

INELASTIC SEISMIC RESPONSE ANALYSIS AND DESIGN OF
TORSIONALLY COUPLED SYSTEMS

A THESIS SUBMITTED TO
THE GRADUATE SCHOOL OF NATURAL AND APPLIED SCIENCES
OF
MIDDLE EAST TECHNICAL UNIVERSITY

BY

KAAN KAATSIZ

IN PARTIAL FULFILLMENT OF THE REQUIREMENTS
FOR
THE DEGREE OF DOCTOR OF PHILOSOPHY
IN
CIVIL ENGINEERING

FEBRUARY 2019

Approval of the thesis:

**INELASTIC SEISMIC RESPONSE ANALYSIS AND DESIGN OF
TORSIONALLY COUPLED SYSTEMS**

submitted by **KAAN KAATSIZ** in partial fulfillment of the requirements for the degree of **Doctor of Philosophy in Civil Engineering Department, Middle East Technical University** by,

Prof. Dr. Halil Kalıpçılar
Dean, Graduate School of **Natural and Applied Sciences**

Prof. Dr. Ahmet Türer
Head of Department, **Civil Engineering**

Prof. Dr. Haluk Sucuoğlu
Supervisor, **Civil Engineering Department, METU**

Examining Committee Members:

Prof. Dr. Polat Gülkan
Department of Architecture, Bilkent University

Prof. Dr. Haluk Sucuoğlu
Department of Civil Engineering, METU

Prof. Dr. Murat Dicleli
Department of Engineering Sciences, METU

Prof. Dr. Afşin Sarıtaş
Department of Civil Engineering, METU

Assist. Prof. Dr. Alper Aldemir
Department of Civil Engineering, Hacettepe University

Date:

I hereby declare that all information in this document has been obtained and presented in accordance with academic rules and ethical conduct. I also declare that, as required by these rules and conduct, I have fully cited and referenced all material and results that are not original to this work.

Name, Surname: Kaan Kaatsız

Signature :

ABSTRACT

INELASTIC SEISMIC RESPONSE ANALYSIS AND DESIGN OF TORSIONALLY COUPLED SYSTEMS

Kaatsız, Kaan

Ph.D., Department of Civil Engineering

Supervisor: Prof. Dr. Haluk Sucuoğlu

February 2019, 299 pages

Torsional coupling due to irregular placement of load resisting members and/or uneven mass distribution along a story plan is a very common phenomenon in structural systems. Unsymmetrical-plan buildings with stiffness and/or mass asymmetry behave considerably different compared to regular buildings when they are subjected to earthquake-induced forces. Modern earthquake resistant design related code provisions that employ capacity design principles aim to achieve a certain amount of ductility in the structural systems while they undergo earthquake excitation. Due to torsional coupling present in asymmetric structures, load-resisting members located at different positions along the plan attain their maximum responses at different times under ground motion excitations. This usually results in unbalanced inelastic demands on members along a story. Consequently, varying ductility demands occur at these members, which are in contrast to the code provisions that utilize a single ductility target. Therefore, following code provisions that aims for a global ductility demand among all structural members can not represent the behaviour of these types of buildings properly.

The proposed thesis study aims at investigating this problem. A comprehensive parametric study on a typical single story, torsionally stiff asymmetric-plan system is conceived. The results obtained are utilized to compile “Unsymmetrical Response Spectra” and “Uniform Ductility Spectra”, which are proposed as assessment and preliminary design tools for estimating the seismic performance of multi-story asymmetric structures. Furthermore, “Optimal Strength Distribution Method” is proposed for use in the design of torsionally coupled systems. This optimal strength distribution, which is determined by utilizing the Uniform Ductility Spectra, is expected to reduce the inherent ductility imbalance in asymmetric systems. The performance of the proposed method is evaluated on three different multi-degree of freedom asymmetric structures and improvements in the seismic response of these systems are evaluated in detail.

Keywords: asymmetric structures, seismic design, ductility balance, overstrength, uniform ductility spectra, optimal strength distribution method

ÖZ

BURULMALI SİSTEMLERİN TASARIMI VE DOĞRUSAL OLMAYAN SİSMİK DAVRANIŞININ ANALİZİ

Kaatsız, Kaan

Doktora, İnşaat Mühendisliği Bölümü

Tez Yöneticisi: Prof. Dr. Haluk Sucuoğlu

Şubat 2019 , 299 sayfa

Yapısal sistemlerde yük taşıyan elemanların simetrik olmayan dağılımı veya düzgün olarak dağıtılmamış kat kütleleri sebebiyle burulma davranışı sık olarak görülmektedir. Düzenli binalarla karşılaştırıldığında kütle yerleşimi ya da taşıyıcıyı sisteme bağlı düzensizliği olan planda asimetrik yapılar deprem kuvvetleri altında oldukça farklı davranış göstermektedirler. Kapasite tasarımı prensiplerini uygulamayı amaçlayan modern depreme dayanıklı tasarım kodları, yer hareketleri sırasında belli bir miktar elastik ötesi deformasyon kapasitesini (süneklik) sağlamayı hedeflemektedir. Burulmalı sistemlerin doğası gereği, dinamik hareket esnasında kat planında farklı yerlerde bulunan yük taşıyıcı elemanların maksimum tepkileri farklı zamanlarda oluşmaktadır. Bu durum da genellikle elemanların üzerinde kat içinde değişen farklı süneklik taleplerine neden olmaktadır. Sonuç olarak, sismik kodların amaçladığı hedefe aykırı şekilde, birbirinden farklı deformasyon talepleri aynı kattaki yapısal elemanlarda gözlenmektedir. Depreme dayanıklı tasarım standartlarının hedeflediği tek bir süneklik değerinin burulmalı sistemlerin gerçek davranışını yansıtmadığı düşünülmektedir.

Önerilen tez çalışması bu durumu araştırmayı amaçlamaktadır. Tek katlı asimetric planlı tipik bir yapısal sistem, kapsamlı bir parametrik çalışma ile incelenmektedir. Çalışmadan, “Asimetric Davranış Spektrumları” ve “Eşit Süneklik Spektrumları” olarak isimlendirilen iki spektral araç üretilmiştir. Bu spektrum setleri çok katlı yapıların sismik performanslarını tasarım aşamasında kestirmek ve değerlendirmek için kullanılabilirler olarak sunulmaktadır. Buna ek olarak, “Optimal Dayanım Dağılım Metodu” isminde bir yöntem burulmalı sistemlerin tasarımlarında kullanılmak için geliştirilmiştir. Bu yöntemde Eşit Süneklik Spektrumları kullanılarak burulmalı sistemlerde en uygun dayanım dağılımı hedeflenmekte ve yapının planı boyunca deprem etkisi altında gözlenen süneklik taleplerinin dengesizliği azaltılmaya çalışılmaktadır. Önerilen bu metodun ortaya koyduğu performans üç farklı asimetric planlı yapı sistemi üzerinde incelenmiş ve bu yapıların sismik performanslarında meydana gelen iyileşmeler kapsamlı olarak incelenerek sunulmuştur.

Anahtar Kelimeler: asimetric yapılar, sismik tasarım, süneklik dengesi, dayanım fazlalığı, eşit süneklik spektrumları, optimal dayanım dağılım metodu

To my mother...

ACKNOWLEDGMENTS

This study was conducted under the supervision of Prof. Dr. Haluk Sucuoğlu. I would like to express my earnest thanks and appreciations for his support, guidance, encouragement and criticisms during this study. It has been a great pleasure to work with him.

I would like to express my gratitude to my family for their endless support throughout my graduate study. Their enthusiasm about my thesis has always been a significant source of motivation for me. I am grateful for the the patience and encouragement shown by them during this period.

I also want to extend my thanks to my close friend and colleague Dr. Fırat Soner Alıcı. His friendship and support has been very valuable throughout my graduate study. His contribution to the research that we have done together over the years is thankfully acknowledged. I am looking forward to work with him in many research topics in the next stage of our careers.

I would like to thank to Erhan Budak for the support he provided while utilizing Perform-3D in the performance assessment phase of the study. Thanks to his tutorial sessions, I have been able to use the software in sufficient capacity in such a short time.

Sincere thanks to M. Başar Mutlu, Dr. Mustafa Can Yücel, Dr. Ahmet Kuşyılmaz and Sadun Tanışer for the great times we shared together in Room Z01. Their support will always be remembered with pleasure.

A very special thanks goes to my dear Dr. Melike Ayça Ay for the enormous support and love she has given to me during the course of this study. Thanks to her understanding and never ending encouragement, I was able to get through the hard times keep my focus. Her immense love and emotional support are gratefully acknowledged.

Finally, my most heartfelt thanks is to my mother who passed away in late stages of my MSc study. Her great love and infinite support have always been the very essential parts of my every success that I have achieved so far. Her self-devotion, encouragement and guidance will never be forgotten. Although she has not been able to see me commence my PhD study, I am sure that she is somewhere up there and proud of her son's achievement. This work is dedicated to her.

TABLE OF CONTENTS

ABSTRACT	v
ÖZ	vii
ACKNOWLEDGMENTS	x
TABLE OF CONTENTS	xii
LIST OF TABLES	xix
LIST OF FIGURES	xxv
CHAPTERS	
1 INTRODUCTION	1
1.1 Statement of the Problem	1
1.2 Review of Past Studies and Investigation of Current Seismic Provisions	5
1.2.1 Review of Research Performed on One-Story Simple Analytical Models	6
1.2.2 Review of Studies Employing Multi-Story Models	16
1.2.3 Discussion on Passive Control Systems for Torsionally Coupled Structures	27
1.2.4 Investigation of Nonlinear Static Analysis Methods Developed for Asymmetric Systems	32
1.2.5 Investigation of Current Seismic Provisions on the Torsional Response	34
1.2.5.1 Provisions in Eurocode 8	35

1.2.5.2	Torsional Provisions in ASCE 7-10	40
1.2.5.3	Provisions in the Turkish Earthquake Code	46
1.2.5.4	Concluding Remarks about Seismic Provisions	49
1.3	Objective and Scope	49
2	A SIMPLE CASE STUDY: ONE-STORY ASYMMETRIC STRUCTURE .	53
2.1	Introduction	53
2.2	General Information and Dynamic Properties	53
2.3	Design and Detailing of Structural Members	58
2.3.1	One-Story Reinforced Concrete Structure	60
2.3.2	One-Story Steel Structure	63
2.4	Analysis of the Designed System	65
2.4.1	Modeling	66
2.4.2	Inelastic Analysis	69
2.4.2.1	Pushover Analysis Results of Reinforced Concrete Structure	70
2.4.3	Pushover Analysis Results of Steel Structure	72
2.5	Discussions on the Observed Asymmetric Performance	73
3	INVESTIGATION OF THE ROLE OF OVERSTRENGTH ON THE SEISMIC PERFORMANCE OF ASYMMETRIC-PLAN STRUCTURES	75
3.1	Introduction	75
3.2	Current Design Practice and Unbalanced Overstrength Distribution .	76
3.3	Parametric Description of the Single-Story Asymmetric System . . .	79
3.3.1	Strong Ground Motions and Dynamic Analyses	82
3.4	Unsymmetrical Response Spectrum	82

3.4.1	Sensitivity of Results to Uncoupled Torsional-to-Lateral Frequency Ratio	88
3.4.2	Sensitivity Analysis for Torsional Performance Parameters . . .	89
3.5	A Simple Design Procedure for Achieving Balanced Inelastic Seismic Response Distribution in Asymmetric-Plan Systems	98
3.6	Discussions	99
4	A PROPOSED METHOD FOR OBTAINING OPTIMAL STRENGTH DISTRIBUTION IN ASYMMETRIC STRUCTURES	103
4.1	Introduction	103
4.2	Identification of the Problem	103
4.3	The Optimal Strength Distribution Method	104
4.3.1	Case I: Strengthening the Stiff Edge Member	106
4.3.2	Case II: Strengthening the Flexible Edge Member	107
4.3.3	Flowchart for the Optimal Strength Distribution Method	109
4.4	Sensitivity of the Method with Respect to Stiff Edge Overstrength . .	109
4.5	Verification of the Optimal Strength Distribution Method	113
4.6	Implementation of the Optimal Strength Distribution Method to Building Structures	117
4.6.1	Construction of Equivalent Strength Allocation Diagrams . . .	117
4.6.2	Determination of Member Strengths	119
4.6.3	Optimal Load Vector and Its Application	122
4.6.4	Revising the Seismic Design	123
4.6.5	Algorithm for the Optimal Strength Distribution Method . . .	123
5	CASE STUDY 1: 8-STORY STIFFNESS ASYMMETRIC STRUCTURE .	125
5.1	Introduction	125

5.2	General Information	125
5.3	Free Vibration Properties	126
5.4	Determination of Static Eccentricity	127
5.5	Linear Elastic Design Spectrum	129
5.6	Seismic Design	130
5.6.1	Frame Design Shears	130
5.6.2	Frame Strengths and Determination of Existing Stiff-to-Flexible Strength Ratio	132
5.6.3	System Overstrength and Computation of Ductility Reduction Factor	132
5.7	Analytical Modeling and Strong Ground Motion Set	134
5.8	Dynamic Analysis Results of the Existing Design	135
5.9	<i>Revised Design</i> : Implementation of the Optimal Strength Distribu- tion Method	141
5.9.1	Determination of $SFSR_{opt}$	141
5.9.2	Strength Allocation Diagram	142
5.9.3	Linear Elastic Analysis and Revised Seismic Design	143
5.10	Dynamic Analysis Results for the Revised Design	145
5.11	Performance Comparison between Existing and Revised Designs . . .	150
5.11.1	Comparison of the Frame Responses	151
5.11.2	Comparison of the Member Ductility Demands	153
5.12	Summary and Discussions	162
6	CASE STUDY 2: 8-STORY MASS ASYMMETRIC STRUCTURE	163
6.1	Introduction	163

6.2	General Information	163
6.3	Free Vibration Properties	165
6.4	Labeling of Frames	165
6.5	Linear Elastic Design Spectrum	166
6.6	Seismic Design	166
6.6.1	Frame Design Shears	168
6.6.2	Computation of Frame Strengths	168
6.6.3	Determination of the Flexible and Stiff Sides of the Structure and $SFSR_{existing}$	168
6.6.4	System Overstrength and Computation of Ductility Reduction Factor	170
6.7	Analytical Modeling and Strong Ground Motion Set	171
6.8	Dynamic Analysis Results of the Existing Design	172
6.9	Implementation of the Optimal Strength Distribution Method	178
6.9.1	Determination of $SFSR_{opt}$	179
6.9.2	Strength Allocation Diagram	179
6.9.3	Linear Elastic Analysis and Revised Seismic Design	181
6.10	Dynamic Analysis Results for the Revised Design	183
6.11	Performance Comparison between Existing and Revised Designs	189
6.11.1	Comparison of Frame Responses	189
6.11.2	Comparison of Member Ductility Demands	189
6.12	Summary and Discussions	200
7	CASE STUDY 3: 12-STORY ASYMMETRIC STRUCTURE	203
7.1	Introduction	203

7.2	General Information	203
7.3	Free Vibration Properties	204
7.4	Determination of Static Eccentricity	204
7.5	Linear Elastic Design Spectrum	207
7.6	Seismic Design	207
7.6.1	Frame Design Shears	209
7.6.2	Frame Strengths and Determination of Existing Stiff-to-Flexible Strength Ratio	209
7.6.3	System Overstrength and Computation of Ductility Reduction Factor	210
7.7	Analytical Modeling and Strong Ground Motions	211
7.8	Dynamic Analysis Results for the Existing Design	212
7.9	<i>Revised Design</i> : Implementation of the Optimal Strength Distribu- tion Method	224
7.9.1	Determination of $SFSR_{opt}$	224
7.9.2	Strength Allocation Diagram	225
7.9.3	Linear Elastic Analysis and Revised Seismic Design	226
7.10	Dynamic Analysis Results for the Revised Design	229
7.11	Performance Comparison between Existing and Revised Designs . . .	240
7.11.1	Comparison of Frame Responses	240
7.11.2	Comparison of Member Ductility Demands	245
7.11.3	Discussion of Results	257
7.12	Performance Comparison between Existing and Revised Designs un- der Scaled Ground Motion Set	257
7.12.1	Comparison of Frame Responses	258

7.12.2	Comparison of Member Ductility Demands	264
7.12.3	Discussion of the Results	275
7.13	Summary and Discussions	275
8	SUMMARY AND CONCLUSIONS	279
8.1	Summary	279
8.2	Conclusion	281
8.3	Recommendations for Future Research	285
	REFERENCES	287
	CURRICULUM VITAE	297

LIST OF TABLES

TABLES

Table 1.1 Basic value of the behavior factor, q_0 , for systems regular in elevation (From Eurocode 8)	39
Table 1.2 Definition of horizontal structural irregularities, taken from ASCE 7-10	42
Table 1.3 Requirements for each story resisting more than 35% of the base shear, taken from ASCE 7-10	45
Table 2.1 Properties of the reinforced concrete one-story structure	61
Table 3.1 Variation of design parameters for the single story structure	80
Table 3.2 The ratios of first and second periods of the parametric systems corresponding to design eccentricities	80
Table 3.3 Unmodified strong ground motions and their properties	83
Table 4.1 Selected design parameters for the single story system	114
Table 4.2 Comparison of mean ductilities for existing and updated designs where $e_s = 0.20$	115
Table 4.3 Comparison of mean ductilities for existing and updated designs where $e_s = 0.30$	116
Table 5.1 Free vibration properties of the eight story stiffness asymmetric structure	127

Table 5.2	Position of CR with respect to CM and the corresponding structural eccentricity (e) at each story. Negative x_{CR} value implies that CR is located on the stiff side.	128
Table 5.3	Strong column - weak beam check for the Existing Design: Ratio of total column moment capacity to total beam moment capacity at each joint of the structure.	131
Table 5.4	Frame design base shear forces ($V_{d,Frame}$) for the <i>Existing Design</i> . Units in kN.	131
Table 5.5	Frame base shear strengths (F_{Frame}) of the <i>Existing Design</i> . Units in kN.	132
Table 5.6	Strong ground motion records that are employed in the dynamic analyses.	135
Table 5.7	Mean beam curvature ductilities of existing design under the ground motion set.	139
Table 5.8	Mean column curvature ductilities of existing design under the ground motion set.	140
Table 5.9	Mean beam curvature ductilities of revised design under the ground motion set.	148
Table 5.10	Mean column curvature ductilities of revised design under the ground motion set.	149
Table 5.11	Beam curvature ductility comparison for the Stiff Edge Frame . . .	154
Table 5.12	Beam curvature ductility comparison for the Stiff Inner Frame . . .	155
Table 5.13	Beam curvature ductility comparison for the Flexible Inner Frame .	156
Table 5.14	Beam curvature ductility comparison for the Flexible Edge Frame .	157
Table 5.15	Column curvature ductility comparison for the Stiff Edge Frame . .	158
Table 5.16	Column curvature ductility comparison for the Stiff Inner Frame . .	159

Table 5.17 Column curvature ductility comparison for the Flexible Inner Frame	160
Table 5.18 Column curvature ductility comparison for the Flexible Edge Frame	161
Table 6.1 Free vibration properties of the eight-story mass-asymmetric structure	165
Table 6.2 Strong column - weak beam checks for the Existing Design: Ratio of total column moment capacity to total beam moment capacity at each joint of the structure.	167
Table 6.3 Frame design shear forces ($V_{d,Frame}$). Units in kN.	168
Table 6.4 Frame base shear strengths (F_{Frame}) of the <i>Existing Design</i> . Units in kN.	168
Table 6.5 Strong ground motion records employed in dynamic analyses. . . .	172
Table 6.6 Mean beam curvature ductilities of existing design under the ground motion set.	176
Table 6.7 Mean column curvature ductilities of existing design under the ground motion set.	177
Table 6.8 Mean beam curvature ductilities of revised design under the ground motion set.	186
Table 6.9 Mean column curvature ductilities of revised design under the ground motion set.	187
Table 6.10 Beam curvature ductility comparison for the Weak Edge Frame . . .	192
Table 6.11 Beam curvature ductility comparison for the Weak Inner Frame . . .	193
Table 6.12 Beam curvature ductility comparison for the Strong Inner Frame . .	194
Table 6.13 Beam curvature ductility comparison for the Strong Edge Frame . .	195
Table 6.14 Column curvature ductility comparison for the Weak Edge Frame . .	196
Table 6.15 Column curvature ductility comparison for the Weak Inner Frame . .	197

Table 6.16 Column curvature ductility comparison for the Strong Inner Frame .	198
Table 6.17 Column curvature ductility comparison for the Strong Edge Frame .	199
Table 7.1 Free vibration properties of the twelve story asymmetric structure .	206
Table 7.2 Position of CR with respect to CM and the corresponding stiffness eccentricity (e) at each story perpendicular to the direction of analysis. Negative x_{CR} value implies that CR is located at left side of the CM as indicated in Figure 7.1.	206
Table 7.3 Frame design shear force demands ($V_{d,Frame}$) for the <i>Existing Design</i> . Units in kN.	209
Table 7.4 Frame base shear strengths (F_{Frame}) of the <i>Existing Design</i> . Units in kN.	210
Table 7.5 Strong ground motion records that are employed in dynamic analyses.	213
Table 7.6 Mean beam curvature ductilities of existing design under the ground motion set.	219
Table 7.7 Shear wall curvature ductilities of existing design computed under the ground motion set.	220
Table 7.8 Mean stiff edge frame column curvature ductilities of existing design under the ground motion set.	221
Table 7.9 Mean stiff inner and center frame column curvature ductilities of the existing design under the ground motion set.	222
Table 7.10 Mean flexible inner and flexible edge frame column curvature ductilities of existing design under the ground motion set.	223
Table 7.11 Mean beam curvature ductilities of revised design under the ground motion set.	235
Table 7.12 Shear wall curvature ductilities of revised design computed under the ground motion set.	236

Table 7.13 Mean stiff edge frame column curvature ductilities of revised design under the ground motion set.	237
Table 7.14 Mean stiff inner and center frame column curvature ductilities of revised design under the ground motion set.	238
Table 7.15 Mean flexible inner and flexible edge frame column curvature duc- tilities of revised design under the ground motion set.	239
Table 7.16 Beam curvature ductility comparison for the Stiff Edge Frame . . .	246
Table 7.17 Beam curvature ductility comparison for the Stiff Inner Frame . . .	247
Table 7.18 Beam curvature ductility comparison for the Center Frame	248
Table 7.19 Beam curvature ductility comparison for the Flexible Inner Frame .	249
Table 7.20 Beam curvature ductility comparison for the Flexible Edge Frame .	250
Table 7.21 Shear wall ductility comparison for both designs.	251
Table 7.22 Column curvature ductility comparison for the Stiff Edge Frame . .	252
Table 7.23 Column curvature ductility comparison for the Stiff Inner Frame . .	253
Table 7.24 Column curvature ductility comparison for the Center Frame	254
Table 7.25 Column curvature ductility comparison for the Flexible Inner Frame	255
Table 7.26 Column curvature ductility comparison for the Flexible Edge Frame	256
Table 7.27 Beam curvature ductility comparison for the Stiff Edge Frame . . .	264
Table 7.28 Beam curvature ductility comparison for the Stiff Inner Frame . . .	265
Table 7.29 Beam curvature ductility comparison for the Center Frame	266
Table 7.30 Beam curvature ductility comparison for the Flexible Inner Frame .	267
Table 7.31 Beam curvature ductility comparison for the Flexible Edge Frame .	268

Table 7.32 Shear wall ductility comparison for both designs under the MCE scaled ground motion set.	269
Table 7.33 Column curvature ductility comparison for the Stiff Edge Frame . .	270
Table 7.34 Column curvature ductility comparison for the Stiff Inner Frame . .	271
Table 7.35 Column curvature ductility comparison for the Center Frame	272
Table 7.36 Column curvature ductility comparison for the Flexible Inner Frame	273
Table 7.37 Column curvature ductility comparison for the Flexible Edge Frame	274

LIST OF FIGURES

FIGURES

Figure 1.1	A torsionally coupled building model with stiffness eccentricity.	2
Figure 1.2	Definition of nominal yield curvature and relationship between section depth and yield strain (from Paulay [69]).	20
Figure 1.3	Relationship between strength and stiffness of a typical reinforced concrete structural member (from Paulay [69]).	20
Figure 2.1	Floor plan of the one story rigid slab structure.	54
Figure 2.2	Locations of <i>CV</i> and <i>CR</i> with respect to the center of mass. . . .	57
Figure 2.3	Design acceleration response spectrum.	58
Figure 2.4	Representative view of the one story structure.	59
Figure 2.5	Deformed shape of a column fixed at both ends and resulting forces during seismic response.	62
Figure 2.6	Section details of reinforced concrete members (units in mm). . .	63
Figure 2.7	Section details of structural steel members (units in mm). . . .	64
Figure 2.8	Fiber section diagram for reinforced concrete members (from OpenSees Example Manual)	67
Figure 2.9	Fiber section diagram for steel members (from OpenSees Example Manual)	68

Figure 2.10	Capacity curve of the one story reinforced concrete system obtained from pushover analysis.	70
Figure 2.11	Capacity curve of reinforced concrete columns obtained from pushover analysis.	71
Figure 2.12	Capacity curve of the one story reinforced steel system obtained under from analysis.	72
Figure 2.13	Capacity curve of steel columns obtained from pushover analysis.	73
Figure 3.1	(a) Schematic distribution of displacement and strength demands in design. (b) Types of strength demands for different choices of e_v . (u_{FD} : flexible edge design displacement, F_{FD} : flexible edge design strength, k_F : flexible edge stiffness. Similar notation for the stiff edge)	76
Figure 3.2	Variation of stiff edge to flexible edge design strength ratio of nominal designs with translational design period and stiffness eccentricity.	77
Figure 3.3	Typical single story shear frame structure.	78
Figure 3.4	Force- displacement behavior of structural members and strength design demands in a single story asymmetric system.	78
Figure 3.5	Acceleration response spectra of the thirty design spectrum compatible ground motions.	81
Figure 3.6	Unsymmetrical response spectra for $e = 0.05$	85
Figure 3.7	Unsymmetrical response spectra for $e = 0.10$	85
Figure 3.8	Unsymmetrical response spectra for $e = 0.15$	86
Figure 3.9	Unsymmetrical response spectra for $e = 0.20$	86
Figure 3.10	Unsymmetrical response spectra for $e = 0.30$	87
Figure 3.11	Mean ductility spectra for $R\mu = 4$ and $SFSR = 1$ at the flexible (left) and stiff (right) edges.	88

Figure 3.12	Mean ductility spectra for constant e and $SFSR = 1$ at the flexible (left) and stiff (right) edges.	89
Figure 3.13	Mean ductility spectra at the flexible (left) and stiff (right) edges for $SFSR = 1$, $R\mu = 4$, $e = 0.15$ (top row) and $e = 0.30$ (bottom row). . .	90
Figure 3.14	The effect of member strength distribution on torsional performance.	93
Figure 3.14	Continued	94
Figure 3.14	Continued	95
Figure 3.15	Uniform Ductility Spectra.	96
Figure 3.16	Variance of $SFSR$ in Uniform Ductility Spectra.	97
Figure 3.17	Force-displacement responses of existing and revised single story asymmetric systems under design ground motions.	100
Figure 3.18	Force-displacement responses of existing and revised single story asymmetric systems under scaled ground motions.	101
Figure 4.1	Schematic representation of the simple asymmetric system. . . .	105
Figure 4.2	Strength Allocation Diagram constructed for Case I type system.	106
Figure 4.3	Strength Allocation Diagram constructed for Case II type system.	108
Figure 4.4	Flowchart for the Optimal Strength Distribution Method.	110
Figure 4.5	Variation of normalized ΔV with Ω_S	112
Figure 4.6	Variation of normalized ΔT with Ω_S	112
Figure 4.7	Typical force-deformation relationships of single story structures.	114
Figure 4.8	Construction of Equivalent Strength Allocation Diagram for a multi-story moment-frame building. Frames of the structure are labeled according to expected deformation patterns during seismic response. . .	118

Figure 4.9	First story mechanism in a moment resisting frame during seismic response. Individual shear forces on columns (V_{ir}) are obtained from plastic moments occurring at both ends of members (M_{itop} and $M_{p,bottom}$).	121
Figure 5.1	Typical story plan of the eight story asymmetric structure and elevation view of the SE-SI-FI frames in the direction of analysis. Center of mass (CM) locations which is located at the geometric center (same for all stories) are marked on the plan (Units in meters).	126
Figure 5.2	Linear elastic design spectrum and acceleration response spectra of amplitude scaled strong ground motions. Mean scaled response spectrum of these records is also plotted in dotted line.	129
Figure 5.3	Distribution of frame shears and strengths along four frames of the structure (units in kN).	133
Figure 5.4	Maximum interstory drift ratios obtained from inelastic dynamic analyses of the existing design under ground motion set and the corresponding mean of maximum values for 9 GM records.	136
Figure 5.5	Beam-end curvatures obtained from inelastic dynamic analyses of the existing design under ground motion set and the corresponding mean of maximum values for 9 GM records.	136
Figure 5.6	Column bottom-end curvatures obtained from inelastic dynamic analyses of the existing design under ground motion set and the corresponding mean values for 9 GM records.	137
Figure 5.7	Frame shear forces obtained from inelastic dynamic analyses of the existing design under ground motion set and the corresponding mean values for 9 GM records.	137
Figure 5.8	Bi-linearized moment curvature relationships of first story columns and computed ductility demands on these columns.	141

Figure 5.9	Equivalent Strength Allocation Diagram constructed for the eight story-stiffness asymmetric structure.	143
Figure 5.10	Schematic view of the four frames with columns that require strengthening (marked as dashed red lines).	144
Figure 5.11	Interstory drift ratios obtained from inelastic dynamic analyses of the revised design under ground motion set and the corresponding mean values for 9 GM records.	146
Figure 5.12	Beam end curvatures obtained from inelastic dynamic analyses of the revised design under ground motion set and the corresponding mean values for 9 GM records.	146
Figure 5.13	Column bottom end curvatures obtained from inelastic dynamic analyses of the revised design under ground motion set and the corresponding mean values for 9 GM records.	147
Figure 5.14	Frame shear forces obtained from inelastic dynamic analyses of the revised design under ground motion set and the corresponding mean values for 9 GM records.	147
Figure 5.15	Bi-linearized moment curvature relationships of first story columns and computed ductility demands on these columns obtained for revised design.	150
Figure 5.16	Comparison of the mean interstory drift ratios calculated for the existing and revised designs.	151
Figure 5.17	Comparison of the mean beam-end curvatures calculated for the existing and revised designs.	152
Figure 5.18	Comparison of the mean column bottom end curvatures calculated for the existing and revised designs.	152

Figure 6.1	Typical story plan of the eight story mass-asymmetric structure and elevation view of the frames in the direction of analysis. Center of Rigidity (<i>CR</i>) and Center of mass (<i>CM</i>) locations (same for all stories) are marked on the plan. (Units in meters)	164
Figure 6.2	Idealized force-deformation relationships of flexible and stiff sides of the system.	169
Figure 6.3	Distribution of frame shears and strengths along four frames of the mass asymmetric system (units in kN).	171
Figure 6.4	Maximum interstory drift ratios obtained from inelastic dynamic analyses of the existing design under ground motion set and the corresponding mean of maximum values.	173
Figure 6.5	Beam-end curvatures obtained from inelastic dynamic analyses of the existing design under ground motion set and the corresponding mean of maximum values.	173
Figure 6.6	Column bottom end curvatures obtained from inelastic dynamic analyses of the existing design under ground motion set and the corresponding mean of maximum values.	174
Figure 6.7	Frame shear forces obtained from inelastic dynamic analyses of the existing design under ground motion set and the corresponding mean of maximum values.	174
Figure 6.8	Bi-linearized moment curvature relationships of first story columns and computed ductility demands on these members.	178
Figure 6.9	Equivalent Strength Allocation Diagram constructed for the eight story mass-asymmetric structure.	180
Figure 6.10	Change in idealized force-deformation relationships of flexible and stiff sides of the revised system and expected deformation levels, which are qualitatively marked on the curves.	181

Figure 6.11	Schematic view of the four frames with columns needing design revision marked as dashed red lines.	182
Figure 6.12	Maximum interstory drift ratios obtained from inelastic dynamic analyses of the revised design under ground motion set and the corresponding mean of maximum values.	183
Figure 6.13	Beam-end curvatures obtained from inelastic dynamic analyses of the revised design under ground motion set and the corresponding mean of maximum values.	184
Figure 6.14	Column bottom-end curvatures obtained from inelastic dynamic analyses of the revised design under ground motion set and the corresponding mean of maximum values.	184
Figure 6.15	Frame shear forces obtained from inelastic dynamic analyses of the revised design under ground motion set and the corresponding mean of maximum values.	185
Figure 6.16	Bi-linearized moment curvature relationships of first story columns and computed ductility demands on these columns obtained for revised design.	188
Figure 6.17	Comparison of mean maximum interstory drift ratios calculated for the existing and revised designs.	190
Figure 6.18	Comparison of the mean maximum beam-end curvatures calculated for the existing and revised designs.	190
Figure 6.19	Comparison of the mean maximum column bottom-end curvatures calculated for the existing and revised designs.	191
Figure 7.1	Typical floor plan of the twelve story asymmetric structure and elevation view of the frames in the direction of analysis. Center of mass (<i>CM</i>) is marked on the plan. (Units in meters)	205

Figure 7.2	Linear elastic design spectrum and acceleration response spectra of the amplitude scaled strong ground motions. Mean response spectrum of the scaled records is plotted in dotted line.	208
Figure 7.3	Distribution of frame base shear demands and base shear strengths along all frames of the structure (units in kN).	211
Figure 7.4	Maximum interstory drift ratios obtained from inelastic dynamic analyses of the existing design under ground motion set, and the corresponding mean of maximum values for 10 GM records.	214
Figure 7.5	Beam-end curvatures obtained from inelastic dynamic analyses of the existing design under ground motion set and the corresponding mean values for 10 GM records.	215
Figure 7.6	Column bottom-end curvatures obtained from inelastic dynamic analyses of the existing design under ground motion set, and the corresponding mean values for 10 GM records.	216
Figure 7.7	<i>SE</i> frame shear wall curvatures obtained from inelastic dynamic analyses of the existing design under the ground motion set, and the corresponding mean values for 10 GM records.	217
Figure 7.8	Maximum interstory drift ratios of the frames in orthogonal direction determined under ground motion set and the corresponding mean of maximum values for 10 GM records.	217
Figure 7.9	Equivalent Strength Allocation Diagram constructed for the twelve story frame-wall structure.	225
Figure 7.10	Schematic view of the five frames where columns and the shear wall that require strengthening at the related stories are marked.	227
Figure 7.11	Maximum interstory drift ratios obtained from inelastic dynamic analyses of the revised design under ground motion set and the corresponding mean of maximum values for 10 GM records.	230

Figure 7.12	Beam end curvatures obtained from inelastic dynamic analyses of the revised design under ground motion set and the corresponding mean values for 10 GM records.	231
Figure 7.13	Column bottom-end curvatures obtained from inelastic dynamic analyses of the revised design under ground motion set and the corresponding mean values for 10 GM records.	232
Figure 7.14	SE frame shear wall curvatures obtained from inelastic dynamic analyses of the revised design under ground motion set and the corresponding mean values for 10 GM records.	233
Figure 7.15	Maximum interstory drift ratios of the frames in orthogonal direction of the revised structure determined under ground motion set and the corresponding mean of maximum values for 10 GM records. . . .	233
Figure 7.16	Comparison of the mean interstory drift ratios in direction of analysis calculated for the existing and revised designs.	241
Figure 7.17	Comparison of the mean beam-end curvatures calculated for the existing and revised designs.	242
Figure 7.18	Comparison of the mean column bottom end curvatures calculated for the existing and revised designs.	243
Figure 7.19	Comparison of the shear wall curvatures calculated for the existing and revised designs.	244
Figure 7.20	Comparison of the mean interstory drift ratios calculated in the orthogonal direction frames for the existing and revised designs. . . .	244
Figure 7.21	Comparison of the mean interstory drift ratios in direction of analysis calculated for the existing and revised designs under the MCE scaled ground motion set.	259
Figure 7.22	Comparison of the mean beam-end curvatures calculated for the existing and revised designs under the MCE scaled ground motion set. .	260

Figure 7.23	Comparison of the mean column bottom end curvatures calculated for the existing and revised designs under the MCE scaled ground motion set.	261
Figure 7.24	Comparison of the shear wall curvatures calculated for the existing and revised designs under the MCE scaled ground motion set. . .	262
Figure 7.25	Comparison of the mean interstory drift ratios calculated in the orthogonal direction frames for the existing and revised designs under the MCE scaled ground motion set.	262

CHAPTER 1

INTRODUCTION

1.1 Statement of the Problem

Torsional coupling due to irregular placement of load resisting members and/or uneven mass distribution across a story plan is a very common phenomenon in structural systems. Unsymmetrical-plan buildings with stiffness and/or mass asymmetry behave considerably different compared to regular buildings when they are subjected to earthquake-induced forces. Modern earthquake resistant design provisions that employ capacity design principles aim to achieve a certain amount of ductility in structural systems while they undergo earthquake excitation. Although inelastic performance of the system is mostly predictable and uniform along each story for regular structures, this is not always the case for asymmetric structures. Due to the presence of torsional coupling in these types of buildings, load-resisting members located at different positions in the plan attain their maximum responses at different times during dynamic response. This usually results in differing demands on members along a story. Consequently, varying deformation and ductility demands are measured on these members, and this is in contrast to the code provisions, which intend to impose a uniform inelastic performance distribution. Moreover, there is a lack of globally accepted performance-based earthquake engineering philosophy for the estimation of the structural performance of torsionally coupled systems. Therefore, it can be stated that the behavior of these types of buildings may not be estimated properly by applying common design and assessment methodologies that are employed in current earthquake engineering practice.

In order to understand torsionally coupled response better, properties associated with

the asymmetric systems and some of the principles in seismic code provisions that are developed for design of torsionally coupled structures can be discussed in detail herein.

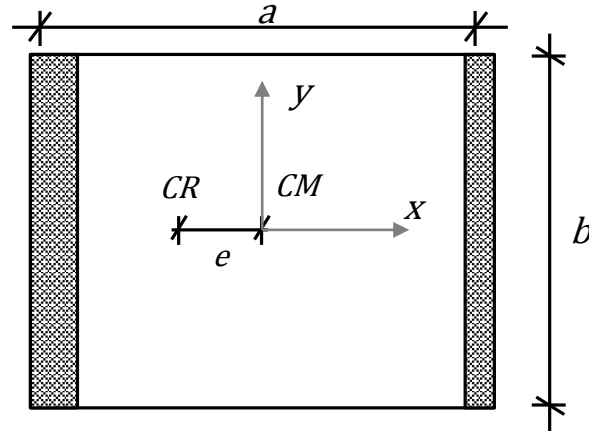


Figure 1.1: A torsionally coupled building model with stiffness eccentricity.

A single story idealized system is presented in Figure 1.1 in order to define the problem. The lateral load resisting members are idealized as shear frames at both edges of the slab. The stiffness values of these members are different from each other with element on one side being stiffer than the other. This also provides the labeling convention for the torsionally coupled systems. *SE* stands for stiff edge where less deformation is anticipated due to stiffer elements; while *FE* stands for flexible edge that is expected to deform larger. *CR* is the center of rigidity (stiffness) of the system that is determined from the individual element stiffness values, and *CM* is the center of mass, which is coincident with the geometric center in this particular structure. System is asymmetric in the direction of consideration (*y* direction). The stiffness eccentricity causing the asymmetry is symbolized by e . Due to eccentricity, the slab does not move uniformly under lateral loading. This results in the occurrence of both translational deformation and rotation at the center of mass; hence a torsionally coupled response. The eccentricity e is a system property and should be considered in the design. Prevalent seismic codes such as Eurocode 8 [30] or ASCE/SEI 7-10 [4] provide means to incorporate this necessity in capacity design principles and consequently design eccentricity was defined. Bustamante and Rosenblueth [10] suggested a definition for the design eccentricity which was later discussed by Rutenberg and De

Stefano [80]. Although the implementation varies among seismic provisions; design eccentricity can be stated as given in Equation 1.1:

$$e_d^+ = \alpha e + \beta \alpha \quad (1.1a)$$

$$e_d^- = \gamma e - \beta \alpha \quad (1.1b)$$

$$e_d^- = \alpha e + \beta \alpha \quad (1.1c)$$

Design eccentricity of the flexible edge elements is defined in Equation 1.1a. For the stiff edge elements, the one that yields maximum forces were selected as the design eccentricity from Equations 1.1b and 1.1c. The plan dimension a is in the perpendicular direction to the analysis as shown in Figure 1.1. The coefficients α and γ are used to amplify the plan (natural) eccentricity and their values vary among seismic provisions. For instance; in the aforementioned study by Rutenberg and De Stefano [80], authors stated that the contemporary values of γ and α given by SEAOC and UBC was 1. It should be noted that α and γ apply only to static analysis and modern seismic provisions only consider β term for dynamic analysis. This β term is the coefficient for accidental eccentricity. It is not included in the design stage, but may occur in the actual constructed system due to unexpected changes in stiffness and/or mass distribution. Value of β varies according to seismic provisions but generally given as 0.05 or 0.10. Many studies performed in the past inspected these coefficients and design eccentricity definitions given in the seismic codes and point out the weaknesses observed in the seismic code provisions. These are discussed in detail in the following sections.

Another important concept that needs to be elaborated is the torsional rigidity of the structure under consideration. When the stiffness eccentricity e for the system given in Figure 1.1 becomes zero, no torsional coupling occurs. In this case the first two pair of elastic vibration frequencies of the uncoupled system can be defined as ω and ω_θ . While ω is the translational vibration frequency; ω_θ is the rotational vibration frequency of the system. The ratio of these uncoupled torsional and lateral frequencies is defined as below:

$$\Omega_\theta = \frac{\omega_\theta}{\omega} \quad (1.2)$$

The frequency ratio Ω_θ in Equation 1.2 provides a measure about the torsional rigid-

ity of the system. When this ratio is close to zero; it can be said that the structure is highly torsionally flexible. In other words, the effects of torsional response are very pronounced in the lateral deformation of the system. On the other hand, when this ratio is close to one or higher, system is torsionally stiff. Consequently torsional effects are less significant in the combined response. The torsional property of a system is an important factor in its seismic response and as can be seen in the review of the past studies, majority of the researchers reach different conclusions on torsionally flexible and torsionally stiff systems. It is also shown in many studies that seismic code provisions are usually inadequate in the seismic response estimation of torsionally flexible systems. These conclusions will be elaborated further in the following sections.

There are a number of studies conducted on the inelastic seismic behavior of torsionally coupled systems over the past years. In some of these studies main behavioral differences of torsionally coupled systems, compared to regular structures were investigated. Moreover, some researchers pointed out the shortcomings of the contemporary code provisions when applied to asymmetric structural systems. Majority of these studies are based on single story analytical models. However, with the advancements of structural analysis software and increasing computational power, studies based on multi-story models were also increasingly published. A portion of the recent studies show contradicting results with that of the older studies based on simpler, single story models. They mostly highlight the inability of the simpler models to represent the actual structural behavior of multi-story torsionally coupled systems and the accompanying misleading results achieved from over-simplified single story models.

In conjunction with the studies inspecting the behavior of this type of systems there is also active research on the application of response control systems on asymmetric structures. Especially over the last decade, many publications became available that investigates the possibility of limiting the ductility and deformation demands of torsionally coupled systems. The basic idea is to introduce energy dissipation devices like friction dampers to control the response in a controllable and predictable manner and in a similar level to that of symmetric structures. This application may be employed to overcome the weaknesses of torsional code provisions or prevent torsional coupling effects on existing structures that could be susceptible to uneven demand

distribution.

Aside from the research focused on seismic response of torsionally coupled systems, there are also studies on the application of newly developed nonlinear static analysis techniques extended to these types of structures. Many analysis methods emerged over the years and they were applied to non-regular structures with mostly satisfactory results. Along with better understanding the behavior of torsionally coupled systems, the advancement of more accurate analysis techniques enables designers with more valuable tools and information than what had been available in the past. This progress has yielded more robust structural design as the engineers had been able to estimate the responses of torsionally coupled systems better. Still, however, there are many issues to be addressed in the subject, on which this thesis study focuses.

1.2 Review of Past Studies and Investigation of Current Seismic Provisions

Behavior of irregular and asymmetric structures has been studied since many decades by a limited number of researchers. The studies conducted in the field were thoroughly reviewed by Rutenberg [78, 79], De Stefano and Pintucchi [26]. In a very comprehensive study, Anagnostopoulos et al. [6] presented the current state-of-the-art regarding earthquake induced torsion in buildings. In a review discussing over five hundred studies that were conducted on torsionally coupled systems, authors discussed the modeling and analysis variations of torsionally coupled systems and reached important conclusions concerning the usage of oversimplified models for assessing the torsional behavior. Moreover, lack of universally accepted observations about torsion and associated performance of asymmetric systems was also noted.

In this section, a further investigation into the previous studies is presented in five major subsections. First, the research which employs simple one-story models is discussed. Next, studies that inspect the behavior of torsionally coupled systems on multi-story analytical models are presented in detail. In the third section, studies involving energy dissipation and control mechanisms in asymmetric systems are investigated. Fourth section summarizes the progress made on the nonlinear static analysis methods that are developed to estimate the response of multi-story torsionally cou-

pled systems. Finally; a discussion on provisions about torsional behavior in three contemporary seismic standards, namely, Eurocode 8 [30], ASCE/SEI 7-10 [4], and Turkish Earthquake Code [73] are presented.

Some studies inspected in this section focus on torsional behavior of the systems while others assess the code provisions regarding asymmetric systems. Another portion of the studies propose design recommendations or new design procedures for torsionally coupled systems. These different topics are not divided into separate titles in the subsections specified. Rather, it was deduced to present the previous work in a chronological order in order to better visualize the progress made over the decades.

1.2.1 Review of Research Performed on One-Story Simple Analytical Models

Very early studies attempted to establish the definition of design eccentricity of the asymmetric structures [10]. With the inclusion of design eccentricity in seismic provisions, regular engineering practice has been long performed such that after the design eccentricity is determined, strength of structural members are allocated according to the strength based formulas. Consequently, peak ductility demands on the system could be maintained in a controlled manner. However, the formulated design eccentricity and resulting strength allocation did not represent the strength of elements beyond their elastic limits. Later Paulay [67] criticized this and stated that the strength of members are related to their geometry, therefore strength allocation based on design eccentricity equations may yield undesired behavior. He later elaborated this argument in his subsequent research, which will be discussed in the following sections.

Kan and Chopra [49] were the earliest researchers who discussed the effects of torsional coupling on seismic response. The influence of basic system parameters on the response and the relationship between base shear and base torque was investigated. They reached an important conclusion: The increase in stiffness eccentricity results in a decrease in base shear while base torque increases. In another well-known study, Kan and Chopra [50] analyzed the effects of torsional coupling on the seismic behavior of single-story structures in both elastic and inelastic response ranges. The models had one-way eccentricity, and the resisting elements were simply idealized by single

element models. Under a set of ground motions, deformation response of the system and structural elements were investigated. A major finding in the study is that with increasing inelastic behavior, effects of torsional coupling diminish compared to the elastic response. They recorded lower effects of torsional deformation when highly inelastic action was observed.

Goel and Chopra [39] conducted a study on the inelastic seismic response of one-story systems. Effects of plan asymmetry were investigated and inelastic deformations were considered. The motive was to better understand the inelastic response of asymmetric-plan systems and consequently reach conclusions that can provide improvements for torsional provisions in building codes. The idealized one-way asymmetric single-story system included elements both in the direction of analysis and in the transverse direction. Torsional coupling was introduced by a stiffness eccentricity. The force-deformation characteristics of structural members were assumed as elastic-perfectly plastic. Effects of many parameters were inspected in the response such as lateral vibration period, torsional rigidity and the amount of stiffness eccentricity. Along with the stiffness eccentricity, strength eccentricity related with the center of strength was also considered. Center of strength, which is the location of the resultant forces on structural members, existed in the initial elastic response. However, if all the elements have the same yield strength and yielding event occurs simultaneously in all members, the center of strength becomes symmetrically located. To account for this change, both cases of strength eccentricity were also considered. In the analysis results, peak deformation demands were compared. It was concluded that response of inelastic systems are affected more from plan asymmetry compared to elastic systems. To add; in terms of inelastic response, strength-symmetric systems (with no strength eccentricity) were affected less from plan asymmetry when compared with systems with equal strength and stiffness eccentricities. This conclusion is of significance since loss of strength eccentricity could be observed in the post-yield response of structures having equal strength allocation in structural members.

There are also some other early studies considering the response of code-designed asymmetric single story systems under ground motion excitation (Rutenberg [77], Chandler et. al. [13]). In these publications, the ductility demands among structural members designed according to provisions such as Eurocode 8, UBC (United States),

NBCC (Canada) were measured and an important result was noted: Static provisions of seismic codes are not suitable for design of structures that are torsionally flexible.

In a paper worth mentioning, Priestley [74] discussed many “myths” that are associated with earthquake engineering such as strength and stiffness allocation to members, detailing of reinforced concrete members or energy absorption during seismic events. In a section of his study, he also proposed a displacement-based design procedure and illustrated this on a simple one-story model. This can be summarized as follows: At the initial stage of the design, yield displacement estimation is made for the structure. Then, critical hinges on the structure is determined. Maximum acceptable structural plastic displacement occurring at the location where seismic force acts on the system is found. This maximum plastic displacement corresponds to the plastic rotation limit of the most critical hinge is determined by considering the mechanism formation. From the plastic displacement, maximum acceptable structural displacement is calculated which enables the designer to find the ductility level of the system. The ductility level and structural system properties are then used to estimate the effective damping of the system which in turn yields the elastic design spectrum. The period can now be estimated and, consequently, equivalent stiffness of the system is calculated. This equivalent stiffness is used to calculate the force acting on the system of which the structural members are determined according to this force. The procedure essentially determines the equivalent stiffness of the system obtained by considering the yield mechanism. Although there is no mention of an extension of the procedure to a torsionally coupled system, it is applicable to any asymmetric structure; therefore this study is also included in the review.

Goel and Chopra [40] presented a dual design approach for seismic design of asymmetric-plan systems. The main postulation in the study is that buildings should be designed in a way to satisfy both serviceability and ultimate limit states (SLS and ULS). Therefore, they state that design procedure for asymmetric-plan systems should be simultaneously investigating both their elastic response to moderate ground motions (SLS) and their inelastic response to intense ground motion (ULS). The response of a single story, asymmetric-plan system designed according to dual design approach. Then its response is investigated and compared with responses of systems designed according to the torsional provisions of U.S. seismic codes. In this approach, design forces of

members are selected as the larger of the forces obtained according to design spectra for each limit state, namely SLS and ULS. In order to investigate performance; response comparison of SLS, ULS and dual-level systems are presented. It is shown that a single limit state may not satisfy the objectives of other limit state. That is, ULS design may not remain elastic under serviceability design earthquake, while SLS design may undergo excessive ductility under ULS earthquake. However, dual level design response of asymmetric-plan system satisfies the requirements of both limit states. The authors conclude that results obtained address a shortcoming of current seismic codes and the concept presented should be extended to multistory systems.

Correnza et al. [17] studied on the seismic response of flexible-edge elements in code-designed structures. They investigated the ductility and deformation demands of the flexible-edge elements in torsionally unbalanced systems and evaluated the adequacy of code torsional provisions. They set up two analytical models with a moderately high and a with low level of torsional stiffnesses which were designed according to UBC (United States), NBCC (Canada), NZS (New Zealand), AUS (Australia) and Eurocode 8 (Europe) provisions. They pointed out that NZS and Eurocode 8 allowed strength reduction in stiff-edge side elements, which resulted in stiff-edge becoming more critical in terms of ductility demands. Upon comparing the response of the asymmetric systems with that of symmetric counterparts, they concluded that torsional stiffness is more sensitive to variations in the normalized static eccentricity rather than plan aspect ratio. For the seismic codes that do not amplify static eccentricity (NZS and UBC), non-conservative results has been determined. Tso and Wong [86] also investigated displacement response of asymmetric systems. They found out that the maximum edge displacements are not sensitive to torsional provisions, but they are affected more by the eccentricity of the system.

Bertero [8] studied the effects of inelastic torsion in the preliminary seismic design process. The purpose of the study was to set a goal to avoid torsional mechanism. He developed a simplified approach to control the inelastic behavior of structures and tested the approach on a parametrical study. In this approach, the expected torsional response of the building is associated with a β parameter which is formulated by considering the eccentricity of the system. If the calculated β for the structure were above 1.2, the design would have to be modified to minimize the effects of torsion.

He concluded his study with design recommendations such as locating centers of rigidity and mass as close as possible and increasing torsional redundancy, which are in consistency with the findings of previously mentioned researchers.

The effects of spatially varying ground motions on asymmetric structures were studied by Hao and Duan [43]. On idealized single story systems (varying from torsionally flexible to torsionally stiff) with mass asymmetry, thirty pairs of ground motions were imposed. These ground motions were spatially correlated, that is, different two ground excitations originating from the same earthquake were produced to form each pair. These pairs were then applied to both flexible and stiff edges of the structure, resulting in a non-uniform excitation. It was deduced that both building asymmetry and non-uniform excitation have the effect of reducing base shear and producing torque. For torsionally stiff systems, reduction in torque due to non-uniform excitation was observed; whereas for torsionally flexible systems this trend was the opposite. Finally, the authors noted inadequacy of provisions for multiple excitations in seismic codes.

Performance of code-designed torsionally coupled systems for both serviceability and ultimate limit states were discussed by Chandler and Duan [12]. In the paper, effects of parameters such as accidental torsional provisions defined in the codes, load reduction factor and uncoupled lateral period on the response of structures were investigated. One-way asymmetric single story idealized structures, which were designed according to Eurocode 8, UBC and NBCC were analyzed under a set of eight ground motions. They performed these analyses by changing the system parameters explained above and compared the ductility demand and peak displacement demand ratios obtained with those obtained from symmetrical counterpart systems. It has been observed that a strength increase in the flexible-edge elements is always present in the results. Similarly, for all models strength demand is shown to be higher in the torsionally coupled systems compared to symmetric ones. They concluded their study with many remarks such as insensitivity of the seismic response to the consideration of accidental eccentricity in the design. This trend, however, was not observed in torsionally flexible systems. It was also noted that reduction factor influences stiff-edge response significantly: high reduction factors yielded higher inelastic action which resulted in loss of torsional response. This finding is consistent with what previously

mentioned researches concluded. Similar to the previous studies, they also stated that stiff-edge elements are more critical at the limit states compared to flexible-edge elements that were designed conservatively; due to code provisions.

In a complementing paper to their previous work, Duan and Chandler [28] described an optimized procedure which considers both serviceability and ultimate limit states for seismic design of torsionally unbalanced (TB) structures. The study is aimed to achieve equal or nearly equal responses in terms of ductility in both rigid and flexible edge. These responses are also aimed to be around similar range with those of observed in torsionally balanced (symmetric) reference system. A parametric study was conducting by changing many system parameters such as radius of gyration, static eccentricity or force reduction factor, R . Two one-story TB systems were utilized in this extensive parametric study and several design charts marking relationships between the aforementioned parameters were prepared. Next, a two-phased design procedure was applied that considers the design eccentricity as dependent to limit state and R via design charts provided. The more unfavorable member demand from both limit state is employed in the detailing and sizing of the members. The authors concluded that the applicability of the method can be generalized torsionally unbalanced systems with or without transverse elements and multi-story systems. However, it is also noted that the validity of the procedure for systems having a significant unbalanced mass distribution should be evaluated further.

Some researchers have also investigated presence of elements normal to the direction of excitation, and their contribution to the torsional stiffness. While Rutenberg [77] found that their presence affected the response little, De la Llera and Chopra [21] found the opposite. Paulay [67] introduced the idea of torsionally restrained structures which have load resisting elements on the transverse direction that are included in the analytical models. These members are designed to remain elastic during seismic response. Study results revealed that the displacements related with torsional coupling are significantly reduced.

There is also some research conducted on single story asymmetric systems under bi-directional excitation. These studies are directly related with the research investigating the effects of transverse elements on the seismic response. Although some of the

previous work suggested that the elements in the orthogonal direction to earthquake should be neglected in the analysis; studies performed by employing bi-directional excitations showed significant interaction among structural members in different directions. Stathopoulos and Anagnostopoulos [83] investigated the effect of period ratio on the longitudinal and transverse members and determined that stiffer period results in higher response on the members that are in the direction of analysis. They also found large ductility demands at the stiff edge elements when the eccentricity of the structure was large. De Stefano et al. [23] suggested considering transverse elements while conducting analysis in two separate directions. Humar and Kumar [46] found consistent results with Paulay [67]. In their study, the transverse elements remained practically elastic, lowering the torsional response. Riddell and Santa-Maria [75] concluded in their study that bi-directional ground motion mostly increases the ductility demands of flexible edge elements of torsionally coupled systems in the short period range. Perus and Fajfar [70] compared bi-directional and unidirectional responses of one story asymmetric models and found that unidirectional analysis approach underestimates the response. They also suggested inclusion of transverse elements for unidirectional analysis.

An interesting study by Goel [36] employed an energy-based approach to investigate the seismic behavior of code-designed torsionally coupled systems. Rather than using a one-way asymmetric system, a structure having large eccentricities in both directions was utilized. This system was excited bi-directionally. Hysteretic energy demands on the flexible and stiff side elements were compared with that of symmetric counterpart systems and contrary to many previous findings, the energy-based performance criterion employed in the study yielded more damage in the flexible-edge elements. In the results, while input energy was the same for both symmetric and asymmetric systems, hysteretic energy dissipation seemed lower in the asymmetric systems while damping energy dissipation was higher. Hysteretic energy demands could not be met by the structural members; resulting in damage especially in flexible-edge elements. Goel deduced in the study that higher vulnerability of asymmetric plan systems is related to how the total hysteretic energy is dissipated by various elements. He also suggested that higher hysteretic energy dissipation capacity should be provided for flexible-edge elements.

Perus and Fajfar [70, 71] investigated the effects of plastic deformations on torsional response compared with the elastic response on single story models under bi-axial excitation. They concluded that the global torsional effects in inelastic structures are similar to the elastic ones. In a study that provides a design recommendation for asymmetric buildings, Gherzi and Rossi [35] formulated a design eccentricity that aims to reduce the ductility demand in torsionally coupled systems. Their proposed procedure started with performing the modal analysis twice. At the design stage, first modal analysis is performed with actual mass distribution; while the second one is conducted after mass center is shifted towards the center of rigidity by a formulated design eccentricity. It was stated that the dynamic properties of the system obtained from the first analysis cover the elastic behavior; whereas the inelastic dynamic response of the system is given by second modal analysis. The strength of each element is then assigned as the larger of the two values determined from these two different dynamic responses of the structure. Then, design eccentricity e_d was defined in terms of a pre-determined target ductility demand and its relation with stiffness eccentricity. It was formulated as a function of various system parameters such as frequency ratio and geometric properties. These relationships were obtained by studying the results of performed analyses on a single story asymmetric system. By testing the proposed formulation of design eccentricity for a wide set of parameters in these analyses, authors concluded that their postulation is highly effective in controlling the ductility demand. A different study by De Stefano and Pintucchi [25] studied the behavior of the torsionally stiff systems, especially the interaction between axial force and bi-directional forces occurring in this type of structures. They concluded that previous models neglecting this interaction overestimate the torsional response.

Many researchers studied the relationship between strength and stiffness of structural members which are determined in the preliminary stages of the design process. Since the ductility of torsionally coupled systems are directly related with the deformation characteristics of structural members, strength and stiffness allocation to these members have always been considered an important aspect of the design stage. Paulay [68] aimed to re-evaluate the traditional structural properties for torsionally coupled systems by discussing the relationship between stiffness of structural members and the strength assigned to them. He stated that yield displacement of a member is related

with the member geometry (inversely proportional with member depth) rather than being a strength related property and consequently inelastic displacement of a member is independent of strength. However this is not the case for member stiffness. Due to this independency, he postulated that strength of the structural members could be arbitrarily allocated while yield deformations can be controlled by changing the member dimensions. He later elaborated this approach more in his subsequent paper investigating multi-story systems. [69, Paulay]. As discussed previously, he brought up the concept of torsionally restrained and torsionally unrestrained systems. In torsionally restrained systems, transverse elements that are designed to remain elastic during response are introduced to the design, providing stability and necessary resistance to the structure while it reaches its limit state. However, in the torsionally unrestrained systems, no members exist in transverse direction; therefore the resistance of the structure at the limit state is severely reduced compared to the torsionally restrained one. Further, he summarized the weaknesses of the seismic codes in terms of design of asymmetric structures such as consideration of only elastic behavior in the design and the way the strength to members are allocated and resulting plastic deformations due to torsional effects. He concluded his study with a noteworthy remark: Rather than asking a structure what it could do during a major earthquake, designers should be telling the structure what it must do in terms of seismic performance.

Tso and Myslimaj [85], also worked on the interdependence between strength and stiffness in lateral resisting elements and its implications on seismic design. Adopting a yield displacement based approach they proposed a balanced center of strength (CV) and center of rigidity (CR) location which they have obtained with a desirable distribution of mass and stiffness along a one-story structure. In the final design they reached a configuration where centers of mass and strength are equidistant from center of rigidity. They tested their procedure under bi-directional ground motion excitation and concluded that a balanced CV – CR location criterion can minimize the edge displacements of torsionally coupled systems by providing a careful strength distribution. In their subsequent study Myslimaj and Tso [63] evaluated their design approach along with single story structures designed according to Eurocode 8 and UBC (ICBO1997). Similar to Paulay's observations on interdependence of strength and stiffness [68], their results displayed a need for re-examination of the efficiency

of the torsional provisions which assume that stiffness and strength of lateral force resisting elements as independent.

In a study about residual deformations in structures, Pettinga et. al. [72] evaluated the effects related with inelastic torsional behavior. Adopting a performance-based approach, residual deformations in 3D irregular buildings were inspected. Their approach is which was originally developed for 2D systems is similar what Priestley [74] described as a displacement based design procedure. However, it is extended to 3D systems and aims to estimate the critical global residual drift. In the following sections of the study, a series of one-way eccentric systems either with torsionally restrained or unrestrained configurations were assessed by using inelastic time history analyses. The applicability of their proposed method for estimation of residual deformations were demonstrated by the authors.

Roy and Chakrobotry [76] studied various strength distribution strategies in the plan-symmetric structures on a single story rigid deck system. Investigated eccentric configurations in the paper are concurrent center of strength (CV) - center of mass (CM) positioning and balanced the center of strength (CV) - center of resistance (CR) locations on the plan. As a part of a conceptual framework, authors formulated the distance of CR to CM and the angle of this distance with horizontal axis of the structural plan in terms of center of yield displacement of members and CM while CV is coinciding with CM. By doing so, they were able to compute the eccentricity at the beginning of the design process. Their formulation is also shown to be applicable to the balanced CV-CR systems. Upon performing analyses on a single story doubly asymmetric system, it is finally concluded in the paper that CV-CM coinciding strength design strategy may be employed for structures that is expected to resist from moderate to high seismic activity.

Over the years, there has been varying conclusions in the seismic response of irregular buildings which were represented as simple one story models. In addition, some design procedures, which had been shown to yield superior performance estimation in comparison with the contemporary seismic regulations, were suggested. These procedures were formulated on one-story torsionally coupled systems and their applicability to multi story systems remained unknown. Moreover, majority of the studies that

assess seismic codes stated that seismic design provisions regarding the asymmetric systems are inadequate in terms of ensuring a uniform demand distribution.

1.2.2 Review of Studies Employing Multi-Story Models

Investigation of seismic response in multi-story systems has progressed in conjunction with the studies that employ single-story models over the last decades. Starting from 1990's research including multi-story torsionally coupled structures also gained momentum. With the advance of analysis environments, research that is more comprehensive became possible. One major advantage that this type of detailed models gave the researches was improved accuracy of the estimated response compared to the one-story models. The complex and highly irregular behavior of torsionally coupled systems and the dynamic phenomena such as modal coupling and higher mode effects can better be observed on more realistic multi-story structural models. In contemporary research, multi-story models are commonly employed and enable researchers to better investigate the inelastic seismic response of structures.

Kan and Chopra [48] performed one of the earliest studies concerning the torsional coupling in buildings. Rather than concentrating on the seismic behavior, their paper presented an approximate way to estimate the dynamic properties (lower modal frequencies and mode shapes) of a torsionally coupled system. By performing perturbation analysis on torsionally uncoupled counterpart systems, they were able to estimate the lower modal frequencies and mode shapes of torsionally coupled systems. To determine the lateral forces acting on the structure they further combined this approach with an elastic analysis procedure that uses the modal frequencies and mode shapes obtained. Upon investigating the results of rigid-deck asymmetric multi-story systems, they concluded that the suggested procedure is accurate enough. Considering the date of publication and the limited computational power available, the study provided a robust approximate tool for a demanding problem and presented an early seismic analysis example for torsionally coupled systems.

Hejal and Chopra [44, 45] investigated lateral and torsional seismic response coupling in frame type buildings. Contrary to many studies that will be discussed shortly, they did not employ a shear beam model; that is, their models had beams and columns

rather than rigid decks connected by columns. Their models were 5-story buildings and have been analyzed by employing an approximate procedure which utilizes torsionally uncoupled counterpart buildings. In the studies, many parameters have been inspected as well as higher mode contributions to the response. It was found that response of the building depends heavily on static eccentricity ratio, uncoupled torsional to lateral frequency ratio, beam to column stiffness ratio and lateral vibration period. Moreover, two pairs of mode couples were found to be sufficient to estimate the earthquake response. Later, they also compared these responses of torsionally coupled buildings with those of uncoupled systems. It was determined that torsional coupling results in decrease in base shear; base overturning moment and top-level displacement at center of rigidity but increase in base torque. This finding seems to be consistent with what was observed in response of single-story systems.

An early work performed by Sedarat and Bertero [82] investigating the seismic response of wall-frame systems revealed that this type of structural configuration allows a significant amount of redistribution of forces after the first yield event occurring at the first floor level of the wall. Accompanying change in the deflected shape also resulted in a very different behavior of this type of structures in the inelastic region. Consequent shift in the rigidity center of the structure placed it closer to center of mass; therefore yielding lower torsional response than predicted in the elastic design.

Duan and Chandler [27] inspected the inelastic seismic response of multi-story frame buildings that were designed according to code provisions. Their work is one of highly cited studies concerning the seismic response of torsionally coupled systems. The influence of higher vibration modes on inelastic torsional response and adequacy of provisions on seismic building codes (Eurocode 8, NZS, UBC, Mexico 87 and NBCC) were evaluated. As the paper concentrates on the inelastic response; they postulated that during nonlinear action, redistribution of stiffness and strength results in a very different behavior compared to that of linear elastic system. Due to weakness of the one-story models to simulate this behavior they preferred using multi-story asymmetric structures in their analyses. One-way asymmetric models with stiffness eccentricity were created with three, five and stories; representing the short, medium and long period systems. These structures were modeled as shear-beam systems (rigid decks) and moment-curvature relationships were defined for structural members. In

addition, symmetric versions of the same structures were analyzed to compare the results. In the design, they employed the dynamic eccentricities dictated by the seismic provisions. It was observed in the results that stiff edge elements registered higher ductility demands while deformation demand for flexible edge members were higher. For the seismic provisions that do not allow reduction of strength for stiff edge elements, analysis results were adequate. They concluded that stiff edge inelastic response increases with eccentricity and increasing value of lateral period. In addition, they generally observed higher ductility demands in the stiff edge elements compared to other members. Finally, their result clearly indicated the insufficiency of linear elastic modal analysis to design the asymmetric buildings conservatively especially when they are expected to be excited well into inelastic range. Even though their models employed the inferior shear-beam assumption and missed some important capacity design principles such as strong column – weak beam connection, conclusions reached in the study were clear enough that more inelastic behavior oriented design methodologies were necessary. Out of this necessity, Chandler and Duan [11] suggested a new static procedure to design torsionally unbalanced multistory frame buildings. Considering the inelastic action of the system, they tried to estimate the peak ductility demands of edge elements on both sides of the structure in a conservative manner. The procedure provided acceptable levels of additional lateral design strength to the structural elements. Australian Earthquake Code later implemented in 1993.

Moghadam and Tso [61] stated the simpler modeling utilizing the shear-beam approach does not lead to reliable estimates of the important design parameters for multi-story asymmetric systems. De Stefano et al. [22] worked on four story buildings designed according to Eurocode 8 with high ductility level provisions. They observed that bilinear hysteretic models underestimate the response of asymmetric structures more than they do in symmetric ones. A study about wall-frame buildings conducted by Nelson et al. [64] tried to single out the problems of using static procedures based on single story models to estimate the dynamic torsional effects in multi-story wall-frame or moment resisting frame buildings. They concluded that for proportionally framed systems composed of either only moment resisting frames or shear wall elements, results obtained from torsional coupling analysis of single-story

buildings can be extrapolated to multi-story ones. On the other hand, in the case of non-proportionally frame systems which possess a mixture of moment resisting frames and shear walls; significant inaccuracy in the results obtained from single-story building analogy was observed. A non-uniform ratio of translational force and torque was present at each floor level. Therefore; the torsional response of each story was dependent on the building as a whole. The estimation of dynamic response of for this type of systems by studying single story typical floor models yielded highly inadequate demands, as stated by the authors.

Medhekar and Kennedy [60, 59] proposed a displacement-based seismic design methodology that is based on research presented by Priestley [74]. The concept is illustrated on a single-story concentrically braced frame (CBF) first. In a similar way to what Priestley suggested, yield displacement of CBF is estimated and a maximum inelastic displacement is selected for an acceptable ductility level. Later, an effective structural damping is selected. An effective period at the maximum displacement for the decided ductility level can now be determined. This yields the effective stiffness and shear force for the single degree of freedom system. Procedure is later extended to multi degree of freedom systems by using an equivalent single degree of freedom system. In order to control torsion in the designed systems, authors suggest a torsional restraint system similar to Paulay [67] described. Method is later tested by analyzing two-story and eight-story buildings that were designed according to the procedure. In the case of two-story building, inelastic response of an asymmetric system is also studied. By changing the location of one CBF, stiffness eccentricity is introduced. After analyses, asymmetric model is found to have greater ductility demands compared to its symmetric counterpart, which is an expected outcome.

Further advancing in his investigation on the relationship of strength and stiffness of structural elements, Paulay [69] studied the displacement capacities of ductile multi-story systems. His behavior-based strategy enabled the designer to estimate the limiting displacements of the system. By calculating the yield curvature and yield moment at the onset of yielding of a structural member, he was able to relate these properties to the section depth of the member rather than its flexural rigidity, EI . Consequently he stated that yield curvature is a section and material property and it is essentially independent of strength (Figure 1.2).

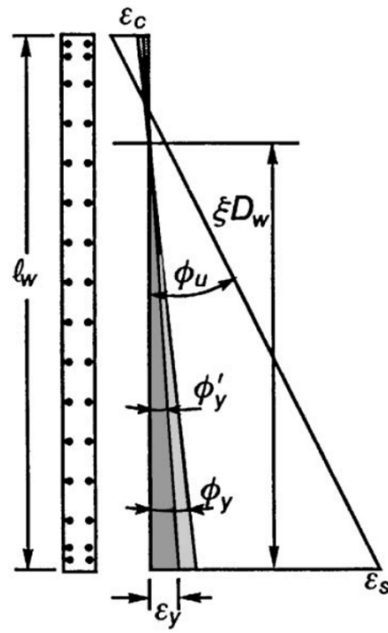


Figure 1.2: Definition of nominal yield curvature and relationship between section depth and yield strain (from Paulay [69]).

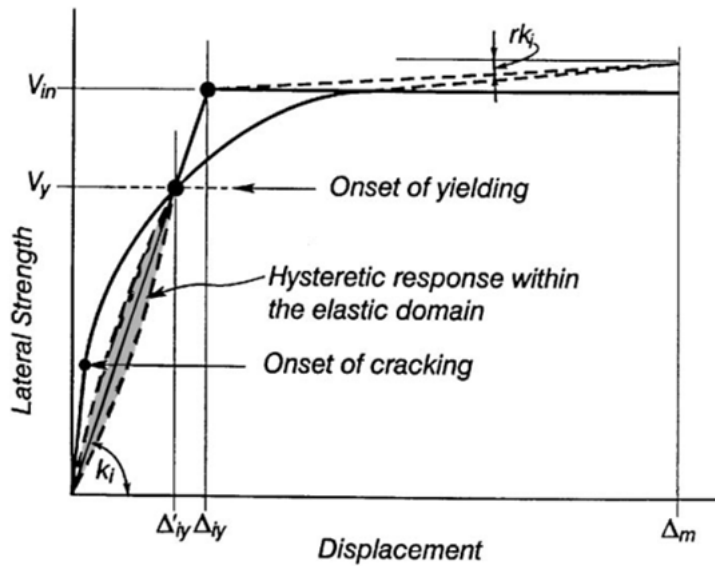


Figure 1.3: Relationship between strength and stiffness of a typical reinforced concrete structural member (from Paulay [69]).

Then, he was able to extrapolate the yield curvature to the nominal yield curvature until which structure essentially attains its initial stiffness. Figure 1.3 provides an illustration to this postulation. Both yield and nominal strengths as well as displacements of a structural member in 1.2 are calculated from its respective moment-curvature relationship. Consequently, he was able to show that stiffness of a component is proportional to its strength as shown in Equation 1.3.

$$k = V_y / \Delta'_y = V_n / \Delta_y \quad (1.3)$$

Using this property, strength values of structural members could be assigned arbitrarily while their yield deformations were dependent on their geometries. This type of strength allocation in design and its performance was evaluated on a ductile reinforced concrete wall-frame system which employed bi-linear inelastic member relationships. Upon analysis, it was observed that due to presence of a shear wall and its dominant displacement pattern, the system behaved predominantly in the first mode. Consequently, higher mode effects hardly affected the ductility demands on frame elements. A major advantage his approach presented was that since the yield displacements can be assessed from geometric properties of structural members, the displacement limits for ductile systems can be estimated even before design commences. Therefore the expected demands on the structure could be calculated beforehand. Moreover, since designer had the freedom of strength allocation, he could use this to minimize the undesired effects of torsional coupling.

As in the case of research performed on one-story models, some studies also considered bi-directional excitation for multi-story asymmetric structures. Marusic and Fajfar [57] conducted analyses on 5-story buildings under bi-directional excitation. They concluded that roof displacements of torsionally flexible structures may be almost twice higher compared to their symmetric counterparts. They also added that this response has been underestimated by unidirectional excitation. Cruz and Cominetti [18] also stated that unidirectional excitation does not predict floor twist adequately. De-la-Colina [19] studied multistory models to assess the design recommendations for torsionally unbalanced multistory buildings. Seven different five-story models having mass or stiffness eccentricities were modeled by employing shear-beam simplifications. Then, they were analyzed under bi-directional excitation. The ductility demands of structural members were compared with demands of corresponding

members in torsionally balanced (symmetric) systems. For a conservative design, the author recommended using static design procedure, which is based on story eccentricities in conjunction with multiplying the design eccentricity with amplification factor, α , defined in the paper.

Marusic and Fajfar [58] inspected the inelastic seismic response of asymmetric structures under bi-axial excitation. They targeted to determine the parameters which have an important effect on inelastic torsional response of buildings with bi-axial eccentricity under bi-directional ground motion excitation. An interesting feature of this study is that asymmetry was intentionally not considered in the design of the test structures to eliminate any torsional code influence from the results. Instead, three five-story steel frame buildings were designed and later two-way mass eccentricity was introduced. Two of them were designed according to Eurocode 3 and Eurocode 8 standards. Another one was detailed such that it was torsionally flexible while the other two were torsionally stiff. The mass eccentricity varied from 5% to 15% in different analyses. These models were analyzed under six ground motion pairs (two horizontal components). During the analyses it was seen that elastic displacements of the models were about 30% higher than the inelastic displacements. According to the authors, this was the consequence of the elasto-plastic hysteresis relationships employed in structural members. Since these models dissipate energy in large amounts, they resulted in lower inelastic displacements compared to elastic response. They reached a conclusion which is consistent with findings of some of the research performed on single-story models: When high intensity ground motion excitations were acted on the systems, initially torsionally flexible and stiff structures' responses became similar due to high inelastic action. Moreover it was observed that center of mass displacements of asymmetric systems and their symmetric counterparts were roughly equal. Finally, they noticed a loss of the favorable torsional effect on the stiff side of the torsionally stiff structures (reduction in displacements) that is estimated by elastic analysis, which could occur when the system is excited well beyond its elastic range. This is again related with the diminishing effect of torsional coupling when all the structural elements behave nonlinear.

Stathopoulos and Anagnostopoulos [84] investigated the inelastic torsional behavior of multi-story buildings extensively. In their study, they questioned the performance

of one-story models that have been predominantly used over the years and wanted to observe the actual multi-story structural behavior. They employed three and five-story Eurocode 8 and UBC97 designed reinforced concrete frame structures. The two-way asymmetry was provided by introducing an offset to mass center from center of rigidity. Rather than using rigid decks in the models, columns and beams were modeled and plastic hinge models were defined for these members to represent the nonlinear behavior. Models were analyzed under ten two-component bi-axial ground excitations. The ductility ratios and damage indices, which are based on hysteretic energy loops, were calculated for members. An important observation the authors made was that the flexible side frames experienced higher ductility demands than the stiff side frames, which is in contrast with what has been previously observed on one-story typical shear beam model studies. In addition, for largely eccentric buildings damage indices were higher in the flexible frames; whereas they were lower in the stiff frames compared to the corresponding symmetric buildings. It was also noted that the behavior of their models reflects the uneven distribution of ductility demands in asymmetric buildings. This is, in fact, a significant shortcoming of the code provisions, which aims for similar level of inelastic action along the structure. Finally, it was concluded that Eurocode 8 provisions do not meet the objective of similar levels of inelastic action when they are applied to asymmetric frame buildings.

De Stefano et al. [24] studied the effects of overstrength on seismic behavior of multi-story asymmetric systems. The main motivation of their study was to investigate the effects of overstrength present in realistic multi-story models during seismic response. In their study the authors criticize the over-simplified one-story systems that neglect the inherent overstrength characteristics of structures. In order to quantify the system overstrength, a collapse multiplier, which yields the amount of overstrength at each story of a structure, is formulated through beam and column strengths. Then, a six-story regularly asymmetric system is presented. The structural model includes rigid decks connected by steel columns and mass asymmetry. To be able to assess the performance of the system, a torsionally balanced (symmetric) version is also designed as the reference structure. Moreover, a reference asymmetric single-story system is also described that has equivalent dynamic properties to the reference system. These case studies are analyzed under a set of thirty artificial accelerograms

matching the Eurocode 8 response spectrum. In the end, authors conclude that the ductility demands of the multi-story asymmetric system may become larger at unexpected locations due to overstrength. These locations are given as upper floors where overstrength is largest. In addition, flexible edge ductility demands were observed to be larger than the reference system while stiff edge shows the opposite. This result is reported by the authors to contradict the findings of the single-story system. Authors finally noted that the code provisions that are developed using one-story models are in need of an improvement in order to account for overstrength effects inherent in multi-story systems. In a slightly related paper, Ghersi et. al. [34] worked on a comparison of static and modal analysis of multi-story asymmetric systems. They used the same multi-story building that De Stefano et. al. [24] employed in a parametric study in which system parameters such as torsional stiffness or amount of static eccentricity varied. They also measured the overstrength of the parametric systems using the collapse multiplier defined by the aforementioned authors. Static and modal analyses were performed on these parametric systems. In addition to these standard procedures, some proposed design methods for asymmetric systems in the literature were also tested. Many conclusions were reached in the study. For instance; regardless of the analysis type, authors stated a need for adjustment of design eccentricities in order to avoid large ductility demands in asymmetric systems compared to those observed in torsionally balanced reference systems. It was also noted that the when proper design eccentricities are employed, modal analysis is a valid design tool for asymmetric structures.

Kosmopoulos and Fardis [53] inspected the inelastic seismic deformations in asymmetric multi-story reinforced concrete buildings. They modeled four real buildings all of which have strong plan irregularity and analyzed those under seven bi-directional Eurocode 8 spectra compatible ground motions. Rather than using conceptual models, actual buildings with plan and/or vertical irregularities were utilized to better understand the response of existing structures which may not be built according to seismic provisions. Inelastic properties were included in the analytical models of these buildings by defining lumped plasticity regions for structural elements. Chord rotations obtained from nonlinear response history analysis were compared with those of linear elastic analyses. They determined that when higher mode effects are present

in buildings, the story average ratio of inelastic to elastic chord rotations is not uniform. As a result of the analyses performed, it was observed that for buildings with low higher mode effects elastic static analysis generally overestimates the inelastic chord rotations even when torsional effects are present. In another study, Georgousis [33] worked on a derivation of a simple approach to estimate the conditions for multistory eccentric buildings under which the effects of torsional coupling could be neglected in the structural design of these buildings. The study was performed by employing monosymmetric and vertically regular rigid frame-shear wall systems. A parametric study was performed to validate the postulation. An approach where shear wall system and frame system are handled separately in the design stage was elaborated. By employing such an approach, these two force-resisting systems were in fact designed to be practically uncoupled even though they are part of the same structure. This is achieved by having the same eccentricity values for both of the systems with respect to center of mass of the structure. To test the approach, a ten-story structure composed of shear-walls and rigid frames were used. To conclude the study, it was claimed by the author that structural systems designed according to this approach experience a practically negligible eccentricity.

Torsional response of buildings with peripheral steel-braced frame lateral systems was inspected by Erduran and Ryan [29]. Their aim was to evaluate the torsional amplification in asymmetric peripheral steel-braced frames analyzed under nonlinear time history analysis, study the effects of modeling assumptions and evaluate the performance of elastic and nonlinear static analysis procedures for this type of structural systems. They employed a 3-story mass eccentric building based on the SAC building that has been extensively used by researchers over the years. A very detailed model was created for the study where a beam-column model was preferred over rigid slab assumption. Another modeling preference that should be noted is that authors employed fiber sections for columns in order to better estimate the actual behavior. This is relatively rarely observed modeling decision in the analysis of complex torsionally coupled systems. Upon completing their analyses authors reached many conclusions. However, they noted that their conclusions are limited to the very specific type of building that they had inspected. They observed larger torsional response during inelastic action compared to that observed in elastic systems, which is in contrast to

many studies had found over the years. A large dynamic shift in center of rigidity (CR) of the system due to yielding of flexible edge braces was postulated as the reason for this behavior by the authors. In addition, response spectrum analysis and pushover analysis were also deemed inadequate in terms of capturing the amplification of story drifts due to torsional behavior caused by strong ground motions for the specific type of steel frame building that was analyzed.

Şahin [81] presented an optimization algorithm for geometrical design of asymmetric tall buildings which intends to minimize torsional response. In a study that concentrates on the orientation of structural members, the target of minimum torsional effect was tried to be targeted. By employing the developed numerical algorithm in the study, orientation of the rectangular columns is positioned in such a way that distance between centers of mass and rigidity is minimized. The method is tested on a 10-story asymmetric reinforced concrete building and reduction of eccentric behavior as well as reduced seismic demands is observed. Krykos and Anagnostopoulos [55] studied Earthquake resistant design of eccentric steel buildings. A design modification that improves the inelastic response of torsionally flexible eccentric steel buildings was proposed by authors. In the suggested procedure, two factors for flexible and stiff edges were computed using displacements obtained from equivalent static method under both directions of analysis. These factor were applied to system such a way that flexible edge of the structural systems are made stronger while stiff edge sides are designed to be weaker compared to reference structures. This design modification was tested on one, three and five-story building sets. By inspecting the results, authors stated that approximate stiffness center of systems becomes substantially closer to mass centers in the modified structures. This results in a more balanced ductility demand distribution as a result of diminished effects of torsional coupling.

As can be deduced from the research discussed, studies performed on multi-story systems converge on the fact that unequal seismic demand and estimation of this demand is a problem in torsionally coupled systems whether they are designed according to code provisions, or not. However, determination of critical members varies according to target response parameter. Some studies concentrates on deformation demands and singles out the flexible edge elements as critical since they undergo more deformation; while others consider ductility demand or amount energy dissipation as a critical

indicator of seismic performance and conclude on stiff edge elements as critical since more inelastic demands are observed in these elements. There are some design recommendations and suggestions to improve seismic codes to better account for torsional coupling in the structures. However, there still lacks a universally reached conclusion that results in an accurate determination inelastic action on all structural members on torsionally coupled systems during seismic response. Moreover, it should be noted that amount of studies on performance-based assessment and design of torsionally coupled systems is very few. In the future this field could be expanding as research on earthquake-engineering also shifts towards performance-based engineering applications.

1.2.3 Discussion on Passive Control Systems for Torsionally Coupled Structures

In order to minimize the undesired effects of torsional-coupling in buildings, there are many applications that utilize passive control systems such as viscous or friction dampers. In conjunction with the increasing number of applications, research in the field has also been highly active, especially for the last decade. It has been noted by many researches that by providing a well-calculated distribution of passive control devices, it is possible to lessen the irregular response of asymmetric systems. In this section, a brief review of some of the well-known studies performed on single or multi-story systems is presented in order to better explain the mechanism and behavioral improvements of these types of systems.

An important design challenge associated with energy dissipation devices is their optimal placement in the buildings to provide the most effectiveness. This condition requires solution of a structural optimization problem and has been investigated by many researchers over the years. Considering this issue, Wu et al. [88] discussed the placement optimal of energy dissipation devices for three-dimensional structures. An N-story shear-type building is utilized in the study and torsional coupling effects were further assessed in a six-story variant. Upon examining the coupled response they developed an iterative procedure that yields an optimal placement for the dampers. The optimality of the procedure was shown by providing numerical examples. It was

noted that the placement of a limited number of energy dissipation devices might have a significant effect on the reduction of response.

Introduction of supplemental viscous damping and its effects on seismic response of asymmetric-plan systems was examined by Goel [37]. The primary objective of the study was to identify the system parameters that control the seismic response of asymmetric-plan systems with fluid viscous dampers. In addition to this, the effects of these parameters on edge deformations of the structures were also investigated. A one-story rigid deck model constituting two structural elements and fluid viscous damper (FVD) was implemented. The structure was one-way symmetric with stiffness eccentricity. In addition to static eccentricity, center of supplemental damping (CSD) which is the centroid of damper forces under uniform translational velocity and related damping eccentricity (e_{sd}) was also defined. To compare the results, a symmetric model having no FVDs was also employed. These two systems were analyzed under a component of 1994 Northridge earthquake. A wide range of structure periods from 0.05 to 3 seconds were considered in the analyses. Some of the inspected parameters were torsional rigidity of the structure (torsionally flexible vs. torsionally stiff systems), static eccentricity, aspect ratio of the deck, eccentricity of CSD, and the spread of the FVDs along the floor slab. It was observed that with the employment of FVDs, edge deformations significantly decreased. However, this was seen to be dependent on damping eccentricity. Effects were more pronounced for torsionally flexible systems. Being more critical, reduction of flexible edge element deformations was suggested by the author by appropriate placement of FVDs. The spread of the FVDs along the floor plan was represented by their radius of gyration. The results indicated that when radius of gyration of FVDs increased, deformations also increased. This effect was again more pronounced for flexible edge elements.

The previous study was conducted by utilizing linear elastic models. Later, Goel [38] discussed the inelastic seismic response of asymmetric systems where supplemental viscous damping was utilized. According to the author, seismic code provisions provide additional strength to certain load resisting elements to account for the torsional coupling effects. However, there is still a need to control the energy dissipation and excessive deformation demands on the structural members. The objective was to control these parameters by employing FVD devices. One-story model with a stiff-

ness asymmetry and FVDs were prepared. A model with no FVD devices and its symmetric counterpart were also created to compare the response. Structures had inelastic member properties and they were analyzed under ground motion excitation. Edge deformation and ductility demands, hysteretic and damping energy dissipations were inspected. Results showed that introduction of FVDs reduced the deformations significantly during inelastic cycles. Also, supplemental damping significantly reduced the deformation and energy dissipation demand on flexible-edge element of the one-story structure. The global reduction in seismic demands was observed to be dependent on plan-wise distribution of supplemental damping in terms of FVD devices. These results are consistent with those obtained from elastic analyses, which shows that supplemental damping is also effective for inelastic range of behavior. When a proper plan-wise distribution was applied, usage of FVDs was found to be very effective to control the excess deformation and ductility demands for flexible-edge element. The analyses were performed for a range of reduction factor (R) values and the variation in this observation was found to be minimal for all R values except for short period systems. The dissipation of damping energy was also determined to be not very sensitive to distribution of FVDs. On the other hand, hysteretic energy dissipation was shown to be dependent. With optimal placement of FVDs, hysteretic energy reduction in flexible edge elements is possible, hence reducing the damage sustained by these members. In conclusion, response parameters decreased with optimal placement of supplemental viscous damping. Accordingly, this optimal placement was recommended to limit the demands of most critical elements located on the flexible-edge side.

Concentrating on the concept of torsional balance, which was also investigated by a number of researchers, a study conducted by De la Llera et al. [20] inspected the implementation of frictional dampers on plan-asymmetric structures. As stated by the authors, torsional balance is defined as a property of an asymmetric structure that leads to similar deformation demands in structural members that are equidistant from geometric center. Moreover, it is noted that frictional dampers are able to influence the center of balance of the structure; therefore, the lateral-torsional coupling of the system can be controlled by a careful placement of these devices. The research was motivated by the fact that frictional dampers dissociate the stiffness and strength of

a system. In other words, the inelastic properties of a building may be modified by introduction of these devices. These modifications on the strength and stiffness properties of a torsionally coupled structure could be used to transform the seismic response of the system into that of a symmetric one. At this point, an empirical center of balance (ECB) was defined as the place where the frictional damper is placed to exploit their effects on system properties. On this center of balance, translations and rotations are statistically uncorrelated. On an asymmetric system, with proper placing of frictional dampers, ECB can be located such that the structure behaves as torsionally uncoupled. The postulation was inspected on a one story asymmetric structure with varying parameters such as period, eccentricity ratio and inclusion of frictional dampers. It was concluded in the study that frictional dampers can control the torsional response. In addition, deformation demands were also observed to decrease due to increasing damping in the system when frictional dampers were included. In a closely related study, Almazan and De la Llera [1] further investigated the torsional balance in the asymmetric structures with energy dissipation devices. Very similar to previously discussed study, linear viscous dampers were utilized to provide a torsional balance to asymmetric systems. These were located in the plan such that they provided the minimum demand at the geometric center. Thus; by minimizing the geometric center response they also tried to minimize the edge deformations which are amplified due to rotational response of floor slabs. It was shown mathematically that this placement of dampers created the case of zero correlation (uncoupled response) between the translations and rotation at the geometric center. As a side advantage, usage of viscous dampers also increased the damping of the whole system; further decreasing the deformations. Along with a single-story model to test their approach, response of an exemplary six-story building was also inspected and it was deduced that torsional balance concept may also be applied to multi-story buildings. From the results of one-story structure, it was shown that optimal damper location on the plan depends on the amount of static eccentricity and the frequency ratio of the bare structure. Total amount of supplemental damping and the frequency content of ground motion excitation also seemed to affect the location.

Recently, Lin et al. [56] studied the optimal locations of viscous dampers in two-way asymmetrical structures by employing an energy-based approach. They tried

to maximize the average dissipation rate of overall strain energy of the building under bi-directional unit impulse by modifying the damper placement. It was pointed out by researchers that many studies that investigate the optimal damper placement on buildings employ optimization algorithms to determine the damper locations, Sequential search algorithm (SSSA), is one of them. It utilized the elastic response history analysis of the structure; therefore the placement of dampers was ground motion dependent. To test the effectiveness of damper placement, an index that displays the dissipation rate of elastic strain energy (IE) was defined. The building analyzed was a SAC building variation. Two nine-story examples (torsionally flexible and torsionally stiff) were prepared and two-way mass eccentricity was introduced to these two models. The optimal damper locations were determined according to SSSA and another approach which is called as generalized optimal location of dampers (GOLD). GOLD was a modified variant of SSSA which employs IE to optimize the location of dampers. Upon comparing responses, it was found that strain energy demands recorded in the models where GOLD procedure was implemented was more uniformly distributed. In these models, less deformation demands compared to SSSA distribution was also recorded. In addition, the computational effort and time requirements for GOLD was less demanding compared to SSSA.

In the studies that are briefly summarized above, the positive effect of implementation of energy dissipation devices can be observed. With a proper placement, they can be implemented to lessen the effects of torsional-coupling. It is even possible to neutralize the coupled seismic response. This phenomenon is well displayed in one-story theoretical models. However, for multi-story systems, determination of damper locations is more complicated. Optimization procedures are utilized to estimate the locations and sometimes this can be a tedious process. If optimally placed in multi-story structures, it is shown that energy dissipation devices may help significantly to control the coupled response. There is very active research continuing in optimization procedures to develop less demanding procedures. In the following years, with implementation of very efficient placement algorithms that does not require a more complex design process: usage of energy dissipation devices can be a very suitable approach in torsionally coupled systems in order to reduce the non-uniform demand distribution.

1.2.4 Investigation of Nonlinear Static Analysis Methods Developed for Asymmetric Systems

An increasing amount of studies investigated the application of nonlinear static analysis procedures developed for torsionally coupled structures. Since the early studies that investigate the seismic response of torsionally coupled systems, it was observed that pushover analysis which employs a single force distribution for lateral load analysis was insufficient due to complex nature of modal response observed in asymmetric systems. To overcome this phenomenon, research published in the recent years mainly concentrated in developing novel static analysis procedures that yield good estimates in torsionally coupled systems. In this section, a review of some major nonlinear static analysis procedures and their superiority to basic static analysis is discussed.

In earlier works that investigate the application of single mode pushover analysis to asymmetric systems, Moghadam and Tso [62], Kilar and Fajfar [52], Fajfar et al. [32] all stated that static analysis that includes the first mode could not predict the response of torsionally flexible structures due to higher mode effects. Moghadam and Tso [62] used 3D response spectrum analysis to estimate the roof displacement and distribution of lateral forces for each resisting elements; then they performed planar pushover analyses for each element using the displacements and force distributions that have been obtained previously. Fajfar et al. [32] extended the N2 method to asymmetric multi story buildings by applying a height wise distribution of lateral forces to center of mass of each floors. The main drawback was that the procedure as in the case of other static analyses methods did not allow for inclusion of dynamic effects of lateral torsional coupling. Fajfar et al. [31] later made improvements to N2 method by combining pushover analysis results in a 3D model with the results from linear dynamic analysis. Kreslin and Fajfar [54] combined their previous work on asymmetric buildings in both plan and elevation and further developed the N2 Method to better suit this type of buildings.

Chopra and Goel [15] extended well-known MPA to 3D structures. Previously MPA was developed for two-dimensional planar structures and proved itself as a reliable nonlinear static analysis tool [14, Chopra and Goel]. In order to account for modal

response in three-dimensional space, both modal forces torques from each mode were applied separately and then the individual responses of each mode were combined using statistical combination methods (CQC). Due to inadequacy of statistical combination methods in structures where high modal coupling is present, results deteriorated for this type of systems. Another drawback of the statistical combination was over-estimated member forces which exceeded member capacities. Goel and Chopra [41] modified the MPA so that it can estimate the member forces correctly. Bosco et al. [9] compared the nonlinear static analyses methods for the assessment of asymmetric buildings. They compared the original N2 method, which is adopted by Eurocode 8, extended N2 method and an improved method which is named as corrective eccentricity method by the authors. The latter one essentially envelopes two nonlinear static analyses results in two directions to obtain the structural response. They concluded that improved nonlinear static methods always enhance the prediction of the displacement demand of asymmetric structures.

Recently, Kaatsız and Sucuoğlu [47] implemented the Generalized Pushover Analysis (GPA) to torsionally coupled systems. The procedure was tested on an 8-story unsymmetrical-plan structure with mass asymmetry. Compared with the benchmark nonlinear response history results, a good match was observed compared to conventional single mode pushover analysis which fails to estimate the behavior of torsionally coupled structures adequately. Moreover, it was stated that GPA were able to estimate the forces on structural members accurately since no modal combination is employed while the results are compiled.

In conclusion, many of the studies discussed are able to identify the problem of non-uniform demand distribution both in plan and elevation for torsionally coupled structures, although the critical structural members that were pointed in these studies vary considerably. As an interesting observation, majority of the studies concentrate on behavior assessment of asymmetric systems that are detailed by employing capacity design. It can be stated that investigation of structural behavior according to performance-based engineering principles has not yet been an important research topic in the case torsionally coupled systems. It is also observed that the implementation of multi-story models has been the trend in the studies since the last decade. This has been beneficial to better pinpoint the shortcomings of code provisions because

the deformation patterns could be inspected more accurately. Moreover, emerging improvements in seismic control devices such as dampers can significantly help to reduce and balance the seismic demands in torsionally coupled systems. Finally, nonlinear static analysis tools developed for torsionally coupled systems are emerging in an ever-increasing rate, helping the researchers to understand the behavior of irregular systems better.

1.2.5 Investigation of Current Seismic Provisions on the Torsional Response

This section of the chapter concentrates on regulations defined in seismic codes about plan irregularities (and resulting asymmetric behavior) as well as accidental eccentricity and torsional behavior of structures. After reviewing the past studies that have been performed to better understand the asymmetric structural behavior over the decades, an investigation considering regulations governing the contemporary practices regarding torsionally coupled behavior is performed in order to provide a very comprehensive background to the problem. Along this section, the term “irregularity” is used rather than “torsional coupling” since structures are classified according to plan and vertical irregularities in seismic standards and provisions considering torsional behavior due to the plan irregularities are detailed following this classification.

In the following discussions, three standards are investigated in detail; ASCE/SEI 7-10 (or simply ASCE 7-10) [4], Eurocode 8 [30] and Turkish Earthquake Code [73]. ASCE 7-10 is a widely applied standard in United States and has an extensive coverage of seismic design requirements for building structures. Eurocode 8, on the other hand, is the standardized technical rule set developed for the structural design of construction works in the European Union. These two codes govern a wide portion of engineering practice in the world; therefore their recommendations about design of torsionally-coupled systems are of significance. Additionally, Turkish Earthquake Code is the mandatory rulebook for construction of buildings in seismic zones in Turkey and it also provides some regulations regarding asymmetric behavior in structures. In conjunction with the purpose of the thesis study, only regulations about plan irregularities and asymmetry in these standards are inspected and topics about elevation irregularities are omitted.

Seismic provisions try to emphasize structural regularity in both plan and elevation. By doing so, a more uniform response under earthquake forces is ensured. In the case of non-uniform behavior along a story, plan regularity is especially important. If a plan-regular structural system can be realized by the designer, accompanying asymmetric behavior and resultant torsional coupling is minimized. There are several principles presented in the mentioned standards and these are discussed in following parts.

1.2.5.1 Provisions in Eurocode 8

In the following parts, definition of structural regularity in Eurocode 8 is described first. Then design requirements for inclusion of accidental torsion effects is explained. Finally, implications of structural irregularities on design and analysis of structural buildings according to Eurocode 8 provisions are discussed in detail.

Eurocode 8 encourages the designer to provide uniformity on the structural plan by even distribution of structural members or subdivision of the entire building into independent units, if possible. Moreover, a closely related mass and stiffness distribution along the plan is promoted in order to prevent large eccentricities between mass and stiffness. In addition; to emphasize the importance of structural redundancy, it is stated that building structures should possess adequate torsional resistance to limit the torsional motions. The aim of promoting plan regularity is to minimize torsionally coupled behavior.

The structural regularity of buildings is inspected in detail and structures are categorized into being regular or non-regular according to a number of factors. Criteria are specified for regularity in plan and elevation. As mentioned previously, conditions for plan regularity are discussed. There are a number of conditions to be checked in order to classify a building as regular in plan. First, it is required that approximately symmetrical distribution of mass and stiffness should be present in the plan. Next, a compact plan configuration is favored. In other words; each floor are required to be delimited by a polygonal convex line. In a convex polygon, all interior angles are less than or equal to 180 degrees. Therefore, it can be stated excessive setbacks like re-entrant corners or edge recesses are recommended to be avoided by the code. If

these kinds of setbacks still exist, they should not affect the in-plan stiffness and for each setback, the ratio of between the outline of the floor and a convex polygonal line enveloping the floor should not exceed the 5% of floor area.

To establish a global uniform behavior, in-plan stiffness of the floors should be sufficiently large in comparison with the lateral stiffness of the vertical structural elements. This condition is particularly important for diaphragm action of plan shapes like letters L, C, H, I or X. It is to be ensured that deformation of the floor should have a small effect on the distribution of forces among the vertical structural elements.

Another consideration is the plan aspect ratio of the building. In Eurocode 8, this is denoted as the slenderness of the building in plan and given as $\lambda = L_{max}/L_{min}$, where L_{max} and L_{min} are the larger and smaller plan dimensions of the building. The maximum limit for the slenderness λ is specified as 4.

Up to this part of the review regarding the Eurocode 8, main focus has been the definitions of plan irregularities which may result in unequal distributions of mass and stiffness along a story. Another important reason for irregularity that is extensively detailed in Eurocode 8 is the torsional flexibility of the building structure. A plan regular structure should satisfy the conditions given in Equation 1.4 for each direction of analysis (the formulation below is for Y-direction of analysis):

$$e_{ox} \leq r_x \quad (1.4a)$$

$$r_x \leq l_s \quad (1.4b)$$

Where e_{ox} is the structural eccentricity (distance between center of stiffness and center of mass), r_x is the torsional radius (square root of the ratio of the torsional stiffness to the lateral stiffness in y direction) and l_s is the radius of gyration of floor mass in plan. If the structure fails to satisfy the criteria stated, then it is considered as torsionally flexible.

The special requirements and design consequences for building systems that are classified as plan-irregular according to definitions given above are to be discussed shortly.

Eurocode 8 imposes a 5% accidental eccentricity in order to account for uncertainties

in the location of mass and in the spatial variation of seismic motion. It is formulated as given in Equation 1.5:

$$e_{ai} \leq \pm 0.05 L_i \quad (1.5)$$

Where e_{ai} is the accidental eccentricity and L_i is the floor dimension that is perpendicular to the direction of the seismic action. Although the accidental eccentricity is defined as stated, the method to include its effect to the design forces depends on the modeling decisions that are based on plan and elevation regularities.

There are also a number of remarks in Eurocode 8 that deal with plan irregularity resulting from distribution of masonry infills. Strongly irregular infill arrangements are advised to be avoided. Moreover; if there is severe irregularity in the system due to infill placement, spatial (3D) analysis models that also incorporates the mathematical modeling of infill walls are required. Also, it is noted that if the irregularity is not severe, the effects of infill walls can be taken into account by multiplying the accidental eccentricity, e_{ai} , by a factor of 2 in the analyses.

Structural systems that are classified as plan-irregular according to criteria discussed previously require a specialized set of rules for both modeling (including analysis) and design. These requirements are summarized below. Normally, Eurocode 8 allows for both planar (2D) and spatial (3D) modeling of structural systems for analysis. However; when plan irregularities exist in a building structure, only a spatial analysis model is allowed. For a small subset of plan-irregular buildings for which the conditions are specified in the Eurocode 8, linear elastic analysis of a structural model composed of two planar frames is also allowed.

Both lateral force and modal analysis are permitted using spatial models of the plan irregular systems; however, appropriate application of accidental eccentricity is to be ensured according to each analysis method. As an alternative to linear elastic method, nonlinear analysis procedures such as pushover analysis or nonlinear time-history analysis of the spatial model are also permitted.

Alternative ways to account for the accidental eccentricity for these analysis methods are also described by Eurocode 8. If lateral force method is used for analysis of a building structure and 5% accidental eccentricity described previously is not considered in the analysis, then Eurocode 8 requires a scaling for action effects in the

individual load resisting elements by multiplying these with a factor δ given as in Equation 1.6:

$$\delta = 1 + 0.6 \frac{x}{L_e} \quad (1.6)$$

Where x is the distance of the element to the center of mass of the building in plan and L_e is the distance between the two outermost lateral load resisting elements perpendicular to the direction of analysis. In the case of modal response spectrum analysis, the effects of accidental torsion can also be represented by the result envelope given by application of torque M_{ai} at each story by performing the calculation shown in Equation 1.7:

$$M_{ai} = e_{ai} * F_i \quad (1.7)$$

F_i in Equation 1.7 is story lateral force and e_{ai} is the accidental eccentricity that has been discussed previously.

Nonlinear static (pushover) analysis, which is presented as an alternative method to the linear elastic analysis procedures, requires constructing a spatial model for plan-irregular systems. Moreover, it is stated 5% accidental eccentricity should be taken into account for all types of systems in the application of lateral loads. There is an important remark to properly estimate the torsional effects while using nonlinear static analysis methods in Eurocode 8. It is stated that stiff side deformations of a torsionally flexible structure may be significantly underestimated due to lateral load distribution (such as uniform loading) used in the analysis. Therefore it is required that displacements at the stiff side of a torsionally flexible system be increased compared to those in the corresponding torsionally balanced structure.

Implications of plan irregularity and torsion in design of building structures according to Eurocode 8 is best discussed by investigating the behavior factor concept. For all kinds of structural systems, behavior factor, q , which accounts for energy dissipation capacity of the system, is the primary tool that is employed by Eurocode 8 in determination of behavior of building structures. It is, in fact, the reduction factor (R) that is employed in earthquake engineering that is used to reduce the spectral forces acting on structures to account for the deformation capability of the system. In other words, q factor in Eurocode 8 is a measure of ductility of the structure.

Reinforced concrete structures are designed according to two ductility classes: Medium

ductility (DCM) and high ductility (DCH). By determining a basic value of the behavior factor, q_0 , which is used to calculate q ; concrete structures are classified into the two ductility categories given. Once classified, structures are designed dimensioned and detailed in accordance with specific earthquake resistant provisions for the ductility class assigned for the basic value of the behavior factor taken from Eurocode 8 is given in Table 1.1

Table 1.1: Basic value of the behavior factor, q_0 , for systems regular in elevation (From Eurocode 8)

STRUCTURAL TYPE	DCM	DCH
Frame system, dual system, coupled wall system	$3.0 \alpha_u/\alpha_1$	$4.5 \alpha_u/\alpha_1$
Uncoupled wall system	3.0	$4.0 \alpha_u/\alpha_1$
Torsionally flexible system	2.0	3.0
Inverted pendulum system	1.5	2.0

In Table 1.1, α_u/α_1 is defined as the overstrength ratio. As expressed in the code; α_1 is the value that horizontal seismic design action is multiplied in order to first reach the flexural resistance in any member in the structure. On the other hand, α_u is the value that horizontal seismic design action is multiplied in order to develop the plastic hinge mechanism in the structure that results in structural instability. There are approximate values given for the ratio in Eurocode 8 but for plan-irregular systems, it is recommended to calculate this ratio in an explicit way such as employing a nonlinear static analysis and determining the α coefficients. This may especially be beneficial in asymmetric systems since it is almost certain that torsional coupling resulting from asymmetry will interfere with α coefficients compared to a symmetric, torsionally uncoupled system. Therefore, it can be stated that Eurocode 8 implicitly takes the effects of torsional-coupling into account when determining the overall ductility capacity of the reinforced concrete structure.

It should be noted that in the case of reinforced concrete structures, q_0 parameter is strongly related with the torsional flexibility of the system. Torsionally flexible reinforced concrete system is defined by Eurocode 8 as a structure that violates the equation about torsional radius and radius of gyration of the system that was previously given (Equation 1.4b). As can be seen from Table 1.1, if a concrete structure is deemed torsionally flexible by checking the criterion, it is not permitted to be de-

signed with a high level of ductility compared to torsionally stiff systems. This is a very explicit way of discouraging the design of torsionally coupled systems as they are penalized in terms of expected ductility.

Contrary to what is specified for concrete structures, there is no explicit reference to avoid torsionally flexible systems while designing steel and steel-concrete composite systems by limiting the expected ductility. For the latter two structural systems, a low ductility level is also introduced (DCL) along with DCM and DCH. Upper limits for behavior factor (q) are given in separate tables according to ductility level and structural system solution for steel and steel-composite systems. It should be noted that the upper limits specified are still related with the overstrength ratio α_u/α_1 therefore it implicitly considers torsionally coupled behavior and resulting non-uniform demand distribution.

There are no more specific design recommendations and regulations defined for plan irregular and/or torsionally coupled systems apart from specified above in Eurocode 8. Overall, code provisions advise against selecting very irregular building layouts that can introduce asymmetry and excessive torsional flexibility into the structure. If any of the specified irregularities still exist in the structure, a number of specifications are given to take into account in modeling and analysis of the structure. By controlling the maximum allowed ductility of the system with parameters that is directly related with the expected performance of the structure under lateral loading; Eurocode 8 tries provide resistance against non-uniform demand distribution resulting from asymmetry related torsional-coupling rather than estimating this demand. There is not any strict set of rules in terms of a maximum design eccentricity or an acceptable level of plan irregularity. Instead, designer is advised to come up with solutions that provides in uniform, symmetric and redundant solutions.

1.2.5.2 Torsional Provisions in ASCE 7-10

ASCE 7-10 is one of the most widely used standards in the United States that is employed for determination of design loads for buildings. It has an extensive coverage about many types of loading such as wind, snow, live or seismic loads. Seismic design requirements are discussed in a number of chapters extensively.

Prior to design specifications for building structures, seismic risk criteria are discussed in a separate chapter in ASCE 7-10. Information regarding design spectrum as well as parameters required for the construction of the design spectrum such as short, 1-second and long period values; corresponding PGA values for these periods are defined in this mentioned part of the standard. Maps on which these PGA values are plotted for United States territories are also provided. Another topic discussed in this chapter is the seismic risk and classification of structures according to seismic risk with regard to their importance. Seismic design categories for building structures are defined by combining the spectral acceleration values where the building is located and importance classification of the structure which is explained in a separate chapter of the standard. Therefore, it can be stated that the seismicity on the site of the structure and its risk classification are the two factors in the assignment of the seismic design categories in ASCE 7-10. To illustrate, a structure in a region with low seismicity and a low risk factor can be assigned to category B. However, an important structure which is classified as an essential building located in a high seismic zone can be in the seismic design category F. Specifications about the selection of the structural system in relation with each seismic design category are given next in the design specifications chapter of ASCE 7-10 along with provisions about structural irregularities.

In ASCE 7-10 design specifications, structural systems are not separated according to load carrying systems such as reinforced concrete, steel or composite structures of which regulations are detailed in distinct chapters. Rather, all structural systems are handled in a single chapter where they are categorized according to type of the load carrying systems (such as concrete-wall system, steel braced frame, etc.) In contrast to Eurocode 8, majority of the specifications is given in a tabulated manner including the irregularity criteria. Limitations about selected seismic force resisting system of building structure are given in these tables. Limiting behavior factors such as Response Modification Factor (R) or Overstrength Factor (Ω_0) are also specified. At the later stages of the design, ASCE 7-10 requires checking of irregularities which yields modeling and analysis decisions. Following this step, design loads are determined according to specifications given. In the following subsections, discussions about irregular and eccentric systems in ASCE 7-10 are inspected in conjunction with the

scope of this study.

As mentioned previously, irregularity types for both plan and elevation are given in design tables. Horizontal structural irregularities defined as in ASCE 7-10 is given in Table 1.2. Also presents are the reference sections of the horizontal irregularities and corresponding seismic design categories so that designer can directly investigate the implications of the type of the irregularity that is considered. Adopting a different approach compared to Eurocode 8, ASCE 7-10 measures the amount torsionally coupled behavior in the structure by simple comparing the maxima of the interstory drifts with the average values obtained under lateral load analysis. Other criteria regarding irregularities such as reentrant corners or diaphragm discontinuities are handled similarly, yet in a simpler form.

Table 1.2: Definition of horizontal structural irregularities, taken from ASCE 7-10

Type	Description	Reference Section	Seismic Design Category Application
1a.	Torsional Irregularity: Torsional irregularity is defined to exist where the maximum story drift, computed including accidental torsion with $A_s = 1.0$, at one end of the structure transverse to an axis is more than 1.2 times the average of the story drifts at the two ends of the structure. Torsional irregularity requirements in the reference sections apply only to structures in which the diaphragms are rigid or semirigid.	12.3.3.4 12.7.3 12.8.4.3 12.12.1 Table 12.6-1 16.2.2	D, E, and F B, C, D, E, and F C, D, E, and F C, D, E, and F D, E, and F B, C, D, E, and F
1b.	Extreme Torsional Irregularity: Extreme torsional irregularity is defined to exist where the maximum story drift, computed including accidental torsion with $A_s = 1.0$, at one end of the structure transverse to an axis is more than 1.4 times the average of the story drifts at the two ends of the structure. Extreme torsional irregularity requirements in the reference sections apply only to structures in which the diaphragms are rigid or semirigid.	12.3.3.1 12.3.3.4 12.3.4.2 12.7.3 12.8.4.3 12.12.1 Table 12.6-1 16.2.2	E and F D D B, C, and D C and D C and D D B, C, and D
2.	Reentrant Corner Irregularity: Reentrant corner irregularity is defined to exist where both plan projections of the structure beyond a reentrant corner are greater than 15% of the plan dimension of the structure in the given direction.	12.3.3.4 Table 12.6-1	D, E, and F D, E, and F
3.	Diaphragm Discontinuity Irregularity: Diaphragm discontinuity irregularity is defined to exist where there is a diaphragm with an abrupt discontinuity or variation in stiffness, including one having a cutout or open area greater than 50% of the gross enclosed diaphragm area, or a change in effective diaphragm stiffness of more than 50% from one story to the next.	12.3.3.4 Table 12.6-1	D, E, and F D, E, and F
4.	Out-of-Plane Offset Irregularity: Out-of-plane offset irregularity is defined to exist where there is a discontinuity in a lateral force-resistance path, such as an out-of-plane offset of at least one of the vertical elements.	12.3.3.3 12.3.3.4 12.7.3 Table 12.6-1 16.2.2	B, C, D, E, and F D, E, and F B, C, D, E, and F D, E, and F B, C, D, E, and F
5.	Nonparallel System Irregularity: Nonparallel system irregularity is defined to exist where vertical lateral force-resisting elements are not parallel to the major orthogonal axes of the seismic force-resisting system.	12.5.3 12.7.3 Table 12.6-1 16.2.2	C, D, E, and F B, C, D, E, and F D, E, and F B, C, D, E, and F

Among the five types given, Type 1 torsional irregularity is regarded as the most important one, as it has many limitations for modeling and analysis. For instance, Type 1.b irregularity is not permitted in seismic design categories of E and F. Consideration of the irregularities in modeling and design are to be discussed in the following subsections in more detail.

In ASCE 7-10, accidental torsion is taken into the account by adding the effect of

the torsional moments, which are caused by a shift of center of mass of the structure by 5% of the plan dimension of the structure perpendicular to the direction of action to calculated floor torques. However, the exact procedure to calculate the accidental eccentricity related forces is not specified. This addition may be done by calculating the accidental eccentricity related torques and applying them to the center of mass in the case of static analysis or offsetting the center of mass by 5% of the plan dimension while performing modal or dynamic analyses.

There is also an amplification factor defined for accidental torsional moment. If Type 1 torsional irregularity exists for selected seismic design categories, accidental eccentricity related torsional moments should be scaled with a factor A_x given as shown in Equation 1.8:

$$A_x = \left(\frac{\delta_{max}}{1.2\delta_{avg}} \right) \quad (1.8)$$

Where δ_{max} is the maximum lateral displacement at the x^{th} story level and δ_{avg} is the average lateral displacement at the x^{th} story level. Both of these quantities obtained under seismic analysis. Minimum limit for A_x is specified as 1 and maximum value A_x can take is given as 3. It should be also noted that set of rules described for accidental torsion is to be applied for two orthogonal directions.

In terms of structural modeling, there is an important specification against oversimplification of torsionally-coupled systems in ASCE 7-10. For structures that possess horizontal irregularity Type 1, 4 or 5 given in Table 1.2, use of planar models are prohibited. They should instead need to be analyzed by a 3D mathematical representation.

ASCE 7-10 permits using three types of analysis procedures according to seismic design categories of structures. These are listed as equivalent lateral force method, modal response spectrum analysis and seismic response history (dynamic analysis – linear or nonlinear) procedures. In selection of the analysis procedure, only limitation in terms of horizontal irregularity is presence of Type 1 irregularity given in Table 1.2. If structure is deemed to sport Type 1 type torsional irregularity, then simpler equivalent static load method is not permitted.

If equivalent static load method is the selected procedure for seismic analysis, then ASCE 7-10 requires consideration of inherent torsion resulting from eccentricity be-

tween center of mass and center of stiffness of the system. It should be noted that a specification about inclusion torsional effects in equivalent static method is not in conflict with the criteria for permitted analysis procedures. Even if a structure is not classified as torsionally irregular (Type 1), it may still have an amount of static eccentricity as well as accidental eccentricity. Therefore, these effects should be included in the design when simplest analysis method is employed. No formulation or procedure for this inclusion is elaborated in the Code, however it should be rather straightforward for the designer. For modal analysis and dynamic analysis there is not any other specific comments are given regarding the inherent torsion since these procedures are able to represent torsionally coupled response compared with the equivalent lateral force method. However; when using any of the latter two analysis methods, amplification factor for accidental torsional moment (A_x) is stated as not required when accidental eccentricity is applied to the structure.

While designing structural systems that are classified as laterally irregular, ASCE 7-10 requires an increase in diaphragm design forces for specific design categories. Structures assigned to D, E or F categories sporting a horizontal irregularity given in Table 1.2 (except for Type 5 irregularity) requires an increase of 25% in design forces of specific members. These specific elements of the load resisting system are given as connections of diaphragms to load carrying members and collector elements which carry the loads of diaphragm elements to vertical load carrying systems. These types of members are discussed in detail in the chapter commentaries which are supplied as appendices to the Code.

Another parameter called redundancy factor, ρ , is also defined in this section of ASCE 7-10. It is employed in calculation of horizontal seismic load effect. The horizontal seismic load effect, which is employed in design load combinations given in a separate chapter of ASCE 7-10, is obtained by multiplying this redundancy factor with the effect of horizontal seismic forces calculated by performing a lateral analysis procedure. Redundancy factor which is determined separately for two orthogonal directions is given as 1 for majority of the cases. However, this value changes for some specific conditions. For building structures that are assigned in seismic design categories D, E or F (higher seismic risk), ρ is given as 1.3. Although this value is specified in the standard, it is still permitted to be taken as 1 provided that two

specific conditions are met in building structures assigned to the mentioned seismic design categories. These conditions focus on stories that resist more than 35 percent of base shear of the base shear in the direction of interest. In a typical structure this type of story is most probably located in lower levels of a building. First condition regarding the mentioned type of stories is given in Table 1.3. A loss of strength scenario and limits this loss at 33% reduction in strength is described in Table 1.3. Moreover, extreme torsional irregularity should not occur in the system due to this strength loss. Other condition is that a plan-regular structure should have a seismic force resistance system that consists of at least two bays of seismic force resisting perimeter framing on each side of the structure at the stories under consideration. If the building structure satisfies these two conditions, then an increase in the force through application of the redundancy factor is deemed unnecessary by ASCE 7-10 (ρ is to be taken as 1). In fact, this regulation is also closely related with Type 1 horizontal irregularity. If the loss of strength during seismic action results in an extreme torsional irregularity (Type 1.b) as well as significant change in strength distribution, ASCE 7-10 opts for an increase in seismic forces in order to prevent the undesired and normally unforeseen behavior.

Table 1.3: Requirements for each story resisting more than 35% of the base shear, taken from ASCE 7-10

Lateral Force-Resisting Element	Requirement
Braced frames	Removal of an individual brace, or connection thereto, would not result in more than a 33% reduction in story strength, nor does the resulting system have an extreme torsional irregularity (horizontal structural irregularity Type 1b).
Moment frames	Loss of moment resistance at the beam-to-column connections at both ends of a single beam would not result in more than a 33% reduction in story strength, nor does the resulting system have an extreme torsional irregularity (horizontal structural irregularity Type 1b).
Shear walls or wall piers with a height-to-length ratio greater than 1.0	Removal of a shear wall or wall pier with a height-to-length ratio greater than 1.0 within any story, or collector connections thereto, would not result in more than a 33% reduction in story strength, nor does the resulting system have an extreme torsional irregularity (horizontal structural irregularity Type 1b). The shear wall and wall pier height-to-length ratios are determined as shown in Figure 12.3-2.
Cantilever columns	Loss of moment resistance at the base connections of any single cantilever column would not result in more than a 33% reduction in story strength, nor does the resulting system have an extreme torsional irregularity (horizontal structural irregularity Type 1b).
Other	No requirements

Adopting quite a different approach compared to Eurocode 8, ASCE 7-10 gives a relatively small number of design guidelines for structures having horizontal irregularities. Limitations about important parameters such as reduction, overstrength and ductility factors are fixed at the beginning of the design phase when structural system is selected and building is assigned to a seismic design category. Countermeasures

for irregularities are taken into account for some structural types assigned to specific design categories. As discussed previously, these measures are in fact scale factors that increases the design forces or design load combinations.

The design approach adopted by ASCE 7-10 is simple and practical but for some buildings in specific design categories, it may result in undesired non-uniform demand distribution among structural plan. This effect could be minimized by adopting a regular and redundant design strategy as promoted by the Code.

1.2.5.3 Provisions in the Turkish Earthquake Code

Turkish Earthquake Code follows a closely related outline about defining structural irregularities and issues regarding torsional response with those observed in ASCE 7-10. Conditions for structural regularities are tabulated and labeled. While it encourages selection of regular and symmetric structural systems like previously discussed seismic codes; ductility definitions are given in a simple way and do not include effect of plan irregularities. These aspects are to be discussed in detail.

Conditions for structural regularity are tabulated for both plan and elevation in Turkish Earthquake Code. There are three types of plan irregularities are identified: A1, A2 and A3. A1 is defined as torsional irregularity and it is measured by torsional irregularity coefficient, η_{bi} , which is given in Equation 1.9:

$$\eta_{bi} = \frac{(\Delta_i)_{max}}{(\Delta_i)_{mean}} > 1.2 \quad (1.9)$$

Where $(\Delta_i)_{max}$ is the maximum interstory drift and $(\Delta_i)_{mean}$ is the mean value of interstory drift for the i^{th} story obtained from analysis under reduced earthquake forces. In determination of the drift values, accidental eccentricity should also be considered. For a torsionally coupled system, this value is expected to be larger than 1 and lower limit for A1 type irregularity classification is given as 1.2 in the Code. Irregularities resulting from slab discontinuities along a story are classified as A2 type; whereas large plan extensions like balconies (larger than 20% of the floor area) that result in plan irregularities are categorized as A3 type. If A2 or A3 type plan irregularities exist in the system, it is required by the Code to verify the ability of floor slabs to transfer earthquake loads to structural members of buildings located in first and second

earthquake zones by performing design calculations.

Accidental eccentricity in structural systems is considered in the analyses by introducing an additional $\pm 5\%$ eccentricity to the system. The application of this additional eccentricity is detailed for given analysis methods which are discussed in the next subsection. Accidental eccentricity is directly applied in the case of equivalent static load method. However for systems where $1.2 < \eta_{bi} < 2.0$, it is scaled with a factor defined in Equation 1.10:

$$D_i = \left(\frac{\eta_{bi}}{1.2} \right) \quad (1.10)$$

This amplification is very similar to what is described in ASCE 7-10 for structures having extreme torsional irregularities. In the case of modal response analysis method, effect of accidental eccentricity is still included while determining the design forces.

For modeling of building structures, Turkish Earthquake Code gives no specific details regarding the irregular structures. However, there are some limitations for simpler analysis methods for non-symmetric systems. In this context, A1 type irregularity is more important than the others as it is an important criterion to select the analysis method for the building structure.

Three analysis methods are defined by Turkish Earthquake Code; namely, equivalent lateral load method, modal superposition method (response spectrum analysis) and time history analysis method. Selection of the appropriate analysis method is governed by two main type of categorizations: Earthquake Design Classification and Building Height Classification. Earthquake Design Classification (*EDC*) categorizes the structures according to expected short period design spectral acceleration coefficients (S_{DS}). A structure having an *EDC* class of 1, 1a, 2 or 2a could be considered as a structure where high spectral accelerations could be expected in the seismic design compared to other classes (3, 3a, 4, 4a). Building Height Classification (*BHC*), on the other hand, separates designed structures into eight different classes with respect to their heights and assign *EDC* categories. *BHC* value of 1 corresponds to tallest structures where buildings classified as *BHC* = 8 are the shortest.

The simplest of the analysis methods, equivalent lateral load method could be applied on structures less than 42 meters high where A1 type irregularity factor, η_{bi} , being less than or equal to 2. In addition to this, there should not be B2 type (weak story) on

the system. This height limit is determined by both *EDC* and *BHC* classes assigned to the building. If the building does not satisfy either one of these two conditions, then height limit reduces to 28 meters. By imposing such a limit on highly irregular building structures, Turkish Earthquake Code aims to better estimate the non-uniform demands in these type of systems by enforcing the designer to use more complex yet accurate analysis methods compared to simplest design tool available.

There are no specific comments for modal superposition or time history methods concerning the irregular structures in Turkish Earthquake Code. However, implementation of accidental eccentricity is stated as required for every node where modal forces are acted upon in the case of modal superposition method.

It should be noted that no specific set of rules are given to be taken into account in the design and detailing of irregular structural systems. As in the case of previously inspected standards, designer is encouraged to select a regular structural system and especially discouraged from having A1 type irregularity in the building structure. In addition, a very brief mention is made for torsional rigidity. To provide sufficient torsional stiffness to the system, appropriate placement of shear walls and structural elements is advised. All of these design recommendations are in the form of general principles regarding earthquake resistant design and no any other detailed provision is present in the current version of the Code.

In terms of ductility targets for different type of structural systems, Turkish Earthquake Code differs significantly from Eurocode 8. For every type of structure, whether they are regular or not, same ductility targets are valid and effect of torsional coupling is not considered. Moreover, any design recommendation against torsional flexibility is missing contrary to Eurocode 8. The approach taken by Turkish Earthquake Code is more similar to ASCE 7-10 in these aspects.

In the case of irregular torsionally coupled systems, main focus of Turkish Earthquake Code, which is subject to a major overhaul in the following years, is to prohibit simple analysis approaches that may underestimate the coupled response. Moreover, it provides a measure of accidental eccentricity for all kinds of systems that is in similar level to the other two standards discussed. It may be a good direction for Turkish Earthquake Code in the future revisions to include design recommendations

for asymmetric systems as in the case of contemporary seismic provisions.

1.2.5.4 Concluding Remarks about Seismic Provisions

Three different seismic design standards reviewed in this section encourages design of horizontally and vertically regular and redundant structural systems within the general earthquake resistant design philosophy. Although they differ in complexity, primary considerations of these seismic provisions can be regarded as the same. Several irregularity types are defined, and severe cases of torsionally coupled behavior are prevented through specific set of rules. Moreover, if designed structures are deemed irregular by these standards, overly simplified analysis and modeling methods that may underestimate the asymmetric behavior are not allowed.

In terms of specifications about seismic design, there are some differences observed. Eurocode 8 prevents design of torsionally flexible systems, and the seismic behavior due to plan irregularities are implicitly included in the calculation of seismic response factors. On the other hand, ASCE 7-10 requires a scaling of design forces for a limited set of structural types in the case of extreme torsional irregularities. Turkish Earthquake Code; however does not present a general design recommendation apart from including the effects of accidental eccentricity in determining the design forces for torsionally coupled systems.

In their current versions, the reviewed seismic design standards do not give any guidelines on how to handle non-uniform force demand and ductility distributions across a story. They rather adopt a preventive approach to avoid excessive undesired behaviour. Future revisions of these provisions may consider these phenomena in order to enable engineers to design building structures that achieve a well-estimated and uniform inelastic seismic behavior.

1.3 Objective and Scope

The phenomenon of torsional coupling is an important aspect of structural dynamics that affects the seismic response of structures. If the inelastic demands and their dis-

tribution in torsionally coupled systems are understood thoroughly, then their performances can be estimated more accurately. Consequently, accurate performance-based evaluations can be made, and design recommendations for future seismic provisions can be developed for these types of complex structures. This is the main motivation behind the thesis study.

The presented thesis study aims to investigate the non-uniform distribution of seismic demands in torsionally coupled (asymmetric) systems. Further, suggesting possible design recommendations in order to minimize the unbalanced inelastic response distribution and providing means for better estimation of the displacement performance of structural elements are considered as possible outcomes.

First, the fundamental characteristics of the seismic response of torsionally coupled systems are presented by inspecting a simple one-story system in the following chapter as an introductory study. Upon designing this simple structure to resist seismic demands with both reinforced concrete and steel members, performance of the load resisting elements and the effect of torsional coupling on these systems is discussed in order to pinpoint the problems associated with non-uniform response. This discussion is based on nonlinear analysis results obtained from pushover analyses.

Following the analyses on the simple structure, a comprehensive parametric study regarding the effect of overstrength on a parametric single-story system is conducted. Several significant design parameters such as eccentricity (e), translational period (T_n), ductility reduction factor (R_μ) and stiff-to-flexible-edge strength ratio ($SFSR$) of the asymmetric systems are considered and dynamic analyses are performed. Results obtained from inelastic dynamic analyses are utilized to compile *Unsymmetrical Response Spectra* and *Uniform Ductility Spectra*, which are proposed as assessment and preliminary design tools for the seismic performance assessment and design of multi-story asymmetric structures. Finally, a simple design strategy is postulated for improving the inelastic torsional performance and seismic response of several single-story systems to validate the outcomes.

In the following chapter, a method to obtain optimal strength distribution in asymmetric structures is developed and investigated in detail. This method employs the *Uniform Ductility Spectra* to determine the optimal $SFSR$ of an asymmetric system

and modifies the existing *SFSR* of the structure by means of a force vector. The procedure alters the design forces such that resulting *SFSR* achieved at the end of *updated* seismic design is expected to yield a more balanced ductility distribution. Then, a flowchart describing the Optimal Strength Distribution Method is presented. Sensitivity of the proposed method to important design parameters such as stiff edge overstrength is also investigated. Later, performance of the procedure in terms of improved ductility distribution is validated on single-story asymmetric systems. Finally, Optimal Strength Distribution Method is expanded to the multi-story structures and an algorithm describing the procedure is given.

Next, seismic performances of three multi-story asymmetric structural systems are investigated as case studies in three different chapters. First, a stiffness-asymmetric eight-story structure is presented. Second, seismic response of a mass-asymmetric eight-story system is studied. Third, a twelve-story plan-asymmetric structure with a shear wall is investigated in detail. In all three case studies, general properties of these structures are presented first, then dynamic properties are defined and seismic design is commenced. Inelastic dynamic analyses are performed using appropriate strong motion sets, and mean seismic response of these structures are presented. Next, *Optimal Strength Distribution Method* is applied to the systems and designs are modified accordingly. Finally, mean results of the inelastic dynamic analyses performed on the modified designs are compiled, and comparisons are made between original and updated designs in terms of ductility distribution.

In the final chapter, a brief summary is given and conclusions are stated. Discussion of the results as well as possible future work regarding the topics covered within the scope of thesis study are presented.

CHAPTER 2

A SIMPLE CASE STUDY: ONE-STORY ASYMMETRIC STRUCTURE

2.1 Introduction

In this chapter, the seismic response of a one-story asymmetric rigid slab structure is investigated. The design capacities of structural members are determined in an effort to better visualize the expected inelastic behavior and demands on the system that has been designed according to linear elastic procedures. Later, design solutions provided according to seismic demands and the inelastic behavior of the system is examined. As in the case of studies performed in the past decades, this parametric study is conducted on the simplest possible one-story model. The case study structure is investigated in the scope of this chapter to better examine the expected deformation demands in an asymmetric (torsionally coupled) system. The observations made in this chapter are considered to form a basis for inspecting structures that are more complex.

2.2 General Information and Dynamic Properties

The schematic floor plan of the initial parametric system is shown in Figure 2.1. The slab is square with length L , and its mass is m . There are two structural members, which are assumed weightless on the two sides of the rigid slab. These are oriented to resist the lateral forces along y-axis. No transverse structural elements are present in the system. The one on the right is two times stiffer from the one on the left, which has a stiffness of k . Therefore, one-way asymmetry along the y-axis is present in the structure. Distribution of stiffness on the system affects the center of rigidity (CR)

which can be described as the hypothetical location of the resulting stiffness centroid of all structural members on the floor plan. Using CR , the stiffness eccentricity e_s , which is shown in Figure 1.1 is obtained by dividing the CR coordinate value with the plan dimension perpendicular to the direction of analysis. The resulting shift of center of rigidity (CR) in the positive x direction gives a %16.7 eccentricity to the system. Expression of CR is given in Equation 2.1.

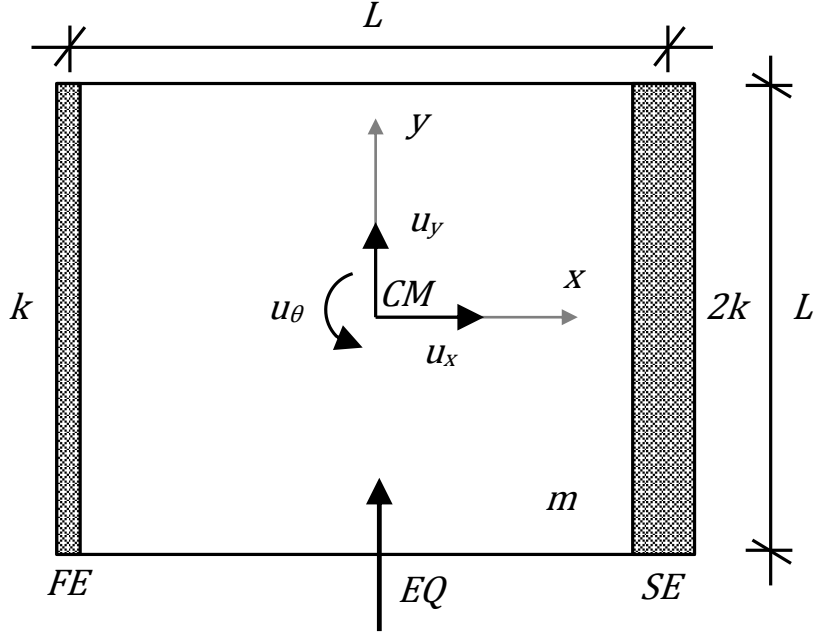


Figure 2.1: Floor plan of the one story rigid slab structure.

$$CR = \frac{\sum k_i * x_i}{\sum k_i} \quad (2.1)$$

k_i value in Equation 2.1 denotes the stiffness of structural member i ; while x_i is the distance of member from center of mass. In accordance with the expected deformation patterns, left hand side of the slab is named as the flexible edge (FE); whereas the right hand side is named as the stiff edge (SE). Since there is one-way asymmetry in the system, only the coupling degrees of freedom are considered in the dynamic response; translation y and rotation θ . Modal analysis of the system yields the vibration frequencies given in Equation 2.2, and the mode shapes expressed in Equation 2.3. The first degree of freedom denotes translation y whereas the second one denotes

rotation θ .

$$\omega_n = \begin{bmatrix} 1.52 \\ 2.28 \end{bmatrix} \sqrt{\frac{k}{m}} \quad (2.2)$$

$$\Phi = \begin{bmatrix} 1 & 1 \\ -1.37/L & 4.37/L \end{bmatrix} \quad (2.3)$$

First mode shape is translation dominant and the second mode shape is rotation dominant. The ratio of uncoupled torsional and lateral modal frequencies, which is defined in Equation 1.2, is around 1.5. Therefore it can be said that the prototype system is torsionally stiff.

The modal participation factors (Γ_n) and effective modal masses (M_n^*) calculated for y-direction are presented in Equation . The sum of effective modal masses calculated from the coupled modes yields the total mass of the structure, as expected.

$$\begin{aligned} \Gamma_1 &= 0.76 & \Gamma_2 &= 0.24 \\ M_{1,y}^* &= 0.76m & M_{2,y}^* &= 0.24m \end{aligned} \quad (2.4)$$

As can be seen in Equations 2.3 and 2.4, the system is torsionally coupled. Next, the modal displacements for each mode are determined. At this stage, the spectral accelerations for both of the two modes are assumed as equal to S_a . The calculated modal displacements of the coupled degrees of freedom are given in Equation 2.5.

$$u_1 = \begin{bmatrix} 0.33 (m S_a)/k \\ -0.45 (m S_a)/(k L) \end{bmatrix} \quad u_2 = \begin{bmatrix} 0.046 (m S_a)/k \\ 0.20 (m S_a)/(k L) \end{bmatrix} \quad (2.5)$$

Using the modal displacements, elastic modal forces on the FE and SE frames are calculated. To do this, rigid diaphragm behavior of the slab is taken into the account. The center of mass displacements are transformed into the edge deformations and these are multiplied by the respective stiffness values of the structural members. Resulting modal shear forces on FE and SE members ($V_{FE,1}$, $V_{SE,1}$, $V_{FE,2}$ and $V_{SE,2}$)

are shown in Equation 2.6.

$$\begin{aligned} V_{FE,1} &= 0.55 m S_a & V_{SE,1} &= 0.21 m S_a \\ V_{FE,2} &= -0.055 m S_a & V_{SE,2} &= 0.29 m S_a \end{aligned} \quad (2.6)$$

It can be observed from Equation 2.6 that for both modes sum of the modal shear forces is equal to the multiplication of effective modal mass and spectral acceleration. By applying modal combination (SRSS) to the modal shear forces, final elastic shear forces on structural members are obtained as presented in Equation 2.7:

$$V_{FE} = 0.55 m S_a \quad V_{SE} = 0.36 m S_a \quad (2.7)$$

A major behavior pattern of torsionally coupled systems can easily be observed at this stage. For the flexible edge member, contribution of rotation dominant mode is negligible. On the other hand, stiff edge displacement is heavily amplified by the rotation dominant mode. It can also be noted that on the flexible side of the structure, torsional coupling does not alter the demand on structural members significantly. This significant amplification of response on the stiff edge is also related to significant rotational response of the system.

In order to determine the inelastic design forces, general seismic design principles are followed. A response reduction factor, $R = 4$, is employed. By reducing the elastic forces on structural members, inelastic design forces are determined (Equation 2.8):

$$V_{FE,design} = 0.140 m S_a \quad V_{SE,design} = 0.090 m S_a \quad (2.8)$$

The inelastic shear forces can be considered as the capacities required by the structural members on both sides of the slab. For these capacities, center of strength (CV) which gives an idea about the strength distribution of the system can now be calculated. During seismic response, center of strength is calculated as the instantaneous location of the resultant force acting on structural members. In the design stage, it can be calculated from the elastic member capacities. CV is calculated as displayed in Equation 2.9. Similar to determination of CR , F_i is the force acting on member i ,

and x_i is the distance of this member from geometric center.

$$CV = \frac{\sum F_i * x_i}{\sum F_i} \quad (2.9)$$

By dividing the CV coordinate value with the plan dimension perpendicular to the direction under consideration, strength eccentricity of the system can be obtained. CV is important in torsionally coupled structures since it is related with the torque that the CM undergoes, and with the resulting deformation patterns. For this specific system, location of design center of strength (CV) is determined as $0.11 L$ to the left of the center of mass. Since the structural member at the flexible edge is expected to carry higher loads, it is designed to be stronger; hence shift of CV towards flexible edge occurs on the system. The location of CR and CV with respect to CM are presented in Figure 2.2.

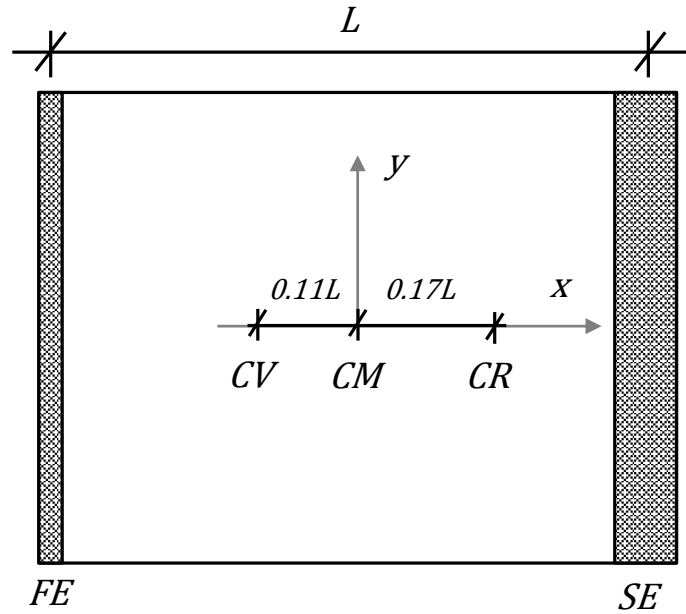


Figure 2.2: Locations of CV and CR with respect to the center of mass.

Since structural analysis is now complete, load-resisting members can be detailed by using code provisions in order to provide member capacities that satisfy the load demands. Due to distribution of force resisting elements, structure is expected to display a non-uniform deformation pattern along its plan while it resists lateral forces. In the actual design of structural members, this is an important factor that affects the

member capacities.

2.3 Design and Detailing of Structural Members

In order to study the expected inelastic behavior and examine the consequent inelastic demands on the one story system, capacity design is performed for two resisting members. At this stage, no seismic code provisions are considered in the design. This strategy is intentionally adopted so that the prohibitive effects of seismic code provisions that limit the undesired consequences of torsional coupling could be omitted. As a result of this, more accurate evaluation of behavior without any other influence on the seismic response is possible. In design, Turkish Earthquake Code [73] is only utilized for determination of spectral acceleration values (S_{an}). The elastic design response spectrum defined by the Turkish Earthquake Code is shown in Figure 2.3. Parameters for design spectrum are selected to simulate an area located in a severe earthquake zone and having the ZC local soil class (medium stiff).

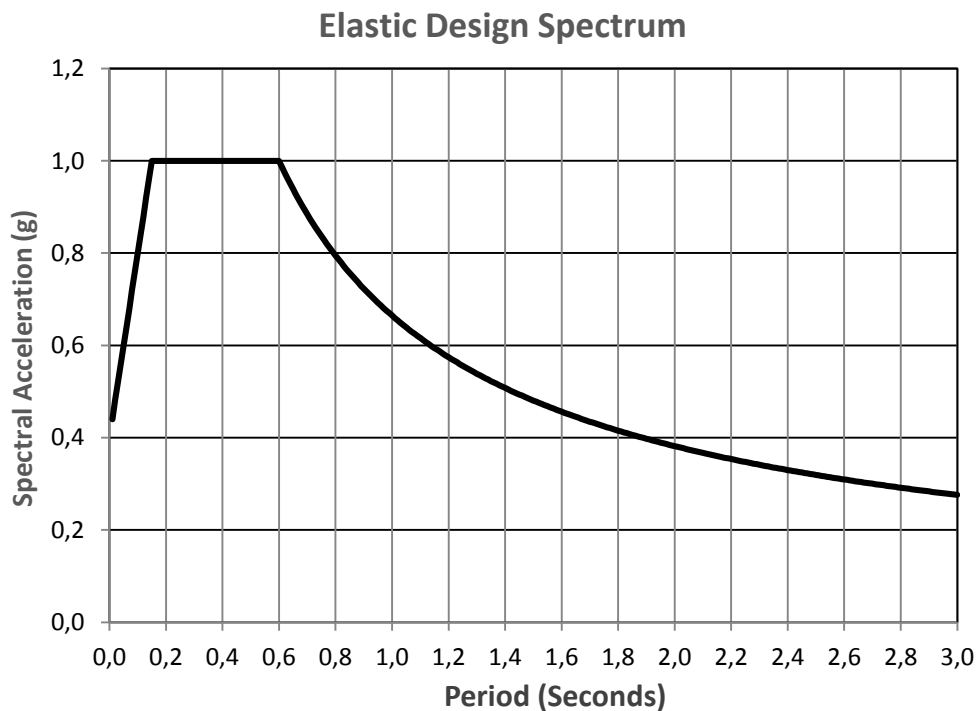


Figure 2.3: Design acceleration response spectrum.

Parametric values described in the previous section are attained for the actual design;

albeit they are replaced with numerical values. Another parameter, h , which is the height of structural members, is also introduced. By doing so, the stiffness values of individual load resisting members could be defined for a rigid deck system in terms of their respective section properties and member lengths (Equation 2.10).

$$k = \frac{12EI}{h^3} \quad (2.10)$$

The section property of the load resisting members, EI , is related with the material and section dimensions of the structural elements. With the inclusion of member dimensions, material properties and member heights; prototype system evolves into a more quantifiable structure that can be designed to resist the seismic demands. This one story rigid slab (having a thickness t) system that is supported by two columns is shown in Figure 2.4. Stiffness asymmetry in the structure is regarded as an architectural constraint and design solutions are provided by taking this constraint into consideration.

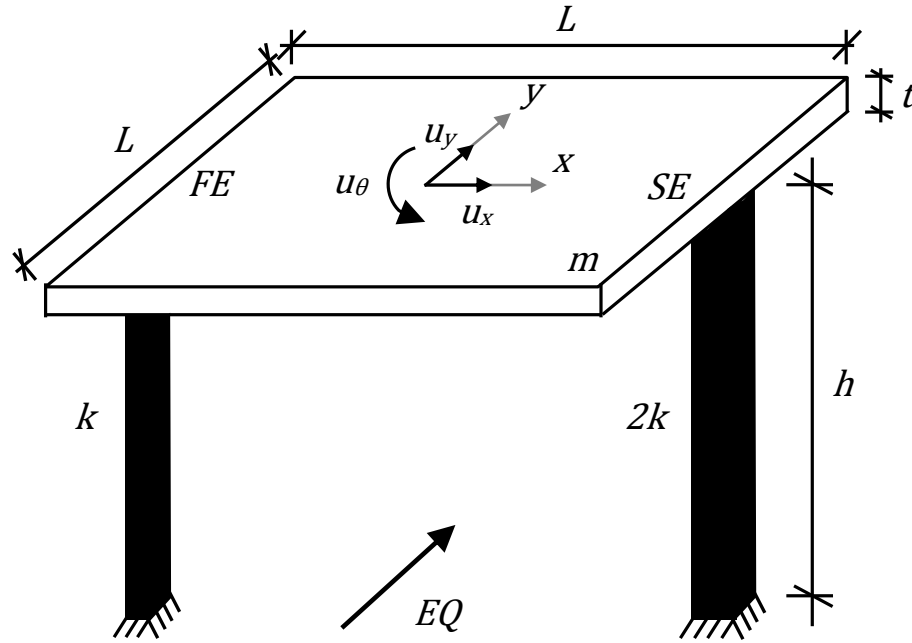


Figure 2.4: Representative view of the one story structure.

In the following subsections, the system under consideration is designed by utilizing two different structural solutions: Reinforced concrete and structural steel. This variation in the design phase is introduced because relationship between strength and stiffness in reinforced concrete elements is different from the relation observed in

steel members. For the case of reinforced concrete members, required capacities can be provided with negligible effect on member stiffness with appropriate reinforcement detailing. However, this is not the case for steel members where stiffness and strength of a section is directly related. The conditions briefly described for two different design philosophies are elaborated in more detail later.

2.3.1 One-Story Reinforced Concrete Structure

Reinforced concrete one story system is composed of a rigid concrete slab carried by two columns whose general properties were described previously. Concrete grade is selected as C25 having 25 MPa strength and 25 GPa modulus of elasticity. Yield strength of reinforcing steel is 420 MPa and its ultimate strength is 500 MPa. (Modulus of elasticity of steel is 200 GPa.) Capacities of designed columns are checked according to provisions defined in Turkish Reinforced Concrete Code [87, TS-500]. In order to preserve the stiffness ratio of two members (stiff edge element being two times stiffer than flexible edge element), column section dimensions are selected. Depths of the columns are decided to be same. However, width of the stiff edge column is two times the width of flexible edge column. Consequently, flexible edge column dimensions are d by b , while stiff edge column dimensions are d by $2b$ where d denotes the section depth and b is the width of the flexible edge column. This dimension arrangement yields two times lateral stiffness (Equation 2.10) to stiff edge member compared to the column at flexible edge, consistent with the architectural constraint regarding the stiffness asymmetry.

Primary criterion for determination of the reinforced concrete system properties is selected as obtaining the highest possible seismic demands on the structure. This enables the investigation of torsional coupling and accompanying inelastic response during severe seismic action. It was previously shown that in order to attain a high demand on the force resisting members, spectral acceleration values for the system should be at maximum (Equations 2.6 and 2.7). Hence, uncoupled translation period target for the one story structure is selected as $T_y = 0.5$ seconds. With the target period set, system parameters discussed previously are assigned numerical values using a goal seek algorithm such that the resulting translational period of the structure is 0.5

seconds. Determined values for the system parameters that are defined in Figure 2.4 are given in Table 2.1.

Table 2.1: Properties of the reinforced concrete one-story structure

Property in Figure 2.4	Value
L (m)	10
t_{slab} (m)	0.275
h (m)	20

In addition to general dimensions of the system, section depth b and width d are also determined. Flexible edge column dimensions are selected as 0.3 by 0.3 meters. Consequently stiff edge column's size is set as 0.3 by 0.6 meters. Mass of the system (m), which directly affects modal periods, is simply calculated from the dimensions of the slab using Equation 2.11. Columns are assumed weightless. ρ_c parameter in Equation 2.11 is the unit mass of concrete and taken as 2.5 tons per m^3 . Using the relationship given, mass m is determined as 68.75 tons.

$$m = L^2 * d_{slab} * \rho_c \quad (2.11)$$

After all the parameters are defined for the asymmetric system, its periods for the first mode coupled can be calculated. Upon performing an eigenvalue analysis, the translation dominant modal period, T_{1y} is calculated as 0.48 seconds and the rotation dominant modal period $T_{1\theta}$ is determined as 0.39 seconds. These period values are within the plateau of the design spectrum; therefore the condition that maximizes the modal spectral acceleration values is satisfied.

Demands on the columns whose dimensions are calculated previously can now be computed. Using Equation 2.8 that was defined in the previous section design shear forces for two column members are calculated for reduction factor $R = 4$. Resulting shear forces are determined as $V_{dFE} = 94$ kN and $V_{dSE} = 61$ kN for flexible and stiff edge column elements, respectively. In order to provide reinforcement detailing for the columns elements, moment and axial load demands on these members should be calculated. Moments for both columns can be approximately calculated by employing

the principles of structural analysis. For a column member that is fixed at both ends, deflected shape and forces acting on the member is displayed in Figure 2.5.

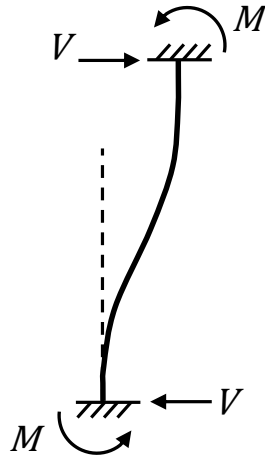


Figure 2.5: Deformed shape of a column fixed at both ends and resulting forces during seismic response.

Deformation pattern of the column shown in Figure 2.5 is the same for structural elements in the one story system since the floor slab is rigid. By taking moment at either one of the supports, relation between moment M and shear force V can be calculated as shown in Equation 2.12:

$$k = \frac{h * V}{2} \quad (2.12)$$

Using Equation 2.12 design moments of column members are obtained as $M_{dFE} = 188$ kNm and $M_{dSE} = 122$ kNm. Axial load on both columns is $P_d = 337$ kN. This single value is calculated by multiplying the floor mass with ground acceleration g , and dividing the resulting slab weight equally to two members.

After all force demands on two column members are determined, reinforcement design can be performed. As mentioned previously, detailing is provided in such a way that only force demands are satisfied with minimal overstrength on both columns. No other detailed seismic design principles are employed. Sections designed according to this strategy are given in Figure 2.6:

Longitudinal reinforcement ratios of both sections (ρ) are given in Figure 2.6. Also

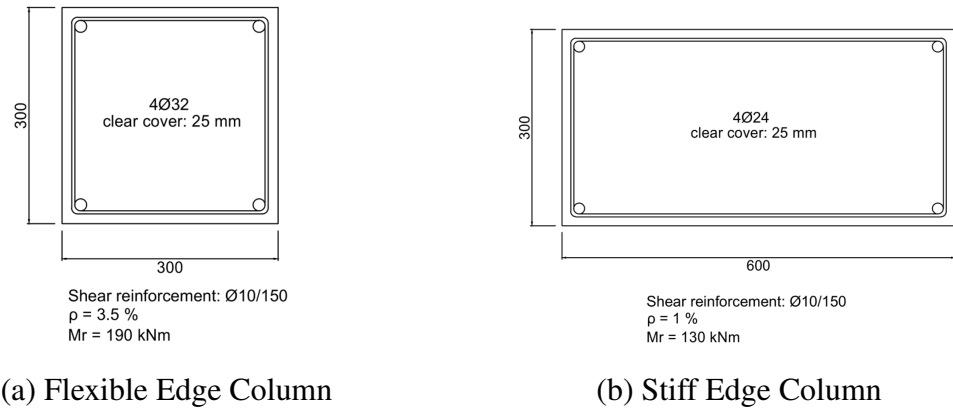


Figure 2.6: Section details of reinforced concrete members (units in mm).

given are the moment capacities of columns under P_d . Typical shear reinforcement is provided for both columns sections with no confinement regions are defined. Its primary purpose is to carry the shear force and form the reinforcement cage along the column.

2.3.2 One-Story Steel Structure

A similar analogy to what was followed in the case of reinforced concrete system is also adopted for steel members. Rigid concrete floor slab whose dimensions and mass is defined previously, is retained as well as the height of the columns is kept same at 4 meters. Again, no detailed seismic design provisions were considered in design. Steel members are selected only to resist lateral load demand. Design checks that include the determination limit states of steel columns such as compression buckling, yielding or lateral torsional buckling are completed as per AISC Specifications for Steel Buildings [2]. Selected steel grade has a yield strength of 344.5 MPa (50 ksi) and a modulus of elasticity of about 200 GPa (29000 ksi).

Main objective of the steel design is to provide a similar level of capacity and initial elastic behavior to the one story structure compared with its reinforced concrete counterpart. As a result, a more straightforward comparison of the seismic response of two systems is possible. The only parameter that can be changed to obtain this level of similarity are the column sections of the two structural members since others are kept constant. Therefore, some design decisions are made at this stage in terms

of member properties. No built-up sections, solid rectangular or circular members are utilized. Rather, wide flange steel members (also denoted as W-Section) which are used extensively in structural engineering applications are employed. A contemporary section list obtained from AISC Steel Construction Manual Shapes Database [3] is utilized for section selection. One final consideration in determining the steel sections is the architectural constraint that causes the stiffness asymmetry: Stiff edge column is two times stiffer from the flexible edge column. Since it is not possible to obtain this relationship by directly altering the section dimensions, special care is given to select two sections such that the stiff edge column's moment of inertia I_{SE} is approximately two times of flexible edge column's moment of inertia, I_{FE} .

Considering all items described previously two steel sections given in Figure 2.7 are selected for the columns. Moments of inertia of two members about their local z (strong) axes are also given in the figure. In the designed system, columns are oriented such that they resist bending moments due to lateral response with their strong axes. As can be seen from the moment of inertia values (I_z), stiffness asymmetry criterion is approximately satisfied.

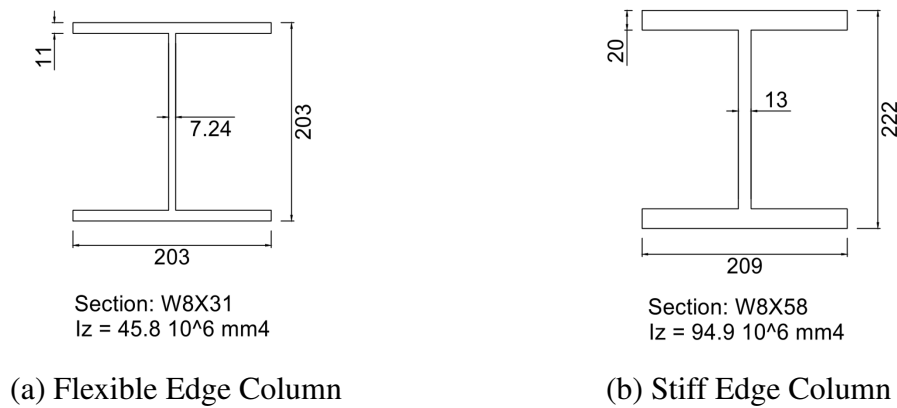


Figure 2.7: Section details of structural steel members (units in mm).

After structural parameters of the steel system are set, its dynamic properties are determined. Translation dominant modal period, T_{1y} is calculated as 0.80 seconds and rotation dominant modal period $T_{1\theta}$ is determined as 0.51 seconds. Compared to reinforced concrete structure, periods of the steel system are longer. Consequently, demands on the system will be lower than demands of the reinforced concrete system. Equation 2.8 is utilized again and for reduction factor $R = 4$, design shear forces

for flexible edge column and stiff edge column are calculated as $V_{dFE} = 73$ kN and $V_{dSE} = 47$ kN, respectively. To calculate design moments, Equation 2.12 has been used and $M_{dFE} = 146$ kN-m and $M_{dSE} = 94$ kN-m values are found for the two respective columns. Design axial force which is $P_d = 337$ kN on columns remains unchanged since rigid story is not altered. Following determination of demands on the system, capacities of the two structural members are calculated with utilization of AISC Specifications for Steel Buildings [2]. The capacities under the design axial load are found as $M_{nFE} = 172$ kN-m for the flexible edge column and $M_{nSE} = 284$ kN-m for the stiff edge column.

As can be deduced from these values, there is an amount of overstrength especially for the stiff edge member. However, this is somewhat anticipated since the adopted design strategy calls for similar levels of capacities for both reinforced concrete and steel systems, particularly for the flexible edge column. Due to interdependency of stiffness and strength on steel members, overstrength in stiff edge column in steel structure is inevitable when a stiffness asymmetry constraint like the one in the considered system is present.

In the upcoming section, seismic performances of one story structures are investigated. Nonlinear models are constructed in computer environment and analyses are performed on these models.

2.4 Analysis of the Designed System

In this section, analyses of designed system is discussed in order to identify the behavior patterns and problems associated with torsionally coupled systems. A nonlinear numerical models are created so that the inelastic action can adequately be observed during analyses. The following subsection gives detailed information about modeling of the one story system. Later, pushover analyses performed on reinforced concrete structure is discussed and results are presented.

2.4.1 Modeling

Analysis model is prepared in the OpenSees Platform [65]. A three-dimensional model is created so that torsional response could be observed properly. Already available inelastic material models are used in member sections.

Two columns of the one story structure are modeled with the implementation of ‘forceBeamColumn’ elements. These are distributed plasticity elements with a number of integration points that can be defined along the member length. For the column members in the models, six integration points along their lengths are defined. Sections that were designed previously are assigned to the integration points for both structural systems. For this purpose, fiber sections are defined. When a section is divided into ‘fibers’ whose strains can be calculated, a more accurate evaluation of response of the section to deformations is possible compared to simple section definitions like idealized moment-curvature relationships. Moreover; this approach takes the interaction of axial loads and moments acting on the section into account, yielding a more proper estimation of demands. A drawback related with the implementation of fiber sections is the requirement for relatively high computational effort. Since the models under consideration are highly simplified, mentioned disadvantage is negligible for this stage of the study.

Analysis model of reinforced concrete structure employs fiber sections along with reinforcement layer definitions. In addition, confinement effects on the concrete are also considered. Different patches of concrete are defined for core and cover areas of the section. Concrete material model “Concrete01” is utilized for both types of unconfined and confined concrete. The model includes a force-deformation relationship (stress-strain in the case of concrete) based on the Modified Kent and Park model [51, Kent and Park]. Compressive strength of the confined concrete material (core concrete) is multiplied by coefficient K_c to account for confinement effects. K_c is calculated by considering the concrete material properties and shear reinforcement all of which are defined in the design stage. After core and cover concrete fibers are created, reinforcement layers are also included in the sections. “ReinforcingSteel” material model, which was specifically written for reinforcement steel that are used in fiber sections is selected for use in reinforcement layers. This uniaxial material

model includes the material properties such as post-yield hardening of steel, ultimate strength and ultimate strain. A very small post-yield stiffness was defined for reinforcing steel model in the system. Resulting reinforced concrete fiber sections for both flexible edge and stiff edge reinforced concrete columns are in same configuration with the analytical model shown in Figure 2.8. The fibers in light gray in Figure 2.8 are core concrete section fibers; while dark grey ones are cover concrete fibers. Reinforcement layers are distributed along boundaries of these regions.

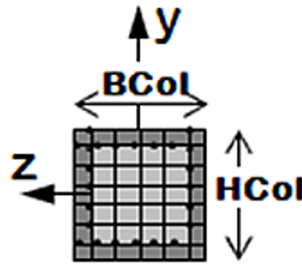


Figure 2.8: Fiber section diagram for reinforced concrete members (from OpenSees Example Manual)

Steel sections that are utilized for the second analytical model are composed in a similar way to reinforced concrete sections. Fiber sections are retained. Instead of rectangular sections, geometric parameters of the designed two W-sections such as depth, flange width, web and flange thicknesses are defined. Uniaxial bilinear “Hardening” material, which has linear kinematic and isotropic hardening properties, is assigned to fibers. Definitions of steel sections are less complex since there are no core zones or reinforcement layers are present. Created sections are similar to the analytical representation that is given in Figure 2.9.

Torsional stiffnesses are also assigned to the fiber sections, as it is required for a proper response in three-dimensional models in OpenSees Platform [65]. Torsional stiffness of the columns are calculated by multiplying material shear modulus, G , with polar moment of inertia of each section. Shear modulus is calculated according to Equation 2.13 where ν is Poisson’s ratio and E is the modulus of elasticity of the material. Later, a uniaxial linear elastic material with stiffness value $G * J$ is defined

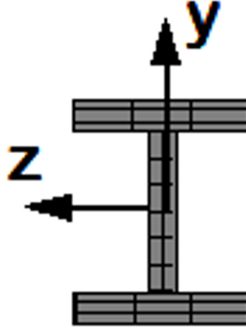


Figure 2.9: Fiber section diagram for steel members (from OpenSees Example Manual)

for each column and assigned to fiber sections accordingly.

$$G = \frac{E}{2(1 + \nu)} \quad (2.13)$$

After section definitions are completed and assigned to column elements that were discussed previously, these members were fixed at their bottom ends. Upper ends of the members are connected to rigid floor slab which bears no load resisting elements. To simulate the behaviour of the rigid slab and fixed-fixed connection of columns; rotations at member upper ends are fixed except for the degree of freedom which yields the torsional deformation. Moreover, rigid diaphragm action of the slab is defined by connecting the center of mass node of the system with upper ends of two columns with rigid links. These rigid links directly transfer the center of mass deformations to the column ends; in a similar fashion with diaphragm constraints. Mass of the system is assigned in two translational directions. Mass moment of inertia of the rigid slab which is defined in Equation 2.14 is calculated and assigned to the rotational degree of freedom of the center of mass.

$$I_{\theta} = 1/6 * m * L^2 \quad (2.14)$$

Since the slab is square, mass moment of inertia formula for a rigid body having dimensions of a by b is simplified into form that is given in Equation 2.14. Axial load on both columns (P_d) is acted on column upper ends as point loads. Second

order effects like P-Delta interaction was not included in the models to preserve the simplistic approach.

2.4.2 Inelastic Analysis

Nonlinear static (pushover) analysis has been performed on both designed systems. By utilizing pushover analysis and obtaining the force deformation relationships for the system, valuable information about inelastic behaviour can be obtained. Consequently, effects of torsional coupling and differences observed on the response due to varying structural solutions can be studied.

Pushover analysis is performed following the gravity analysis during the run sequence. Therefore the effect of the slab weight on the columns and initial deformations can also be included in the response. A single unit load is acted upon the center of mass in the direction of analysis. In order to estimate the expected seismic demand on the system, Displacement Coefficient Method (DCM) that is defined in ASCE 41-13 [5] was utilized. Calculated values from DCM are marked on pushover curves. A very high target drift ratio is defined to terminate the pushover analysis. This high value was chosen so that the system properties could be inspected well beyond the elastic range. Since geometric nonlinearity is not defined, steel system is able to reach this center of mass drift ratio. Reinforced concrete structure, however, fails to attain such high drift ratios. This is due to concrete and reinforcement material models employed, having definitive ultimate strain values. Consequently, results given for that design are up to the point where system fails to converge.

All of the force deformation relationships that are presented in the subsequent sections are normalized with respect to weight of the structure and height of the columns. Weight of the system is same for both structures which is 675 kN. Height of the columns is 4 meters, as discussed previously.

2.4.2.1 Pushover Analysis Results of Reinforced Concrete Structure

Capacity curve of the reinforced concrete one-story structure obtained from the pushover analysis is given in Figure 2.10. Drift ratio demand calculated by DCM is also indicated on the plot. As can be inspected from the figure, the center of mass of the system is able to reach up to 5% drift ratio. Since main motive is to inspect the behaviour of structural members during torsionally coupled response, overall capacity curve of the system fails to reveal much. However, failure to convergence occurs at the moment when global stiffness of the system degrades significantly.

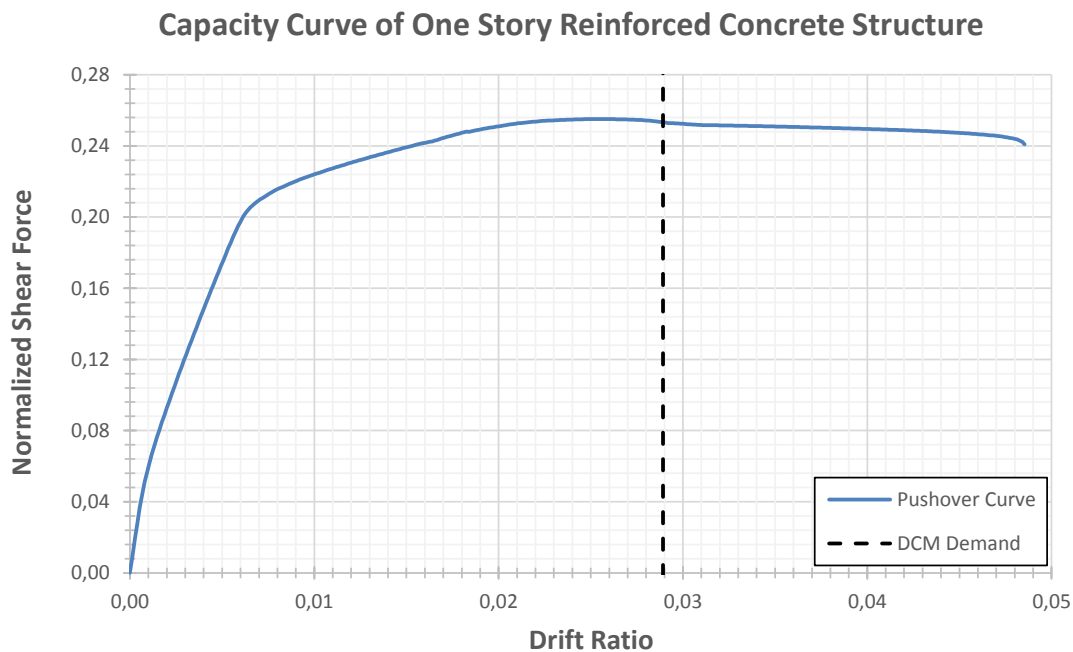


Figure 2.10: Capacity curve of the one story reinforced concrete system obtained from pushover analysis.

Individual responses of both flexible edge and stiff edge columns during pushover analysis are presented in Figure 2.11. To better visualize their respective deformation patterns, some of the points in column capacity curves are labeled in an incremental form. Points having the same label are recorded at the same pushover analysis step. In addition, drift ratio demands on columns at both edges are also marked on the curves. These demands are determined by inspecting the drift ratio values for two column members when center of mass reaches the drift ratio that is estimated by DCM.

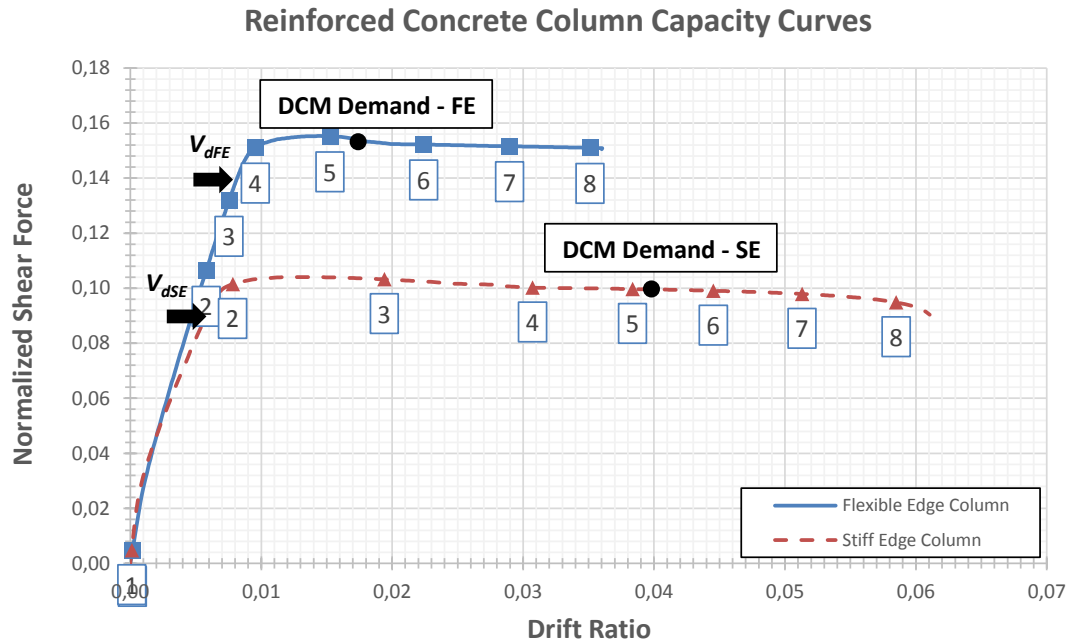


Figure 2.11: Capacity curve of reinforced concrete columns obtained from pushover analysis.

Investigation of Figure 2.11 yields some interesting observations. Although the stiff edge column is stiffer, it starts to exhibit inelastic behaviour before the flexible edge member. Moreover, both columns yield at forces close to their design force demands, which are indicated on the figure. Hence, little amount of overstrength is present. When data labels showing the same steps of pushover analysis are inspected, occurrence of significant amount of slab rotation after yielding of stiff edge column can also be seen. This results in a high amount of floor twist, resulting in highly irregular deformation of the structure in the inelastic phase. Drift ratio demands estimated by DCM falls in the highly inelastic behaviour range where torsional effects distort the uniform demand distribution on members.

Another important aspect is that the ductilities calculated with respect to the computed DCM demands vary among both members. Even without making any calculations, it can be observed from Figure 2.11 that ductility demand of the stiff edge member is considerably higher than the flexible edge one. Stiff edge member yields at the second event marked at Figure 2.11 while flexible edge member is still behaving elastic. Hence, it deforms mostly in its inelastic range until it reaches the drift demand. The

nominal reinforced concrete design, which provides no overstrength to the structural elements results in uneven ductility distribution along structural plan.

2.4.3 Pushover Analysis Results of Steel Structure

Capacity curve of the single story steel structure is presented in Figure 2.12. Due to modeling choices discussed previously, steel structure shows no stiffness degradation properties and it is able to reach the maximum drift ratio specified without any loss of strength. There is some amount of post-yield hardening on the system due to kinematic hardening parameter specified for the uniaxial material that is used for steel systems. Center of mass drift demand estimated by DCM is higher than the demand calculated for reinforced concrete system due to longer periods. In addition, base shear capacity of the system is significantly higher compared to the reinforced concrete structure. Reason behind this can better be discussed upon inspecting the capacity curves of steel columns given in Figure 2.13.

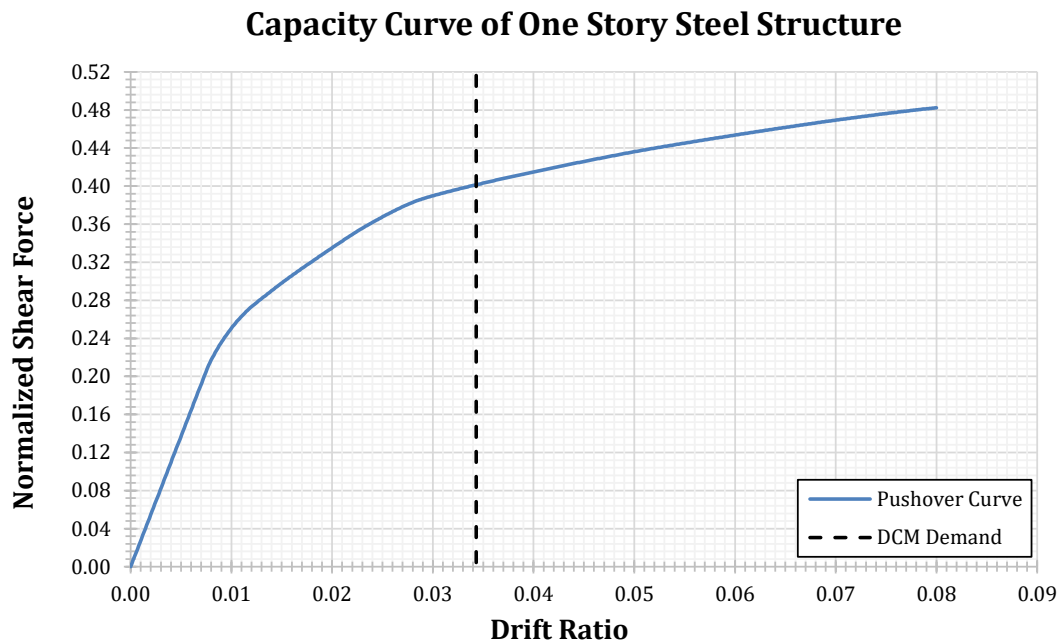


Figure 2.12: Capacity curve of the one story reinforced steel system obtained under from analysis.

As it can be seen from Figure 2.13, flexible edge column overstrength is in similar level compared to those observed in the reinforced concrete system whereas that of

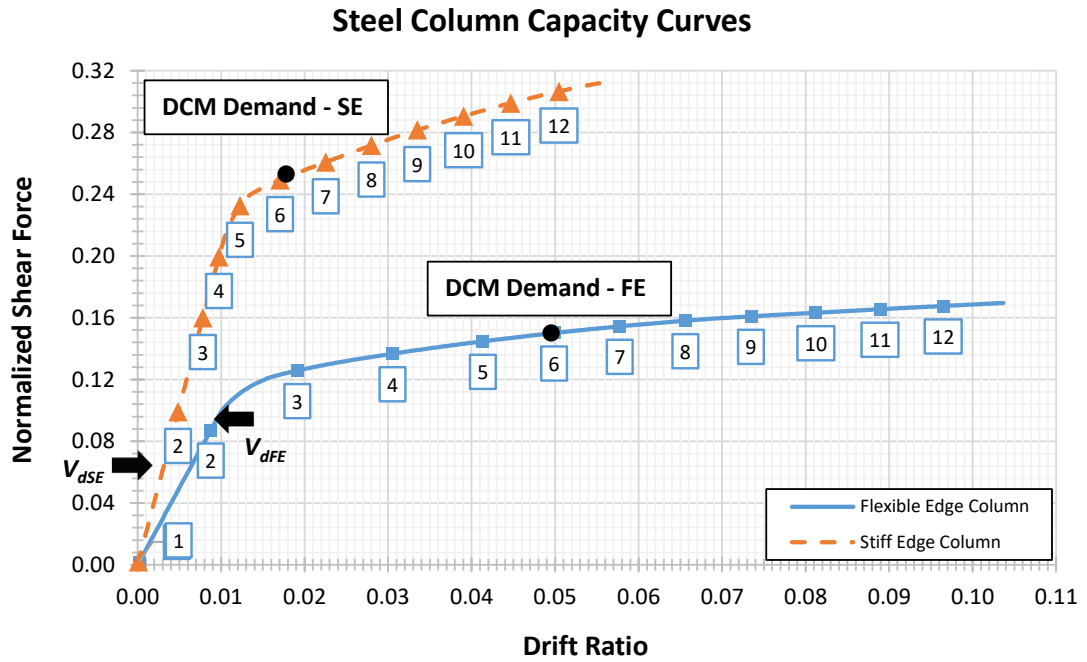


Figure 2.13: Capacity curve of steel columns obtained from pushover analysis.

the stiff edge column is considerably higher. In addition, design forces of reinforced concrete and elastic systems are not widely different from each other and the initial elastic behaviour of both systems is similar. What creates the main difference is very high overstrength present in the stiff edge column. The architectural constraint that dictates the stiffness asymmetry directly affects the response of torsionally coupled system. Since it is not possible to disassociate the strength and stiffness of a steel member, stiffer column becomes stronger even though it experiences less demand compared with the more flexible one. If the labels on the capacity curves are traced, it can also be seen that center of mass rotations increase dramatically as flexible edge column yields. Stiff edge column starts to yield when flexible edge column is already well beyond its elastic response.

2.5 Discussions on the Observed Asymmetric Performance

Omitting the effects of seismic detailing required by code provisions in both reinforced concrete and steel designs yields to a very clear performance comparison for the two torsionally coupled systems: a nominally designed one, and another one hav-

ing a high amount of stiff edge overstrength. In both cases, the ductility distribution is unbalanced which yields to an uneven damage distribution. Stiff edge member of the nominally designed reinforced concrete system registers a high ductility when it reaches the displacement demand estimated by DCM. On the other hand, steel system having a high amount of stiff edge overstrength almost fails to exhibit inelastic behaviour on its stiff edge member. Therefore, it can be concluded that the amount of overstrength present in a system effects the global ductility distribution considerably.

Overstrength present in structures could be a result of architectural constraints, construction materials or simply a requirement of seismic code provisions. Had the reinforced concrete members were detailed according to seismic provisions, stiff edge column's capacity would have been higher due to the code-induced overstrength implemented in concrete design. Irregular response of the system observed previously would have been less pronounced. It can be stated here that seismic code provisions may have a positive but somewhat limited effect to minimize the non-uniform response in the case of reinforced concrete structures.

Controlling the provided overstrength in steel structures is more of a challenge due to aforementioned strength and stiffness relation. Due to this phenomenon, it is also possible that a high amount of overstrength could be concentrated in stiff side of the structure which distorts the ductility distribution.

Reinforced concrete and steel designs presented in the scope of this chapter are the two extreme cases in terms of the presence of asymmetric overstrength distribution and its effects on torsionally coupled seismic response. However, a common ground between these two extreme cases should be investigated further in order to address the problem of uneven ductility distribution. To do this, a comprehensive parametric study is developed in the next chapter by employing another single story structure similar to that is presented here. Many design parameters as well as the stiff edge member strength vary among different designs so that their effects on the ductility distribution could be studied thoroughly. Effects of different strength levels assigned to the stiff edge on the global seismic performance is discussed in detail.

CHAPTER 3

INVESTIGATION OF THE ROLE OF OVERSTRENGTH ON THE SEISMIC PERFORMANCE OF ASYMMETRIC-PLAN STRUCTURES

3.1 Introduction

This chapter investigates the prediction of seismic demand distribution among structural members of a single story, torsionally stiff asymmetric-plan system. The focus is on the effect of inherent unbalanced overstrength, resulting from current force-based design practices, on the seismic response of code-designed single story asymmetric structures. The results obtained are utilized to compile *Unsymmetrical Response Spectra* and *Uniform Ductility Spectra*, which are proposed as assessment and preliminary design tools for estimating the seismic performance of multi-story asymmetric structures. A simple design strategy is further suggested for improving the inelastic torsional performance of asymmetric systems. Providing additional strength to stiff edge members over their nominal design strength demands leads to a more balanced ductility distribution. Finally, seismic responses of several asymmetric case study structures designed with the aid of the proposed strategy are assessed for validating their improved performance.

Throughout the past decades, notable changes did not occur in major seismic codes regarding the design of asymmetric-plan systems, despite enormous amount of research carried out as presented in Chapter 1. This is a clear indication of the complexity of the problem, which does not render itself to simple robust solutions. Yet another parameter is further complicating the problem and not investigated sufficiently in the past. This is the intrinsically unbalanced distribution of overstrength resulting from conventional design practices, introduced in the following section.

3.2 Current Design Practice and Unbalanced Overstrength Distribution

According to the current force based design practice (ASCE/SEI 7-10 [4], Eurocode 8 [30], Turkish Earthquake Code [73]), a lateral displacement distribution is calculated by linear elastic (equivalent static or modal) analysis by considering stiffness eccentricity, and design forces are assigned to members in the story plan in proportion to their lateral displacements and stiffnesses. Then they are reduced by the seismic load reduction factor R . This procedure is schematized in Figure 3.1a for a simple, one story shear frame composed of two lateral load resisting members, by using the equivalent static lateral load procedure. The lateral strength demands on flexible and stiff edge members are also indicated on the figure where accidental eccentricity is not considered and mass distribution is uniform. Depending on the modal vibration periods, design spectrum and static eccentricity e_s , three different types of design strength distributions may occur with regard to the strength eccentricity e_v . They are shown in Figure 3.1b.

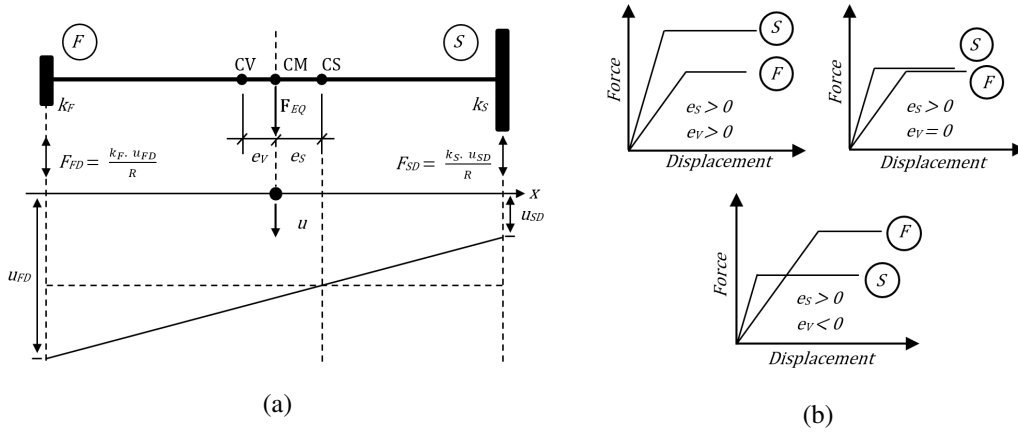


Figure 3.1: (a) Schematic distribution of displacement and strength demands in design. (b) Types of strength demands for different choices of e_v . (u_{FD} : flexible edge design displacement, F_{FD} : flexible edge design strength, k_F : flexible edge stiffness. Similar notation for the stiff edge)

The first type in Figure 3.1b ($F_{FD} < F_{SD}$) is less likely to occur whereas the other two types ($F_{FD} \geq F_{SD}$) are most likely in view of the 600 nominal designs under 475-year design earthquake carried out in this chapter on torsionally stiff, one

story shear frames. It must be noted that torsionally flexible systems, even torsionally equally stiff systems with the uncoupled torsional-to-lateral frequency ratios Ω close to one are highly discouraged in modern seismic design codes, as discussed previously. Stiff edge to flexible edge design strength demands obtained from these torsionally stiff designs are plotted in Figure 3.2. Flexible edge strength less than the stiff edge strength is obtained only for $e = 0.3$, and at periods longer than 0.8 seconds. These cases account for 96 of the 600 designs.

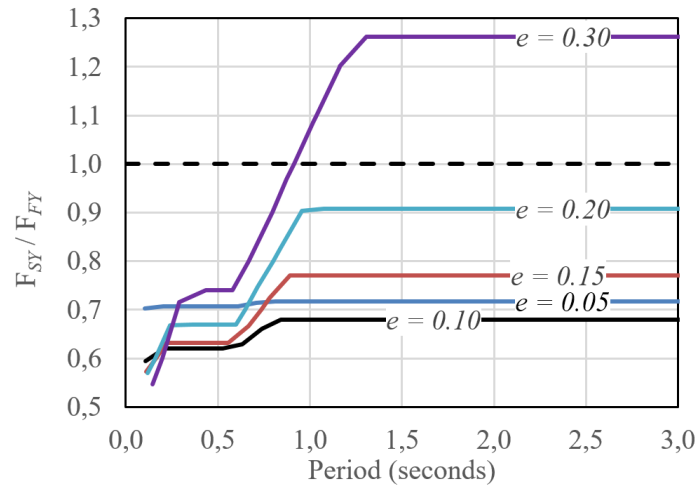


Figure 3.2: Variation of stiff edge to flexible edge design strength ratio of nominal designs with translational design period and stiffness eccentricity.

It is well known that strength is strongly dependent on stiffness in steel members, and it is highly dependent on stiffness in reinforced concrete members (Paulay [68, 69]). Higher strength assigned to flexible edge members and lower strength to stiff edge members as a result of the current design approach requires the opposite. A nominal design can be achieved for the flexible edge members for the higher strength demand, however it is difficult, usually impossible to achieve a strength for the stiff edge members lower than the flexible edge members. Higher stiffness of the stiff edge members in building structures is a consequence of architectural requirements primarily and gravity load distribution to a lesser extent, but not a natural result of structural design requirements. Accordingly, the section sizes at the stiff edge that are larger than those required by the lateral load demands lead to a significant inconsistency between strength and stiffness. Although the flexible edge members can be designed nominally with reasonable overstrength due to the actual material strengths

compared to design strengths basically, this is not possible for the stiff edge members. Strongly proportional strength-stiffness relation in steel sections and minimum section dimensions as well as minimum reinforcement and detailing requirements in concrete sections inevitably lead to excessive overstrength values at the stiff edge members. These phenomena result in a strength distribution in plan that is contrary to the strength demands obtained from current design practice, which is explained graphically with the aid of Figures 3.3 and 3.4.

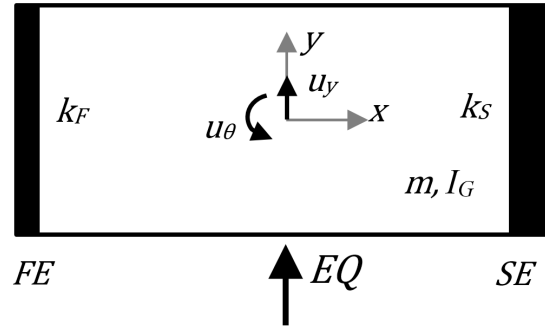


Figure 3.3: Typical single story shear frame structure.

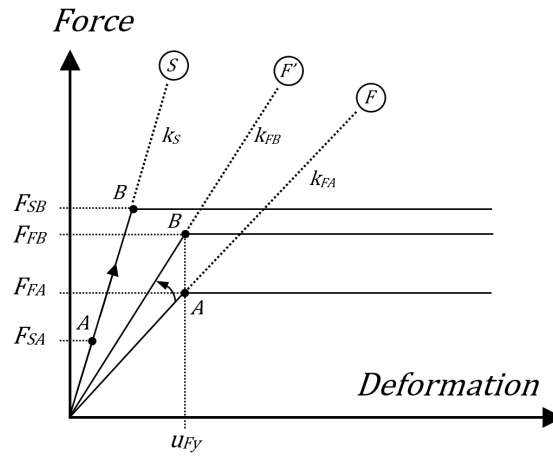


Figure 3.4: Force- displacement behavior of structural members and strength design demands in a single story asymmetric system.

Typical plan of a single story stiffness eccentric shear frame is shown in Figure 3.3. The force-deformation relations of the stiff edge and flexible edge members are schematized in Figure 3.4. Strength demands from both edge members are marked by A, lower at the stiff edge (F_{SA}) and higher at the flexible edge (F_{FA}), as a consequence of the design approach explained above. The existing strength supply at

the stiff edge F_{SB} however is much larger than the design demand F_{SA} due to the strength-stiffness dependent overstrength. Designer has no control over this value, it is a direct consequence of preliminary design. There is no such problem at the flexible edge because stiffness related overstrength does not exist. Then the only option for the designer is to increase the flexible edge strength from F_{FA} to F_{FB} in order to obtain a balanced inelastic seismic performance. Such modification in the flexible edge strength is also accompanied by the increase of stiffness, from k_{FA} to k_{FB} , hence leading to a reduction in the stiffness eccentricity as well as reduction in free vibration periods. Yield displacement u_{FY} is not affected significantly from strength increase. In fact, this is the main reason behind strength-stiffness dependency.

An inelastic single-story asymmetric structure with varying system parameters is developed in the next subsection, and analyzed under design spectrum compatible ground motions. Then using these analysis results, unsymmetrical response spectra are derived in order to classify and elaborate the correlations between system parameters and asymmetric response. Later, sensitivity of torsionally coupled response to structural system parameters, particularly to the asymmetric strength distribution is further investigated in detail. Finally, a design strategy is proposed for achieving a balanced ductility distribution.

3.3 Parametric Description of the Single-Story Asymmetric System

Schematic representation of the single story shear frame was shown above in Figures 3.3 and 3.4. It is composed of two lateral load resisting members carrying an infinitely rigid slab. Lateral stiffness of the flexible edge (FE) member is k_F and that of stiff edge (SE) member is k_S . Translational mass and mass moment of inertia of the slab in each unique model are constant. CM is located at the middle of flexible and stiff edge members. The resulting model possesses one-way asymmetry and two degrees of freedom; translation (u_y) in the direction of analysis (y-axis) and rotation (u_θ) induced by stiffness asymmetry.

The analytical model is conceived in an entirely parametric manner so that a multitude of parameter variations could be investigated. The stiffness eccentricity (e_s in

Figure 3.1), two vibration periods and earthquake response reduction factor (R_μ) due to ductility vary among different variants. Additionally, Stiff to Flexible Strength Ratio ($SFSR$) is also considered as a system parameter, where $SFSR = F_{SY}/F_{FY}$ simply.

The ranges of each system (model) parameter are listed in Table 3.1. The translation dominant fundamental period T_n for each system is obtained by selecting the associated k_F and k_S . Vibration period of the rotation dominant second mode is always kept smaller than T_n , accordingly all systems are torsionally stiff. As discussed in Chapter 1, this is consistent with the provisions of contemporary seismic design codes. The ratio of the two periods depend on the stiffness eccentricity. They are given in Table 3.2 for the considered eccentricities. The ratio of equivalent uncoupled rotational to translational frequencies w_θ/w_y is 1.23 for all parametric systems. The effect of this choice on the presented results is discussed at the end of Subsection 3.4.1.

Table 3.1: Variation of design parameters for the single story structure

Design Parameter	Selected Values
e	0.05 – 0.10 – 0.15 – 0.20 – 0.30
T_n (s)	0.1 to 3.0 with 0.1 second increments (30 values)
R_μ	2 – 3 – 4 – 6
$SFSR$	0.5 to 3 with 0.1 increments (26 values)

Table 3.2: The ratios of first and second periods of the parametric systems corresponding to design eccentricities

e	0.05	0.10	0.15	0.20	0.30
T_1/T_2	1.25	1.33	1.45	1.60	2.07

Linear elastic response spectrum analysis is first conducted for each model under the design spectrum in Figure 3.5, for calculating the linear elastic strength demands at the flexible and stiff edge members in view of seismic code procedures (ASCE/SEI 7-10 [4], Eurocode 8 [30], Turkish Earthquake Code [73]). Design strengths of both components are calculated by introducing the load reduction factor R . Then the ratio

of the stiff edge strength to the flexible edge strength $SFSR$ is varied incrementally by imposing intrinsic overstrength to the stiff edge nominal strength, i.e. increasing F_{SA} to F_{SB} as shown in Figure 3.4, while keeping the flexible edge strength at its nominal design value F_{FA} as described above. This strength increase at the stiff edge does not necessitate a stiffness change in our analytical approach since the stiff edge stiffness is inherently associated with its existing strength F_{SB} . The stiff edge strength demand F_{SA} here is not related with its existing stiffness in reality, which is in fact the actual cause of the problem.

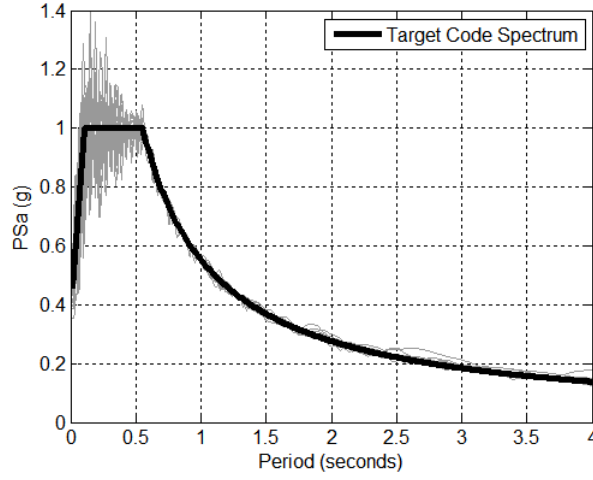


Figure 3.5: Acceleration response spectra of the thirty design spectrum compatible ground motions.

The seismic load reduction factor R employed in the description of single story asymmetric inelastic system models only consists of the ductility reduction component R_μ , hence $R = R_\mu$.

Following this step, a nonlinear model of each parametric system is prepared in OpenSees platform [65], which is used to perform nonlinear dynamic analyses for each unsymmetrical system under design level ground motions. Both structural members are represented by “zeroLength” elements available in the OpenSees element library. Elastic-perfectly plastic bilinear force-displacement relationships are defined for the two structural elements in the direction of analysis. These bilinear response curves are then assigned to the zeroLength members in the direction of analysis. Since mass distribution is assumed uniform over the rigid slab, center of mass coincides

with the geometric center of the model.

3.3.1 Strong Ground Motions and Dynamic Analyses

Nonlinear response history analyses are performed under several strong ground motions in order to study the seismic response of asymmetric single story systems with several design variants. A set of design spectrum matched strong ground motion records is generated for this purpose. Thirty different strong ground motion records are arbitrarily selected from the PEER NGA Database [66]. Detailed information on the selected records are presented in Table 3.3. These records are processed by using RSPMatch2005 [42] to match the design response spectrum defined in ASCE/SEI 7-10 [4]. An imaginary location in downtown San Francisco on Site Class C is selected in order to construct the target design spectrum. Consequently, mapped MCE_R spectral response acceleration parameters at short periods (S_S) and at 1 second (S_1) are determined for the representative site. The parameters associated with this site yields $S_{DS} = 1.0g$. Using the constructed design spectrum, a spectrum-matched strong ground motion set composed of thirty records is produced where their response spectra are presented in Figure 3.5. Design (target) spectrum is also plotted on the same figure. The differences between the individual and target spectra at short periods is a natural consequence of the spectrum matching procedure. However, we do not expect significant influence of these differences on the results since the evaluations are based on mean results of 30 ground motions.

In total, 468,000 dynamic analyses have been carried out on 15,600 analytical models constructed for each combination of design parameters, under the set of 30 strong ground motions. Mean response quantities obtained from these analyses are compiled for the classification and evaluation of results.

3.4 Unsymmetrical Response Spectrum

The focus of this thesis study is detailed investigation of inelastic member displacements and their distribution in asymmetric systems. Damage expected in the structural members of the representative single story frame is a direct consequence of the

Table 3.3: Unmodified strong ground motions and their properties

GM No.	NGA Code	Earthquake	M_w	PGA (g)	Site Geology
GM1	TMB205	Parkfield - 1966	6,19	0,293	C
GM2	UC2090	Loma Prieta - 1989	6,93	0,342	C
GM3	WPI046	Northridge - 1994	6,69	0,385	D
GM4	A-TAR000	Whittier Narrows - 1987	5,99	0,596	D
GM5	ABBAR-L	Manjil, Iran - 1990	7,37	0,505	C
GM6	AND250	Morgan Hill - 1984	6,19	0,343	C
GM7	B-PTS225	Superstition Hills - 1987	6,54	0,451	D
GM8	C05085	Parkfield - 1966	6,19	0,377	D
GM9	CPE045	Victoria, Mexico - 1980	6,33	0,572	C
GM10	375-E	Düzce, Turkey - 1999	7,14	0,737	C
GM11	DAY-LN	Tabas, Iran - 1978	7,35	0,351	C
GM12	DZC270	Kocaeli, Turkey - 1999	7,51	0,326	D
GM13	G02090	Loma Prieta - 1989	6,93	0,353	D
GM14	G03090	Loma Prieta - 1989	6,93	0,462	D
GM15	H-E07230	Imperial Valley - 1979	6,53	0,42	D
GM16	H-E08230	Imperial Valley - 1979	6,53	0,538	D
GM17	HEC090	Hector Mine - 1999	7,13	0,306	C
GM18	KAK090	Kobe, Japan - 1995	6,9	0,267	D
GM19	LGP090	Loma Prieta - 1989	6,93	0,783	C
GM20	LOB000	Loma Prieta - 1989	6,93	0,457	C
GM21	MU2035	Northridge - 1994	6,69	0,51	C
GM22	NWH360	Northridge - 1994	6,69	0,698	D
GM23	OBR360	Northridge - 1994	6,69	0,467	D
GM24	ORR360	Northridge - 1994	6,69	0,49	C
GM25	PAR-T	Northridge - 1994	6,69	0,505	D
GM26	A-MAT353	New Zealand - 1987	6,6	0,293	C
GM27	STG000	Loma Prieta - 1989	6,93	0,382	C
GM28	STM360	Northridge - 1994	6,69	0,591	D
GM29	STN110	Whittier Narrows - 1987	5,99	0,123	D
GM30	SYL090	Whiter Narrows - 1987	5,99	0,056	C

maximum ductility demands. Accordingly, the main response parameter obtained from the analyses has been selected as the maximum mean ductility demands from the stiff and flexible edge members calculated for each parametric design under the set of ground motions. The stiff edge ductility demand μ_S and the flexible edge ductility demand μ_F indicate the damage levels in these members. Plastic displacements cannot be transformed into plastic rotations and accordingly to damage with the employed model, because member lengths and section properties are not assigned.

Due to the large number of parametric systems, mean results are obtained from non-linear response history analyses under the set of 30 ground motions. Mean maximum member ductility demands are then categorized and mapped onto the Stiff to Flexible Strength Distribution Ratio ($SFSR = F_{SY}/F_{FY}$) vs. fundamental (translation dominant) period (T_n) plane. These graphics are prepared separately for the design eccentricity (e) and ductility reduction factor ($R\mu$) values. The resulting contours of the mapped response parameters yield charts that are called as *unsymmetrical response spectrum*. Each $SFSR$ vs. T_n plot for a specific set of e and $R\mu$ pair displays two sets of contour lines; one for the maximum mean ductility ratio observed at the flexible edge member ($\mu_{F,max}$), and the other at the stiff edge ($\mu_{S,max}$). Unsymmetrical response spectra provide a handy tool for the structural engineer in performing structural design, and can help structural engineer to estimate the system performance conveniently by using the specific design parameters T_n , $R\mu$, e and F_{SY}/F_{FY} in the early stages of seismic design.

Unsymmetrical response spectra are grouped per static eccentricity (e), and presented in Figures 3.6-3.10. In each Figure, spectra compiled for values of $R\mu = 2, 3, 4$ and 6 are displayed in a subplot format. For a specified system period T_n and $SFSR$, the corresponding contour values for maximum ductility demands from the flexible and stiff edge members are obtained.

The new parameter introduced in this research is the strength distribution ratio $SFSR = F_{SY}/F_{FY}$, describing the distribution of strength between stiff and flexible edge members. Accordingly, the results presented in Figures 3.6 - 3.10 are primarily evaluated in order to assess the influence of strength distribution ratio $SFSR$ on seismic performance. However, common trends can be observed from the unsymmetrical

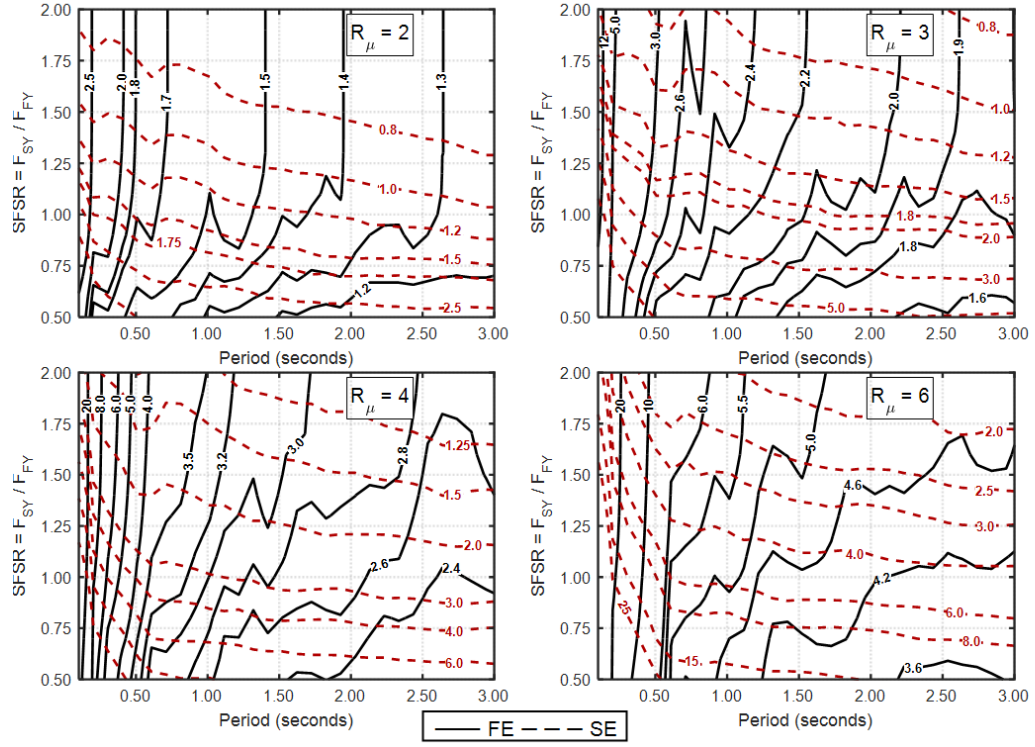


Figure 3.6: Unsymmetrical response spectra for $e = 0.05$.

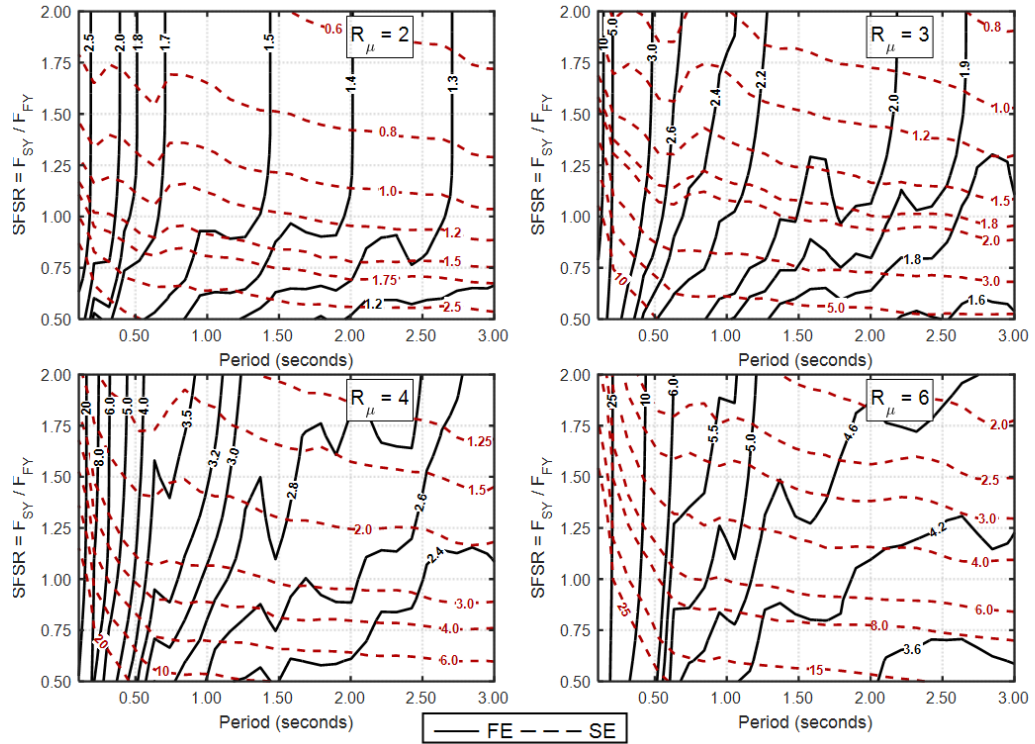


Figure 3.7: Unsymmetrical response spectra for $e = 0.10$.

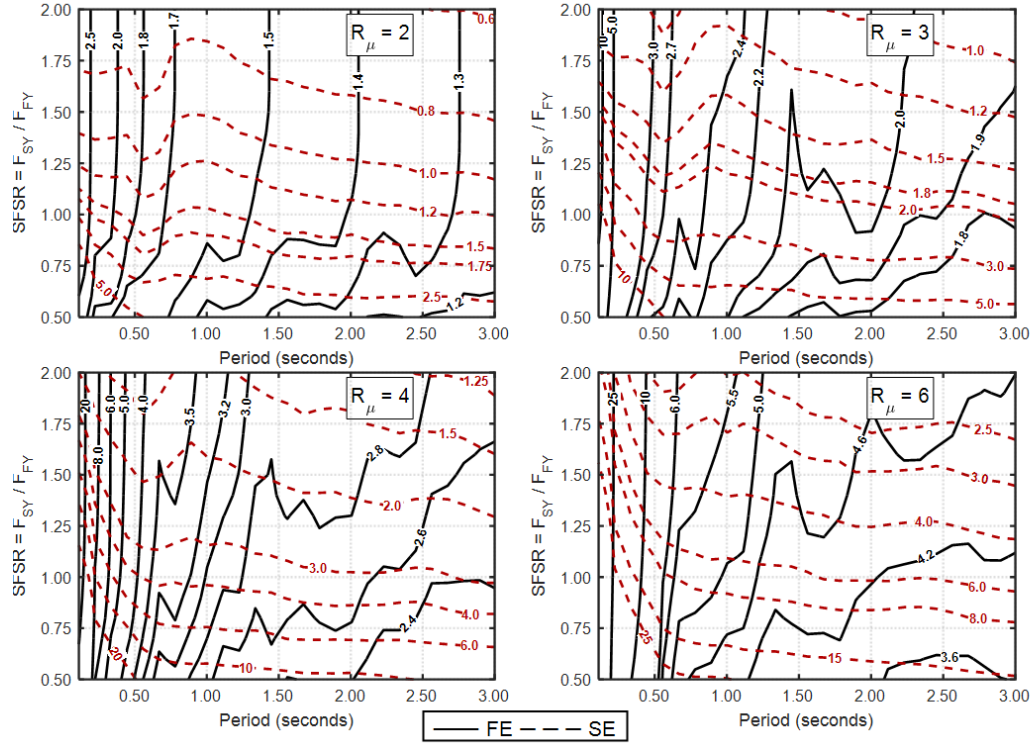


Figure 3.8: Unsymmetrical response spectra for $e = 0.15$.

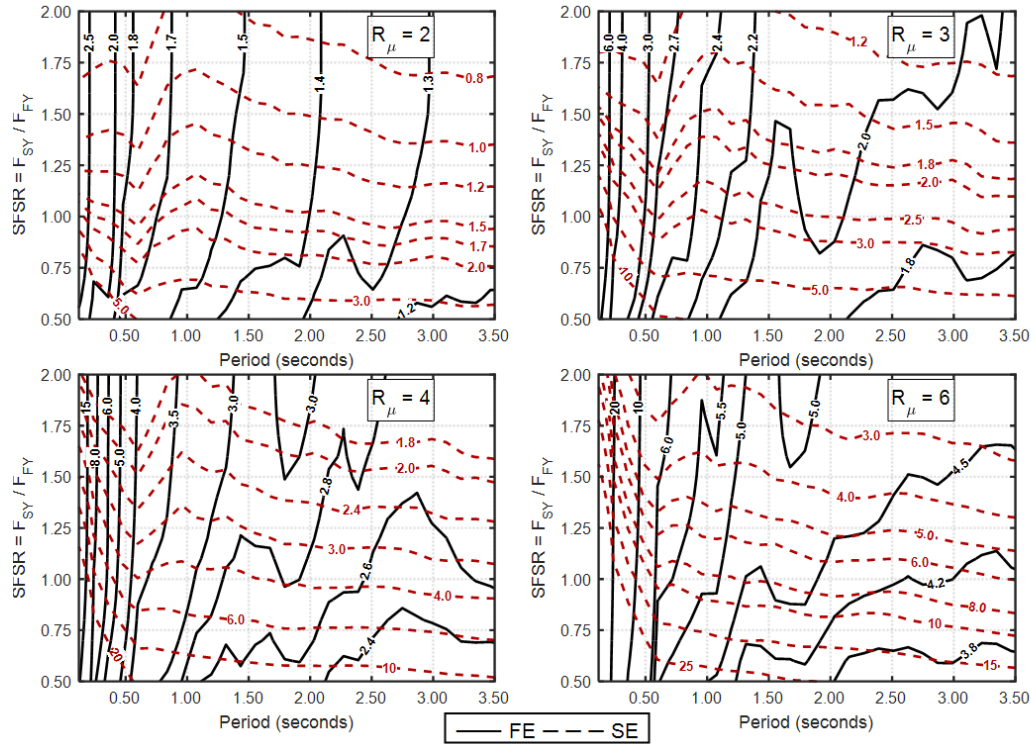


Figure 3.9: Unsymmetrical response spectra for $e = 0.20$.

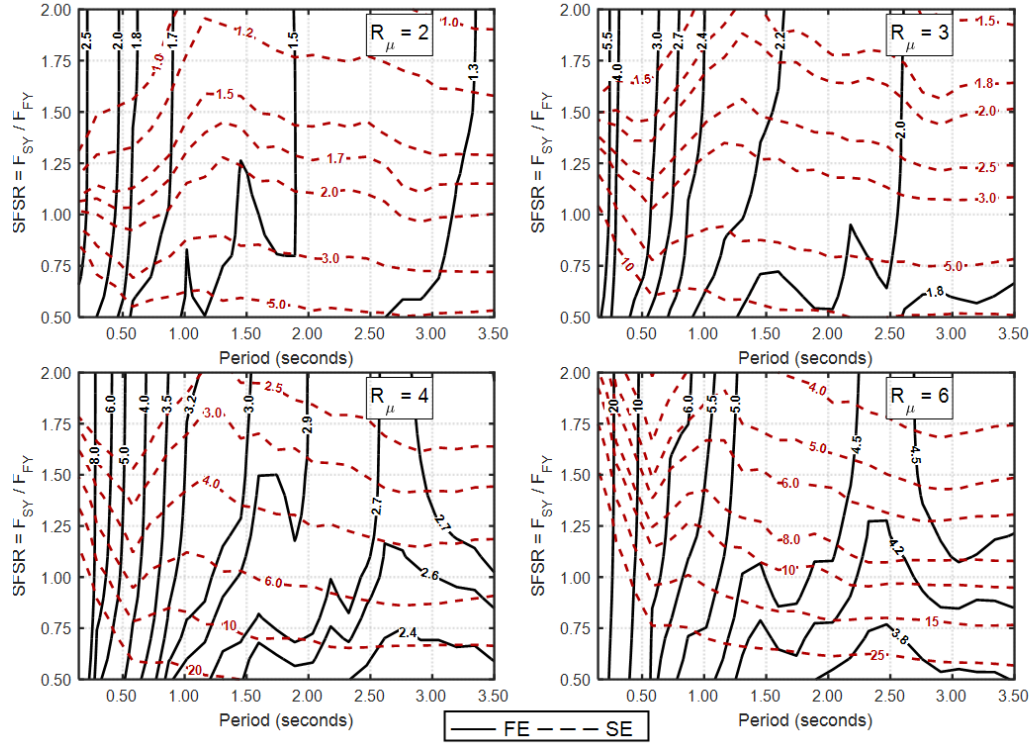


Figure 3.10: Unsymmetrical response spectra for $e = 0.30$.

response spectra presented in Figures 3.6 - 3.10, regarding the variations of the performance parameters μ_S and μ_F with the other system parameters e , $R\mu$, and T_n as well.

- (a) It can be observed in all figures that maximum ductility demand at the stiff edge μ_S reduces with increasing strength ratio whereas maximum ductility demand at the flexible edge μ_F reduces with increasing translational vibration period. This observation is valid for all e and $R\mu$ combinations. Therefore, it can be concluded in general that stiff edge ductility demand is primarily sensitive to strength ratio but less sensitive to period, whereas the flexible edge ductility demand is primarily sensitive to translational vibration period but less sensitive to strength ratio.
- (b) When $R\mu$ is larger than 3, flexible edge ductility demands increase significantly at very short periods, and stiff edge ductility demands increase significantly as $SFSR$ ratio falls below 1.

- (c) For constant ductility reduction factors $R\mu$, the flexible edge ductility demand is not sensitive at all to stiffness eccentricity e whereas the stiff edge ductility demand is more sensitive to e . μ_S increases slowly with e as e changes from 0.05 to 0.10 and to 0.15, then increases faster as e exceeds 0.20. This observation is elaborated in Figure 3.11 below for $R\mu = 4$ and $SFSR = 1$.

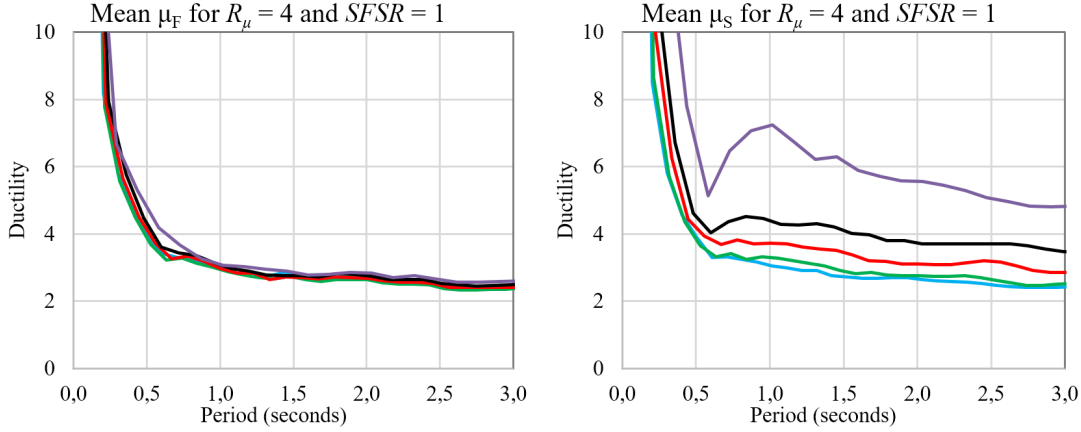


Figure 3.11: Mean ductility spectra for $R\mu = 4$ and $SFSR = 1$ at the flexible (left) and stiff (right) edges.

- (d) For constant stiffness eccentricities e , both the stiff edge and flexible edge ductility demands increase with the ductility reduction factor $R\mu$, although at different rates. The rate of increase of the flexible edge ductility demands with $R\mu$ is fairly independent of e , however the rate of increase of the stiff edge ductility demands with $R\mu$ increases with e . These observations are indeed consistent with the observations stated in (b). Graphical interpretations are presented in Figure 3.12 for $e = 0.10$ and $e = 0.20$.

In summary, it can simply be concluded that the ductility demands of the stiff and flexible edges of an asymmetrical system depend quite differently on the system parameters.

3.4.1 Sensitivity of Results to Uncoupled Torsional-to-Lateral Frequency Ratio

The single story asymmetrical systems employed for obtaining the presented results have been designed for an arbitrary constant torsional-to-lateral frequency ratio

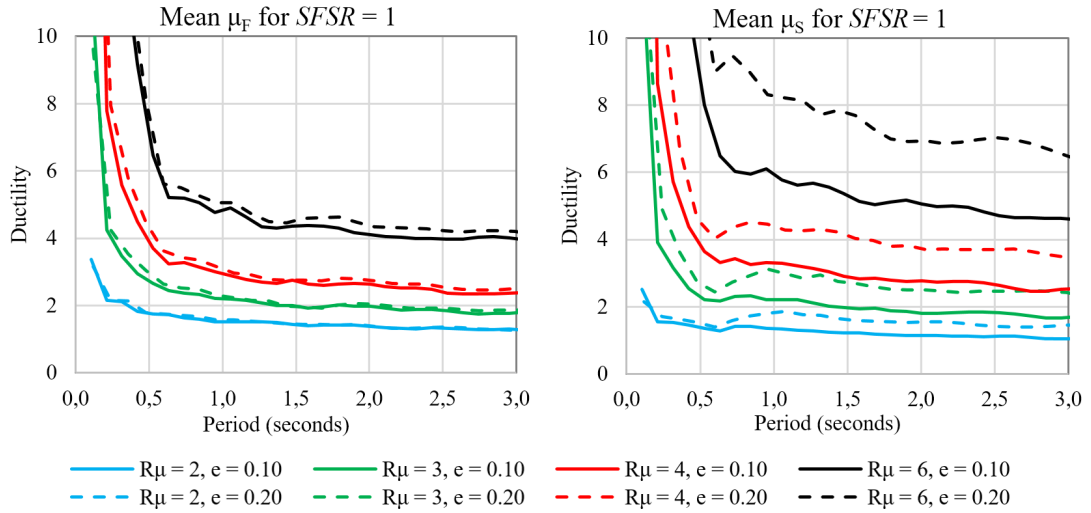


Figure 3.12: Mean ductility spectra for constant e and $SFSR = 1$ at the flexible (left) and stiff (right) edges.

$\Omega \equiv w_\theta/w_y = 1.23$ in order to limit the variable system parameters to a reasonable number. $\Omega = 1.23$ represents a torsionally stiff system. A sensitivity analysis is conducted for investigating the effect of Ω on the results obtained. Mean ductility spectra for the flexible and stiff sides are calculated for constant values of $SFSR = 1$, $R\mu = 4$, $e = 0.15$ and $e = 0.30$ whereas Ω is varied from 1.0 (torsionally equally stiff) to 1.12, 1.23, 1.39 and 1.58 in each combination.

The results are presented in Figure 3.13. It can be observed that mean ductilities at the flexible side are insensitive to Ω for both e value of 0.15 and 0.30. Only the bounding value of $\Omega = 1$ differs slightly from the other curves. Mean ductility spectral curves at the stiff side display more variations with Ω , yet the only significant separation noticed is for $\Omega = 1$. Mean ductility spectra for all other torsionally stiff systems are quite close to each other, and $\Omega = 1.23$ employed in the analyses is a central value representing all torsionally stiff systems. Moreover, the variations in the spectral ductility curves vanish when Ω exceeds 1.5.

3.4.2 Sensitivity Analysis for Torsional Performance Parameters

Unsymmetrical response spectra facilitate observing the effects of system parameters on seismic performance. Each chart contains a large amount of response data

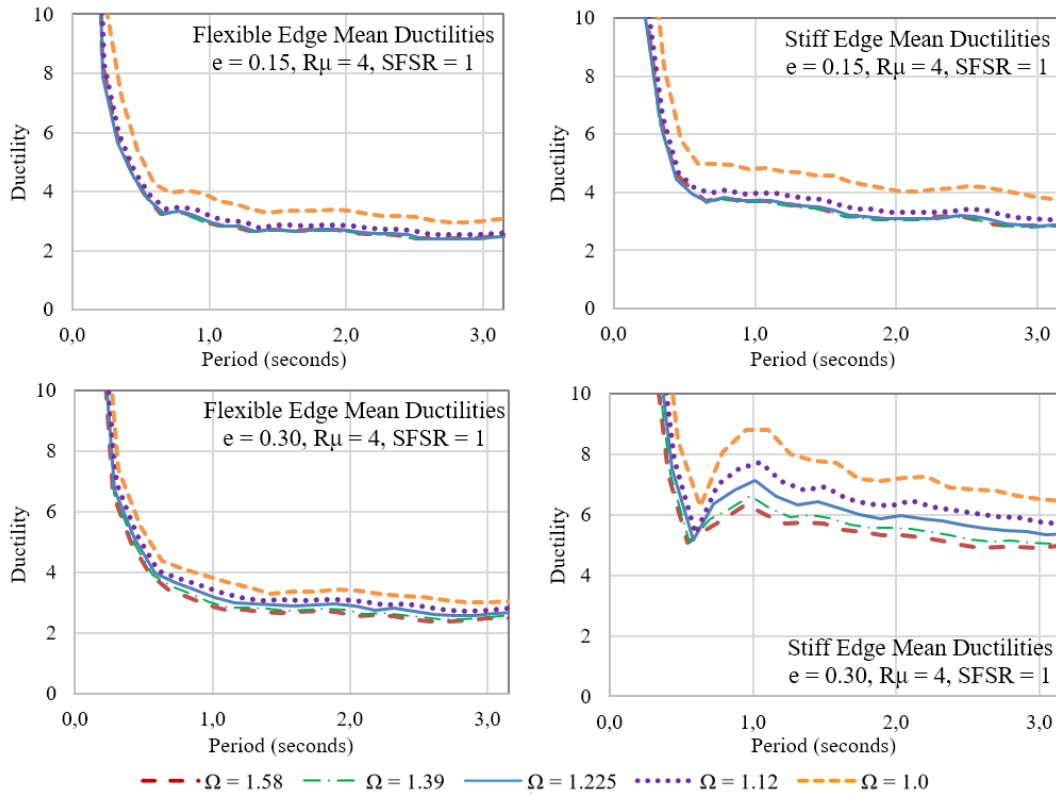


Figure 3.13: Mean ductility spectra at the flexible (left) and stiff (right) edges for $SFSR = 1$, $R\mu = 4$, $e = 0.15$ (top row) and $e = 0.30$ (bottom row).

regarding complex interactions among the set of design parameters. A more detailed inspection of the analysis result is carried out herein for having a better understanding of the correlations among the system and performance parameters of asymmetric systems. The effects of load reduction factor $R\mu$, strength distribution ratio $SFSR$, design eccentricity e and period T_n on unsymmetrical performance are investigated systematically in detail. The purpose of this investigation is to quantify the sensitivity of the asymmetric system response to variations in these design parameters, and reach informative conclusions.

Before progressing with the interpretation of asymmetric inelastic seismic response, design targets for acceptable seismic response should be revisited. An efficient seismic design for a structure that undergo inelastic response under severe ground motions can be considered as attaining reasonable and uniform distribution of ductility demands from ductile members. Modern seismic code provisions aim for a balanced inelastic deformation response such that a properly designed system is expected to exhibit a fairly uniform distribution of plastic deformations over the individual frames, and the resulting member damages satisfy the design assumptions under design level seismic excitation. The translation of this criteria to the simple one story asymmetric system employed in this part of the thesis study is simply achieving uniform ductility demands at the flexible and stiff edge members where the maximum member ductility $\mu_{max} \approx R$.

Figure 3.14 displays the variations of maximum ductility demands from flexible and stiff edge members with strength ratio for different load reduction factors $R\mu$. These results are obtained from the unsymmetrical response spectra presented above. Figure 3.14 is divided into subfigures for five different design eccentricities e and four separate T_n values of 0.5, 1.0, 1.7 and 2.5 seconds representing short, medium and long period systems. Consequently, inelastic response of both rigid-short period and flexible-long period structures are represented in Figure 3.14. Certain combination of design parameters leads to balanced ductility demand distributions as revealed by the results presented in Figure 3.14.

One can determine the intersection points of the flexible and stiff edge ductility ratios from the figure boxes in each sub-plot, and calculate the corresponding $SFSR =$

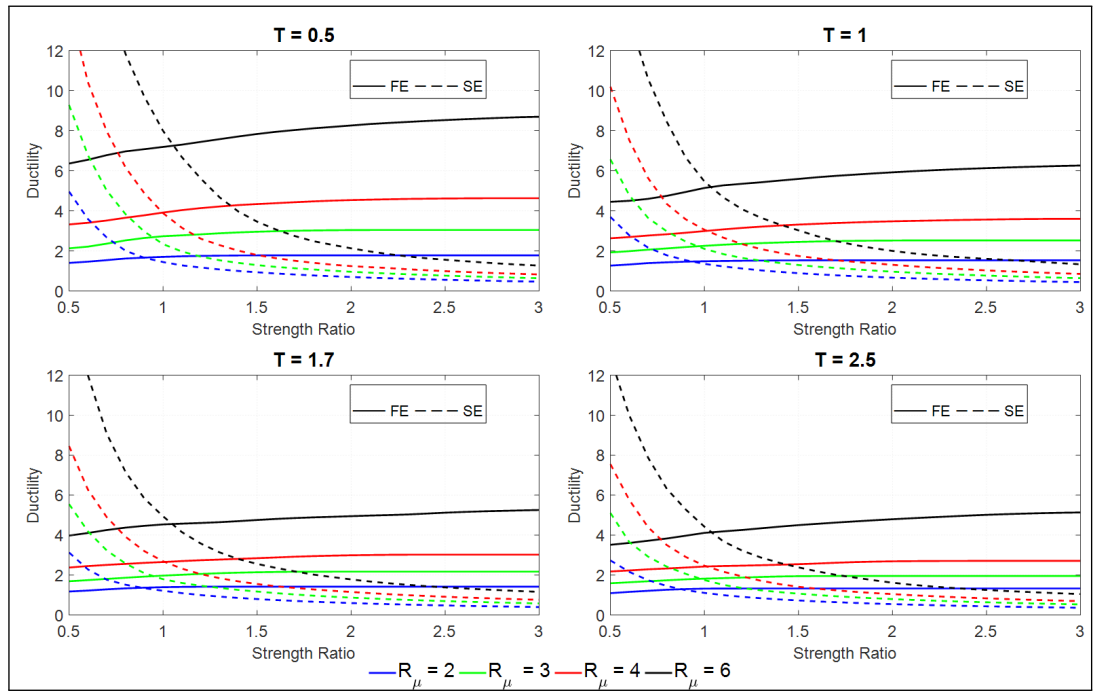
F_{SY}/F_{FY} for each $R\mu$, Tn and e . It can be observed that these ductility values at the intersection of the flexible edge and stiff edge curves at the associated strength ratios are fairly close to the force reduction factors $R\mu$ employed in design for short period systems whereas they are lower than $R\mu$ at medium and longer periods. For example, when $e = 0.10$ and $R\mu = 4$, the intersection of the red curves indicates that $\mu = 3.8$ at $T = 0.5$ s, $\mu = 3.0$ at $T = 1.0$ s, $\mu = 2.7$ at $T = 1.7$ s and $\mu = 2.3$ at $T = 2.5$ s.

The information obtained from Figure 3.14 can be presented graphically in a very useful format, in the form of a uniform ductility spectra as shown in Figure 3.15, for fixed values of $e = 0.05, 0.10, 0.15, 0.20, 0.30$ and 0.40 . Each figure box provides the optimum $SFSR$ for a given Tn , $R\mu$ and e combination corresponding to uniform ductility. Accordingly, we can choose an $SFSR$ value for our structure for a balanced ductility distribution. This is of course a design problem, transformed from an assessment problem. The basic difference is $SFSR$, which is the strength distribution ratio in asymmetric systems. We can simply impose this optimum strength distribution in the design of asymmetric systems for obtaining a balanced inelastic response.

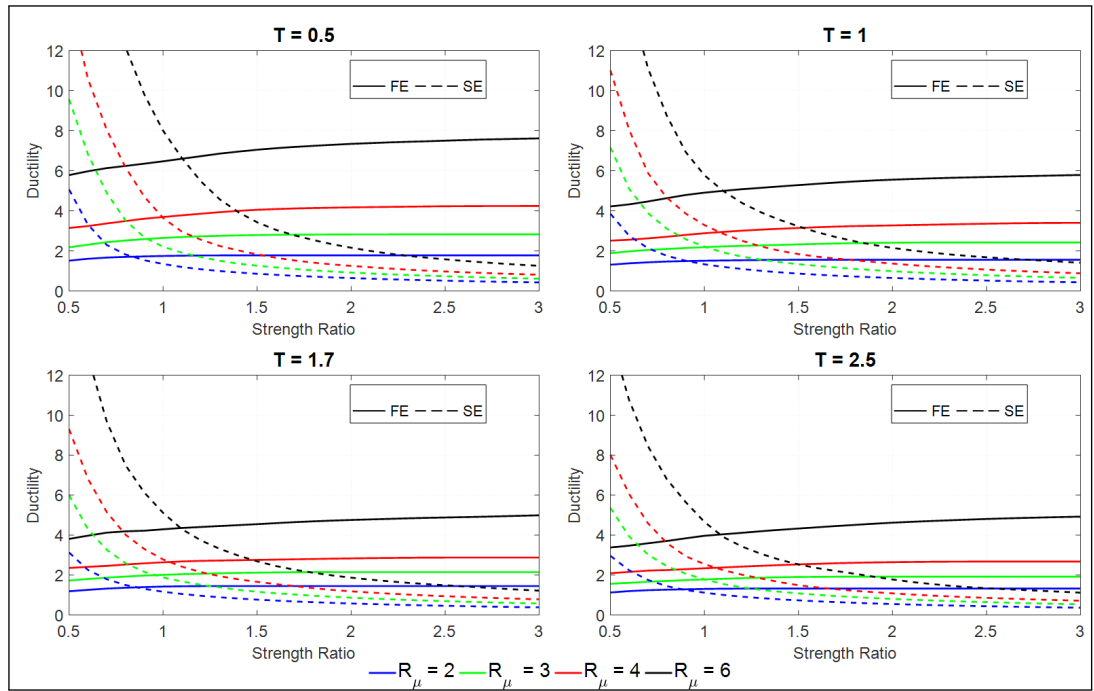
The nominal $SFSR$ values obtained from the code-based designs are also plotted in Figure 3.15. Note that the nominal $SFSR$ does not depend on R . The optimal strength ratios however increase with $R\mu$, and their dispersion slightly increases with e . When e is zero (symmetric system), the dispersion certainly becomes zero.

It is interesting to observe that the optimal $SFSR$ values are significantly higher than the nominal $SFSR$ values in all cases, except for $e = 0.4$ at long periods. However, the variations of optimal and nominal strength ratios with period are somewhat similar, despite significant differences in the amplitudes. They tend to get closer for more extreme eccentricities at longer periods. Accordingly, it can be concluded that the nominal strength distribution suggested by the current code approaches may only be reasonable for long period systems with large eccentricities exceeding 0.3. They are quite unrealistic for $e < 0.30$, which likely leads to unbalanced distribution of inelastic deformations. The differences are more severe at short periods.

One very interesting point is worth noticing here. The intrinsic overstrength of the stiff edge helps improving the inelastic seismic performance up to a certain level, without intention though. If the nominal design strengths had been possible to imple-

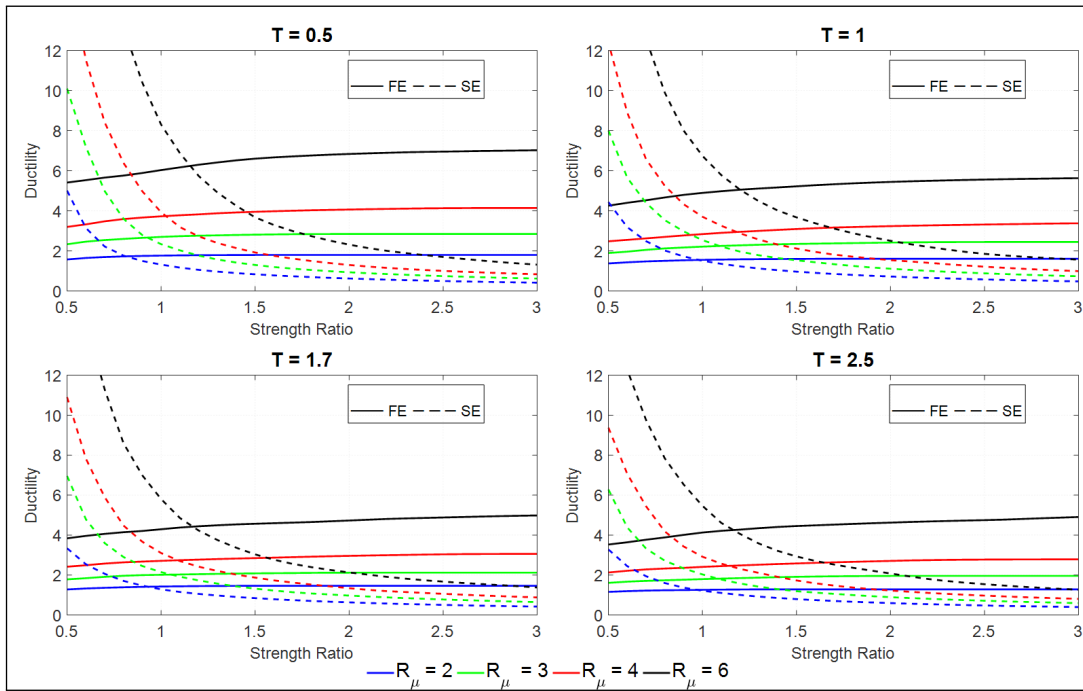


(a) $e = 0.05$

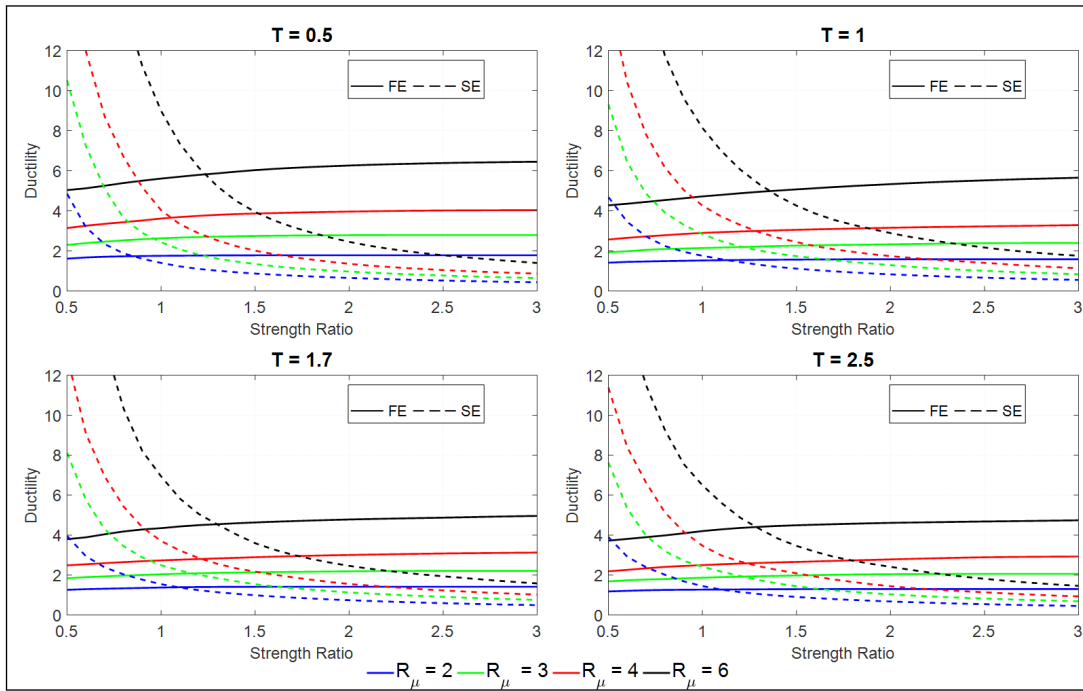


(b) $e = 0.10$

Figure 3.14: The effect of member strength distribution on torsional performance.

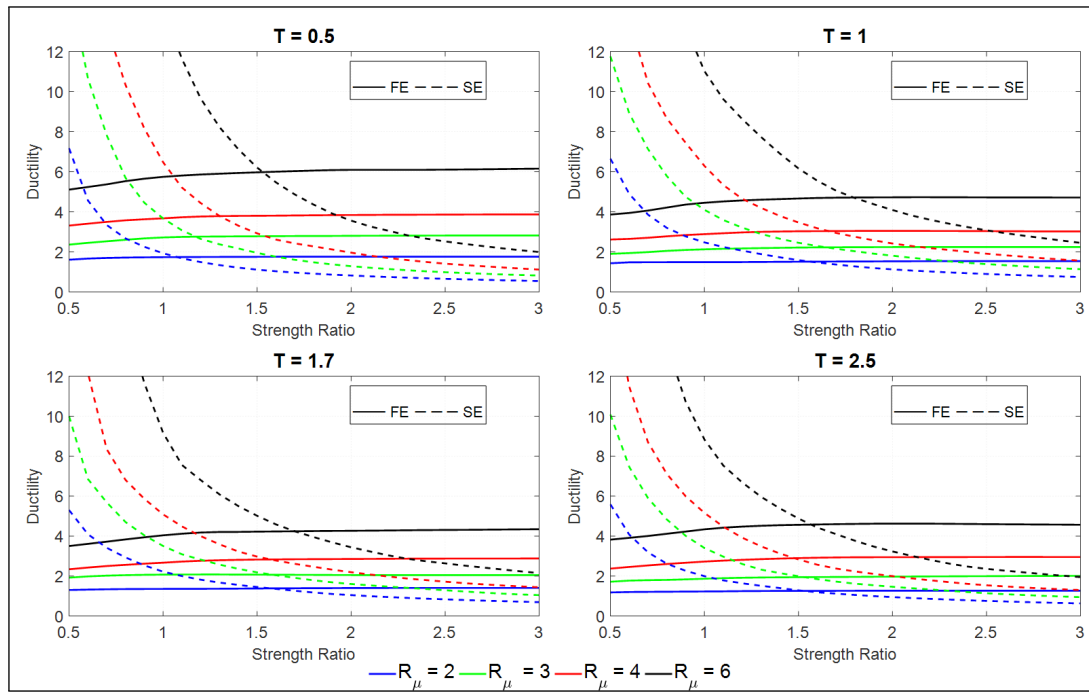


(c) $e = 0.15$



(d) $e = 0.20$

Figure 3.14: Continued



(e) $e = 0.30$

Figure 3.14: Continued

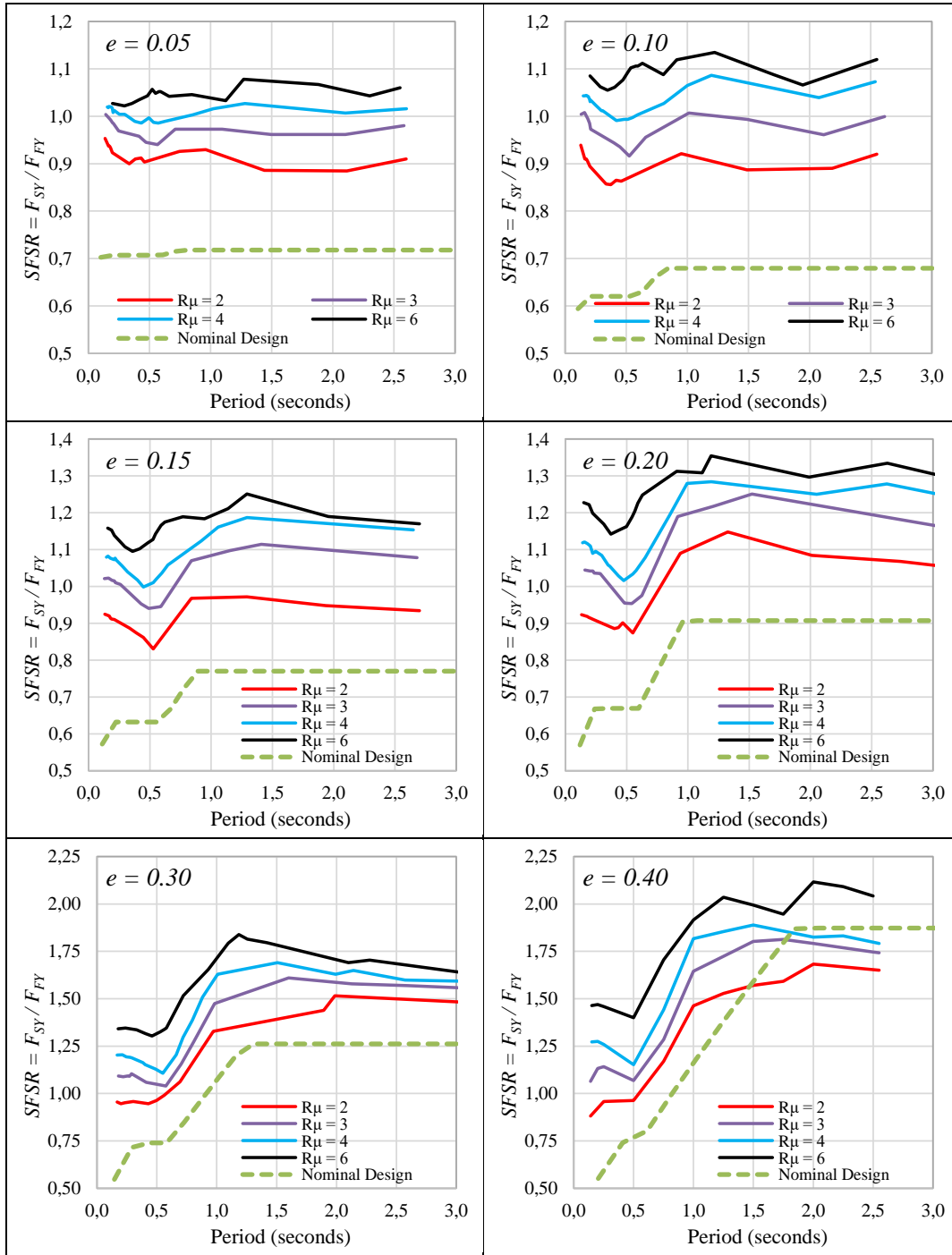


Figure 3.15: Uniform Ductility Spectra.

ment in the structural systems, this would have led to a very poor seismic performance in terms of the distribution of inelastic deformations. The overstrength available at the stiff edge improves inelastic seismic performance if $SFSR$ increases toward the optimal value. However, if it exceeds the optimal value due to excessive overstrength at the stiff edge, then a different strategy is required for obtaining a balanced inelastic deformation distribution. These alternative design strategies are discussed in the following section on simple numerical examples. In any case, the strength distribution obtained from the code procedures leads to almost the worst possible inelastic seismic performance. Accidental eccentricity cannot help correcting it. The “unintended” overstrength of the stiff edge masks this incorrect approach up to a certain level, although this is not recognized at all in the classical design approaches of modern seismic codes (ASCE/SEI 7-10 [4], Eurocode 8 [30], Turkish Earthquake Code [73]).

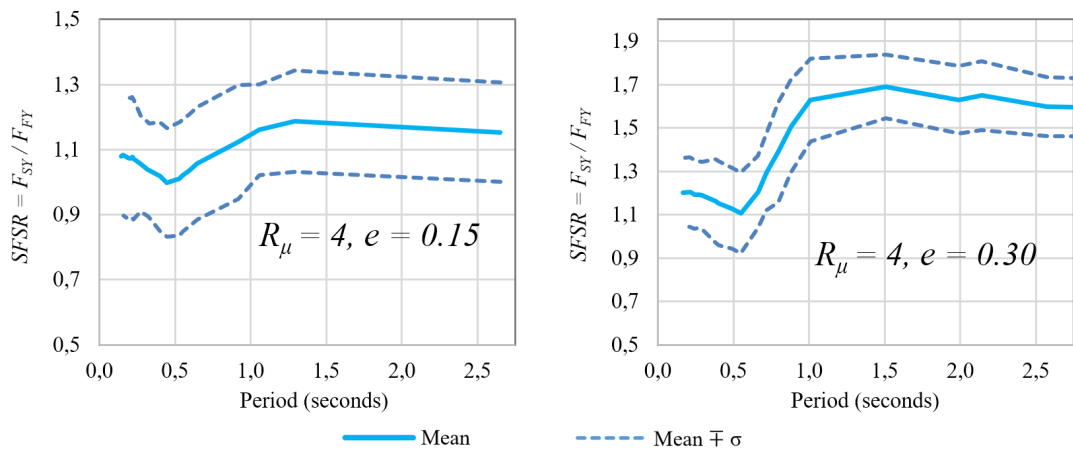


Figure 3.16: Variance of $SFSR$ in Uniform Ductility Spectra.

The variance of $SFSR$ in uniform ductility spectra is further investigated for $R_\mu = 4$ and $e = 0.15, 0.30$. The results for both combinations are plotted in Figure 3.16. Coefficients of variation in Figure 3.16 for $e = 0.15$ are approximately 0.17 for $T < 1$ s, and 0.13 for $T > 1$ s. Similar values for $e = 0.30$ are 0.14 and 0.10. These variations for 30 ground motions can be considered quite reasonable, and justify the stability of mean values.

3.5 A Simple Design Procedure for Achieving Balanced Inelastic Seismic Response Distribution in Asymmetric-Plan Systems

The previous part of this chapter is devoted to investigating the basic characteristics of unbalanced inelastic seismic response distribution in single story asymmetric systems, mainly resulting from the existing strength distribution. In this section, a simple procedure is proposed where strength distribution ratio *SFSR* is employed as a design parameter for obtaining a balanced inelastic response distribution.

The proposed procedure is introduced on 12 representative case studies with three different fundamental periods of 0.5, 1.0 and 2.5 seconds, and four stiff edge overstrength ratios Ω_{SE} of 1.0 (nominal), 1.5, 2.0 and 2.5, combined accordingly. All 12 systems are torsionally stiff where $w_\theta/w_y = 1.23$, and $e = 0.3$ in all cases.

The nominal design strengths are first determined according to seismic codes (ASCE/SEI 7-10 [4], Eurocode 8 [30], Turkish Earthquake Code [73]) for $R\mu = 4$ under the design spectrum in Figure 3.5, without considering accidental eccentricity. Stiff edge overstrengths (Ω_{SE}) are imposed on the nominal design strength demands. Then their mean seismic displacements are calculated under the set of 30 ground motions by assuming elasto-plastic force-displacement hysteresis. The capacity curves and mean maximum displacements of the flexible and stiff edge members of the 12 systems are presented in Figure 3.17.

Uniform ductility spectra given in Figure 3.15 are utilized with the associated T_n , $R\mu$ and e values of the 12 systems, and optimal *SFSR* values are determined which ensure uniform ductility demand at both edges. If the existing *SFSR* value is less than the optimal *SFSR* value (first row in Figure 3.17), then the stiff edge strength is increased to reach the optimal *SFSR*, and the stiff edge stiffness is adjusted accordingly to maintain the strength-stiffness relation, i.e. the stiff edge yield displacement is kept unchanged. On the other hand, if the existing *SFSR* value is larger than the optimal *SFSR* value (third and fourth rows in Figure 3.17), then the flexible edge strength is increased in order to reach the optimal *SFSR*, and the flexible edge stiffness is adjusted accordingly to maintain the strength-stiffness relation. The flexible edge yield displacement is kept unchanged in this case. The existing and the revised system

responses are marked in Figure 3.17 on the bi-linear capacity curves, with solid and dashed lines, respectively. Ductility demands from the existing system components are marked by a solid dot, and the ductility demands from the revised system are marked by a vertical bar.

Coincidentally, the existing and optimal *SFSR* of the systems with stiff edge over-strength ratios of 1.5, shown at the second row are close to each other. Hence, a design revision in their existing states may not be required.

Mean values of the stiff and flexible edge ductilities of the existing systems (μ_S and μ_F) and the revised systems (μ'_S and μ'_F) have been calculated under the set of 30 ground motions, and marked in Figure 3.17. Apparently, stiff and flexible edge ductility ratios of the revised systems approach notable uniformity compared to the existing systems. However exact equality $\mu'_S = \mu'_F$ cannot be achieved since the system properties, namely the modal vibration periods change during the design revisions. An iterative approach is not suggested because the improvements can be considered satisfactory.

Seismic responses of the 12 pairs of existing and revised systems under the set of 30 ground motions with amplitudes scaled by 1.5 have also been calculated. The results are shown in Figure 3.18. Significant improvements in the distribution of inelastic deformations are observed similarly under higher intensity ground motions that represent maximum expected earthquake intensity in probabilistic terms.

3.6 Discussions

The *Unsymmetrical Response Spectra* proposed enable the designer to estimate the inelastic seismic response of asymmetric structures and the associated damage distribution before detailed analysis. This is also valid for the existing structures. Common preliminary design parameters such as stiffness eccentricity, fundamental period and response reduction factor as well as the strength distribution ratio after preliminary design are sufficient for obtaining a reliable performance estimation of an asymmetric plan system.

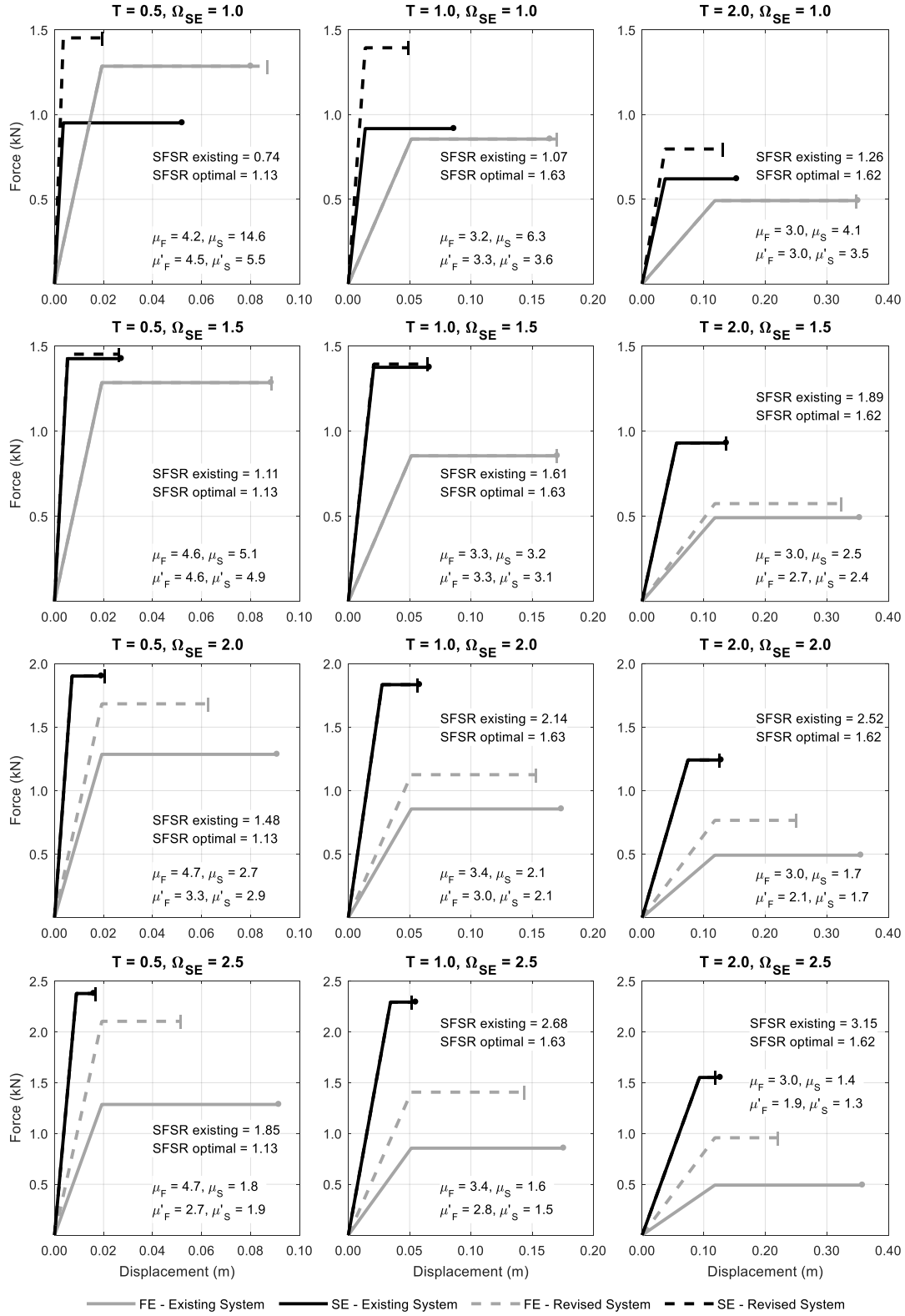


Figure 3.17: Force-displacement responses of existing and revised single story asymmetric systems under design ground motions.

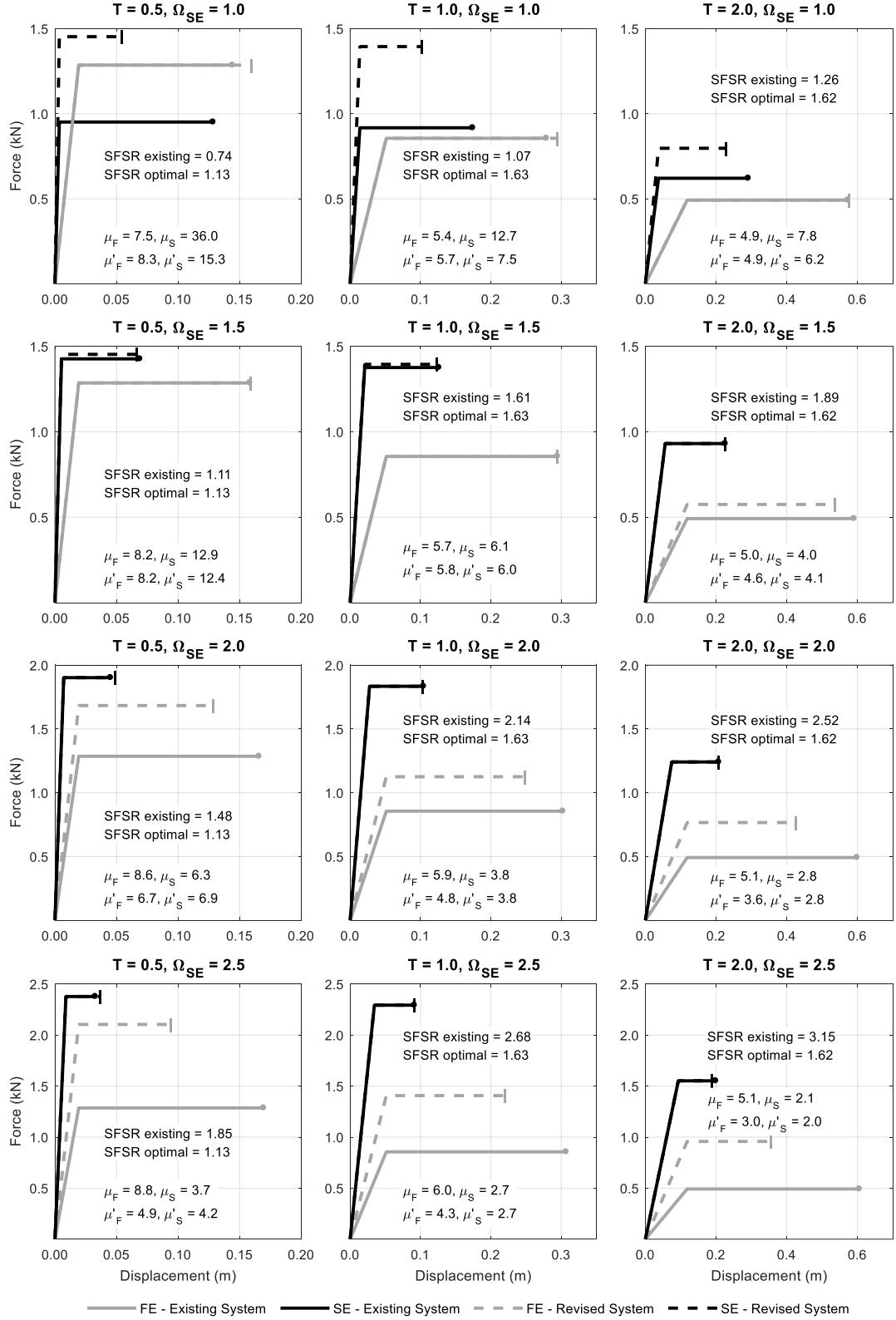


Figure 3.18: Force-displacement responses of existing and revised single story asymmetric systems under scaled ground motions.

The simple design rule developed in the previous section simply suggests increasing the nominal stiff edge to flexible edge strength ratio, or *SFSR* in asymmetric systems where the amount of increase is related with the ductility reduction factor, stiffness eccentricity and vibration period. By doing so, an optimal design could be achieved compared to the associated nominal system, which results in a balanced ductility demand from the stiff and flexible edges of asymmetric systems. *Uniform Ductility Spectra* is developed accordingly for facilitating seismic design.

Investigation of the obtained results indicates that the current code approaches lead to a very unfavorable, unbalanced strength distribution in asymmetric systems regarding their inelastic seismic response under design level ground motions. Code regulations appear only reasonable for long period asymmetric systems possessing extreme eccentricities. The results presented in this study are obtained from a simple two degree of freedom parametric inelastic model. Hence, they cannot be directly generalized to multistory structural systems without proper evaluation. In order to expand the concept presented here to more complex frame systems, a thorough procedure is developed in the next chapter for multistory structures in order to achieve a balanced design in terms of ductility demands and seismic responses. Case studies have been designed with the proposed procedure and investigated in detail in the following chapters.

CHAPTER 4

A PROPOSED METHOD FOR OBTAINING OPTIMAL STRENGTH DISTRIBUTION IN ASYMMETRIC STRUCTURES

4.1 Introduction

A methodology is proposed in this chapter for achieving an optimal strength distribution in the design of asymmetric-plan MDOF structures. It is postulated that a strength distribution that results in a balanced ductility distribution can be achieved by using the *Uniform Ductility Spectra* (Figure 3.15) that was introduced in Chapter 3. The optimal value of Stiff-to-Flexible-Edge Strength Ratio ($SFSR_{opt}$) is obtained from the Uniform Ductility Spectra associated with the investigated structure. This ratio is then utilized to revise the strength distribution of lateral load resisting elements for improved inelastic seismic performance.

4.2 Identification of the Problem

There are well-known causes for uneven strength distribution in asymmetric-plan structures. The most important one is the stiffness asymmetry, which is the focus of this study. Due to factors such as design code requirements and more importantly because of the natural relationship between stiffness and strength, stiff side members usually attain much higher strengths than what is required by analysis. The stiff side of an asymmetric system tends to attract lower seismic demands compared with the flexible side because of code based linear elastic analysis. This situation results in a structural design with large overstrength at the stiff side members while the flexible side members can be assigned capacities close to their demands. As seen in the

results of the parametric study discussed in Chapter 3, the resulting system exhibits irregular response due to this overstrength. Hence, ductility distribution is mostly far from being uniform.

In order to address this issue, a new design method is developed herein, and presented in the following sections.

4.3 The Optimal Strength Distribution Method

A simple one-story, two degree of freedom system with stiffness asymmetry is shown in Figure 4.1. Having determined the structural eccentricity (e_s), first mode period (T_n) and estimating the ductility reduction factor (R_μ) of the structure, lateral load analysis could be performed to determine the strength demands on both stiff and flexible members. In fact, computed demands are the nominal strengths where the effect of overstrength is not present. When these nominal strengths are assigned to both end members as $F_{S,nominal}$ and $F_{F,nominal}$, a line connecting the two values in Figure 4.1 express the nominal strength distribution. However, nominal strength distribution cannot be attained in a structure due to the reasons explained previously, related to different sources of overstrength. Significant overstrength of the stiff side due to strength-stiffness dependency and inherent overstrength associated with the flexible side member yields two existing member strengths which are denoted as $F_{S,existing}$ and $F_{F,existing}$. The line between these values yields the existing strength distribution in Figure 4.1. Stiff-to-Flexible Strength Ratio associated with the existing strength distribution ($SFSR_{existing}$) can simply be computed by using the existing strengths of both members. $SFSR_{existing}$ is instrumental in estimating the level of expected uneven inelastic response from the existing design of the structure.

It is also possible to determine the optimal Stiff-to-Flexible Strength Ratio ($SFSR_{opt}$) for the system. $SFSR_{opt}$ can be obtained from the Uniform Ductility Spectra (Figure 3.15) by using the basic structural characteristics. Then, both structural members can be assigned the strengths ($F_{S,optimal}$ and $F_{F,optimal}$) such that $SFSR_{opt}$ is attained. The resulting strength distribution associated with $SFSR_{opt}$ is called optimal strength distribution in Figure 4.1.

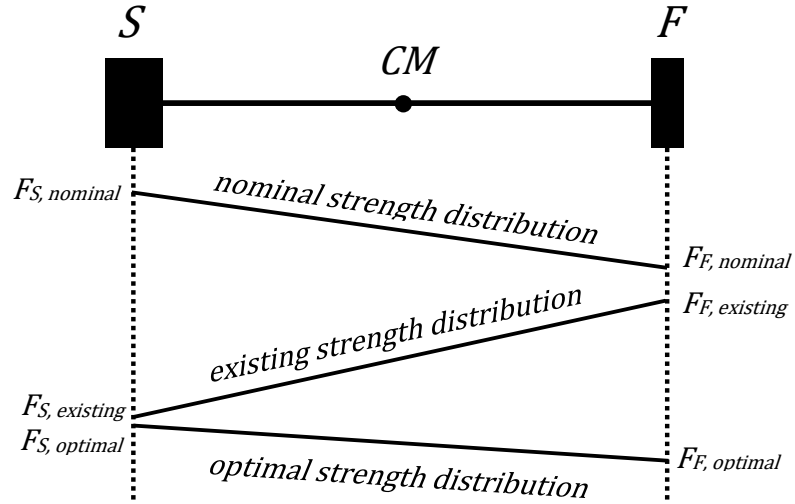


Figure 4.1: Schematic representation of the simple asymmetric system.

It is postulated here that if the existing strength distribution of the system after its design can be modified in a way such that it is brought to the optimal strength distribution; then the system is expected to exhibit balanced ductility performance under strong ground motions. This can be achieved by applying an additional equivalent lateral static force/torque to the system. The structure is then analyzed under the superimposed combination of this additional force and the code based seismic design forces. Structural members designed under the combined effect of both loads are expected to attain their optimal strengths for a balanced inelastic seismic performance. Consequently, $SFSR_{opt}$ is achieved.

The additional load consisting of a translational force and a torque is applied at the mass center of the structure in Figure 4.1. It is called the Optimal Load Vector in this study, and expressed in Equation 4.1.

$$\Delta F = \begin{bmatrix} \Delta V \\ \Delta T \end{bmatrix} \quad (4.1)$$

Derivation of this load vector depends on the existing strengths of structural members in a system. It is preferred to perform the derivation for two distinct cases in terms of the $SFSR$ values. The first case is for a structure where $SFSR_{existing}$ is lower than $SFSR_{opt}$ (Case I). In order to achieve optimal $SFSR$ value, stiff edge member strength

needs to be increased. In the second case, $SFSR_{existing}$ is higher than the $SFSR_{opt}$ (Case II). This time, flexible edge member strength is to be increased in order to attain the optimal SFSR value. Both of these cases are presented on simplified sketches which are called the Strength Allocation Diagrams. They yield the formulation of Optimal Load Vector.

4.3.1 Case I: Strengthening the Stiff Edge Member

The Strength Allocation Diagram for the single story, two degree of freedom system is presented in Figure 4.2. For the sake of simplicity, flexible edge member of this structure has been designed to meet its design demand exactly. Hence, flexible edge member has the nominal strength (F_F) as its existing strength. On the other hand, there is an overstrength (Ω_S) on the stiff edge member; therefore its existing strength is $\Omega_S F_S$. The line connecting these strength values designates the existing strength distribution of the structure.

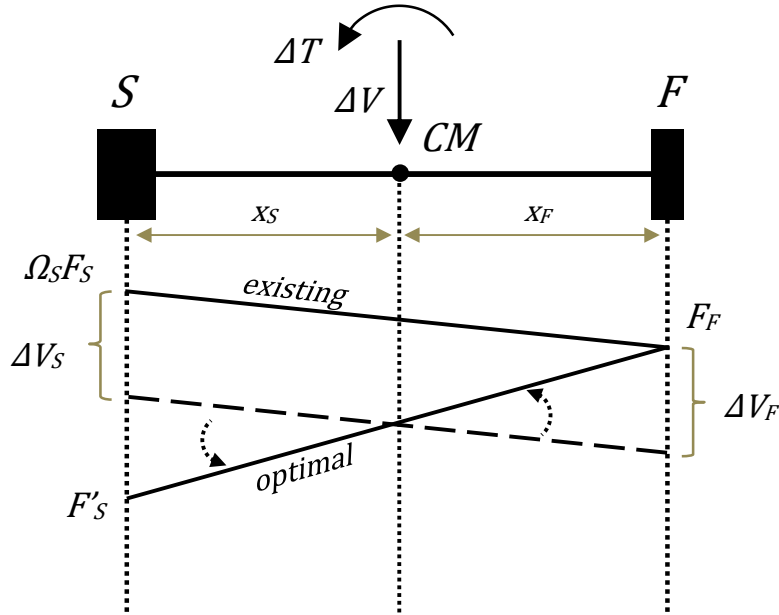


Figure 4.2: Strength Allocation Diagram constructed for Case I type system.

In order to achieve $SFSR_{opt}$, stiff edge member has to be strengthened to attain its new value, F'_S . The line between the updated stiff edge strength and the nominal flexible edge strength yields the optimal strength distribution of the structure. Through

the application of the method, existing strength line will be brought to the optimal strength line. This is achieved by applying ΔV and ΔT to the center of mass. The process can be presented in two steps for clarity. First, ΔV is obtained by computing the difference between the total values of optimal and existing strengths as shown in Equation 4.2. The difference arises from the stiff side only.

$$\Delta V = F'_S - \Omega_S F_S \quad (4.2)$$

When ΔV is applied to the system, it is shared by both edge members with respect to their distances to the center of mass (x_F and x_S). If the center of mass is at the middle for this specific system, both members attain the same force increment, i.e. half of ΔV . The dashed line in Figure 4.2 drawn from these increased strength values now needs to be "*rotated*" by means of a torque in order to match it with the *optimal* strength profile. ΔT which would yield the intended rotation can simply be obtained by computing the moment of the force differences between both ends of the dashed line and the *optimal* strength line. It is given in Equation 4.3 below.

$$\Delta T = \Delta V_F x_F + \left(F'_S - (\Omega_S F_S + \Delta V_S) \right) x_S \quad (4.3)$$

The revised capacity of the stiff edge F'_S is expressed in Equation 4.4 in terms of $SFSR_{opt}$.

$$F'_S = F_F SFSR_{opt} \quad (4.4)$$

4.3.2 Case II: Strengthening the Flexible Edge Member

Strength Allocation Diagram for a structure where flexible edge member requires additional strength is shown in Figure 4.3. The nominal strength demands of the stiff and flexible edge members are denoted by F_S and F_F , respectively. Existing strength of the stiff edge member that includes overstrength is shown by $\Omega_S F_S$. The value of the revised flexible edge strength, which is required to attain $SFSR_{opt}$, is indicated by F'_F . Since the existing stiff edge strength $\Omega_S F_S$ is kept constant in this case, the line

drawn from $\Omega_S F_S$ to F'_F gives the *optimal* strength line.

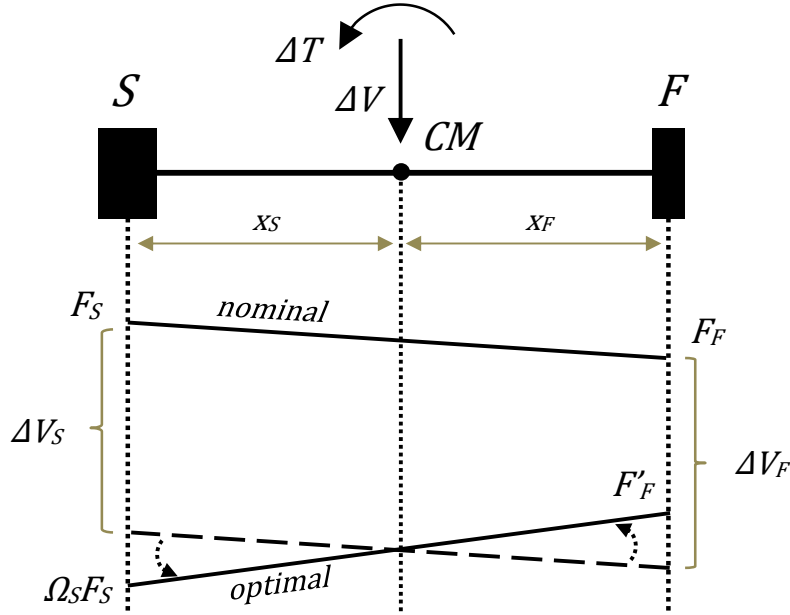


Figure 4.3: Strength Allocation Diagram constructed for Case II type system.

In order to compute the required translational force increment ΔV , the difference between the total nominal and updated strengths are computed in Equation 4.5.

$$\Delta V = (F'_F + \Omega_S F_S) - (F_F + F_S) \quad (4.5)$$

Similar to what has been observed in Case I, both members share this force increment with respect to their distances to the center of mass (x_F and x_S). Addition of the force increments to the nominal strengths of both members results in the strength distribution given by the dashed line in Figure 4.3. This line again needs to be "rotated" to match the *optimal* strength profile by applying the torque ΔT to the system. The required torque is computed in Equation 4.6 from the moment of the force difference between the updated strengths and member forces denoted by the dashed line.

$$\Delta T = (F_F + \Delta V_F - F'_F) x_F + (F_S (\Omega_S - 1) - \Delta V_S) x_S \quad (4.6)$$

The revised capacity of the stiff edge F'_F is given in terms of SFSR_{opt} in Equation 4.7

$$F'_F = \frac{F_S}{SFSR_{opt}} \quad (4.7)$$

The required amount of translational force and torque is computed directly from nominal strength values which are governed by the demands, stiff edge overstrength ratio and $SFSR_{opt}$.

4.3.3 Flowchart for the Optimal Strength Distribution Method

A flowchart describing the method is given in Figure 4.4. The procedure requires a decision about whether to strengthen the stiff or the flexible edge of a structure based on the comparison of $SFSR_{existing}$ and $SFSR_{opt}$. It should be noted that structures where stiff edge needs to be strengthened (Case I) are much rare due to the nature of the systems that are being investigated in the scope of this study. In stiffness asymmetric structures where significant stiff edge overstrength usually exists, flexible edge strength should be increased in order to achieve the optimal SFSR value that yields uniform ductility. This outcome is also supported by the results obtained from Unsymmetrical Response Spectra (Figures 3.6 - 3.10).

Considering its significant positive effect on improving the uneven seismic response, stiff edge overstrength is regarded as the most crucial parameter in calculating the Optimal Load Vector. Consequently, a sensitivity study about this parameter is conducted and presented in the following Section.

4.4 Sensitivity of the Method with Respect to Stiff Edge Overstrength

In this part of the study, sensitivity of the Optimal Load Vector elements to changing levels of stiff edge overstrength (Ω_S) is investigated. Specifically, systems where flexible edge needs to be strengthened (Case II) are studied due to reasons explained in the previous section. A suit of single-story, two degree of freedom parametric systems are evaluated to compute their corresponding Optimal Load Vectors. These parametric asymmetric systems have been previously discussed in detail in Section 3.3 and their schematic diagrams are presented in Figure 3.3.

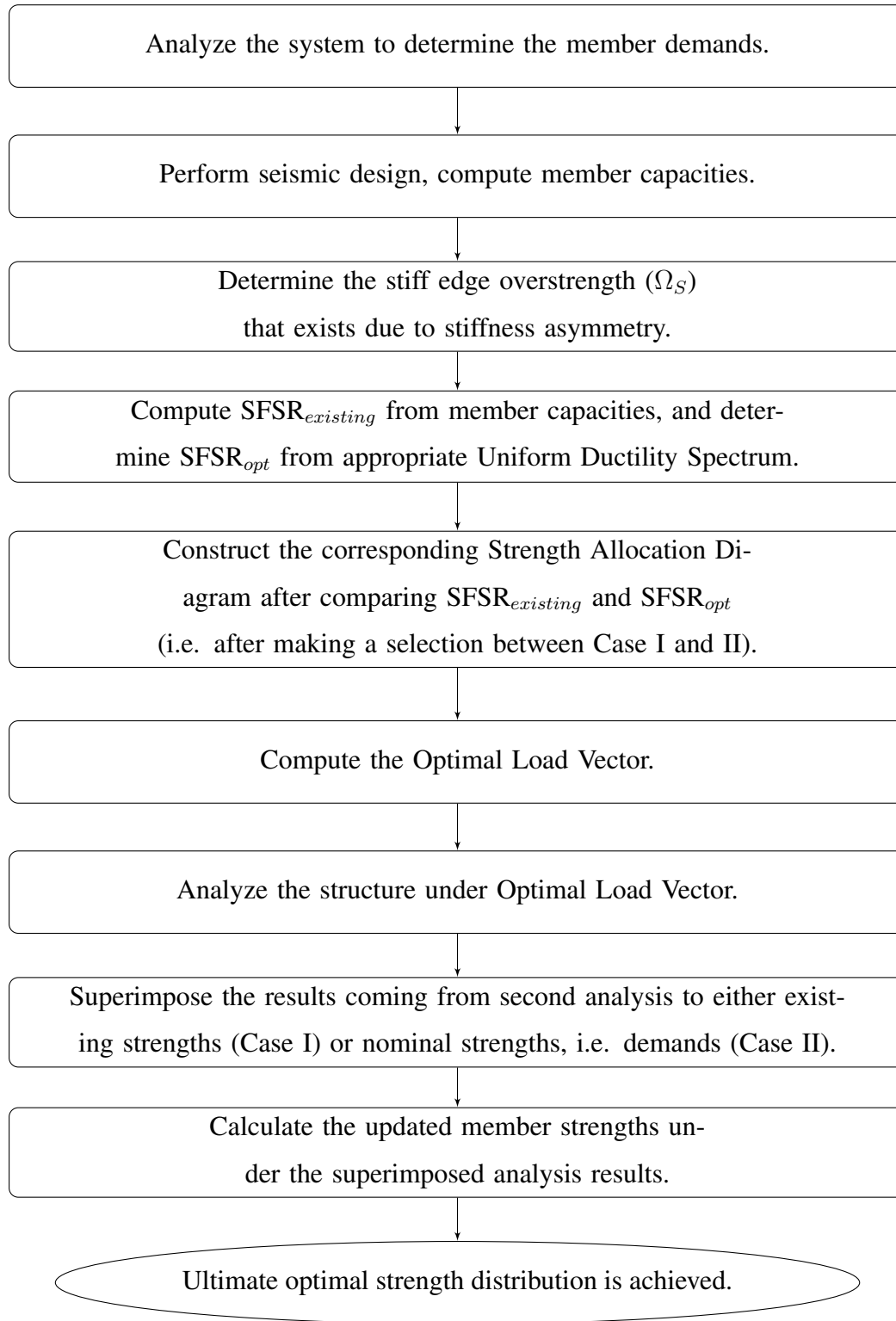


Figure 4.4: Flowchart for the Optimal Strength Distribution Method.

All of the selected parametric systems have a ductility reduction factor (R_μ) of 4 and a stiffness eccentricity of (e_s) 20%. Their fundamental periods (T_n) vary from 0.25 seconds to 3.0 seconds, with a period increment of 0.25 seconds. Thus, there are eleven structures having different dynamic properties. The stiff edge overstrength (Ω_S) of these individual systems are also selected as a design parameter. Ω_S ranges from 1.75 to 3.0 with increments of 0.25. In total, eleven separate systems had six different designs in terms of their stiff edge strength values. Consequently, sixty-six unique single story asymmetric structures are constructed.

These individual systems are analyzed under the Turkish Earthquake Code [73] design spectrum given in Figure 3.5 in order to determine the demands on stiff and flexible edge members. Then, the corresponding Ω_S is applied to the stiff edge member of each parametric system for determining their existing strengths. $\text{SFSR}_{\text{existing}}$ is then calculated and SFSR_{opt} value is determined from the appropriate Uniform Ductility Spectrum. ΔV and ΔT values for each system are then computed by employing the described procedure (Section 4.3). In order to normalize the values of calculated Optimal Load Vector elements, translational force ΔV and torque ΔT are divided by the base shear (V_b) and base torque (T_b) of each system, respectively. Finally, the variations of normalized force and torque values calculated for each system having different translational periods are plotted against stiff edge overstrength. These curves are shown in Figure 4.5 and Figure 4.6, respectively.

Results shown in Figures 4.5 and 4.6 display the expected relations between the required force increment and the stiff edge overstrength. Increasing levels of Ω_S requires an increase in the value of updated flexible edge strength (F'_F) in order to achieve SFSR_{opt} . Consequently; an upward trend is observed in normalized values of ΔV and ΔT . This trend is quite consistent; a linear correlation between stiff edge overstrength and force vector increment is seen, except for the normalized ΔT values computed for short-medium period systems ($T_n < 0.75$ seconds). In these systems, the required torque increment (ΔT) is somewhat insensitive to Ω_S .

Another interesting outcome is that both ΔV and ΔT are quite insensitive to translational period (T_n) of the designed system. The only exceptions to this observation are medium-short period structures where $T_n < 0.75$ seconds. Member strengths are a di-

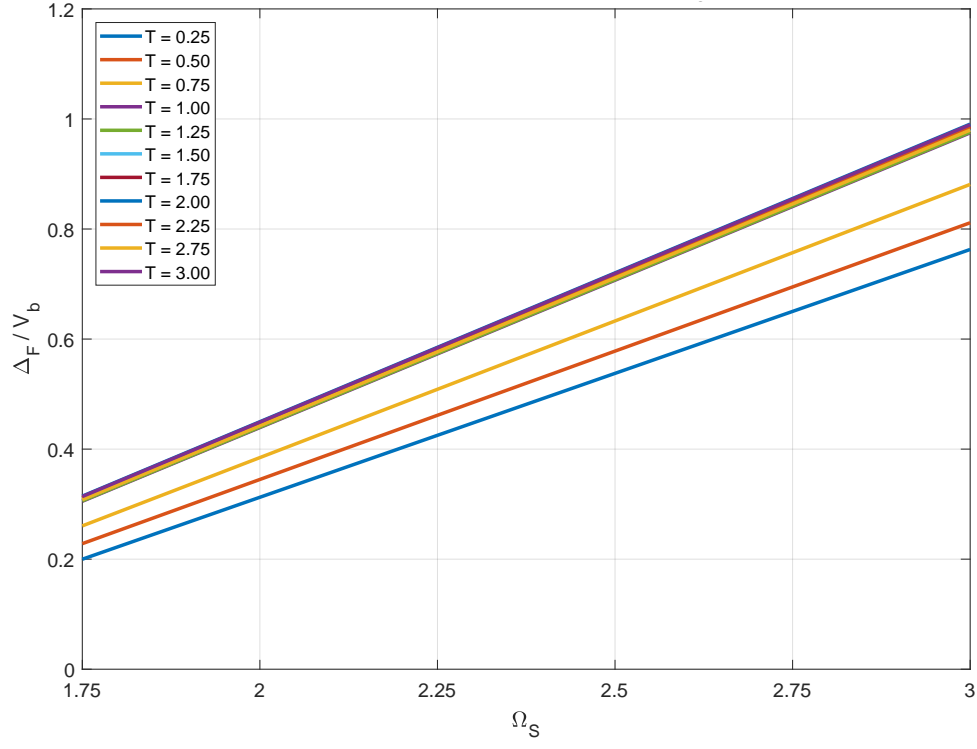


Figure 4.5: Variation of normalized ΔV with Ω_S .

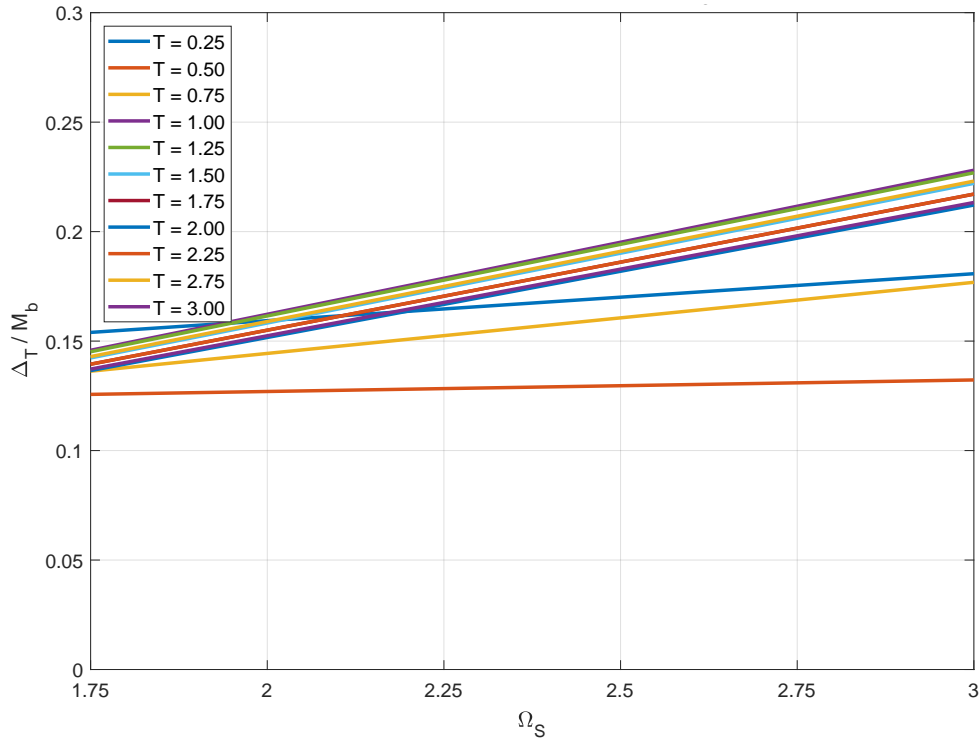


Figure 4.6: Variation of normalized ΔT with Ω_S .

rect function of the spectral acceleration values (Sa_n) that are used in seismic design. Spectral acceleration values corresponding to the first and second modes of these specific systems are on the spectral plateau where highest demands are registered. This is not the case for systems where $T_n > 0.75$ seconds. Sa_1 and Sa_2 values determined for these structures are located on the declining portion of the design spectrum. Consequently, ratio of spectral acceleration (Sa_1/Sa_2) of short period systems is different from what is observed for longer period structures. Distribution of strength demand along both structural members can be affected from this behaviour. In turn, computed ΔV and ΔT for short-medium period systems are quite different from longer period structures.

4.5 Verification of the Optimal Strength Distribution Method

In this section, a parametric case study is performed in order to test the performance of the Optimal Strength Distribution Method in achieving a balanced ductility distribution. Two DOF, single story shear frame parametric systems are again utilized and the improvement in their seismic performances with the suggested method is investigated.

Schematic representation of the single story shear frame was given in Figure 3.3. The two degrees of freedom of the model are translation (u_y) in the direction of analysis (y-axis) and rotation (u_θ) induced by stiffness asymmetry. Since the same parametric model presented in Section 3.3 is used, all constructed systems are again torsionally stiff. The ratio of equivalent uncoupled rotational to translational frequencies ω_θ/ω_y is 1.23 for all systems. The varying design parameters utilized for this verification study are stiffness eccentricity (e_s), fundamental period (T_n), ductility reduction factor (R_μ) and stiff edge overstrength (Ω_S). Selected values of these parameters are given in Table 4.1.

Table 4.1 yields six distinct nominal designs ($\Omega_S = 1$) with different dynamic properties. Typical force - displacement relationships of single story structures are shown in Figure 4.7 for a nominal design case where the stiff edge member has lower strength demand than the flexible edge member ($F_{SY} < F_{FY}$). The stiff edge strength F_{SY} is

Table 4.1: Selected design parameters for the single story system

Design Parameter	Selected Values
e_s	0.20 - 0.30
T_n (s)	0.5 - 1.0 - 2.0
R_μ	4
Ω_S	1.0 - 1.5 - 2.0 - 2.5

then increased incrementally from its nominal value by applying different values of Ω_S . Consequently, twenty-four unique designs are obtained.

In order to compute the ductility demands, nonlinear response history analyses under several strong ground motions are performed on analytical models of these systems prepared in the OpenSees Platform [65]. Same modeling techniques described in Section 3.3 are employed. For dynamic analyses, a set of 30 design spectrum-matched strong ground motion records that was generated and presented in Chapter 3 is utilized.

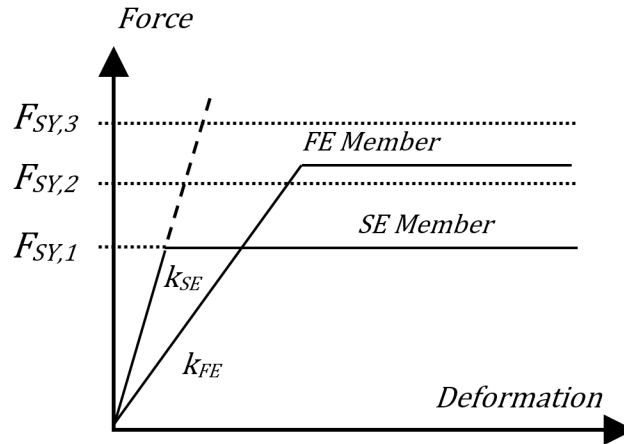


Figure 4.7: Typical force-deformation relationships of single story structures.

The procedure to analyze and compare the seismic responses of the existing and revised designs of asymmetric systems is as follows. First, each structure having a determined stiffness eccentricity (e_s), fundamental period (T_n), ductility reduction factor (R_{mu}) and stiff edge overstrength (Ω_S) has been designed, and this configuration was labeled as the *Existing Design*. $SFSR_{existing}$ values of these existing designs

have been calculated. Nonlinear dynamic analyses are then performed on analytical models and mean ductility demands computed for both flexible (μ_{FE}) and stiff (μ_{SE}) edges under the ground motion set has been recorded. Later, $SFSR_{opt}$ for each structure has been determined from their associated Uniform Ductility Spectrum. Using $SFSR_{opt}$, Optimal Strength Distribution Method has been applied to each systems and resulting structures has been labeled as *Updated Design*. These updated systems have also been analyzed under the ground motion set and mean ductility demands on both members have been recorded.

Two sets of ductility demands obtained both for existing and updated designs are grouped per design parameter and compared in Tables 4.2 and 4.3. Results are grouped in separate tables according to the two selected e_s values. In both Tables 4.2 and 4.3, main columns denote the selected fundamental periods of structures while each row displays their stiff edge overstrength. Ductilities recorded for each design are given in two groups labeled as *Existing* and *Updated*. $SFSR_{existing}$ values, which vary among different designs, are also given. $SFSR_{opt}$ associated with the updated designs are presented in both Tables, under the *Updated* label.

Table 4.2: Comparison of mean ductilities for existing and updated designs where $e_s = 0.20$

T_n (sec)	0.5					1.0					2.0				
Design	Existing			Updated		Existing			Updated		Existing			Updated	
				SFSR	1,01				SFSR	1,28				SFSR	1,26
Ω_S	SFSR	μ_{FE}	μ_{SE}	μ_{FE}	μ_{SE}	SFSR	μ_{FE}	μ_{SE}	μ_{FE}	μ_{SE}	SFSR	μ_{FE}	μ_{SE}	μ_{FE}	μ_{SE}
1	0,67	3,86	13,17	4,28	4,27	0,91	3,02	5,15	3,16	3,21	0,91	2,72	4,35	2,83	2,69
1,5	1,00	4,27	4,33	4,28	4,27	1,36	3,18	2,99	2,97	3,00	1,36	2,86	2,43	2,60	2,44
2	1,34	4,45	2,53	2,91	2,57	1,81	3,29	2,12	2,23	2,13	1,81	2,99	1,75	1,95	1,74
2,5	1,67	4,52	1,85	2,15	1,92	2,27	3,36	1,62	1,77	1,62	2,27	3,07	1,38	1,56	1,34

Comparison of μ_{FE} and μ_{SE} given in Tables 4.2 and 4.3 for both existing and updated designs reveals an improvement in terms of balanced ductility distribution. This is most pronounced in the cases where Ω_S is 1 (nominal design) and 2.5. In the case of $\Omega_S = 1$, there is no overstrength in the system; hence stiff edge members exhibit excessive ductility. The proposed method provides the required amount of strength to the stiff edge member (Case I) to bring the SFSR to the optimal value. Consequently, ductility distribution is considerably improved. In the other extreme case

Table 4.3: Comparison of mean ductilities for existing and updated designs where $e_s = 0.30$

T_n (sec)	0,5					1					2				
Design	Existing			Updated		Existing			Updated		Existing			Updated	
				SFSR	1,13				SFSR	1,63				SFSR	1,62
Ω_S	SFSR	μ FE	μ SE	μ FE	μ SE	SFSR	μ FE	μ SE	μ FE	μ SE	SFSR	μ FE	μ SE	μ FE	μ SE
1	0,67	4,15	14,61	4,60	4,89	0,91	3,21	6,27	3,33	3,13	0,91	2,97	4,13	2,99	2,97
1,5	1,00	4,59	5,10	4,60	4,89	1,36	3,32	3,20	3,33	3,13	1,36	2,99	2,45	2,49	2,48
2	1,34	4,71	2,68	3,18	2,83	1,81	3,39	2,11	2,47	2,14	1,81	3,01	1,72	1,80	1,75
2,5	1,67	4,75	1,80	2,29	1,92	2,27	3,42	1,60	1,94	1,60	2,27	3,03	1,36	1,44	1,38

where Ω_S is 2.5, there is hardly any ductility observed at the stiff edge members of the existing designs. Flexible edge ductilities are also fairly limited. By increasing the strength of flexible edge member through implementation of the proposed method (Case II), observed ductilities in updated designs are notably brought to a more even distribution.

Another observation is that as stiff edge overstrength increases, mean ductilities computed for stiff edge members of existing designs decreases. In the meantime, flexible edge ductilities do not change considerably. Updated designs obtained after Optimal Strength Distribution Method is applied remedy this ductility unbalance noticeably. When $\Omega_S = 1.5$, existing systems yield a somewhat balanced ductility distribution even before application of the method. Consequently, it can be concluded that an amount of stiff edge overstrength around $\Omega_S = 1.5$ is beneficial to achieve a reasonably uniform ductility in both members for this specific family of asymmetric structures.

It should also be added that $SFSR_{existing}$ values of structures having the same Ω_S do not differ from each other for $T_n = 1.0$ and 2.0 seconds. This is not the case for designs where T_n is 0.5 seconds, though. These structures are short period systems and their strength distribution is more sensitive to dynamic properties. This phenomenon was explained in detail during discussion of the sensitivity analysis in the previous section.

4.6 Implementation of the Optimal Strength Distribution Method to Building Structures

As shown in the previous section, application of Optimal Strength Distribution Method results in more uniform distribution of member ductilities in single-story shear frame systems. In this section, it is further extended to actual asymmetric structures composed of complex load resisting systems.

4.6.1 Construction of Equivalent Strength Allocation Diagrams

Proposed method utilizes Strength Allocation Diagram, which is a simple schematic tool for the strength distribution of an asymmetric system. Using the diagram, Optimal Load Vector is computed and design is updated. In order to use the same analogy, strength distribution of an actual asymmetric structure can be simplified such that it is possible to construct the equivalent Strength Allocation Diagram.

Force resisting planes in a structure can be represented in a simpler way by using equivalent structural elements. By doing so, systems such as moment-frames, frame-walls or shear walls can be idealized as single elements while keeping their stiffnesses and strengths the same. Later, these simplified structural elements can be separated into two groups with respect to their locations along structural plan. That is, multiple stiff side elements can be bundled up to form the equivalent stiff edge member. Similarly, equivalent flexible edge member can be obtained by combining the flexible edge elements. The two members are then placed at each side of the center of mass with respect to their locations. Finally, an equivalent Strength Allocation Diagram is obtained, which attains the total amount of stiffness and strength of the structure. The procedure explained here can be visualized in Figure 4.8. Respective locations of both flexible and stiff edge elements with respect to the center of mass of the final diagram is governed by the point of action of the resultant lateral force in both sides of the actual structural plan.

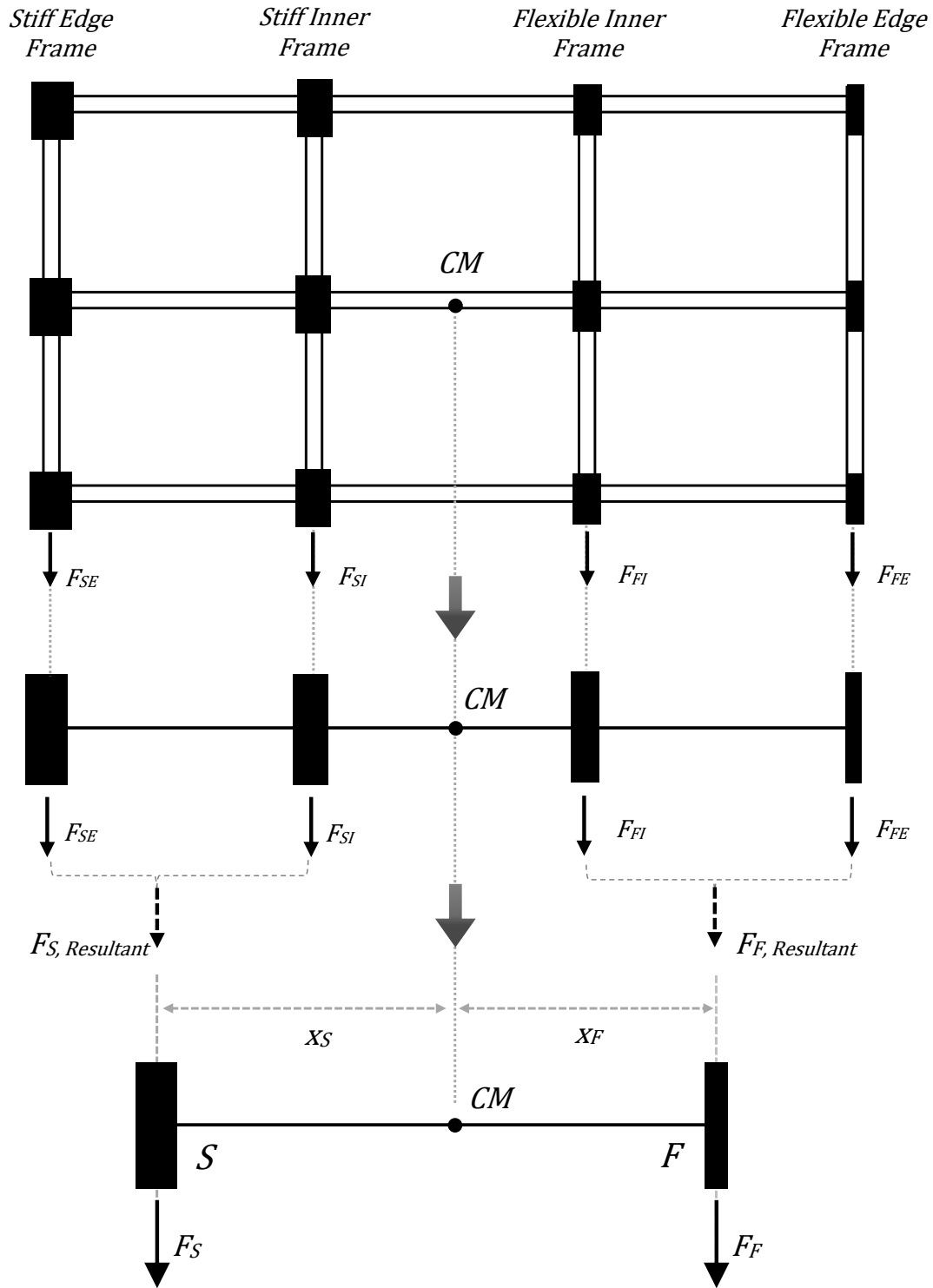


Figure 4.8: Construction of Equivalent Strength Allocation Diagram for a multi-story moment-frame building. Frames of the structure are labeled according to expected deformation patterns during seismic response.

4.6.2 Determination of Member Strengths

Strengths computed for the simplified elements that are utilized in the final diagram should be discussed in further detail. In case of simple shear frame structures, determining the strength of a load-resisting element is fairly straightforward. Since these elements resist loading in the direction of lateral response only, their assigned nominal capacities determined per seismic demands are indeed their own strengths. This is not the case for a building structure where beams, columns or shear walls undergo bending, shear or axial deformations simultaneously. It is a fact that the strength of a structural element is dependent on a complex interaction of these deformations. In addition, code regulated minimum dimension and seismic detailing requirements for structural members are major factors affecting the capacities. All these separate structural elements work together to resist forces and contribute towards the global capacity of a force resisting system. Consequently, it is not an easy task to compute the lateral load capacity of a structure with satisfactory accuracy. Instead, a single strength parameter can be defined for a load resisting system that is composed of structural elements rather than dealing with the strength of every member.

Determining the strength of a properly designed moment-frame system is rather simple since capacity design principles should be adhered. Force-based design procedure followed by seismic codes rely on the principle that columns should be designed stronger than beams. By ensuring this, it is guaranteed that bending failure occurs in structural elements rather than the shear failure. Computed shear forces observed at the instant where bending moment capacities of members are attained are the capacity shears. Moreover, story mechanism is expected to occur when a moment frame undergo significant plastic hinging once bending capacities are reached. In fact, story mechanism event is the ultimate state of a moment-frame where global load resisting capacity is realized. Hence, it is postulated here that if capacity shears of elements forming a load resisting plane such as a moment frame system could be computed at the instant of story mechanism, then it is possible to calculate the strength of the system with adequate accuracy.

In a regular frame where the story mechanism is expected to happen at the first story, bottom end of all the first story columns and both ends of the first story beams exhibit

plastic hinging behaviour by reaching their bending moment capacities. Plastic moment capacities of i and j ends of beams (M_{pi} and M_{pj}) and bottom ends of columns ($M_{p,bottom}$) can be utilized to compute capacity shear of each column. This step is displayed in Equation 4.8 where M_{top} is the bending moment occurring on top end of the column at the instant of mechanism and l_n is the height of the column. Due to beams reaching their capacities before columns, value of M_{top} limited by the total joint moment $M_{pjoint,total}$ that is governed by the plastic moment capacities of connecting beams to that joint. Total plastic moment at the joint is shared by the two connecting columns with respect to their rotational stiffnesses, $k_{col,i}$ and $k_{col,i+1}$ (Equation 4.9).

$$V_r = \frac{M_{p,bottom} + M_{top}}{l_n} \quad (4.8)$$

$$M_{top} = \frac{k_{col,i}}{k_{col,i} + k_{col,i+1}} * M_{pjoint,total} \quad (4.9)$$

Summation of these capacity shear forces computed per Equation 4.8 are considered as the shear strength $V_r, frame$ of the frame. To visualize this explanation, deformation state of a regular moment frame at the instant first (i th) story mechanism develops is shown in Figure 4.9. Plastic moment capacities reached at the ends of the first story beams and at the bottom of the first story columns are also marked as points showing the hinge locations. $M_{pjoint,total}$ used in Equation 4.9 is obtained by summation of each M_{pi} and M_{pj} in Figure 4.9.

In case of shear walls, shear force occurring on the bottom end of the wall at the instant that the wall reaches its plastic moment capacity ($M_{p,bottom}$) is designated as the shear strength of the wall ($V_r, wall$). In order to compute this force, the design shear force V_d that is associated with the design moment M_d at the bottom of the shear wall can be scaled as given in Equation 4.10.

$$V_{r,wall} = \frac{M_{p,bottom}}{M_d} * V_d \quad (4.10)$$

It is assumed that correlation between V_d and M_d is linear until the bending moment capacity is reached. Hence; shear force $V_r, wall$ that is observed when moment de-

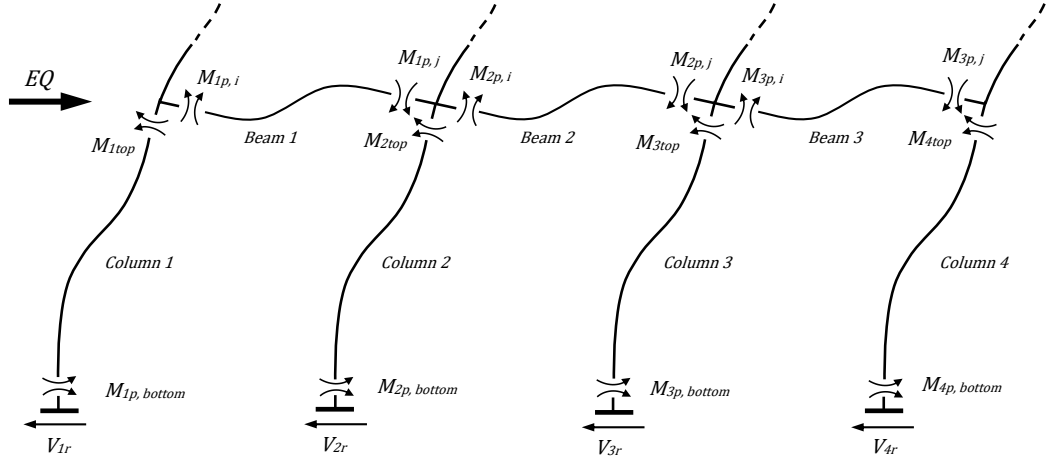


Figure 4.9: First story mechanism in a moment resisting frame during seismic response. Individual shear forces on columns (V_{ir}) are obtained from plastic moments occurring at both ends of members (M_{itop} and $M_{p,bottom}$).

mand reaches to $M_{p,bottom}$ is directly obtained by scaling the design shear force V_d and registered as the strength of the wall.

In a load resisting system consisting of beams, columns and shear walls; it can be assumed that the mechanism occurs when plastic hinges appear in bottom end of all columns, all first story beam ends and the bottom of the shear walls. Then, the associated capacity shears of columns and shear walls can be calculated as described and added together to determine the shear strength of the system.

It should be noted here that first story mechanism may not develop during actual seismic response. Even if all first story columns exhibit plastic hinging, the mechanism itself may develop in upper floors due to beams in different locations developing plastic hinges throughout the dynamic response. Moreover, a mechanism event may not even appear on the structure at all if ultimate member capacities are not realized. However, it is very difficult to exactly determine whether ultimate state is reached or expected mechanism occurs due to randomness of the dynamic response. Therefore, it can be deduced that first story mechanism assumption made in the context of this study is a conservative approach. It yields the highest theoretical capacity shear that can be achieved for the ultimate deformation state of a moment-frame. Although conservative, computed strength values still provide a reasonable estimate about the

expected strength levels. In addition, the only required data to compute capacity shears are section properties which are already available to the engineer after design has been completed. It is of course possible to improve the strength estimation of the load resisting systems by using inelastic analysis techniques. For instance, pushover analysis could be utilized to compute strength related parameters like base shears in a more accurate manner. However, one of the main objectives of this study is to provide means to improve the seismic response by using the parameters obtained through linear elastic analysis and accompanying seismic design. Due to reasons explained, the method of estimating strength levels through capacity shears of load resisting systems is adopted in the scope of this study.

4.6.3 Optimal Load Vector and Its Application

After the Equivalent Strength Allocation Diagram for a multi-story structure have been constructed and strength of the equivalent stiff end flexible members have been computed using capacity shears, existing Stiff-to-Flexible Strength Ratio ($SFSR_{existing}$) can be calculated. Once $SFSR_{existing}$ is compared with the $SFSR_{opt}$ estimated from the associated Uniform Ductility Spectrum, the flowchart given in Figure 4.3 is followed and elements of Optimal Load Vector (ΔV and ΔT) are calculated. The only difference in the procedure for building structures is that base shear force ΔV and base torque ΔT is distributed to each floor with respect to their masses (m_i) and mass moment of inertias (I_{0i}). ΔV_i and ΔT_i that are applied to each floor can be computed by using Equations 4.11 and 4.12.

$$\Delta V_i = \frac{\Delta V * m_i}{\Sigma m_i} \quad (4.11)$$

$$\Delta T_i = \frac{\Delta T * I_{0i}}{\Sigma I_{0i}} \quad (4.12)$$

4.6.4 Revising the Seismic Design

Updated demands on structural members are obtained from combined effect of previously performed seismic analysis and the linear elastic analysis under Optimal Load Vector. Modification of the design under this ultimate loading condition requires further discussion.

As discussed extensively, main source of strength unbalance in asymmetric building structures are the vertical members (columns and shear walls) rather than beams. In a code-conforming structure, beams can be designed optimally with little overstrength. However, this could not be the case for columns and shear walls due to overstrength supplied from various sources. The ultimate loading condition given by the Method results in new strength demands for vertical members that remedy the effect of uneven overstrength distribution. On the other hand, it yields additional demands on beam members as well. Beams, which have already been designed optimally, do not need any revision to their capacities. Therefore, additional demands on beams are ignored. In other words, design of columns and shear walls are updated through the application of the Method in order to address the strength unbalance. Design of optimally designed beams remain unchanged throughout the procedure.

4.6.5 Algorithm for the Optimal Strength Distribution Method

Optimal Strength Distribution Method developed for building structures is given in an algorithmic format below:

1. Design parameters (e_s , T_n , R_μ) associated with the structure are determined.
2. Linear elastic analysis (Response Spectrum Analysis) is carried out.
3. Code conforming seismic design is performed under loading conditions determined by linear elastic analysis.
4. Using computed member capacities obtained from seismic design, capacity shears of first story structural members are calculated. Strength of load-resisting

systems along plan is then determined using the capacity shears of structural members of which these systems are composed.

5. Computed strengths are utilized to form the Equivalent Strength Allocation Diagram as shown in Figure 4.8.
6. Existing and optimal Stiff to Flexible Strength Ratios are determined. Equivalent Strength Allocation Diagram is used to calculate $SFSR_{existing}$; while Uniform Ductility Spectra given in Figure 3.15 yields the $SFSR_{opt}$.
7. Optimal Load Vector is computed. Story shears ΔV_i and story torques ΔT_i are calculated per Equations 4.11 and 4.12.
8. ΔV_i and ΔT_i are applied to the analytical model of the structure simultaneously and linear elastic analysis performed.
9. Demands obtained under ΔV_i and ΔT_i are superimposed to the seismic demands computed from Response Spectrum Analysis. Superposition of these two analysis results is carried out in two senses (positive and negative). This step yields the ultimate, updated design demands.
10. Design of vertical members is revised with respect to the updated demands determined in the previous step. Revised design is expected to yield an $SFSR$ value closer to the optimal, and hence exhibit a more balanced ductility distribution.

An iterative approach can also be applied to the algorithm given above. Updated design could further be modified by performing the procedure repeatedly (steps 4 to 10) until $SFSR_{opt}$ is reached.

The algorithm given above is tested on three separate multistory case study structures in the following chapters. An eight-story stiffness-asymmetric moment-frame structure, another eight-story mass-asymmetric moment-frame structure and a twelve-story stiffness asymmetric structure with a shear wall are investigated in detail. In the following chapters, these structures are first designed and their dynamic responses are recorded. Then, Optimal Strength Distribution Method is implemented to each of these three systems and improvement in their seismic performances are investigated.

CHAPTER 5

CASE STUDY 1: 8-STORY STIFFNESS ASYMMETRIC STRUCTURE

5.1 Introduction

In this section, an eight-story stiffness asymmetric structure is presented as a case study to assess the performance of the Optimal Strength Distribution Method. First, seismic performance of the code designed system (labeled as *existing design*) is investigated. Then the design is revised by implementing the proposed method. Finally, a performance evaluation of the existing and revised designs is carried out comparatively.

5.2 General Information

Case study building is designed in compliance with ASCE 7-10 [4], the Turkish Earthquake Code [73] and Reinforced Concrete Standard of Turkey (TS-500) [87]. Capacity design principles are imposed in design. The building is a reinforced concrete moment-frame that is composed of eight identical stories. First story is 4 meters high, while the story height is 3 meters for the above stories. The floor centers of mass (*CM*) are coincident with the geometric centers of all stories. Characteristic strengths of concrete and reinforcing steel are 35 MPa and 420 MPa, respectively. Width of all beams is 0.30 m and their depth is 0.55 m. Slab thickness is 0.14 m at all stories. As per Turkish Earthquake Code [73], cracked section properties are imposed for beams and columns by multiplying section stiffnesses by 0.35 and 0.70, respectively.

Size of the square columns in three of the four frames in the direction of analysis is 0.55 m by 0.55 m. Columns are 0.4 m by 0.4 m in one of the outer frames. Due to this

difference, structure has one-way asymmetry. Column dimensions are constant along elevation in all frames. Typical story plan and elevation view are presented in Figure 5.1. Direction of excitation is the same as direction of one-way asymmetry (Y-axis).

Identification of the frames in Figure 5.1 is done according to expected deformation patterns of these frames. Flexible Edge frame is less stiff than the other three frames due to smaller size columns; hence more lateral deformation is likely to occur in this frame. The opposite is valid for the Stiff Edge frame. The inner frames are also expected to exhibit similar deformation trends with their adjacent exterior frames.

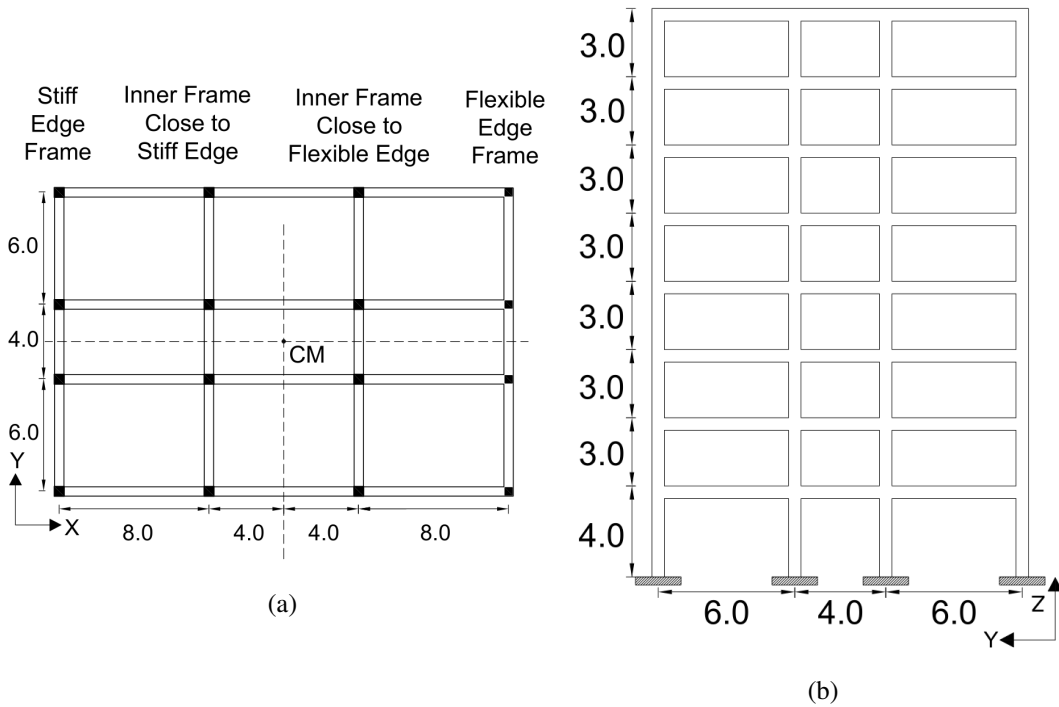


Figure 5.1: Typical story plan of the eight story asymmetric structure and elevation view of the SE-SI-FI frames in the direction of analysis. Center of mass (*CM*) locations which is located at the geometric center (same for all stories) are marked on the plan (Units in meters).

5.3 Free Vibration Properties

Dynamic properties associated with the first six modes of the structure are presented in Table 5.1. Modes denoted with *X* and *Y* are translation dominant modes in respec-

tive directions, and modes denoted with θ are the rotation dominant modes. Along with the periods belonging to each mode, effective modal masses and their ratios calculated in each direction are given. The frequency ratio ω_θ for Y direction is 1.26. Hence, the system is torsionally stiff in the direction of analysis.

Table 5.1: Free vibration properties of the eight story stiffness asymmetric structure

Mode	Period (Seconds)	Effective Modal Mass - Y (tons)	Effective Modal Mass Ratio - Y	Effective Modal Mass - X (tons)	Effective Modal Mass Ratio - X
1X	1.881	0	0	1582	0.825
1Y	1.617	1534	0.8	0	0
1 θ	1.281	49	0.025	0	0
2X	0.574	0	0	0	0.103
2Y	0.508	185	0.096	198	0
2 θ	0.398	12	0.0066	0	0

5.4 Determination of Static Eccentricity

All stories exhibit rigid diaphragm behavior. Center of rigidity (CR) at each floor is dependent on both stiffness variation along plan and stiffness distribution along height. Therefore, CR should be determined for every story diaphragm separately. There is limited research in literature on this issue. However, some practical procedures to find location of CR are suggested in a study by Basu and Jain [7]. In their paper, location of CR is computed by defining it in two different ways: single floor CR and all floor CR . In the first case, story CR is calculated independently per floor. On the other hand, all floor CR is determined by considering the effect of upper floors on the stiffness distribution. In the scope of this thesis study, location of CR is estimated by employing the single floor method. Only torsional and lateral stiffness distributions along a single story are employed in this procedure. At each diaphragm level, a unit load is applied at the center of mass and the rotation of the diaphragm (θ_{yi}) is recorded. Then, a unit moment is applied and the related rotation ($\theta_{\theta i}$) is measured. Position of the center of rigidity with respect to location of center of mass can simply

be computed by using these response quantities from Equation 5.1.

$$x_{CR,i} = -\theta_{Yi}/\theta_{\theta i} \quad (5.1)$$

In fact, $x_{CR,i}$ is the structural eccentricity (e) of the eight-story structure obtained per floor. Variation of this important design parameter along height is given in Table 5.2.

Table 5.2: Position of CR with respect to CM and the corresponding structural eccentricity (e) at each story. Negative x_{CR} value implies that CR is located on the stiff side.

Story	x_{CR} (m)	e (%)
1	-2.17	9.0
2	-1.69	7.0
3	-1.41	5.9
4	-1.25	5.2
5	-1.15	4.8
6	-1.08	4.5
7	-1.03	4.3
8	-0.97	4.0

As can be seen from Table 5.2, stiffness eccentricity varies from top to bottom stories. However, a single representative value of stiffness eccentricity for the structure is required so that the Optimum Strength Distribution Method could be applied accordingly. In order to do this, an equivalent structural eccentricity is conceived. It is defined as the e value attained at the height that corresponds to the shear span of the building. Shear span (L_s) can be defined by dividing the base moment (M_b) to the base shear force (V_b), both of which are obtained from seismic design (Equation 5.2). Story level corresponding to the computed L_s can then be identified, and the related structural eccentricity is taken from Table 5.2.

$$L_s = M_b/V_b \quad (5.2)$$

For the eight story asymmetric structure, L_s is computed as 16 meters, which corresponds to fifth story. Consequently, value of e is determined as $4.8\% \approx 5.0\%$.

5.5 Linear Elastic Design Spectrum

Design spectrum for the structure is constructed by using an imaginary location in downtown San Francisco on Site Class C. Mapped MCE_R spectral response acceleration parameters at short periods (S_S) and at 1 second (S_1) are computed for the representative site. The parameters associated with this site yields $S_{DS} = 1.0g$. The design spectrum, which was reduced by response reduction factor $R = 8$ in design is shown in Figure 5.2. Spectrum matched spectra of the selected ground motions are also given in the figure, which will be explained later in Section 5.7.

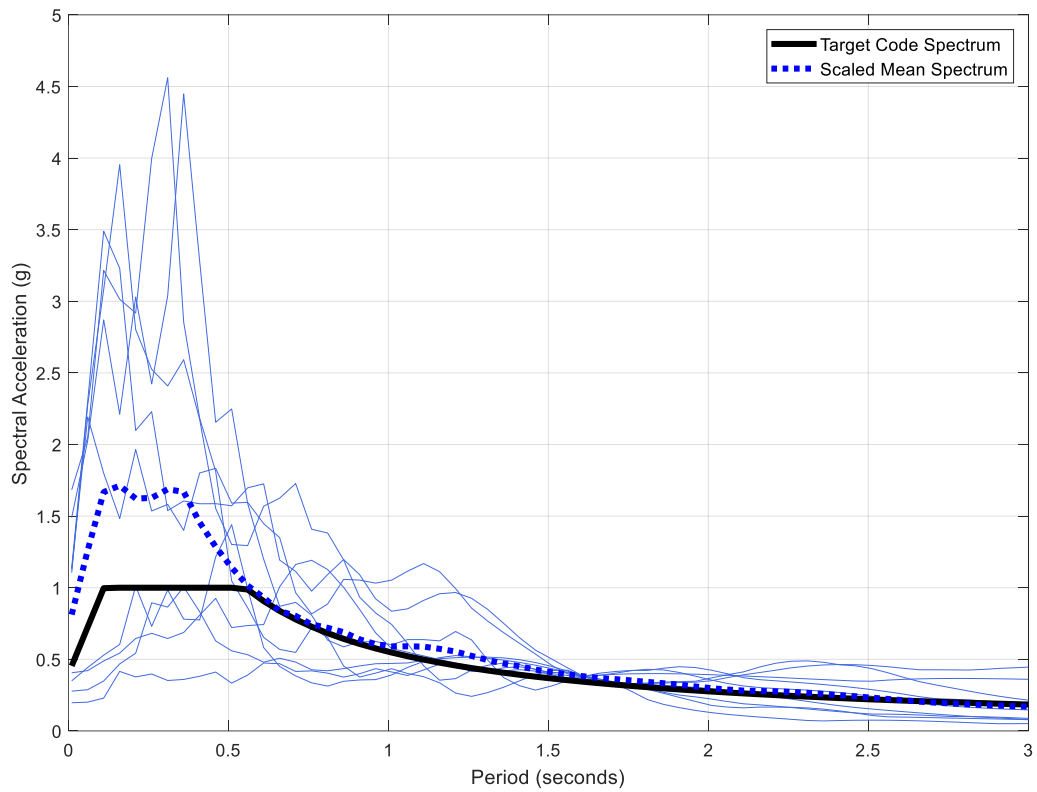


Figure 5.2: Linear elastic design spectrum and acceleration response spectra of amplitude scaled strong ground motions. Mean scaled response spectrum of these records is also plotted in dotted line.

5.6 Seismic Design

Capacity design principles are employed in the seismic design. Reinforcement detailing of beams is performed such that they are designed optimally, i.e. there is little overstrength in these members. Column reinforcement detailing, however, is governed by the minimum longitudinal reinforcement ratio ($\rho_{min} = 1\%$) in accordance with the relevant seismic design standards. In order to satisfy the $\rho_{min} = 1\%$ criterion, 0.55 m by 0.55 m columns are detailed with twelve 18 mm longitudinal bars. Similarly, eight 16 mm bars are provided for 0.40 m by 0.40 m columns. Accordingly, significant amount of overstrength is expected especially at the stiffer frames of the building. Calculations to check the strong column-weak condition are performed at each joint. Ratio of total column moments to the total beam moments at every joint is given in Table 5.3. It should be noted here that joints at each story of each frame in Figure 5.1 are labeled along Y direction from bottom (joint 1) to top (joint 4) in Table 5.3.

The unaltered, code compliant seismic design presented up to this point is denoted as *Existing Design* throughout the study and the dynamic response of the structure having this design is to be used as benchmark for further improvements by using the proposed design methodology.

5.6.1 Frame Design Shears

After seismic design is completed, design shear forces calculated at the bases of four frames. It should be noted that these shear forces are obtained under reduced design spectrum. The calculated base shear forces at each frame are given in Table 5.4. Being more flexible, *FE* frame has lower shear force demand than those of other frames. Design shears of the *SE* and *SI* frames are found to be close to each other. Although column sizes are the same for *SE*, *SI* and *FI* frames, *FI* frame has higher displacement demands compared to stiffer frames. Consequently, *FI* frame attains higher shear forces with respect to the *SE* and *SI* frames.

Table 5.3: Strong column - weak beam check for the Existing Design: Ratio of total column moment capacity to total beam moment capacity at each joint of the structure.

Story	Joint	SE FRAME	SI FRAME	FI FRAME	FE FRAME
1	1	7.9	10.1	10.1	3.8
	2	4.5	5.0	5.0	1.9
	3	4.5	6.0	5.0	1.9
	4	7.9	7.0	7.1	2.7
2	1	7.5	9.5	9.5	3.6
	2	4.3	4.6	4.6	1.7
	3	4.3	4.6	4.6	1.7
	4	7.5	6.6	6.6	2.5
3	1	7.1	8.8	8.8	3.3
	2	4.0	4.2	4.3	1.9
	3	4.0	5.1	4.3	1.9
	4	7.1	6.2	6.2	2.3
4	1	6.7	8.2	8.2	3.1
	2	3.7	3.9	3.9	1.7
	3	3.7	4.7	3.9	1.7
	4	6.7	5.7	5.7	2.2
5	1	6.3	7.5	7.5	2.8
	2	3.4	4.2	3.5	1.6
	3	3.4	4.2	4.2	1.6
	4	6.3	5.3	5.2	2.8
6	1	5.9	6.8	6.8	2.5
	2	3.1	3.7	3.7	1.4
	3	3.1	3.7	3.7	1.4
	4	5.9	4.7	4.7	2.5
7	1	5.4	5.9	5.9	2.2
	2	2.8	3.2	3.2	1.2
	3	2.8	3.2	3.2	1.2
	4	5.4	5.9	5.9	2.2
8	1	2.6	2.8	2.8	1.0
	2	1.3	1.5	1.5	0.6
	3	1.3	1.5	1.5	0.6
	4	2.6	2.8	2.8	1.1

Table 5.4: Frame design base shear forces ($V_{d,Frame}$) for the *Existing Design*. Units in kN.

SE Frame	SI Frame	FI Frame	FE Frame
199	211	295	156

5.6.2 Frame Strengths and Determination of Existing Stiff-to-Flexible Strength Ratio

Frame strengths are determined as discussed in Section 4.6. Frame capacity shears computed at the instant of first story column yielding mechanism are calculated and given in Table 5.5. Although they possess the same column dimensions, inner frames exhibit higher strength compared with to the *SE* Frame. Greater amounts of axial load at the base of the first story columns located at inner frames result in higher column capacities, which in turn increases the lateral strength of these frames.

Table 5.5: Frame base shear strengths (F_{Frame}) of the *Existing Design*. Units in kN.

SE Frame	SI Frame	FI Frame	FE Frame
643	858	882	398

Using the frame strengths given in Table 5.5, $SFSR_{existing}$ value for the eight-story system is computed by dividing the summation of *SE* - *SI* frame strengths by the summation of *FE* - *FI* frames strengths (Equation 5.3). $SFSR_{existing}$ is calculated as 1.17.

$$SFSR = \frac{(F_{SE} + F_{SI})}{(F_{FE} + F_{FI})} \quad (5.3)$$

5.6.3 System Overstrength and Computation of Ductility Reduction Factor

Frame design shears given in Table 5.4 and frame base shear strengths given in Table 5.5 are plotted along the frame axis of the structure in Figure 5.3. As observed in the Figure, there is some amount of reserved capacity (overstrength) in all frames due to seismic detailing. This is particularly pronounced in the frames of the structure having larger column sizes (*FI*, *SI* and *SE*).

The amount of overstrength present in each frame can be computed by simply calculating the ratio of frame strength to the frame design shear force (Equation 5.4). These Ω_{Frame} values are also displayed in Figure 5.3. In addition to Ω_{Frame} , global overstrength (Ω_{Global}) of the structure can be calculated in a similar manner. By di-

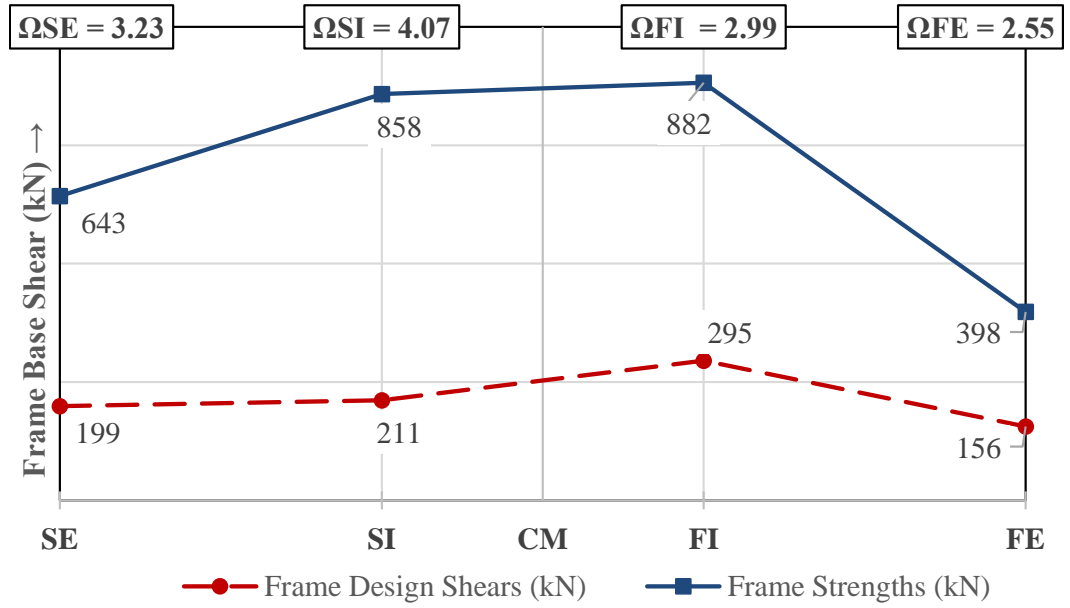


Figure 5.3: Distribution of frame shears and strengths along four frames of the structure (units in kN).

viding the summation of the frame strengths to summation of the frame design shear forces, Ω_{Global} is obtained as 3.21.

$$\Omega_{Frame} = \frac{F_{Frame}}{V_{d,Frame}} \quad (5.4)$$

In fact, Ω_{Global} is the realized value of overstrength factor denoted as Ω_0 in ASCE 7-10 [4]. In Table 12.2-1 of ASCE 7-10 [4], Ω_0 value given for the associated type of moment-frame structure is 3. Computed Ω_{Global} is close to this value, which indicates that the existing design is code compliant in terms of system overstrength. However, distribution of this overstrength is far from ideal. This will be addressed when the design is revised through application of the proposed method.

Overstrength factor is one of the two parameters that response reduction factor (R) is composed of (Equation 5.5). The other parameter, ductility reduction factor (R_{mu}), can be calculated by using Ω_{Global} and $R = 8$ that is employed in design. By doing so,

R_{mu} is determined as 2.48 for the system.

$$R = \Omega_0 * R_{mu} \quad (5.5)$$

5.7 Analytical Modeling and Strong Ground Motion Set

In order to perform nonlinear dynamic analyses for seismic performance assessment, three dimensional mathematical model of the structure is prepared by using the OpenSees Platform [65]. The mathematical model employs “forceBeamColumn” element from the element library with the “HingeRadau” option enabled. This element utilizes plastic hinge regions defined at member ends according to the specified plastic hinge lengths. Inelastic properties for beam-ends are assigned by implementing the moment-curvature relationships of the designed beam sections. In case of columns, fiber sections are defined at plastic hinge regions so that an accurate interaction of axial force and section capacity could be accounted. Cracked section stiffnesses are considered for linear elastic members, by reducing the gross section inertias with the previously defined coefficients.

Nonlinear response history analyses are performed under several strong ground motions. Ten strong ground motion records are selected from the PEER NGA Database [66]. These strong ground motion records are from various earthquakes having similar magnitudes from around the world and all possess strike slip fault mechanism. The site classes associated with these records are either C or D. Detailed information regarding the selected strong ground motions are given in Table 5.6.

Simple amplitude scaling is performed on the set of strong ground motion records in two steps. First, each ground motion record is scaled to match their computed spectral acceleration values at first translation period of the structure ($S_a(T_{1Y})$) to the spectral acceleration value given by the design spectrum ($S_{ae}(T_{1Y})$). Next, another amplitude scaling is performed such that the spectral acceleration values given by the mean response spectra of the scaled ground motions exceed those of the design spectrum over the period range of $0.2T_{1Y} \leq T \leq 1.5T_{1Y}$. Consequently, an ultimate scale factor for each strong ground motion is obtained by multiplying these two scale

factors determined in two steps. These factors are also given in Table 5.6. Scaled acceleration response spectra of the selected ground motions and their mean spectrum were plotted in Figure 5.2 above.

Table 5.6: Strong ground motion records that are employed in the dynamic analyses.

Earthquake Name	GM CODE	YEAR	Mw	EpiD (km) -R	HypD (km)	Joyner-Boore Dist. (km)	Preferred NEHRP Based on Vs30	Preferred Vs30 (m/s)	PGA (g)	PGV (cm/sec)	PGD (cm)	Scale Factor
Manjil, Iran	ABBAR-L	1990	7.37	40.43	43.47	12.56	C	724.0	0.5051	43.78	18.96	2.16
Superstition Hills-02	B-PTS225	1987	6.54	15.99	18.35	0.95	D	348.7	0.4509	77.19	37.19	0.43
Parkfield	C05085	1966	6.19	32.56	34.06	9.58	D	289.6	0.3768	23.92	3.85	3.36
Victoria, Mexico	CPE045	1980	6.33	33.73	35.48	13.80	C	659.6	0.5722	27.06	10.85	1.77
Duzce, Turkey	375-E	1999	7.14	24.05	27.83	3.93	C	424.8	0.7367	28.24	6.09	3.17
Kocaeli, Turkey	DZC270	1999	7.51	98.22	99.52	13.60	D	276.0	0.3255	55.32	29.58	0.76
Imperial Valley-06	H-E07230	1979	6.53	27.64	29.38	0.56	D	210.5	0.4200	79.15	40.83	0.87
Imperial Valley-06	H-E08230	1979	6.53	28.09	29.80	3.86	D	206.1	0.5379	56.80	32.99	2.45
Hector Mine	HEC090	1999	7.13	26.53	30.38	10.35	C	684.9	0.3062	34.21	17.71	1.02
Kobe, Japan	KAK090	1995	6.90	24.20	30.10	22.50	D	312.0	0.2668	21.66	7.60	1.02

5.8 Dynamic Analysis Results of the Existing Design

Convergence has been achieved for nine of the ten dynamic analyses performed under the scaled ground motion set. Dynamic analysis under scaled H-E08230 record has led to excessive frame deformations, indicating collapse. Consequently, results compiled for analyses under nine strong ground motion records are presented herein. Interstory drifts, beam end curvatures, column bottom-end curvatures and story shears are calculated for each frame under each ground motion throughout inelastic dynamic analyses. Figure 5.4 displays the maximum interstory drift ratios of the four frames obtained from dynamic analyses performed under each ground motion. Story mean of maximum curvatures measured at beam ends at each story of each frame are given in Figure 5.5. Similarly, story mean of maximum column bottom-end curvatures computed at each story of each frame are given in Figure 5.6. Finally, frame shear forces at each story for each dynamic analysis are shown in Figure 5.7. Mean results for the 9 ground motions are plotted in red bold line for each response parameter given in Figures 5.4 - 5.7.

Upon inspecting the results given in Figures 5.4 - 5.6, it can be stated that interstory drift ratios and mean beam end curvatures exhibit slightly uniform distribution; albeit higher response is observed in flexible side frames compared with the stiffer side

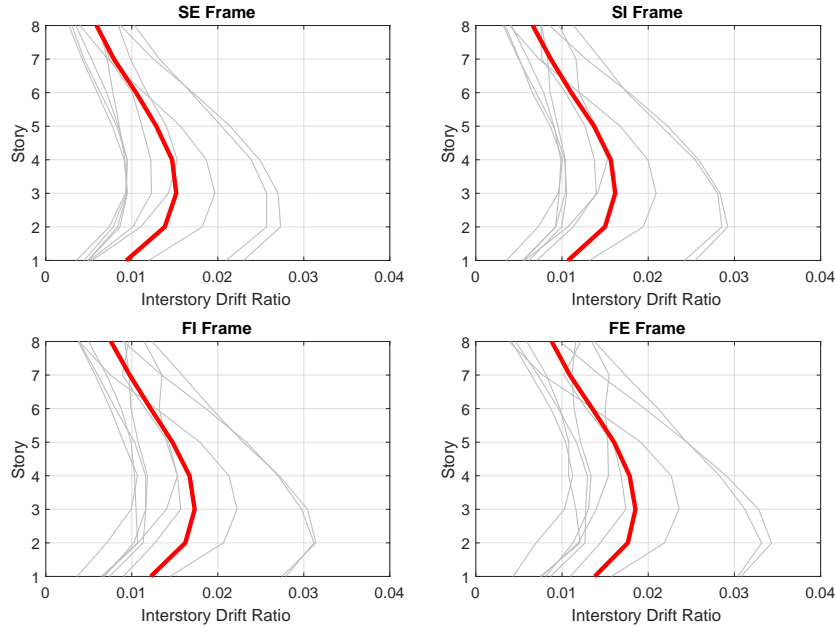


Figure 5.4: Maximum interstory drift ratios obtained from inelastic dynamic analyses of the existing design under ground motion set and the corresponding mean of maximum values for 9 GM records.

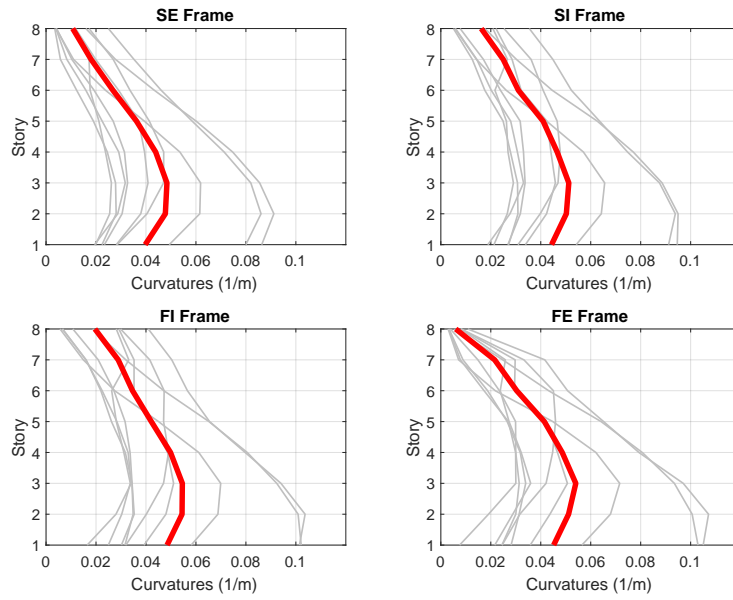


Figure 5.5: Beam-end curvatures obtained from inelastic dynamic analyses of the existing design under ground motion set and the corresponding mean of maximum values for 9 GM records.

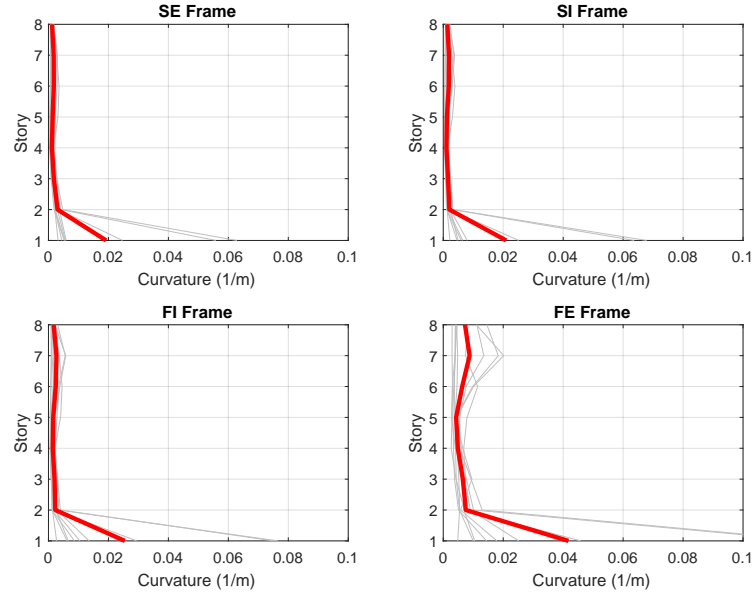


Figure 5.6: Column bottom-end curvatures obtained from inelastic dynamic analyses of the existing design under ground motion set and the corresponding mean values for 9 GM records.

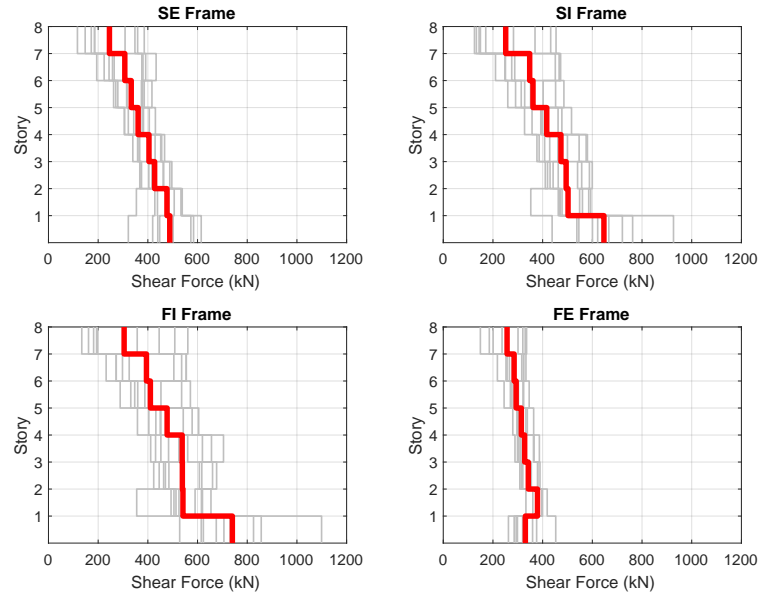


Figure 5.7: Frame shear forces obtained from inelastic dynamic analyses of the existing design under ground motion set and the corresponding mean values for 9 GM records.

frames. However, there are high curvature demands at the bottom ends of first story columns located on the *FE* and *FI* frames, compared with those of *SE* and *SI* frames. An interesting observation is that some of the ground motions in the set yield considerably higher curvature demands in these members. Frame base shears in Figure 5.6 are quite consistent with the expected capacities of frames, which were given in Table 5.5. Hence, it can be concluded that the computed frame strengths are quite representative of the frame shears achieved at the end of dynamic analyses.

The ground motion set mean values of curvature ductilities computed at each beam and column end are also given Tables 5.7 and 5.8. Mean curvature ductilities at both ends (denoted as I and J ends) of the three beams at each story of the four frames are displayed in Table 5.7. In a similar format, top and bottom end curvature ductilities of the four columns at each story of the four frames are presented in Table 5.8.

Results in Table 5.7 further validates the conclusions made for Figure 5.5. In addition, frame average beam ductilities given in the Table do not exhibit dramatic variations among frames. Column ends where curvature ductility ratios exceed 1.0 are marked in colored cells in Table 5.8. These marked ductility ratios denote the column ends where plastic deformations did occur during dynamic analyses. Non-uniform curvature ductility distribution in first story columns can clearly be seen in Table 5.8. Moreover, the majority of the columns in the *FE* frame have experienced inelastic deformations during seismic response as can be seen from the recorded ductilities for these members.

Table 5.7: Mean beam curvature ductilities of existing design under the ground motion set.

Story	Beam	Stiff Edge Frame		Stiff Inner Frame		Flexbile Inner Frame		Flexible Edge Frame	
		I End	J End	I End	J End	I End	J End	I End	J End
1	Beam1	7.5	8.4	8.3	9.1	9.4	9.9	9.4	8.4
	Beam2	7.6	8.0	9.0	9.3	9.7	9.7	9.2	9.3
	Beam3	7.3	8.7	8.2	9.3	9.2	10.2	8.5	9.4
2	Beam1	8.8	10.3	9.4	10.7	10.3	11.5	10.3	9.9
	Beam2	9.2	9.8	10.1	10.0	10.9	10.8	10.5	10.3
	Beam3	8.6	10.5	9.1	11.0	10.1	11.7	9.5	10.8
3	Beam1	8.7	10.5	9.1	11.0	9.9	11.8	9.5	12.0
	Beam2	9.4	10.1	10.1	11.1	11.1	11.0	10.8	11.5
	Beam3	8.5	10.8	8.9	11.3	9.7	12.1	10.2	11.0
4	Beam1	8.0	9.5	8.4	9.9	9.2	10.7	8.7	10.6
	Beam2	8.4	9.1	9.1	10.1	10.0	9.9	9.7	10.1
	Beam3	7.8	9.9	8.2	10.3	9.0	11.0	9.4	9.8
5	Beam1	6.7	7.9	6.9	9.8	7.8	8.8	8.5	8.3
	Beam2	6.9	7.4	7.6	8.2	8.3	8.8	7.8	8.0
	Beam3	6.4	8.3	8.0	8.7	7.5	9.3	7.3	9.8
6	Beam1	5.0	5.8	5.1	7.6	5.8	8.4	6.3	6.1
	Beam2	5.0	5.4	5.6	6.2	6.4	6.9	5.5	5.9
	Beam3	4.6	6.3	6.1	6.6	6.8	7.3	5.0	7.8
7	Beam1	3.3	3.9	5.0	5.6	5.8	6.5	4.8	4.2
	Beam2	3.5	3.7	4.1	4.5	4.8	5.2	3.7	3.9
	Beam3	3.0	4.3	4.5	6.2	5.3	7.1	3.4	5.9
8	Beam1	2.0	2.2	3.4	3.6	4.1	4.3	1.8	0.8
	Beam2	2.0	2.1	2.5	2.7	3.1	3.3	0.6	0.7
	Beam3	1.7	2.7	2.8	4.3	3.5	5.2	0.8	2.4
Average		6.3	7.3	7.1	8.2	7.8	8.8	7.1	7.8
Frame average		6.8		7.6		8.3		7.5	

Table 5.8: Mean column curvature ductilities of existing design under the ground motion set.

Story	Column	Stiff Edge Frame		Stiff Inner Frame		Flexible Inner Frame		Flexible Edge Frame	
		Top End	Bottom End	Top End	Bottom End	Top End	Bottom End	Top End	Bottom End
1	Column 1	3.8	0.3	4.6	0.2	5.6	0.3	6.9	0.4
	Column 2	3.9	0.2	4.3	0.2	5.3	0.3	6.9	0.6
	Column 3	3.9	0.2	4.3	0.2	5.2	0.3	6.8	0.5
	Column 4	3.7	0.3	4.6	0.2	5.5	0.3	6.7	0.4
2	Column 1	0.6	0.2	0.4	0.2	0.5	0.3	0.9	0.6
	Column 2	0.7	0.3	0.5	0.3	0.5	0.4	1.7	1.1
	Column 3	0.6	0.3	0.4	0.3	0.5	0.3	1.4	1.0
	Column 4	0.5	0.2	0.4	0.3	0.4	0.3	0.8	0.6
3	Column 1	0.3	0.3	0.3	0.3	0.4	0.4	0.8	0.7
	Column 2	0.4	0.4	0.4	0.4	0.5	0.4	1.4	1.1
	Column 3	0.3	0.4	0.3	0.3	0.4	0.4	1.2	1.1
	Column 4	0.3	0.3	0.3	0.3	0.4	0.4	0.7	0.7
4	Column 1	0.2	0.4	0.2	0.4	0.3	0.5	0.6	0.9
	Column 2	0.2	0.6	0.2	0.5	0.3	0.6	0.9	1.5
	Column 3	0.2	0.5	0.2	0.5	0.3	0.6	0.9	1.4
	Column 4	0.2	0.4	0.2	0.5	0.3	0.6	0.6	1.1
5	Column 1	0.3	0.5	0.2	0.5	0.3	0.6	0.5	1.1
	Column 2	0.3	0.6	0.2	0.6	0.3	0.8	0.8	2.0
	Column 3	0.2	0.6	0.2	0.6	0.3	0.7	0.8	1.9
	Column 4	0.2	0.5	0.2	0.5	0.3	0.6	0.5	1.1
6	Column 1	0.3	0.5	0.3	0.5	0.4	0.6	0.6	1.1
	Column 2	0.3	0.7	0.3	0.6	0.5	0.8	1.3	2.4
	Column 3	0.3	0.7	0.3	0.6	0.4	0.7	1.1	2.3
	Column 4	0.3	0.5	0.3	0.5	0.4	0.7	0.6	1.1
7	Column 1	0.3	0.4	0.4	0.4	0.5	0.5	0.8	0.9
	Column 2	0.3	0.6	0.3	0.5	0.5	0.6	1.5	2.2
	Column 3	0.3	0.6	0.3	0.5	0.5	0.6	1.5	2.0
	Column 4	0.3	0.4	0.3	0.4	0.4	0.5	0.8	0.8
8	Column 1	0.2	0.3	0.3	0.3	0.3	0.3	0.5	1.8
	Column 2	0.2	0.6	0.2	0.6	0.3	0.6	1.3	4.0
	Column 3	0.2	0.6	0.2	0.5	0.3	0.6	1.3	3.7
	Column 4	0.2	0.3	0.2	0.3	0.3	0.3	0.5	1.6
Average		0.7	0.4	0.8	0.4	1.0	0.5	1.7	1.4
Frame Average		0.6		0.6		0.8		1.5	

Bi-linearized first story column moment-curvature backbone curves are plotted for each frame in Figure 5.8. These backbone curves are computed under the design axial loads. It should be noted that there are two curves at each plot; one for the inner column (higher moment capacity due to larger axial loads), and the other one for the outer column (lower moment capacity). Inner column curve is plotted in green while outer column moment-curvature curve is plotted in magenta. Mean column bottom-end curvature demands are also marked on these lines with dots. Curvature ductilities of the columns are written on each plot, as well. Although the yield curva-

ture values of the first story columns are similar in all four frames, curvature demands vary significantly. Therefore, it can be decided that the ductility unbalance observed at the first story columns is due to uneven distribution of demands rather than yield deformations of these members.

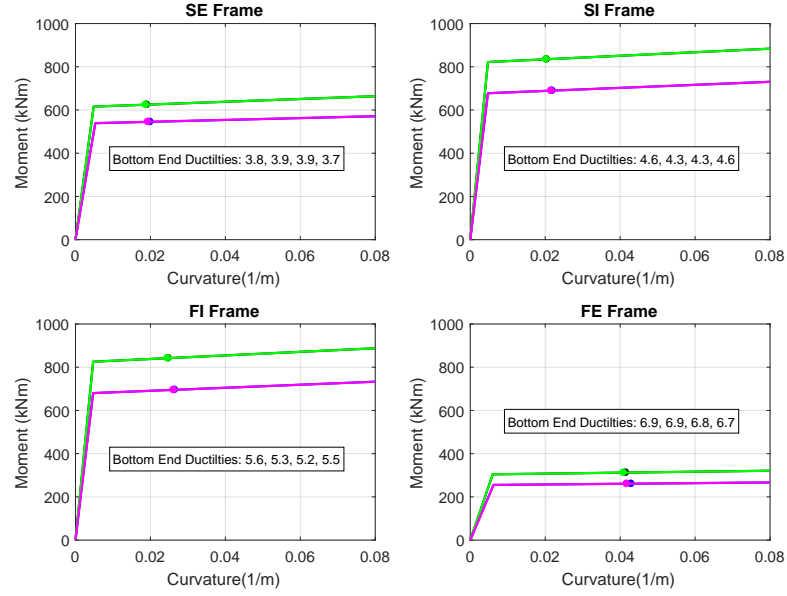


Figure 5.8: Bi-linearized moment curvature relationships of first story columns and computed ductility demands on these columns.

5.9 Revised Design: Implementation of the Optimal Strength Distribution Method

All of the observed issues regarding the uneven damage distribution in the system is addressed in this section through the application of Optimal Strength Distribution Method. The procedure will result in a *Revised Design* where some of the members experiencing high ductility demands would be strengthened.

5.9.1 Determination of $SFSR_{opt}$

First, Optimal Stiff-to-Flexible Strength Ratio affiliated with the structure should be determined. The system parameters e_s , T_n , and ductility reduction factor R_{mu} are needed in order to utilize the associated Uniform Ductility Spectrum given in Figure

3.15. R_{mu} is used rather than the design response reduction factor R for this purpose. This is due to the definition of Uniform Ductility Spectra that is based on results obtained from the parametric case study where only R_{mu} was employed in seismic design and no overstrength was considered. Since capacities of force resisting members in the parametric study are directly determined from seismic demands, there is no material related overstrength in these members. Hence, overstrength reduction factor is unity throughout the utilized structures. In order to take this situation into account, R_{mu} value is used when utilizing the Uniform Ductility Spectra.

It was previously determined that T_n is 1.62 seconds in the direction of analysis. Stiffness eccentricity e is 5.0% and R_{mu} is 2.48. Optimal Stiff-to-Flexible Strength Ratio ($SFSR_{opt}$) associated with these system parameters is determined as 0.923 from Figure 3.15. The optimal strength ratio is compared with $SFSR_{existing}$, which was previously determined as 1.17. Hence, the flexible side of the structure should be strengthened in order to achieve the optimal SFSR value. This situation corresponds to Case II variant of the Optimal Strength Distribution Method that was presented in Section 4.3.2.

5.9.2 Strength Allocation Diagram

Equivalent Strength Allocation Diagram constructed for the eight-story stiffness asymmetric structure is shown in Figure 5.9. The up to scale diagram shown in Figure 5.9 is prepared in a similar way to Figure 4.3 that was presented for a general Case II type system. Distances of flexible and stiff side elements to the center of mass in the Figure are computed as described in Section 4.6.1. The target flexible edge strength (F'_F) that yields $SFSR_{opt}$ is computed as shown in Equation 5.6. It is determined as 1626 kN. Nominal design strengths of F_S and F_F in Figure 5.9 are the design shears associated with both sides of the structure (given in Table 5.4). $\Omega_S F_S$ is the existing strength of the stiff side, which is computed as the summation of the strengths of SE and SI frames given in Table 5.5.

$$F'_F = \frac{\Omega_S F_S}{SFSR_{opt}} \quad (5.6)$$

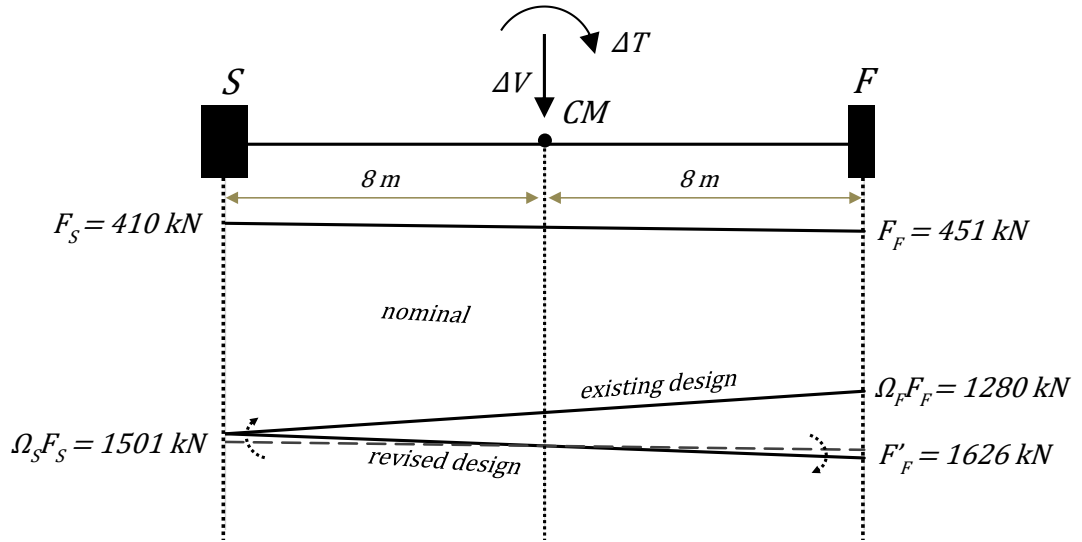


Figure 5.9: Equivalent Strength Allocation Diagram constructed for the eight story-stiffness asymmetric structure.

In order to compute ΔV , Equation 4.5 is utilized. Similarly, ΔT is computed per Equation 4.6. Consequently, the force vector consisting of ΔV and ΔT that should be applied to the frame structure is constructed as given in Equation 5.7.

$$\Delta F = \begin{bmatrix} 2266 \text{ kN} \\ 672 \text{ kNm} \end{bmatrix} \quad (5.7)$$

It should be noted here that torque ΔT is applied towards flexible side. The dashed line in Figure 5.9 representing the combination of ΔV with the nominal strength distribution should be *rotated* by application of ΔT in this direction in order to obtain the *revised design* strength distribution.

5.9.3 Linear Elastic Analysis and Revised Seismic Design

After ΔF force vector is calculated, items 8, 9 and 10 of the Optimal Strength Distribution Method algorithm given in Section 4.6.5 are followed. Consequently, revised force demands in column members are determined. Columns that require an increase in their capacities are marked in frame schematics given in Figure 5.10 as red dashed lines. The updated frame design base shears, $V_{d,Frame}$, are also given be-

neath each frame in Figure 6.11. Other than increasing longitudinal reinforcement ratio (ρ_l) of columns marked in Figure 5.10, no additional design modification has been performed. In order to satisfy the revised demands, ρ_l value of the 0.40 m

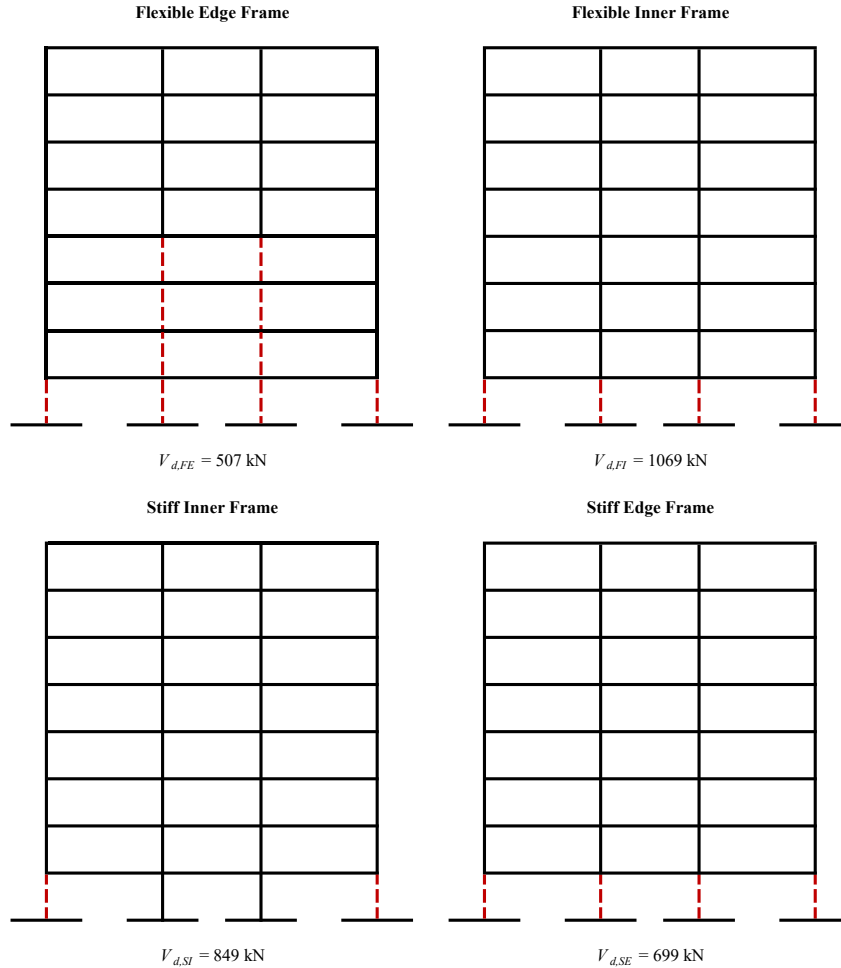


Figure 5.10: Schematic view of the four frames with columns that require strengthening (marked as dashed red lines).

by 0.40 m columns located in the *FE* frame has been increased from 1% to 1.9%. This ratio is achieved by providing eight 22 mm diameter bars in these columns. The strengthened 0.50 m by 0.50 m columns that are located in the other frames has a ρ_l value of 1.5%. These revised columns are detailed such that twelve bars of 22 mm diameter are provided to achieve this reinforcement ratio.

As can be seen from Figure 5.10, revised demands necessitate capacity increase for quite a number of *FE* columns as well as the first story columns located in the *FI*

frame. Contrary to what is anticipated from the procedure, there is also a slight increase in the demand of first story columns located in the *SE* Frame and outer first story columns in the *SI* frame. This could be related to the redistribution of response due to the applied ΔF to the multi-story system. All four frames of the structure react to the additional loading condition collaboratively; therefore, they all exhibit varying levels of deformations under this loading. Due to the interaction of four frames, additional force demands are observed at the stiffer side elements as well.

5.10 Dynamic Analysis Results for the Revised Design

The revised structure has also been analyzed under the scaled strong ground motion set that was previously introduced. Dynamic analysis results were compiled for nine of ten strong ground motions where convergence had been achieved. Interstory drifts, beam end curvatures, column bottom-end curvatures and story shears that were calculated for each frame under each ground motion are presented in Figures 5.11 - 5.14, respectively. In addition, mean of maximum results from the dynamic analyses under nine ground motions are also plotted as red bold lines for each response parameter displayed per frame in these figures.

Similar to what has been observed in dynamic analyses results for the existing design, interstory drifts and mean beam curvature demands computed per story are quite uniform among frames. A slightly higher response is noted in the flexible side frames. A remarkable observation is that first story column bottom-end curvature demands given in Figure 5.13 are quite close to each other in all frames. This outcome illustrates the improvement in damage distribution through revising the design. Computed frame shears in Figure 5.14 are found at similar levels for the *SE*, *SI* and *FI* frames, having same column dimensions. *FE* frame has lower shear demands due to smaller sections.

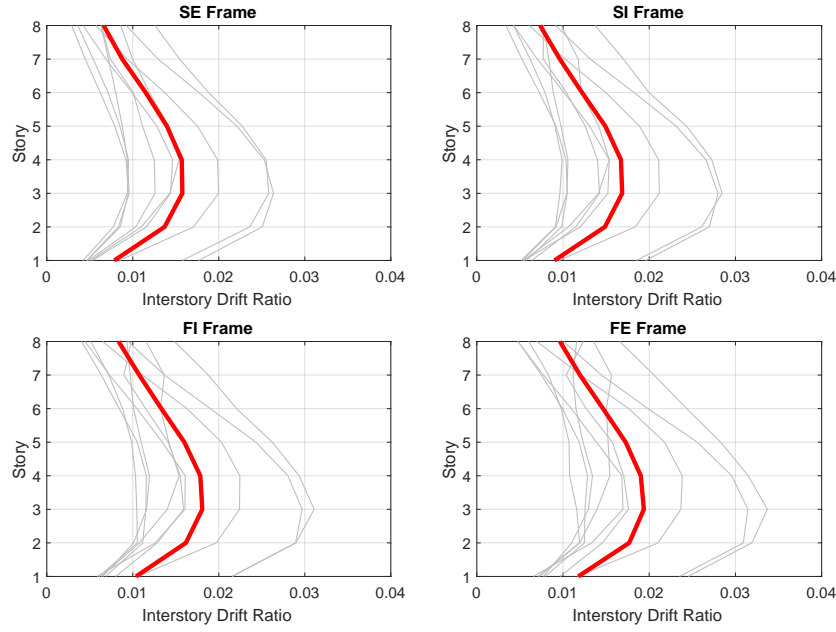


Figure 5.11: Interstory drift ratios obtained from inelastic dynamic analyses of the revised design under ground motion set and the corresponding mean values for 9 GM records.

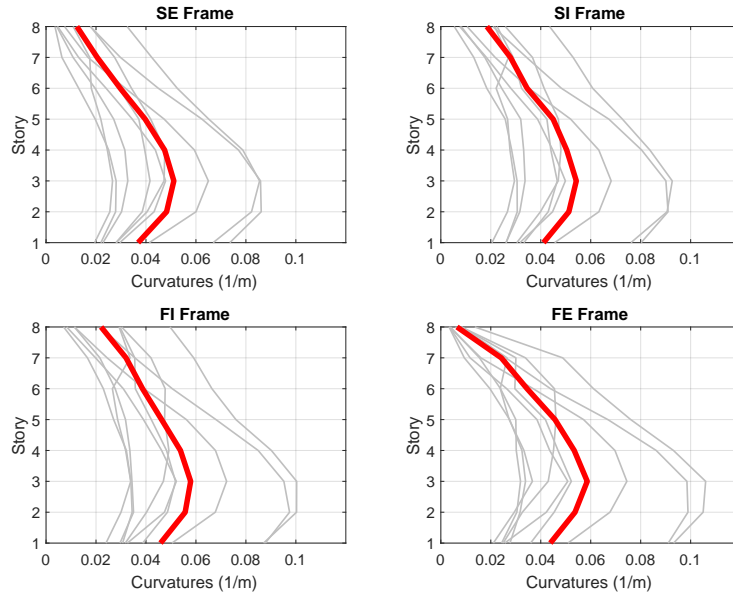


Figure 5.12: Beam end curvatures obtained from inelastic dynamic analyses of the revised design under ground motion set and the corresponding mean values for 9 GM records.

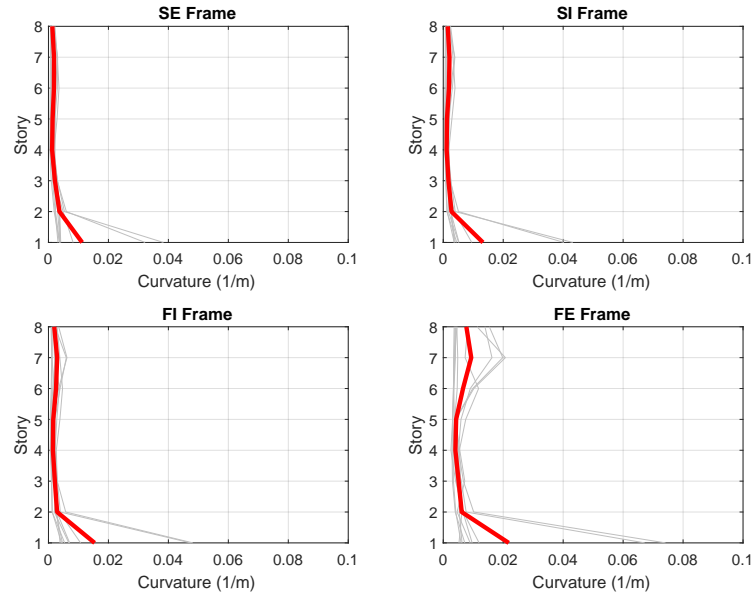


Figure 5.13: Column bottom end curvatures obtained from inelastic dynamic analyses of the revised design under ground motion set and the corresponding mean values for 9 GM records.

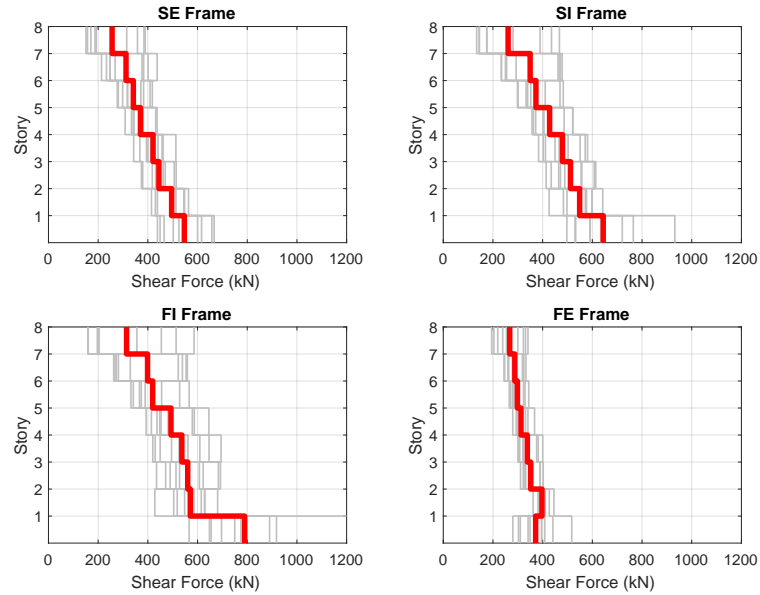


Figure 5.14: Frame shear forces obtained from inelastic dynamic analyses of the revised design under ground motion set and the corresponding mean values for 9 GM records.

The mean curvature ductilities are computed from dynamic analyses of the revised structure under the ground motion set, and tabulated for each beam and column end. These are given in Tables 5.9 and 5.10. The format of these tables is the same as those given for the existing design results (Tables 5.7 and 5.8). It can be observed that the beam curvature ductility demands in are similar levels for all frames. Frame average beam curvature ductilities are found to be approximately equal to the response reduction factor employed ($R = 8$). It is clear in Table 5.10 that bottom ends of the first story columns located in all frames experience inelastic behavior. *FE* columns located at higher stories also exhibit small amounts of ductilities. In fact, these affected columns are the unaltered members of the *FE* Frame according to the revised demands as shown in Figure 5.10.

Table 5.9: Mean beam curvature ductilities of revised design under the ground motion set.

Story	Beam	Stiff Edge Frame		Stiff Inner Frame		Flexible Inner Frame		Flexible Edge Frame	
		I End	J End	I End	J End	I End	J End	I End	J End
1	Beam1	6.9	7.9	7.7	8.5	8.9	9.5	9.0	8.2
	Beam2	6.9	7.5	8.2	8.6	9.1	9.1	9.1	9.1
	Beam3	6.7	8.2	7.5	8.8	8.7	9.7	8.2	9.0
2	Beam1	8.8	10.5	9.4	11.0	10.4	11.8	10.6	10.5
	Beam2	9.3	10.0	10.4	10.2	11.2	11.1	11.2	11.0
	Beam3	8.6	10.7	9.2	11.2	10.2	12.0	10.0	11.2
3	Beam1	9.1	11.2	9.6	11.7	10.4	12.5	10.1	13.0
	Beam2	10.0	10.7	10.7	11.8	11.9	11.7	11.8	12.5
	Beam3	8.9	11.4	9.4	12.0	10.2	12.8	11.1	11.8
4	Beam1	8.6	10.3	9.0	10.8	9.9	11.5	9.4	11.7
	Beam2	9.2	9.9	9.9	10.9	10.9	10.8	10.7	11.3
	Beam3	8.4	10.6	8.8	11.1	9.6	11.9	10.3	10.6
5	Beam1	7.3	8.6	7.7	10.6	8.6	9.6	9.4	9.2
	Beam2	7.7	8.1	8.3	9.1	9.1	9.8	8.6	8.9
	Beam3	7.0	8.9	8.8	9.4	8.3	10.1	8.1	10.8
6	Beam1	5.4	6.5	5.7	8.4	6.5	9.3	7.1	7.0
	Beam2	5.6	6.1	6.2	7.0	7.1	7.8	6.2	6.7
	Beam3	5.1	6.9	6.7	7.4	7.6	8.2	5.7	8.7
7	Beam1	3.6	4.5	5.5	6.4	6.3	7.3	5.2	4.8
	Beam2	3.9	4.3	4.6	5.1	5.3	5.8	4.1	4.5
	Beam3	3.3	4.9	5.0	6.9	5.8	7.9	3.6	6.8
8	Beam1	2.3	2.6	3.8	4.2	4.5	4.9	2.0	0.9
	Beam2	2.3	2.5	2.8	3.2	3.4	3.9	0.7	0.7
	Beam3	1.9	3.2	3.2	4.9	3.8	5.9	0.8	2.7
Average		6.5	7.8	7.4	8.7	8.2	9.4	7.6	8.4
Frame average		7.1		8.1		8.8		8.0	

Table 5.10: Mean column curvature ductilities of revised design under the ground motion set.

Story	Column	Stiff Edge Frame		Stiff Inner Frame		Flexible Inner Frame		Flexible Edge Frame	
		Top End	Bottom End	Top End	Bottom End	Top End	Bottom End	Top End	Bottom End
1	Column 1	1.8	0.2	2.1	0.2	2.6	0.2	2.5	0.2
	Column 2	1.8	0.2	2.9	0.3	2.4	0.2	2.5	0.3
	Column 3	1.7	0.2	2.9	0.3	2.4	0.2	2.4	0.3
	Column 4	1.8	0.2	2.0	0.2	2.5	0.2	2.4	0.2
2	Column 1	0.7	0.3	0.6	0.3	0.6	0.3	0.9	0.6
	Column 2	0.8	0.3	0.6	0.3	0.6	0.4	0.7	0.5
	Column 3	0.7	0.3	0.6	0.3	0.6	0.3	0.7	0.5
	Column 4	0.6	0.3	0.5	0.3	0.6	0.3	1.0	0.7
3	Column 1	0.4	0.3	0.3	0.3	0.4	0.4	0.8	0.7
	Column 2	0.4	0.4	0.4	0.3	0.5	0.4	0.6	0.5
	Column 3	0.4	0.4	0.4	0.3	0.4	0.4	0.6	0.5
	Column 4	0.3	0.3	0.3	0.3	0.4	0.4	0.7	0.7
4	Column 1	0.2	0.4	0.2	0.4	0.3	0.5	0.6	0.9
	Column 2	0.2	0.6	0.2	0.5	0.3	0.6	0.4	0.6
	Column 3	0.2	0.6	0.2	0.5	0.3	0.6	0.4	0.6
	Column 4	0.2	0.5	0.2	0.5	0.3	0.5	0.6	1.1
5	Column 1	0.2	0.5	0.2	0.5	0.3	0.6	0.5	1.2
	Column 2	0.2	0.7	0.2	0.6	0.3	0.8	0.8	2.1
	Column 3	0.2	0.7	0.2	0.6	0.3	0.8	0.8	1.9
	Column 4	0.2	0.5	0.2	0.6	0.3	0.7	0.5	1.2
6	Column 1	0.3	0.5	0.4	0.5	0.5	0.7	0.7	1.2
	Column 2	0.3	0.7	0.4	0.7	0.5	0.9	1.3	2.6
	Column 3	0.3	0.7	0.3	0.7	0.4	0.8	1.1	2.5
	Column 4	0.3	0.5	0.3	0.6	0.5	0.8	0.6	1.3
7	Column 1	0.3	0.5	0.4	0.5	0.5	0.6	0.8	1.1
	Column 2	0.3	0.6	0.3	0.6	0.5	0.7	1.6	2.5
	Column 3	0.3	0.6	0.4	0.6	0.5	0.7	1.6	2.3
	Column 4	0.3	0.5	0.3	0.5	0.5	0.6	0.9	1.0
8	Column 1	0.2	0.3	0.3	0.3	0.4	0.3	0.5	1.8
	Column 2	0.2	0.6	0.2	0.6	0.3	0.7	1.4	4.6
	Column 3	0.2	0.6	0.2	0.5	0.3	0.6	1.4	4.1
	Column 4	0.2	0.3	0.3	0.3	0.3	0.3	0.5	1.8
Average		0.5	0.4	0.6	0.4	0.7	0.5	1.0	1.3
Frame Average		0.5		0.5		0.6		1.2	

Moment-curvature relationships calculated for the first story columns of the revised design are presented in Figure 5.15. The figure format and the calculation procedure is the same as that of Figure 5.8, which was presented for existing design. Curvature demands are marked as dots on bilinear curves. Some variation in curvature demand among frames can be observed in Figure 5.15. Compared with the yield curvature, computed inelastic deformation is somewhat limited. Consequently, relatively low ductilities are registered for the first story columns.

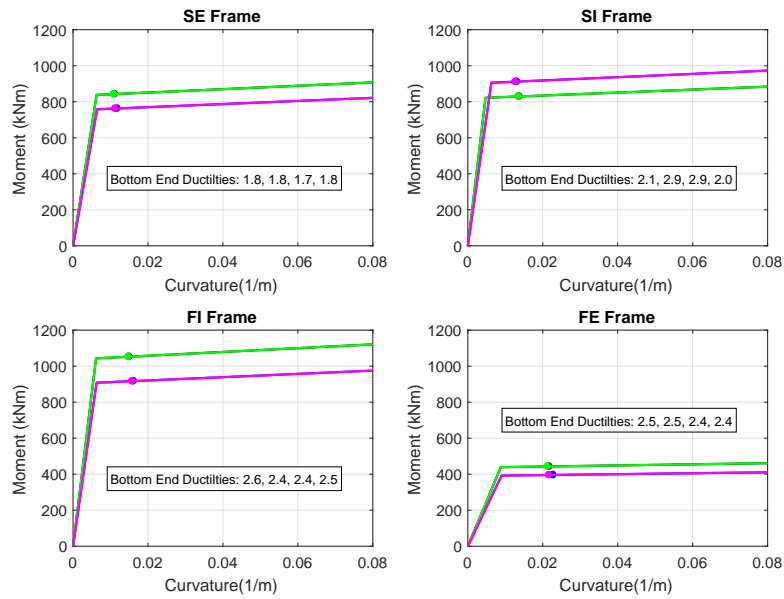


Figure 5.15: Bi-linearized moment curvature relationships of first story columns and computed ductility demands on these columns obtained for revised design.

5.11 Performance Comparison between Existing and Revised Designs

Seismic performances of existing and revised designs have been discussed individually in the previous sections. Here, the seismic response quantities from two designs are compared, and the performance improvement provided by the Optimal Strength Distribution Method is evaluated.

5.11.1 Comparison of the Frame Responses

Mean interstory drifts, beam end curvatures and column bottom-end curvatures obtained from inelastic dynamic analyses of both existing and revised designs under the set of ground motions are compared in Figures 5.16 - 5.18, respectively. Mean value of the response parameters are plotted for four different frames in each figure. Black line in Figures 5.16 - 5.18 indicate the mean response of existing design; whereas red line illustrates the mean deformations associated with the revised design.

Mean interstory drifts given in Figure 5.16 for all four frames do not differ significantly between two designs. Since the columns at the lower stories are strengthened in the revised design, drift demands at the lower stories reduce while a slight increase occurs at the upper stories.

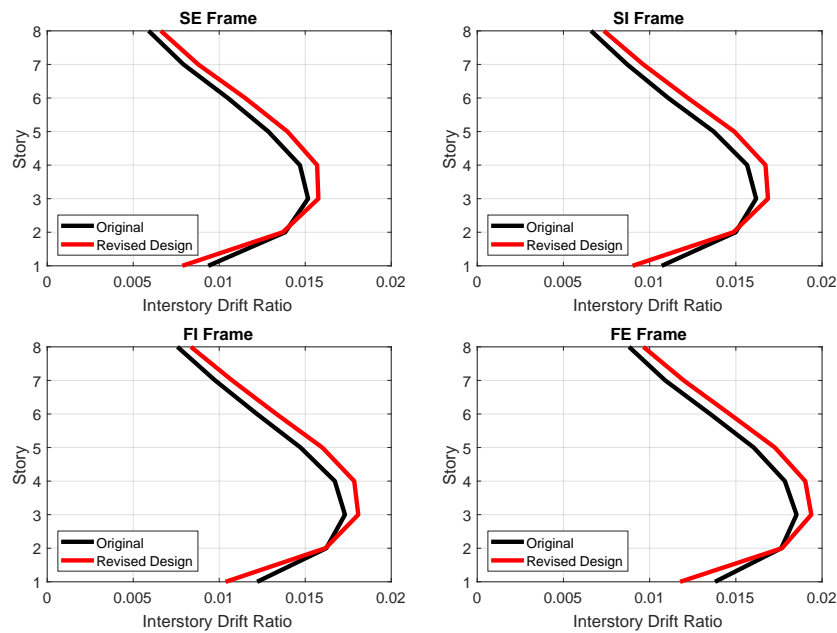


Figure 5.16: Comparison of the mean interstory drift ratios calculated for the existing and revised designs.

As observed in Figure 5.18, there is a dramatic reduction in the mean column curvature demands estimated at the bottom ends of the first story columns. This observation clearly demonstrates the positive effect of the Optimal Strength Distribution Method on damage distribution. Strengthening the columns remedies the very prominent un-

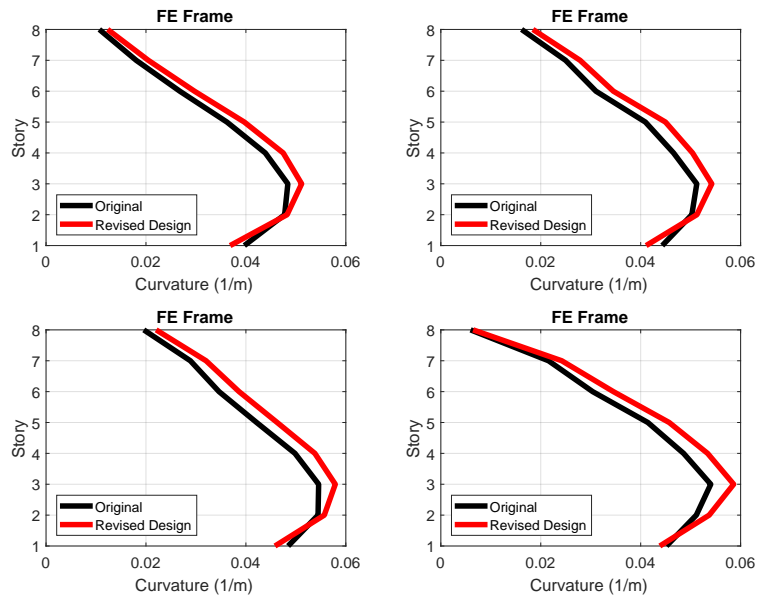


Figure 5.17: Comparison of the mean beam-end curvatures calculated for the existing and revised designs.

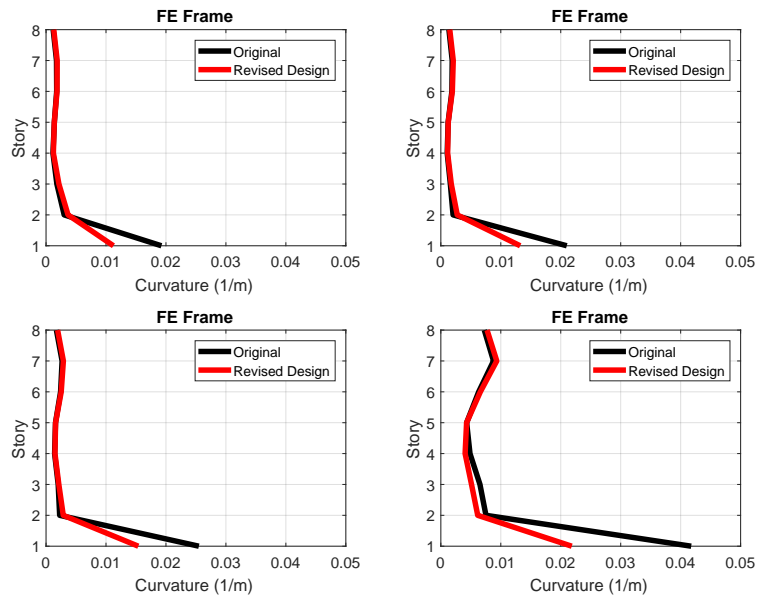


Figure 5.18: Comparison of the mean column bottom end curvatures calculated for the existing and revised designs.

balanced ductility distribution in these members. This conclusion is to be discussed further while curvature ductilities are compared.

5.11.2 Comparison of the Member Ductility Demands

Member ductilities previously given for existing (Tables 5.7 - 5.8) and revised (Tables 5.9 - 5.10) designs individually are presented here in a frame by frame comparison format. Ground motion set mean curvature ductility demands computed for two designs at both ends of each beam located in *SE*, *SI*, *FI* and *FE* frames are compared in Tables 5.11 to 5.14, respectively. Each table is presented in a format such that ductility demands at the ends of three beams located in a story of a frame are given for the two cases. In addition, percent differences of the ductility demands estimated by the revised design to those given by existing design are also presented.

Mean curvature ductility demands that were previously presented for the existing (Tables 5.7 and 5.8) and revised (Tables 5.9 and 5.10) designs separately are presented here in a frame-by-frame comparison format. Member ductilities computed for the two designs at both ends of each beam located in the *SE*, *SI*, *FI* and *FE* frames are compared in Tables 5.11 - 5.14, respectively.

The minor increase in the calculated beam ductilities for the revised design is also seen in Tables 5.11 to 5.14. Some upper story beams undergo a ductility demand increase up to 15%. In the case of first story beams however, significant reduction in ductilities is observed.

Mean column curvature ductility demands computed for the *SE*, *SI*, *FI*, and *FE* frames of the two designs are compared in Tables 5.15 - 5.18, respectively. One striking observation in Tables 5.15 to 5.18 is that column ductility values of the revised design exhibit both a reduction and a more balanced distribution compared with the existing design results. In all frames, first story column bottom-end ductilities are approximately reduced by half. Revised design yields values that range between 1.7 to 3. In the existing design, these ductilities were ranging from 4 in the *SE* frame to 7 in the *FE* frame. In addition, inelastic behavior in the *FE* frame, where a significant number of columns are modified, reduces considerably.

Table 5.11: Beam curvature ductility comparison for the Stiff Edge Frame

Story	Beam Name	Existing Design		Revised Design	
		I End	J End	I End	J End
1	BEAM1	7.5	8.4	6.9	7.9
	BEAM2	7.6	8.0	6.9	7.5
	BEAM3	7.3	8.7	6.7	8.2
2	BEAM1	8.8	10.3	8.8	10.5
	BEAM2	9.2	9.8	9.3	10.0
	BEAM3	8.6	10.5	8.6	10.7
3	BEAM1	8.7	10.5	9.1	11.2
	BEAM2	9.4	10.1	10.0	10.7
	BEAM3	8.5	10.8	8.9	11.4
4	BEAM1	8.0	9.5	8.6	10.3
	BEAM2	8.4	9.1	9.2	9.9
	BEAM3	7.8	9.9	8.4	10.6
5	BEAM1	6.7	7.9	7.3	8.6
	BEAM2	6.9	7.4	7.7	8.1
	BEAM3	6.4	8.3	7.0	8.9
6	BEAM1	5.0	5.8	5.4	6.5
	BEAM2	5.0	5.4	5.6	6.1
	BEAM3	4.6	6.3	5.1	6.9
7	BEAM1	3.3	3.9	3.6	4.5
	BEAM2	3.5	3.7	3.9	4.3
	BEAM3	3.0	4.3	3.3	4.9
8	BEAM1	2.0	2.2	2.3	2.6
	BEAM2	2.0	2.1	2.3	2.5
	BEAM3	1.7	2.7	1.9	3.2
Beam End Average		6.3	7.3	6.5	7.8
Frame Average		6.8		7.1	

Table 5.12: Beam curvature ductility comparison for the Stiff Inner Frame

Story	Beam Name	Existing Design		Revised Design	
		I End	J End	I End	J End
1	BEAM1	8.3	9.1	7.7	8.5
	BEAM2	9.0	9.3	8.2	8.6
	BEAM3	8.2	9.3	7.5	8.8
2	BEAM1	9.4	10.7	9.4	11.0
	BEAM2	10.1	10.0	10.4	10.2
	BEAM3	9.1	11.0	9.2	11.2
3	BEAM1	9.1	11.0	9.6	11.7
	BEAM2	10.1	11.1	10.7	11.8
	BEAM3	8.9	11.3	9.4	12.0
4	BEAM1	8.4	9.9	9.0	10.8
	BEAM2	9.1	10.1	9.9	10.9
	BEAM3	8.2	10.3	8.8	11.1
5	BEAM1	6.9	9.8	7.7	10.6
	BEAM2	7.6	8.2	8.3	9.1
	BEAM3	8.0	8.7	8.8	9.4
6	BEAM1	5.1	7.6	5.7	8.4
	BEAM2	5.6	6.2	6.2	7.0
	BEAM3	6.1	6.6	6.7	7.4
7	BEAM1	5.0	5.6	5.5	6.4
	BEAM2	4.1	4.5	4.6	5.1
	BEAM3	4.5	6.2	5.0	6.9
8	BEAM1	3.4	3.6	3.8	4.2
	BEAM2	2.5	2.7	2.8	3.2
	BEAM3	2.8	4.3	3.2	4.9
Beam End Average		7.1	8.2	7.4	8.7
Frame Average		7.6		8.1	

Table 5.13: Beam curvature ductility comparison for the Flexible Inner Frame

Story	Beam Name	Existing Design		Revised Design	
		I End	J End	I End	J End
1	BEAM1	9.4	9.9	8.9	9.5
	BEAM2	9.7	9.7	9.1	9.1
	BEAM3	9.2	10.2	8.7	9.7
2	BEAM1	10.3	11.5	10.4	11.8
	BEAM2	10.9	10.8	11.2	11.1
	BEAM3	10.1	11.7	10.2	12.0
3	BEAM1	9.9	11.8	10.4	12.5
	BEAM2	11.1	11.0	11.9	11.7
	BEAM3	9.7	12.1	10.2	12.8
4	BEAM1	9.2	10.7	9.9	11.5
	BEAM2	10.0	9.9	10.9	10.8
	BEAM3	9.0	11.0	9.6	11.9
5	BEAM1	7.8	8.8	8.6	9.6
	BEAM2	8.3	8.8	9.1	9.8
	BEAM3	7.5	9.3	8.3	10.1
6	BEAM1	5.8	8.4	6.5	9.3
	BEAM2	6.4	6.9	7.1	7.8
	BEAM3	6.8	7.3	7.6	8.2
7	BEAM1	5.8	6.5	6.3	7.3
	BEAM2	4.8	5.2	5.3	5.8
	BEAM3	5.3	7.1	5.8	7.9
8	BEAM1	4.1	4.3	4.5	4.9
	BEAM2	3.1	3.3	3.4	3.9
	BEAM3	3.5	5.2	3.8	5.9
Beam End Average		7.8	8.8	8.2	9.4
Frame Average		8.3		8.8	

Table 5.14: Beam curvature ductility comparison for the Flexible Edge Frame

Story	Beam Name	Existing Design		Revised Design	
		I End	J End	I End	J End
1	BEAM1	9.4	8.4	9.0	8.2
	BEAM2	9.2	9.3	9.1	9.1
	BEAM3	8.5	9.4	8.2	9.0
2	BEAM1	10.3	9.9	10.6	10.5
	BEAM2	10.5	10.3	11.2	11.0
	BEAM3	9.5	10.8	10.0	11.2
3	BEAM1	9.5	12.0	10.1	13.0
	BEAM2	10.8	11.5	11.8	12.5
	BEAM3	10.2	11.0	11.1	11.8
4	BEAM1	8.7	10.6	9.4	11.7
	BEAM2	9.7	10.1	10.7	11.3
	BEAM3	9.4	9.8	10.3	10.6
5	BEAM1	8.5	8.3	9.4	9.2
	BEAM2	7.8	8.0	8.6	8.9
	BEAM3	7.3	9.8	8.1	10.8
6	BEAM1	6.3	6.1	7.1	7.0
	BEAM2	5.5	5.9	6.2	6.7
	BEAM3	5.0	7.8	5.7	8.7
7	BEAM1	4.8	4.2	5.2	4.8
	BEAM2	3.7	3.9	4.1	4.5
	BEAM3	3.4	5.9	3.6	6.8
8	BEAM1	1.8	0.8	2.0	0.9
	BEAM2	0.6	0.7	0.7	0.7
	BEAM3	0.8	2.4	0.8	2.7
Beam End Average		7.1	7.8	7.6	8.4
Frame Average		7.5		8.0	

Table 5.15: Column curvature ductility comparison for the Stiff Edge Frame

Story	Column Name	Existing Design		Revised Design	
		Bottom End	Top End	Bottom End	Top End
1	COLUMN1	3.8	0.3	1.8	0.2
	COLUMN2	3.9	0.2	1.8	0.2
	COLUMN3	3.9	0.2	1.7	0.2
	COLUMN4	3.7	0.3	1.8	0.2
2	COLUMN1	0.6	0.2	0.7	0.3
	COLUMN2	0.7	0.3	0.8	0.3
	COLUMN3	0.6	0.3	0.7	0.3
	COLUMN4	0.5	0.2	0.6	0.3
3	COLUMN1	0.3	0.3	0.4	0.3
	COLUMN2	0.4	0.4	0.4	0.4
	COLUMN3	0.3	0.4	0.4	0.4
	COLUMN4	0.3	0.3	0.3	0.3
4	COLUMN1	0.2	0.4	0.2	0.4
	COLUMN2	0.2	0.6	0.2	0.6
	COLUMN3	0.2	0.5	0.2	0.6
	COLUMN4	0.2	0.4	0.2	0.5
5	COLUMN1	0.3	0.5	0.2	0.5
	COLUMN2	0.3	0.6	0.2	0.7
	COLUMN3	0.2	0.6	0.2	0.7
	COLUMN4	0.2	0.5	0.2	0.5
6	COLUMN1	0.3	0.5	0.3	0.5
	COLUMN2	0.3	0.7	0.3	0.7
	COLUMN3	0.3	0.7	0.3	0.7
	COLUMN4	0.3	0.5	0.3	0.5
7	COLUMN1	0.3	0.4	0.3	0.5
	COLUMN2	0.3	0.6	0.3	0.6
	COLUMN3	0.3	0.6	0.3	0.6
	COLUMN4	0.3	0.4	0.3	0.5
8	COLUMN1	0.2	0.3	0.2	0.3
	COLUMN2	0.2	0.6	0.2	0.6
	COLUMN3	0.2	0.6	0.2	0.6
	COLUMN4	0.2	0.3	0.2	0.3
Column End Average		0.7	0.4	0.5	0.4
Frame Average		0.6		0.5	

Table 5.16: Column curvature ductility comparison for the Stiff Inner Frame

Story	Column Name	Existing Design		Revised Design	
		Bottom End	Top End	Bottom End	Top End
1	COLUMN1	4.6	0.2	2.1	0.2
	COLUMN2	4.3	0.2	2.9	0.3
	COLUMN3	4.3	0.2	2.9	0.3
	COLUMN4	4.6	0.2	2.0	0.2
2	COLUMN1	0.4	0.2	0.6	0.3
	COLUMN2	0.5	0.3	0.6	0.3
	COLUMN3	0.4	0.3	0.6	0.3
	COLUMN4	0.4	0.3	0.5	0.3
3	COLUMN1	0.3	0.3	0.3	0.3
	COLUMN2	0.4	0.4	0.4	0.3
	COLUMN3	0.3	0.3	0.4	0.3
	COLUMN4	0.3	0.3	0.3	0.3
4	COLUMN1	0.2	0.4	0.2	0.4
	COLUMN2	0.2	0.5	0.2	0.5
	COLUMN3	0.2	0.5	0.2	0.5
	COLUMN4	0.2	0.5	0.2	0.5
5	COLUMN1	0.2	0.5	0.2	0.5
	COLUMN2	0.2	0.6	0.2	0.6
	COLUMN3	0.2	0.6	0.2	0.6
	COLUMN4	0.2	0.5	0.2	0.6
6	COLUMN1	0.3	0.5	0.4	0.5
	COLUMN2	0.3	0.6	0.4	0.7
	COLUMN3	0.3	0.6	0.3	0.7
	COLUMN4	0.3	0.5	0.3	0.6
7	COLUMN1	0.4	0.4	0.4	0.5
	COLUMN2	0.3	0.5	0.3	0.6
	COLUMN3	0.3	0.5	0.4	0.6
	COLUMN4	0.3	0.4	0.3	0.5
8	COLUMN1	0.3	0.3	0.3	0.3
	COLUMN2	0.2	0.6	0.2	0.6
	COLUMN3	0.2	0.5	0.2	0.5
	COLUMN4	0.2	0.3	0.3	0.3
Column End Average		0.8	0.4	0.6	0.4
Frame Average		0.6		0.5	

Table 5.17: Column curvature ductility comparison for the Flexible Inner Frame

Story	Column Name	Existing Design		Revised Design	
		Bottom End	Top End	Bottom End	Top End
1	COLUMN1	5.6	0.3	2.6	0.2
	COLUMN2	5.3	0.3	2.4	0.2
	COLUMN3	5.2	0.3	2.4	0.2
	COLUMN4	5.5	0.3	2.5	0.2
2	COLUMN1	0.5	0.3	0.6	0.3
	COLUMN2	0.5	0.4	0.6	0.4
	COLUMN3	0.5	0.3	0.6	0.3
	COLUMN4	0.4	0.3	0.6	0.3
3	COLUMN1	0.4	0.4	0.4	0.4
	COLUMN2	0.5	0.4	0.5	0.4
	COLUMN3	0.4	0.4	0.4	0.4
	COLUMN4	0.4	0.4	0.4	0.4
4	COLUMN1	0.3	0.5	0.3	0.5
	COLUMN2	0.3	0.6	0.3	0.6
	COLUMN3	0.3	0.6	0.3	0.6
	COLUMN4	0.3	0.6	0.3	0.5
5	COLUMN1	0.3	0.6	0.3	0.6
	COLUMN2	0.3	0.8	0.3	0.8
	COLUMN3	0.3	0.7	0.3	0.8
	COLUMN4	0.3	0.6	0.3	0.7
6	COLUMN1	0.4	0.6	0.5	0.7
	COLUMN2	0.5	0.8	0.5	0.9
	COLUMN3	0.4	0.7	0.4	0.8
	COLUMN4	0.4	0.7	0.5	0.8
7	COLUMN1	0.5	0.5	0.5	0.6
	COLUMN2	0.5	0.6	0.5	0.7
	COLUMN3	0.5	0.6	0.5	0.7
	COLUMN4	0.4	0.5	0.5	0.6
8	COLUMN1	0.3	0.3	0.4	0.3
	COLUMN2	0.3	0.6	0.3	0.7
	COLUMN3	0.3	0.6	0.3	0.6
	COLUMN4	0.3	0.3	0.3	0.3
Column End Average		1.0	0.5	0.7	0.5
Frame Average		0.8		0.6	

Table 5.18: Column curvature ductility comparison for the Flexible Edge Frame

Story	Column Name	Existing Design		Revised Design	
		Bottom End	Top End	Bottom End	Top End
1	COLUMN1	6.9	0.4	2.5	0.2
	COLUMN2	6.9	0.6	2.5	0.3
	COLUMN3	6.8	0.5	2.4	0.3
	COLUMN4	6.7	0.4	2.4	0.2
2	COLUMN1	0.9	0.6	0.9	0.6
	COLUMN2	1.7	1.1	0.7	0.5
	COLUMN3	1.4	1.0	0.7	0.5
	COLUMN4	0.8	0.6	1.0	0.7
3	COLUMN1	0.8	0.7	0.8	0.7
	COLUMN2	1.4	1.1	0.6	0.5
	COLUMN3	1.2	1.1	0.6	0.5
	COLUMN4	0.7	0.7	0.7	0.7
4	COLUMN1	0.6	0.9	0.6	0.9
	COLUMN2	0.9	1.5	0.4	0.6
	COLUMN3	0.9	1.4	0.4	0.6
	COLUMN4	0.6	1.1	0.6	1.1
5	COLUMN1	0.5	1.1	0.5	1.2
	COLUMN2	0.8	2.0	0.8	2.1
	COLUMN3	0.8	1.9	0.8	1.9
	COLUMN4	0.5	1.1	0.5	1.2
6	COLUMN1	0.6	1.1	0.7	1.2
	COLUMN2	1.3	2.4	1.3	2.6
	COLUMN3	1.1	2.3	1.1	2.5
	COLUMN4	0.6	1.1	0.6	1.3
7	COLUMN1	0.8	0.9	0.8	1.1
	COLUMN2	1.5	2.2	1.6	2.5
	COLUMN3	1.5	2.0	1.6	2.3
	COLUMN4	0.8	0.8	0.9	1.0
8	COLUMN1	0.5	1.8	0.5	1.8
	COLUMN2	1.3	4.0	1.4	4.6
	COLUMN3	1.3	3.7	1.4	4.1
	COLUMN4	0.5	1.6	0.5	1.8
Column End Average		1.7	1.4	1.0	1.3
Frame Average		1.5		1.2	

5.12 Summary and Discussions

In this chapter, a stiffness asymmetric eight-story reinforced concrete structure is designed per code regulations and its seismic response has been investigated through inelastic dynamic analyses under the set of compatible, design spectrum scaled ground motions. Then, the Optimal Strength Distribution Method proposed herein is applied to the structure and the existing design is revised by altering the reinforcement detailing of some columns as indicated by the procedure. Finally, inelastic dynamic analyses are performed for the revised structure under the same ground motion set. Seismic response associated with the revised design is compiled, and frame inter-story drifts, beam-column curvatures and curvature ductilities from the existing and modified systems are compared.

Upon inspecting the comparisons carried out in Section 5.11, it is observed that the implementation of Optimal Strength Distribution Method clearly improves the seismic performance of eight story asymmetric structure in terms of damage distribution. Not only uneven, unbalanced ductility distribution decreases, but also significant curvature ductility that was present in the first story columns is also reduced.

In the following Chapter, seismic response of another eight-story structure having mass asymmetry is investigated as a second case study. The flow of next chapter closely follows what has been presented here.

CHAPTER 6

CASE STUDY 2: 8-STORY MASS ASYMMETRIC STRUCTURE

6.1 Introduction

In this section, a mass-asymmetric eight-story structure is investigated. It is the second case study that is devised to assess the performance of the Optimal Strength Distribution Method. The seismic response of the code-designed structure (*existing design*) is inspected first. Next, the design is revised and the improvement in inelastic response is assessed comparatively.

6.2 General Information

The building is designed in compliance with ASCE 7-10 [4], the Turkish Earthquake Code [73] and Reinforced Concrete Standard of Turkey (TS-500) [87]. Capacity design principles are imposed in design. The structure is a reinforced concrete moment-frame that is composed of eight identical stories. Typical story plan and elevation view are presented in Figure 6.1. Direction of seismic excitation is along the Y-axis. Characteristic strengths of concrete and reinforcing steel are 35 MPa and 420 MPa, respectively. Width of all beams is 0.30 m and the depth is 0.55 m. Size of all columns is 0.5 m by 0.5 m and the slab thickness is 0.14 m at all stories. Story height is 3.5 meters at the first story, while other stories are 3 meters high. As specified in the Turkish Earthquake Code, cracked section properties are imposed for beams and columns by multiplying the section stiffnesses by 0.35 and 0.70, respectively. The plan view indicates that the stiffness distribution is symmetrical with respect to the geometric centroid. Asymmetric behavior in the system is due to the shifted mass center (*CM*)

of each story by 15% of the plan dimension with respect to the center of rigidity (CR), perpendicular to the direction of analysis. Consequently, a one-way asymmetric system is obtained along the Y-axis as shown in Figure 6.1. Frames in the figure are labeled in view of their expected lateral strengths. This issue is elaborated further in the following sections. Geometric properties of members are kept constant along the height of the structure. Since there is no variation in member sizes, system does not exhibit stiffness asymmetry. Therefore, Center of Rigidity (CR) is coincident with the geometric center (CG). Consequently, design eccentricity is equal to the amount of shift in the CM location.

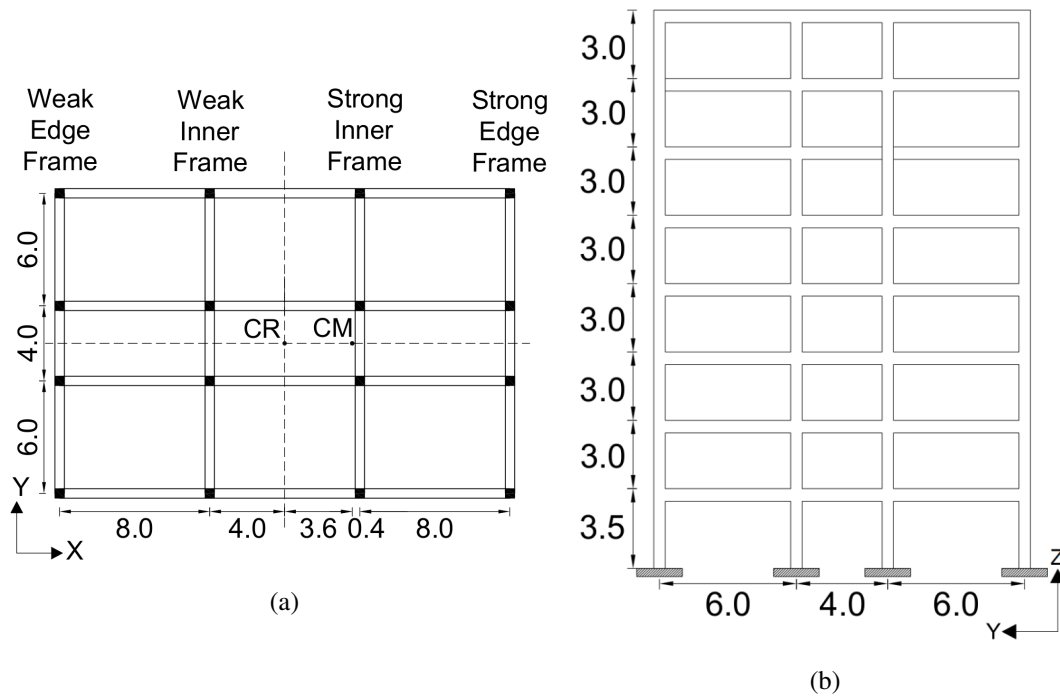


Figure 6.1: Typical story plan of the eight story mass-asymmetric structure and elevation view of the frames in the direction of analysis. Center of Rigidity (CR) and Center of mass (CM) locations (same for all stories) are marked on the plan. (Units in meters)

6.3 Free Vibration Properties

Free vibration properties for the first six modes are presented in Table 6.1. Modes denoted with X and Y are translation dominant modes in the respective directions, and modes denoted with θ are the torsion dominant modes. Effective modal masses calculated in each direction as well as effective modal mass ratios are also given for each mode. Frequency ratios ω_θ computed for X and Y directions are both 1.44. Hence, the eight-story structure is torsionally stiff in both orthogonal directions.

Table 6.1: Free vibration properties of the eight-story mass-asymmetric structure

Mode	Period (Seconds)	Effective Modal Mass - Y (tons)	Effective Modal Mass Ratio - Y	Effective Modal Mass - X (tons)	Effective Modal Mass Ratio - X
1X	1.663	1280	0.667	0	0
1Y	1.662	0	0	1616	0.842
1 θ	1.156	345	0.180	0	0
2X	0.543	144	0.075	0	0
2Y	0.527	0	0	184	0.096
2 θ	0.374	42	0.022	0	0

6.4 Labeling of Frames

Due to the position of the center of mass, frames to the right of the CM in Figure 6.1 are expected to receive higher force demands. This would necessitate designing them *stronger* compared with the remaining frames. Considering that the section sizes are constant, such a design can be achieved by utilizing higher reinforcement amounts in these members. Similarly, frames to the left of CM would exhibit lesser lateral force demands. Members located in these frames can be designed such that they are *weaker* compared with frames with higher lateral strength capacities. Frames in the direction of analysis are labeled according to the expected strength levels through their designs. Frame at the strong edge is denoted as the strong edge frame and the next one on this side is called the strong inner frame. Similarly, the frame at the weak edge is denoted as the weak edge frame and the inner one on this side is called the weak inner frame. Using the same analogy, the right side of structure with respect to CM is labeled as

strong side while the other side is designated as the *weak side*. The frame notation adopted herein is in contrast to the classical notation for linear elastic asymmetric plan systems where the edge that displaces more, the exterior frame close to the *CM* in this case, is called the *flexible side*, while the other side is the *stiff side*. The stiff side usually demands less strength; hence it is the weak side in terms of strength. Since the focus in this study is the strength distribution rather than the stiffness, strong-weak notation has more sense than the stiff-flexible notation.

6.5 Linear Elastic Design Spectrum

Linear elastic design spectrum discussed in Section 5.5 is utilized for this case study as well. It was previously shown in Figure 5.2. The design spectrum has been constructed for an imaginary location in downtown San Francisco on Site Class C. The parameters associated with this site yields $S_{DS} = 1.0g$. While performing seismic design, linear elastic spectrum has been reduced by the response reduction factor $R = 8$.

6.6 Seismic Design

Capacity design principles are employed in seismic design. Beams are designed optimally to meet their demands throughout the structure. There is little amount of overstrength available in these members. Column design is governed by the minimum longitudinal reinforcement ratio ($\rho_{min} = 1\%$) as per code requirements. Therefore, eight 20 mm bars are provided for columns. Due to the minimum longitudinal reinforcement requirement, significant amount of overstrength is expected especially at the weak side frames that attain lower demands. Upon completion of the *existing design*, strong column-weak beam checks are performed at each joint in the direction of analysis. Ratio of total column moments to the total beam moments at every joint is given in Table 6.2. It should be noted here that joints in each story of each frame in Table 6.2 are labeled along the Y direction from right (joint 1) to left (joint 4) as shown in the frame elevation view given in Figure 6.1.

Table 6.2: Strong column - weak beam checks for the Existing Design: Ratio of total column moment capacity to total beam moment capacity at each joint of the structure.

Story	Joint	WE Frame	WI Frame	SI Frame	SE Frame
1	1	6.4	7.7	6.0	3.5
	2	3.0	3.6	2.9	1.8
	3	3.0	3.6	2.9	1.8
	4	4.5	5.4	4.3	3.0
2	1	6.1	7.4	5.7	3.3
	2	2.8	3.5	2.8	1.7
	3	2.8	3.5	2.8	1.7
	4	4.2	5.1	4.1	2.8
3	1	5.7	7.0	3.8	3.1
	2	2.7	3.3	2.3	1.6
	3	2.7	3.3	2.2	1.6
	4	4.0	4.9	3.2	2.7
4	1	5.4	6.5	5.1	4.2
	2	2.5	3.0	2.6	2.0
	3	3.0	3.6	2.7	2.0
	4	3.8	4.5	3.6	3.0
5	1	4.9	6.0	6.0	3.9
	2	2.7	2.7	2.8	2.0
	3	2.7	3.3	2.8	2.1
	4	4.9	4.2	4.2	2.8
6	1	4.6	5.4	5.4	4.7
	2	2.5	2.4	2.4	2.1
	3	2.5	3.0	3.0	2.1
	4	4.6	3.8	3.8	3.3
7	1	4.1	4.7	4.7	4.1
	2	2.2	2.1	2.1	2.2
	3	2.2	2.5	2.5	2.2
	4	4.1	3.3	3.3	4.1
8	1	2.0	2.1	2.1	2.0
	2	1.0	1.2	1.2	1.0
	3	1.0	1.2	1.2	1.0
	4	2.0	2.1	2.1	2.0

6.6.1 Frame Design Shears

Design shear forces obtained from linear elastic response spectrum analysis are calculated at the base of four frames. It should be noted that these shear forces are obtained under reduced design spectrum. Frame shear forces at each frame are given in Table 6.3. Strong side frames attain higher shear forces compared with the weak side frames. Design shears of the weak side frames are found to be close to each other. Since weak inner frame is expected to deform least under seismic loads, it exhibits lowest shear demands.

Table 6.3: Frame design shear forces ($V_{d,Frame}$). Units in kN.

Weak Edge Frame	Weak Inner Frame	Strong Inner Frame	Strong Edge Frame
217	188	261	390

6.6.2 Computation of Frame Strengths

Frame strengths of the mass-asymmetric structure are determined as discussed in Section 4.6. Capacity shears of the frames computed at the formation of first story mechanism are given in Table 6.4. The inner frames exhibit higher strength compared with the outer frames. This is due to larger axial loads carried by the first story columns located at the inner frames.

Table 6.4: Frame base shear strengths (F_{Frame}) of the *Existing Design*. Units in kN.

Weak Edge Frame	Weak Inner Frame	Strong Inner Frame	Strong Edge Frame
591	691	729	673

6.6.3 Determination of the Flexible and Stiff Sides of the Structure and $SFSR_{existing}$

As mentioned previously, dimensions of columns and beams do not show any variation among frames of the mass-asymmetric structure. However, strengths of these frames vary due to the seismic design requirements of their members as discussed in Section 6.4. The correlation between strength and stiffness of reinforced concrete

members has been studied over the decades by a number of researchers. Paulay [69] noted that yield deformations of reinforced concrete sections are directly related with section geometries and yield strain of longitudinal reinforcement. Since section sizes and material properties do not vary throughout the structure, yield deformations of all beams are expected to be similar. This is also valid for the columns. Consequently, individual frames of the mass-asymmetric system are expected to exhibit inelastic behavior at same yield deformation levels (u_y). Although four frames of the structure yield at u_y , they attain different strengths. Column sizes are governed by the gravity load requirements and the sizes of column members do not vary. On the other hand, bending moment capacities of beams change according to their seismic demands. This results in stronger frames that experience higher seismic demands than the other ones. In the case of particular mass-asymmetric system, frames to the right of CM in Figure 6.1 register higher demands; hence, they are designed stronger. Due to the relationship between strength and stiffness when u_y is constant, frames having stronger beams are indeed stiffer. This discussion given above is presented visually in Figure 6.2. The idealized force-deformation relationships of the strong and weak sides of the system are shown in the Figure. Since all frames yield approximately at the same deformation, the stronger side is the stiff side of the mass-asymmetric system. Similarly, weak side of the structure is the flexible side.

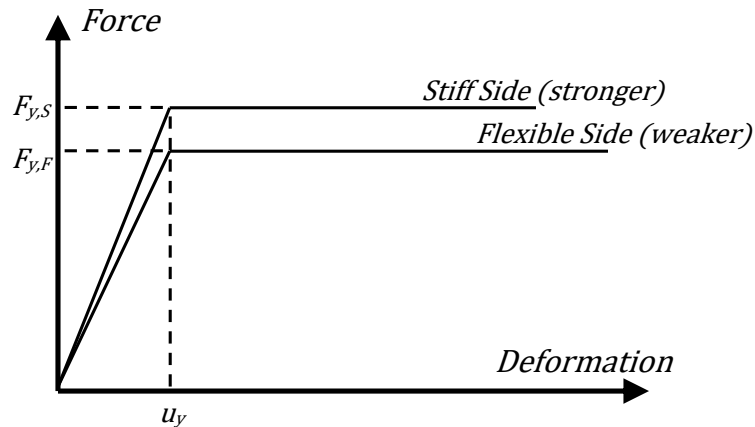


Figure 6.2: Idealized force-deformation relationships of flexible and stiff sides of the system.

The stiff side of the particular system is associated with the right side of the CM in Figure 6.1 where stronger frames are located. Similarly, flexible side is defined as the

side where Weak Edge and Weak Inner Frames are located. After frames are identified with respect to their strengths and expected stiffnesses, existing Stiff to Flexible Strength Ratio ($SFSR_{existing}$) can be computed. According to the discussion given above, stiff side strength is computed by summing the strengths of Strong Edge and Strong Inner frames given in Table 6.4. Similarly, flexible side strength is determined through summation of Weak Edge and Weak Inner frame strengths. By dividing stiff side strength to flexible side strength, $SFSR_{existing}$ is determined as 1.09.

6.6.4 System Overstrength and Computation of Ductility Reduction Factor

Distribution of frame strengths and design shears given in Tables 6.3 and 6.4, respectively are displayed graphically in Figure 6.3. Values for each frame are plotted along the location of four frames. There is significant amount of overstrength resulting from the code compliant seismic design in all frames in Figure 6.3. This is most pronounced at the Weak Inner frame where lowest shear demands are registered. On the other hand, least amount of overstrength occurs in the strong edge frame due to the highest seismic force demands. As it was shown in Equation 5.4, overstrength in each frame (Ω_{Frame}) is the ratio of frame base shear strength (existing capacity) to the frame base shear design shear force (demand). The computed Ω_{Frame} values are given in Figure 6.3, as well. Similarly, overstrength of the structure (Ω_{Global}) is also determined as 2.54. This value is obtained by dividing the sum of frame strengths with the sum of frame design shear forces.

As discussed in Section 5.6.3, Ω_{Global} is the actual value of the overstrength factor. Using Ω_{Global} and response reduction factor (R) associated with the seismic design of structure, ductility reduction factor (R_{mu}) can be estimated as shown Equation 6.1. Since $R = 8$ is employed in design, R_{mu} is computed as 3.15 for the mass-asymmetric structure from Equation 6.1.

$$R_{mu} = \frac{R}{\Omega_{Global}} \quad (6.1)$$

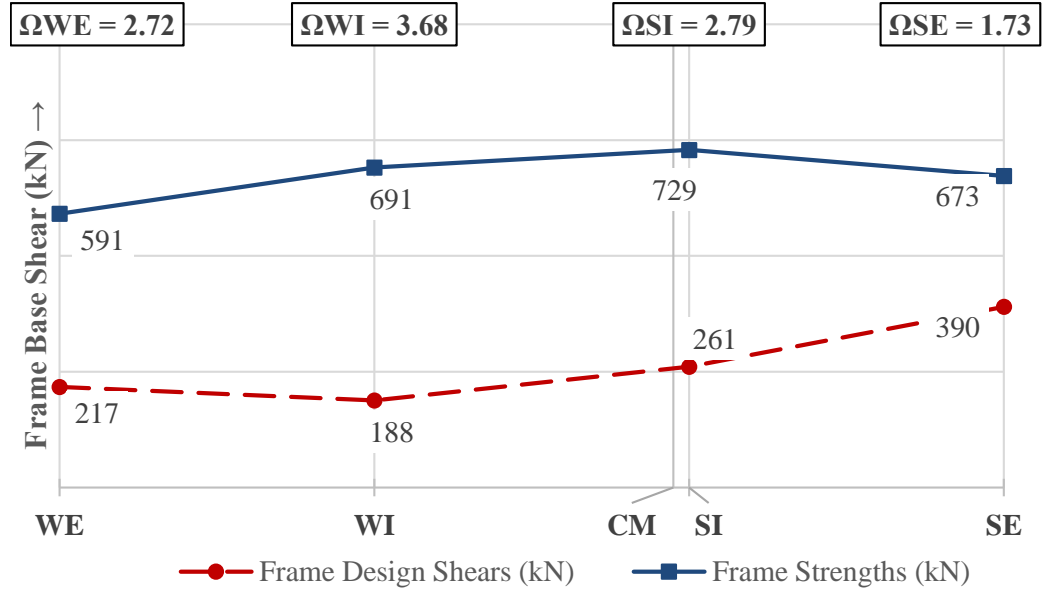


Figure 6.3: Distribution of frame shears and strengths along four frames of the mass asymmetric system (units in kN).

6.7 Analytical Modeling and Strong Ground Motion Set

Three-dimensional mathematical model of the structure is prepared in the OpenSees Platform [65] so that nonlinear dynamic analyses could be performed for performance assessment. “forceBeamColumn” elements with “HingeRadau” option enabled are utilized for both columns and beams in the mathematical model. Moment-curvature relationships obtained from beam sections are defined for beam ends, fiber sections are used in column ends. Behavior of these elements and implementation of inelastic properties for beams and columns was discussed in Section 5.7. Cracked section stiffness is considered for linear elastic portions of all members by reducing the gross section inertias by previously defined coefficients. Same strong ground motion set that has been used in Chapter 5 is utilized in nonlinear response history analyses. Strong ground motion records having similar characteristics had been selected from the PEER NGA Database [66]. Detailed information regarding the selected strong ground motions were given in Table 5.6. Simple amplitude scaling, which was discussed in Section 5.7, is applied to the strong ground motion set. At the end of the two-step scaling procedure, scale factors associated with each strong ground motion

are obtained. These factors calculated for the eight story asymmetric structure are tabulated in Table 6.5.

Table 6.5: Strong ground motion records employed in dynamic analyses.

Earthquake Name	GMCODE	YEAR	Mw	Scale Factor
Manjil, Iran	ABBAR-L	1990	7.37	2.23
Superstition Hills-02	B-PTS225	1987	6.54	0.41
Parkfield	C05085	1966	6.19	3.04
Victoria, Mexico	CPE045	1980	6.33	1.78
Duzce, Turkey	375-E	1999	7.14	3.19
Kocaeli, Turkey	DZC270	1999	7.51	0.82
Imperial Valley-06	H-E07230	1979	6.53	0.81
Imperial Valley-06	H-E08230	1979	6.53	2.69
Hector Mine	HEC090	1999	7.13	1.05
Kobe, Japan	KAK090	1995	6.9	0.91

6.8 Dynamic Analysis Results of the Existing Design

Convergence has been achieved for the seven of ten dynamic analyses performed under the scaled ground motion set. Inelastic response history analyses under scaled H-E08230, H-E07230 and DZC270 records could not be completed due to excessive deformations experienced by the analytical model. Therefore, results compiled for analyses under seven strong ground motion records are presented. Response parameters that are calculated for each frame during the dynamic analyses are given below. Maximum interstory drift ratios calculated for the four frames are given in Figure 6.4. Story mean values of maximum curvatures measured at the beam-ends at each story are presented in Figure 6.5 for all frames. Similarly, story mean of maximum column bottom-end curvatures of each frame are displayed in Figure 6.6. Finally, frame shear forces are given in Figure 6.7. Mean results for the seven ground motions are also plotted in red bold line for each response parameter given in Figures 6.4 - 6.7.

As can be seen in Figures 6.4 and 6.5, interstory drift ratios and story mean beam-end curvature demands are slightly increasing towards the strong edge frame. In two of the seven dynamic analyses, significant amount of deformation is registered at the

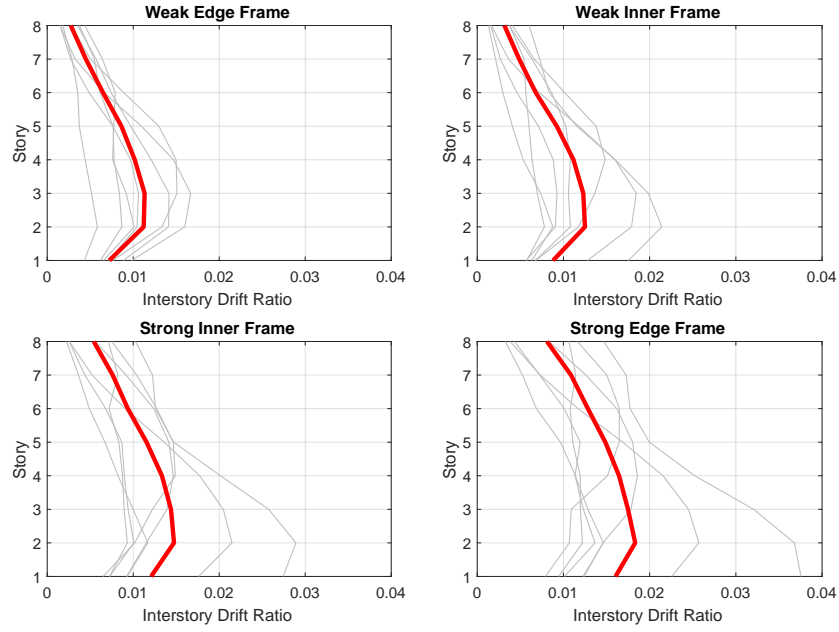


Figure 6.4: Maximum interstory drift ratios obtained from inelastic dynamic analyses of the existing design under ground motion set and the corresponding mean of maximum values.

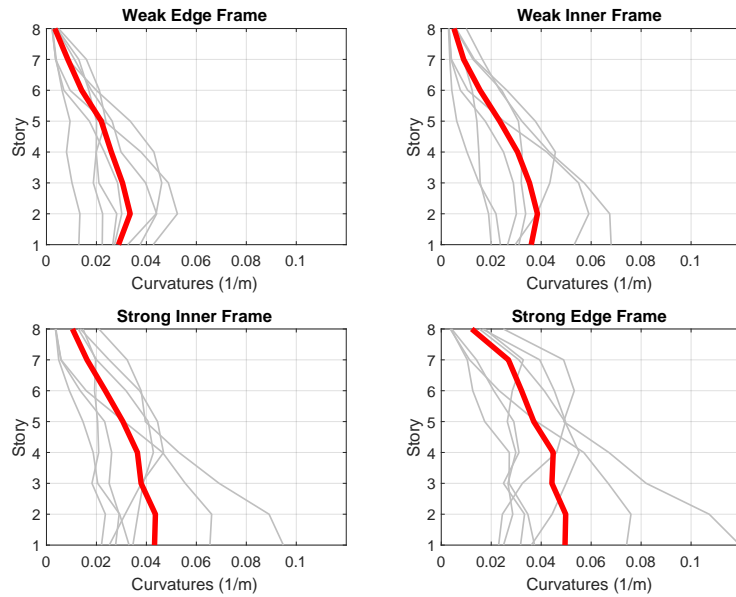


Figure 6.5: Beam-end curvatures obtained from inelastic dynamic analyses of the existing design under ground motion set and the corresponding mean of maximum values.

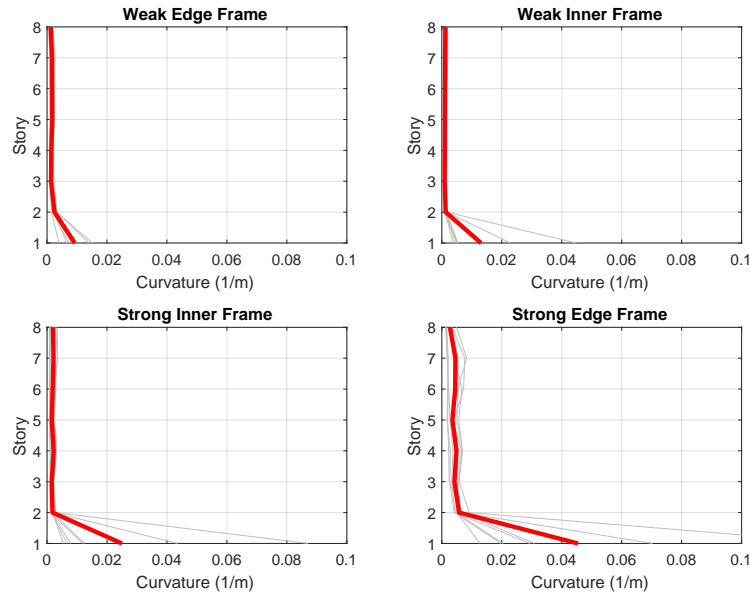


Figure 6.6: Column bottom end curvatures obtained from inelastic dynamic analyses of the existing design under ground motion set and the corresponding mean of maximum values.

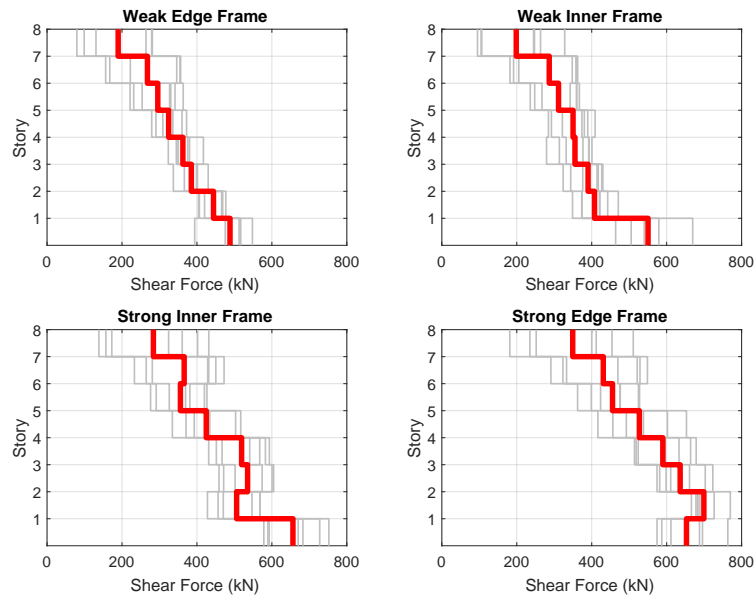


Figure 6.7: Frame shear forces obtained from inelastic dynamic analyses of the existing design under ground motion set and the corresponding mean of maximum values.

strong side frames. These large demands result in an increase in the mean values of interstory drift and beam end curvature demands computed for these frames.

High curvature demands are observed at the bottom ends of first story columns located at the strong side compared with those at the weak side of the structure in Figure 6.6. Similar to what has been observed in Figures 6.4 and 6.5, two of the ground motions yielded greater curvature demands at first story columns of strong side frames. Little variation among frame shears is observed in Figure 6.7. This is considered as an expected outcome since stiffness of all four frames are approximately the same. Mean frame base shears computed at the end of dynamic analyses are also close to frame base shear strengths given in Table 6.4.

The ground motion set mean values of curvature ductilities computed at each beam and column end are presented in Tables 6.6 and 6.7. The format of the tables is the same as Tables 5.7 and 5.8 presented in Chapter 5. Each beam and column located on every story are numbered from bottom to top along Y Axis as given in Figure 6.1. As can be seen in Table 6.6, beam curvature ductilities exhibit an increasing trend towards the strong edge frame. Average curvature ductility measured for beams located at the middle stories of inner frames is determined to be close to the value of response reduction factor ($R = 8$). However, it can also be seen that curvature ductility demands of beams located at the first four stories of the strong edge frame exceed the value of response reduction factor. Inelastic deformation in columns is observed only at the first story in the weak, weak inner and strong inner frames in Table 6.7. However, strong edge frame exhibits some inelastic column deformations in the upper stories, as well as significant plasticity at the first story. An important point to note is that ductility demand at the bottom end of the first story columns in the strong edge frame is nearly four times that of measured in the weak edge frame. It can be concluded from Table 6.7 that there is strong unbalanced ductility demand at the bottom end of the first story columns.

Bi-linearized first story column moment-curvature backbone curves are plotted for each frame in Figure 6.8. These backbone curves are computed under design axial loads. It should be noted that there are two curves at each plot; one for the inner column (higher moment capacity due to greater axial loads), and the other one for

Table 6.6: Mean beam curvature ductilities of existing design under the ground motion set.

Story	Beam	Weak Edge Frame		Weak Inner Frame		Strong Inner Frame		Strong Edge Frame	
		I End	J End	I End	J End	I End	J End	I End	J End
1	Beam1	5.5	5.7	6.7	7.7	8.3	8.4	9.5	8.6
	Beam2	6.1	5.9	7.3	7.3	8.5	8.5	9.5	9.6
	Beam3	5.2	6.2	6.3	8.0	7.9	8.9	8.8	9.5
2	Beam1	6.4	6.7	7.0	8.2	7.9	8.8	9.3	8.9
	Beam2	7.1	6.8	7.9	7.8	8.8	8.7	9.6	9.6
	Beam3	6.1	7.1	6.7	8.6	7.6	9.2	8.6	9.6
3	Beam1	5.9	6.0	6.3	7.6	6.3	7.4	8.3	8.0
	Beam2	6.4	6.2	7.2	7.1	7.9	7.7	8.5	8.5
	Beam3	5.5	6.5	6.0	8.1	5.8	8.0	7.5	8.9
4	Beam1	4.9	5.0	5.4	6.6	6.4	7.3	8.8	8.4
	Beam2	5.4	5.8	5.8	6.7	7.6	7.6	9.1	8.8
	Beam3	4.7	5.4	5.0	7.2	6.1	7.8	8.2	9.0
5	Beam1	4.3	4.6	4.3	4.9	6.0	6.4	7.2	6.8
	Beam2	4.1	4.3	4.3	5.0	5.9	5.9	7.9	7.8
	Beam3	3.8	5.1	3.9	5.6	5.4	7.1	6.7	7.4
6	Beam1	3.1	2.8	2.9	3.2	4.1	4.9	6.4	6.3
	Beam2	2.4	2.6	2.9	3.4	4.5	5.2	6.6	6.4
	Beam3	2.6	3.4	2.5	3.8	3.7	5.7	5.8	7.0
7	Beam1	2.0	1.6	1.7	1.8	2.7	3.5	4.9	5.9
	Beam2	1.5	1.5	1.6	2.1	3.0	3.8	5.0	5.5
	Beam3	1.7	2.0	1.2	2.3	2.4	4.1	4.5	6.5
8	Beam1	0.8	0.7	1.0	1.1	2.1	2.3	3.2	2.0
	Beam2	0.6	0.6	0.6	0.9	1.2	2.0	1.5	2.2
	Beam3	0.7	0.8	0.8	1.6	1.5	3.4	1.6	4.2
Average		4.0	4.3	4.4	5.3	5.5	6.4	7.0	7.3
Frame average		4.2		4.8		5.9		7.1	

Table 6.7: Mean column curvature ductilities of existing design under the ground motion set.

Story	Column	Weak Edge Frame		Weak Inner Frame		Strong Inner Frame		Strong Edge Frame	
		Bottom End	Top End	Bottom End	Top End	Bottom End	Top End	Bottom End	Top End
1	Column 1	2.0	0.3	3.3	0.2	6.0	0.3	8.6	0.5
	Column 2	1.8	0.3	3.0	0.3	6.1	0.4	9.6	0.8
	Column 3	1.7	0.3	3.0	0.3	6.0	0.4	9.5	0.7
	Column 4	1.8	0.3	3.2	0.2	5.9	0.3	8.4	0.5
2	Column 1	0.4	0.3	0.3	0.2	0.4	0.4	0.9	0.8
	Column 2	0.6	0.5	0.3	0.4	0.5	0.5	1.5	1.4
	Column 3	0.5	0.5	0.3	0.3	0.5	0.5	1.3	1.4
	Column 4	0.3	0.3	0.2	0.3	0.3	0.4	0.7	0.8
3	Column 1	0.2	0.4	0.2	0.3	0.3	0.5	0.6	0.9
	Column 2	0.3	0.6	0.2	0.4	0.4	0.7	1.1	1.6
	Column 3	0.3	0.6	0.2	0.4	0.4	0.7	1.0	1.6
	Column 4	0.2	0.4	0.2	0.3	0.3	0.5	0.5	0.9
4	Column 1	0.2	0.4	0.2	0.3	0.4	0.5	0.6	0.8
	Column 2	0.3	0.6	0.2	0.5	0.5	0.7	1.2	1.3
	Column 3	0.3	0.6	0.2	0.4	0.5	0.7	1.1	1.3
	Column 4	0.2	0.4	0.2	0.3	0.4	0.5	0.6	0.8
5	Column 1	0.2	0.4	0.2	0.3	0.3	0.5	0.5	0.8
	Column 2	0.4	0.6	0.2	0.5	0.3	0.7	0.7	1.2
	Column 3	0.4	0.5	0.3	0.4	0.4	0.6	0.7	1.2
	Column 4	0.2	0.4	0.2	0.4	0.3	0.5	0.5	0.9
6	Column 1	0.2	0.4	0.2	0.3	0.3	0.5	0.6	0.7
	Column 2	0.3	0.6	0.2	0.6	0.4	0.7	0.9	1.2
	Column 3	0.3	0.6	0.2	0.5	0.3	0.6	0.8	1.1
	Column 4	0.2	0.4	0.2	0.4	0.3	0.5	0.6	0.7
7	Column 1	0.2	0.3	0.1	0.3	0.3	0.5	0.6	0.7
	Column 2	0.3	0.5	0.2	0.5	0.4	0.7	0.8	1.0
	Column 3	0.3	0.5	0.2	0.5	0.4	0.6	0.9	1.0
	Column 4	0.2	0.3	0.2	0.4	0.3	0.5	0.6	0.7
8	Column 1	0.1	0.4	0.2	0.3	0.3	0.4	0.3	0.5
	Column 2	0.3	0.5	0.2	0.5	0.3	1.0	0.5	2.4
	Column 3	0.2	0.5	0.2	0.4	0.4	0.7	0.5	1.8
	Column 4	0.1	0.4	0.2	0.4	0.3	0.4	0.3	0.5
Average		0.5	0.4	0.6	0.4	1.1	0.5	1.8	1.0
Frame average		0.5		0.5		0.8		1.4	

the outer column (lower moment capacity) of each frame. Inner column curve is plotted in green while outer column moment-curvature curve is plotted in magenta. Mean column bottom-end curvature demands are marked on these lines with dots. Curvature ductilities of first story columns are written on each plot, as well. Although the yield curvature values of the first story columns are similar in all four frames, amount of curvature demand vary significantly. Therefore, it can be concluded that the ductility unbalance observed at the first story columns is due to uneven demands rather than yield deformations of these members.

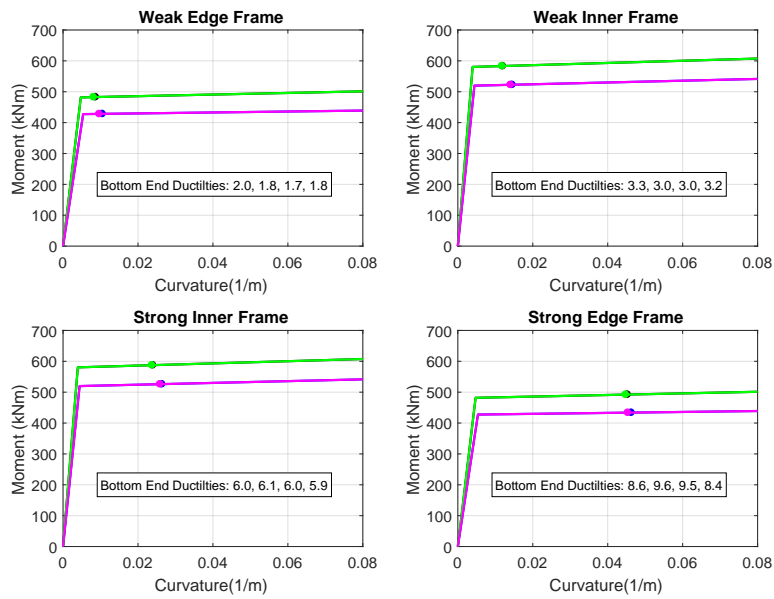


Figure 6.8: Bi-linearized moment curvature relationships of first story columns and computed ductility demands on these members.

6.9 Implementation of the Optimal Strength Distribution Method

Design of the mass-asymmetric system is to be revised through the application of Optimal Strength Distribution Method. A more balanced ductility distribution is aimed by revising the strength of the columns which are indicated by the procedure.

6.9.1 Determination of $SFSR_{opt}$

Using the system parameters e_s , T_n , and ductility reduction factor R_{mu} , optimal stiff to flexible strength ratio ($SFSR_{opt}$) is determined. Uniform Ductility Spectrum that is associated with the structural properties is utilized for this purpose. T_n was determined as 1.66 seconds previously in the direction of analysis. Furthermore, structural eccentricity (e) is 15% for all stories and R_{mu} is 3.15. Optimal Stiff to Flexible Strength Ratio ($SFSR_{opt}$) associated with these system parameters is then determined as 1.2 from Figure 3.15. After $SFSR_{opt}$ is obtained, it is compared with the $SFSR_{existing}$, which was previously determined as 1.09. Upon this comparison, it is concluded that a minor revision at the stiff side is required in order to achieve the optimal strength distribution. This situation corresponds to Case I variant of the Optimal Strength Distribution Method discussed in Section 4.3.1. It should be noted here that the stiff side of the structure has been previously associated with the strong side of the structure in Section 6.6.3.

6.9.2 Strength Allocation Diagram

Equivalent Strength Allocation Diagram of the mass-asymmetric system is shown in Figure 6.9. Target stiff edge strength (F'_S) is computed by utilizing $SFSR_{opt}$ as shown in Equation 6.2.. It is determined as 1430 kN. Nominal design strengths of F_S and F_F in Figure 6.9 are obtained from the design shears given in Table 6.3. The flexible side strength ($\Omega_F F_F$) is the summation of the capacity shears computed for the weak side frames and they are given in Table 6.4.

$$F'_S = \Omega_F F_F * SFSR_{opt} \quad (6.2)$$

ΔV and ΔT are computed according to Section 4.3.1. Optimal Load Vector that includes ΔV and ΔT is given in Equation 6.3.

$$\Delta F = \begin{bmatrix} 1656 \text{ kN} \\ 6736 \text{ kNm} \end{bmatrix} \quad (6.3)$$

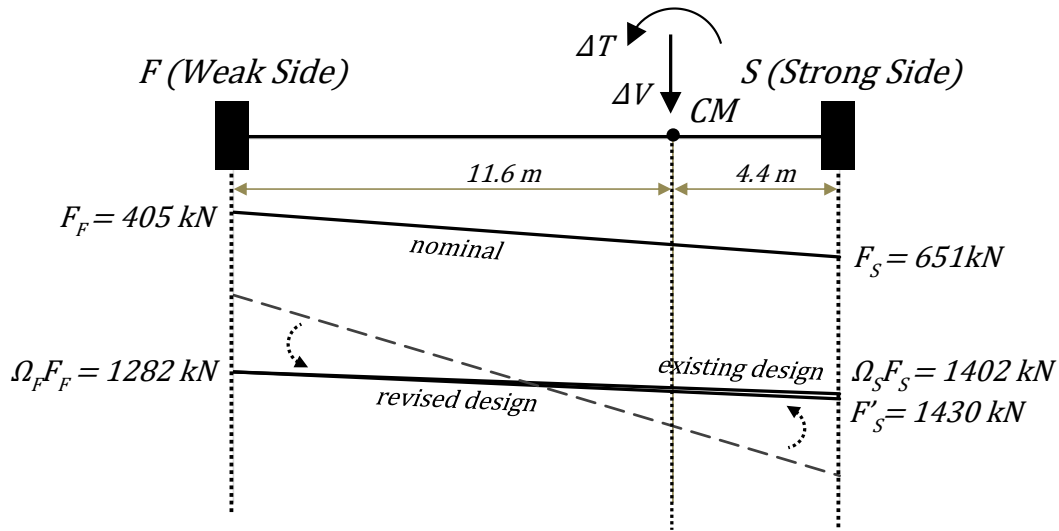


Figure 6.9: Equivalent Strength Allocation Diagram constructed for the eight story mass-asymmetric structure.

It should be noted here that both sides of the system share the applied ΔV with respect to their distances to the center of mass (CM) as displayed in Figure 6.8. Computation of these distances has been explained previously in Figure 4.8. Consequent force distribution is shown by a dashed line in the figure, as well. By applying the torque ΔT towards flexible side (positive torque with respect to sign convention in Figure 6.9), this dashed line is rotated so that the revised design strength distribution could be achieved. As can be seen in Figure 6.9, strength distribution of the existing design is quite similar to that of the revised design. A very small strength increase is necessary at the strong side of the structure in order to achieve the optimal value of SFSR, which is very close to $\text{SFSR}_{\text{existing}}$. In fact, code compliant existing design is successful in attaining near-optimal strength distribution for this specific structure. Therefore, application of the rest of the procedure is a design decision. At this stage, the engineer could decide that the existing design is satisfactory in terms of achieving optimal strength distribution. Consequently, a design alteration may not be utilized. However, design is revised within the scope of this Chapter so that the effect of the applied procedure on the unbalanced ductilities could be inspected comprehensively. The idealized force-deformation response of both sides of the structure that is expected to be achieved at the end of design revision is shown in Figure 6.10. As discussed in Section 6.6.3, the stronger side of the structure is anticipated to attain a higher

strength while yield deformations observed globally on the structure stay same.

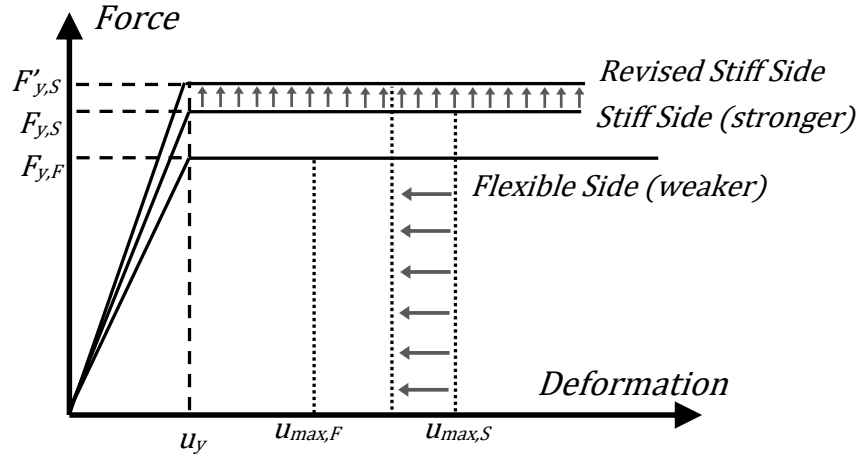


Figure 6.10: Change in idealized force-deformation relationships of flexible and stiff sides of the revised system and expected deformation levels, which are qualitatively marked on the curves.

6.9.3 Linear Elastic Analysis and Revised Seismic Design

Optimal Strength Distribution Method is carried out further after the Optimal Load Vector is determined. The complete algorithm given in Section 4.6.5 is applied and the revised demands are computed. Column members requiring strengthening due of the revised demands are given in Figure 6.11. They are marked as red dashed lines in the Figure. The updated frame design base shears, $V_{d,Frame}$, are also given beneath each frame in Figure 6.11. As can be seen in Figure 6.11, only the first story columns located at the strong edge frame requires a slight increase in their capacities. In order to achieve this target, longitudinal reinforcement ratio (ρ_l) of these columns has been increased from the minimum of 1% to 1.7% by providing 8-26 mm diameter bars. A design modification necessitated only for a very limited number of columns in the revised design of the mass-asymmetric system. This could be due to the fact that existing strength ratio of the structure and determined $SFSR_{opt}$ associated with the system are quite close to each other. Strengthening the first story columns at the strong edge has been found to be sufficient in order to achieve the modest capacity increases to obtain the optimal strength distribution.

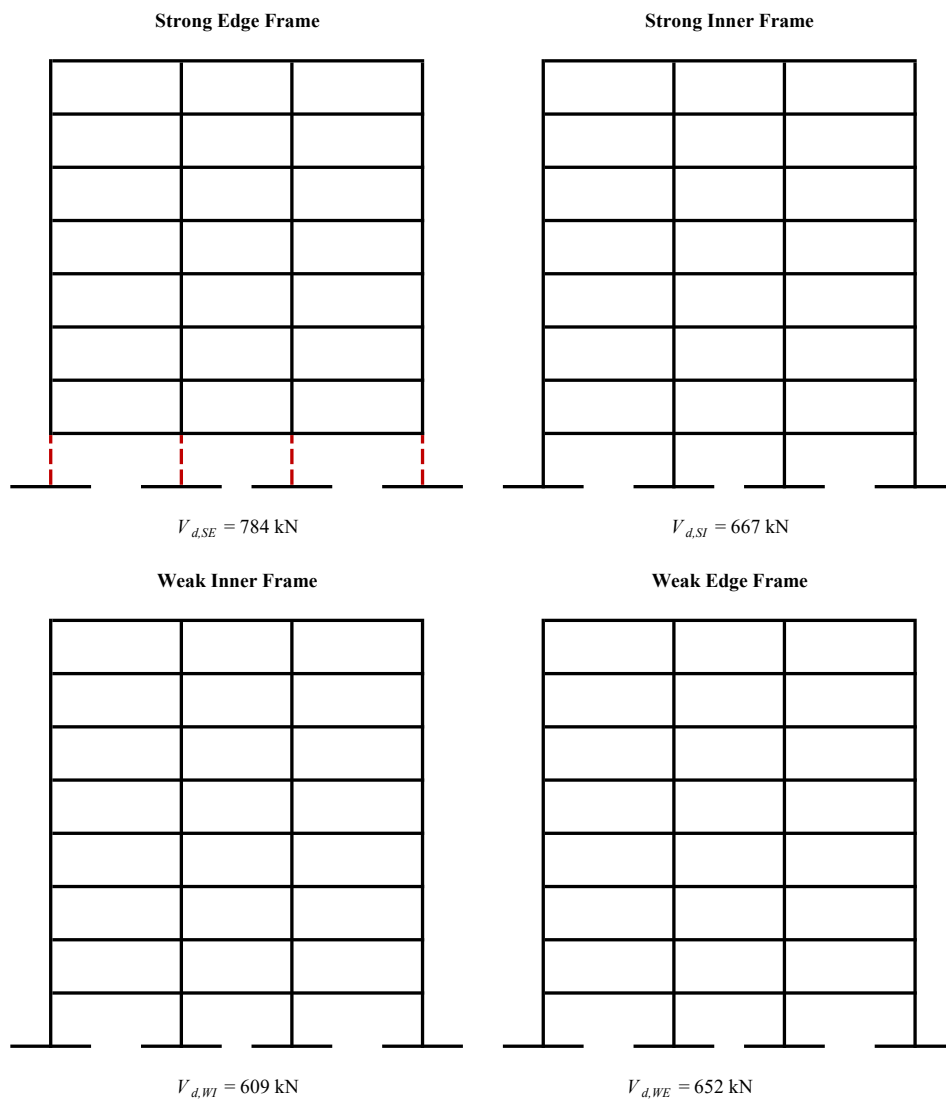


Figure 6.11: Schematic view of the four frames with columns needing design revision marked as dashed red lines.

6.10 Dynamic Analysis Results for the Revised Design

The revised system has been re-analyzed under the scaled ground motions. Analysis results are obtained for the seven ground motions for which convergence had been achieved. Interstory drifts, beam end curvatures, column bottom-end curvatures and story shears that are calculated for each frame under each ground motion and they are presented in Figures 6.12 - 6.15, respectively. Ground motion set means of the response parameters given in Figures 6.12 - 6.15 are plotted in red bold lines for each frame.

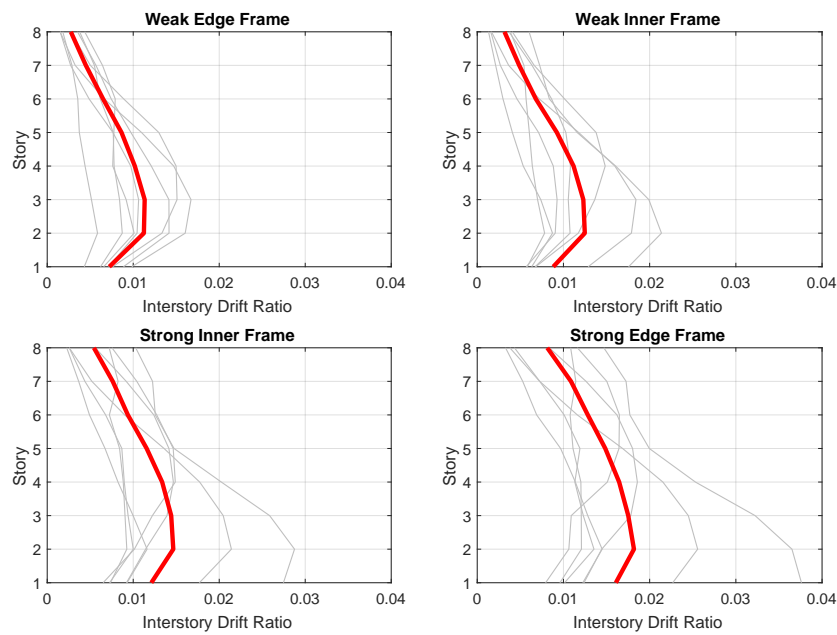


Figure 6.12: Maximum interstory drift ratios obtained from inelastic dynamic analyses of the revised design under ground motion set and the corresponding mean of maximum values.

Similar to the analysis results of existing design, interstory drift and beam end curvature demands given in Figures 6.12 and 6.13 exhibit an increasing trend towards strong edge frame. Two of the ground motions yield considerably higher demands on strong side frames. In addition, ground motion set means of the response parameters plotted in red are greater in strong side of the structure. Significant amount of curvature demand exists only at the bottom ends of first story columns in Figure 6.14. Ground motion set mean values of column end curvatures are grater in strong

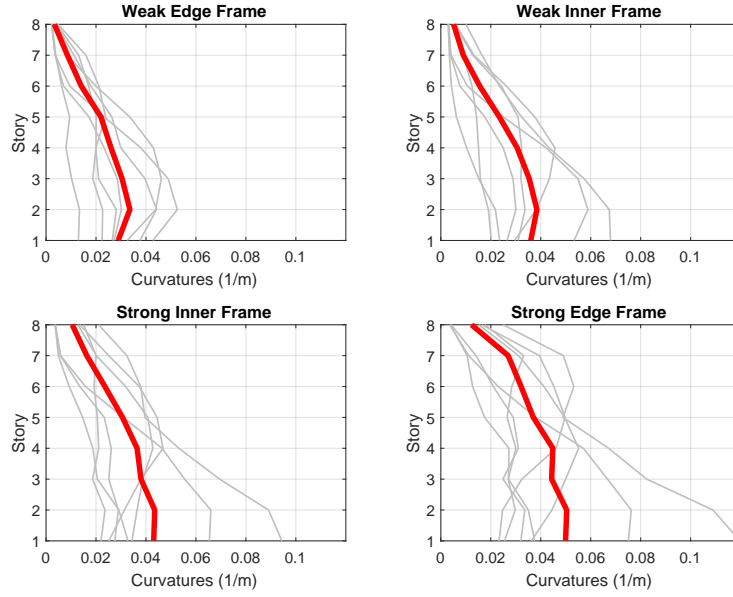


Figure 6.13: Beam-end curvatures obtained from inelastic dynamic analyses of the revised design under ground motion set and the corresponding mean of maximum values.

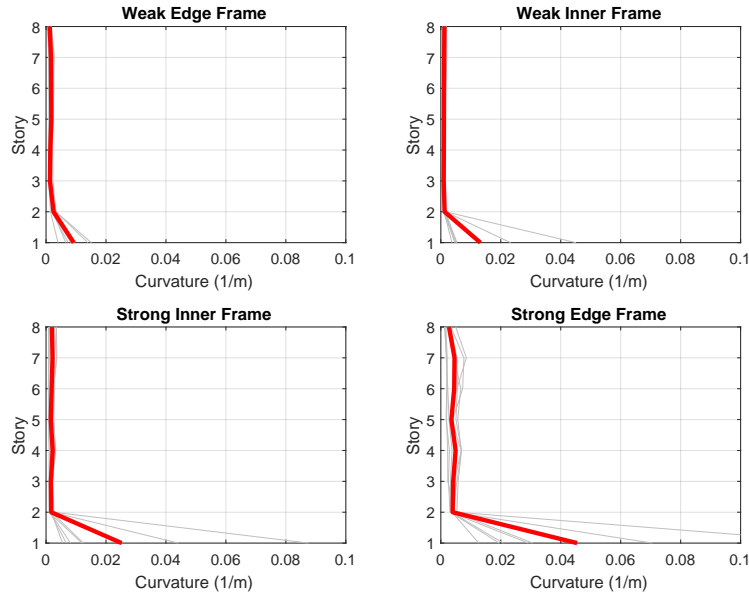


Figure 6.14: Column bottom-end curvatures obtained from inelastic dynamic analyses of the revised design under ground motion set and the corresponding mean of maximum values.

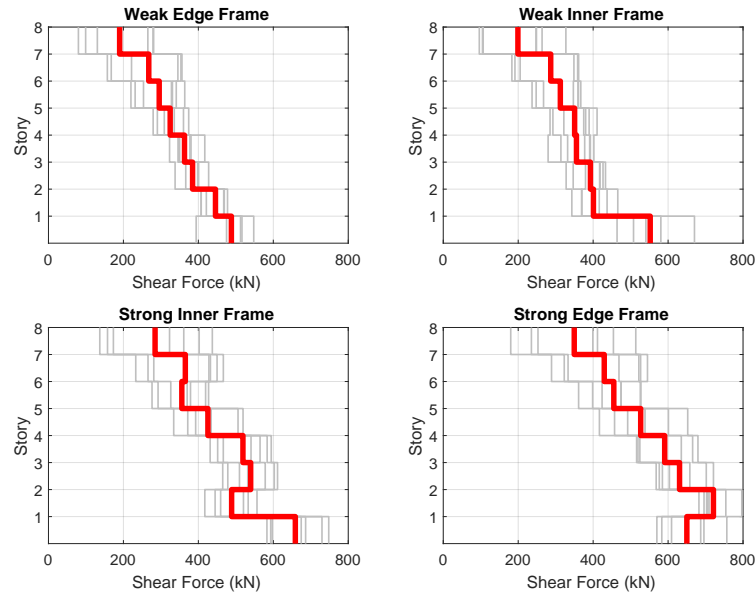


Figure 6.15: Frame shear forces obtained from inelastic dynamic analyses of the revised design under ground motion set and the corresponding mean of maximum values.

side frames. Similar shear force distribution is observed among all frames in Figure 6.15 due to constant beam and column sizes along the structure. Strong side frames, however, attain slightly higher shear forces especially at lower stories.

Ground motion set mean curvature ductilities measured at the end of beams and column members at the end of dynamic analyses of the revised design are given in Tables 6.8 and 6.9, respectively. Computed column end ductilities exceeding 1.0 are indicated in colored cells in Table 6.9.

In conjunction with what has been observed in Figure 6.11, beam curvature ductilities generally increase towards strong edge frame in Table 6.8. Frame average beam curvature ductility of the strong edge frame is close to value of response reduction factor ($R = 8$) employed in design. It should also be stated that apart from top story beams located in weak side frames, all beam ends exhibit inelastic behaviour with ductilities larger than 1.

Significant ductility demand is observed only at the bottom ends of the first story

Table 6.8: Mean beam curvature ductilities of revised design under the ground motion set.

Story	Beam	Weak Edge Frame		Weak Inner Frame		Strong Inner Frame		Strong Edge Frame	
		I End	J End	I End	J End	I End	J End	I End	J End
1	Beam1	5.5	5.7	6.7	7.7	8.2	8.4	9.5	8.7
	Beam2	6.1	5.9	7.3	7.3	8.5	8.5	9.6	9.7
	Beam3	5.2	6.2	6.3	8.0	7.8	8.9	8.9	9.5
2	Beam1	6.4	6.7	7.0	8.2	7.9	8.7	9.3	9.1
	Beam2	7.2	6.8	7.8	7.8	8.8	8.7	9.8	9.8
	Beam3	6.1	7.1	6.7	8.6	7.5	9.1	8.8	9.7
3	Beam1	5.9	6.0	6.3	7.6	6.3	7.4	8.3	8.0
	Beam2	6.4	6.2	7.2	7.1	7.9	7.7	8.5	8.5
	Beam3	5.5	6.5	6.0	8.1	5.9	8.0	7.5	8.9
4	Beam1	5.0	5.0	5.4	6.6	6.4	7.3	8.8	8.4
	Beam2	5.4	5.8	5.8	6.7	7.6	7.6	9.1	8.8
	Beam3	4.7	5.4	5.0	7.2	6.1	7.9	8.2	9.0
5	Beam1	4.3	4.6	4.3	4.9	6.0	6.4	7.2	6.8
	Beam2	4.1	4.3	4.3	5.0	5.9	5.9	7.9	7.8
	Beam3	3.8	5.1	3.9	5.6	5.4	7.1	6.7	7.4
6	Beam1	3.1	2.8	2.9	3.2	4.1	4.9	6.4	6.3
	Beam2	2.4	2.6	2.9	3.4	4.5	5.2	6.6	6.4
	Beam3	2.6	3.4	2.5	3.8	3.7	5.7	5.8	7.0
7	Beam1	2.0	1.6	1.7	1.8	2.7	3.6	4.9	5.9
	Beam2	1.5	1.5	1.6	2.1	3.0	3.8	5.1	5.5
	Beam3	1.7	2.0	1.2	2.3	2.4	4.1	4.5	6.5
8	Beam1	0.8	0.7	1.0	1.1	2.1	2.3	3.2	2.0
	Beam2	0.6	0.6	0.6	0.9	1.3	2.0	1.5	2.2
	Beam3	0.7	0.8	0.8	1.6	1.5	3.4	1.6	4.2
Average		4.0	4.3	4.4	5.3	5.5	6.4	7.0	7.3
Frame average		4.2		4.8		5.9		7.2	

Table 6.9: Mean column curvature ductilities of revised design under the ground motion set.

Story	Column	Weak Edge Frame		Weak Inner Frame		Strong Inner Frame		Strong Edge Frame	
		Bottom End	Top End	Bottom End	Top End	Bottom End	Top End	Bottom End	Top End
1	Column 1	2.0	0.3	3.3	0.2	6.0	0.3	6.7	0.4
	Column 2	1.8	0.3	3.1	0.3	6.1	0.4	7.0	0.6
	Column 3	1.7	0.3	3.0	0.3	6.1	0.4	6.9	0.5
	Column 4	1.8	0.3	3.2	0.2	5.9	0.3	6.6	0.4
2	Column 1	0.4	0.3	0.2	0.2	0.3	0.3	0.6	0.6
	Column 2	0.6	0.5	0.3	0.4	0.5	0.5	1.0	1.0
	Column 3	0.5	0.5	0.3	0.3	0.4	0.5	0.9	0.9
	Column 4	0.4	0.3	0.2	0.3	0.3	0.4	0.5	0.6
3	Column 1	0.2	0.4	0.2	0.3	0.3	0.5	0.6	0.9
	Column 2	0.3	0.6	0.3	0.4	0.4	0.8	1.0	1.5
	Column 3	0.3	0.6	0.2	0.4	0.4	0.7	0.9	1.5
	Column 4	0.2	0.4	0.2	0.3	0.3	0.6	0.5	0.9
4	Column 1	0.2	0.4	0.2	0.3	0.4	0.5	0.6	0.8
	Column 2	0.3	0.6	0.2	0.5	0.5	0.7	1.2	1.3
	Column 3	0.3	0.6	0.2	0.4	0.5	0.7	1.1	1.4
	Column 4	0.2	0.4	0.2	0.3	0.4	0.5	0.6	0.8
5	Column 1	0.2	0.4	0.2	0.3	0.3	0.5	0.5	0.8
	Column 2	0.4	0.6	0.2	0.5	0.3	0.7	0.7	1.2
	Column 3	0.4	0.5	0.3	0.4	0.4	0.6	0.7	1.2
	Column 4	0.2	0.4	0.2	0.4	0.3	0.5	0.5	0.9
6	Column 1	0.2	0.4	0.2	0.3	0.3	0.5	0.6	0.7
	Column 2	0.3	0.6	0.2	0.6	0.4	0.7	0.9	1.2
	Column 3	0.3	0.6	0.2	0.5	0.3	0.6	0.8	1.1
	Column 4	0.2	0.4	0.2	0.4	0.3	0.5	0.6	0.7
7	Column 1	0.2	0.3	0.1	0.3	0.3	0.5	0.6	0.7
	Column 2	0.3	0.5	0.2	0.5	0.4	0.7	0.8	1.0
	Column 3	0.3	0.5	0.2	0.5	0.4	0.6	0.9	1.0
	Column 4	0.2	0.3	0.2	0.4	0.3	0.5	0.6	0.7
8	Column 1	0.1	0.4	0.2	0.3	0.3	0.4	0.3	0.5
	Column 2	0.3	0.5	0.2	0.5	0.3	1.0	0.5	2.4
	Column 3	0.2	0.5	0.2	0.4	0.4	0.7	0.5	1.8
	Column 4	0.1	0.4	0.2	0.4	0.3	0.4	0.3	0.5
Average		0.5	0.4	0.6	0.4	1.1	0.5	1.5	1.0
Frame average		0.5		0.5		0.8		1.2	

columns as can be seen in Table 6.9. These values are at similar levels at the strong side frames. Apart from these localized inelastic demands, columns remain elastic in other stories of the weak edge, weak inner and strong inner frames. There is slight inelastic behaviour recorded in some upper story columns of the strong edge frame. However, computed ductilities are relatively low on these members, indicating a limited amount of plasticity.

First story column moment-curvature relationships of the revised design are computed and given in Figure 6.16. The figure format and the calculation procedure is the same as that of Figure 6.8, which was presented for the existing design. The effect of the capacity increase in the first story columns in the strong edge frame is clearly seen in Figure 6.16 where high yield moments are obtained for these columns.

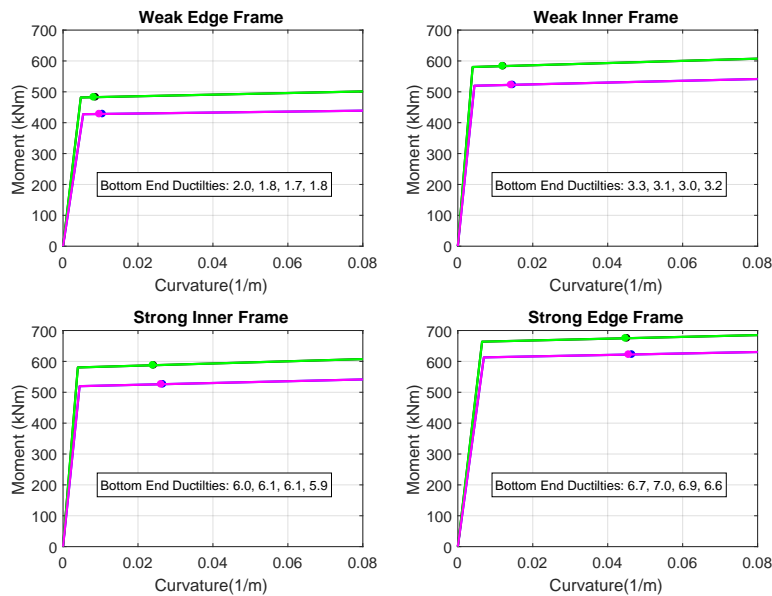


Figure 6.16: Bi-linearized moment curvature relationships of first story columns and computed ductility demands on these columns obtained for revised design.

An interesting observation could be made by comparing the moment-curvature curves of strong edge frame columns given both for existing and revised designs. Due to the relationship between strength and stiffness, column yield curvatures computed at the strong edge frame in Figure 6.16 are higher than those given in Figure 6.8 for the existing design. On the other hand, curvature demands of strong edge columns

marked in both figures are at similar levels. Although the demands vary slightly in both systems, the increase in yield moment and yield curvature in the case of revised design results in lower ductilities.

6.11 Performance Comparison between Existing and Revised Designs

Seismic response quantities that were given previously for both systems are compared with each other and performance of the Optimal Strength Distribution Method in improving the seismic response of mass-asymmetric structure is evaluated in this section.

6.11.1 Comparison of Frame Responses

Mean values of maximum interstory drifts, beam end curvatures and column bottom-end curvatures obtained from inelastic dynamic analyses of both existing and revised designs under the set of ground motions are compared in Figures 6.17 - 6.19, respectively. Red line in these Figures represents the mean response of the revised design, whereas black line is the mean response of the existing system.

As can be seen in Figures 6.17 - 6.19, mean responses of both existing and revised systems are nearly indistinguishable with each other. This observation is expected since strength distributions of existing and revised designs are very similar. Very slight decrease in the second story interstory drift ratio of strong side frames is observed. While mean beam-end curvature plots are coincident with each other for both designs, a modest reduction in column bottom end curvature demands at the second story columns of strong edge frame can be seen.

6.11.2 Comparison of Member Ductility Demands

Previously presented curvature ductility demands, compiled for existing and revised systems, are given in this section in a frame-by-frame comparison format. Ground motion set mean beam ductilities at both ends are compared in Tables 6.10 – 6.13 for

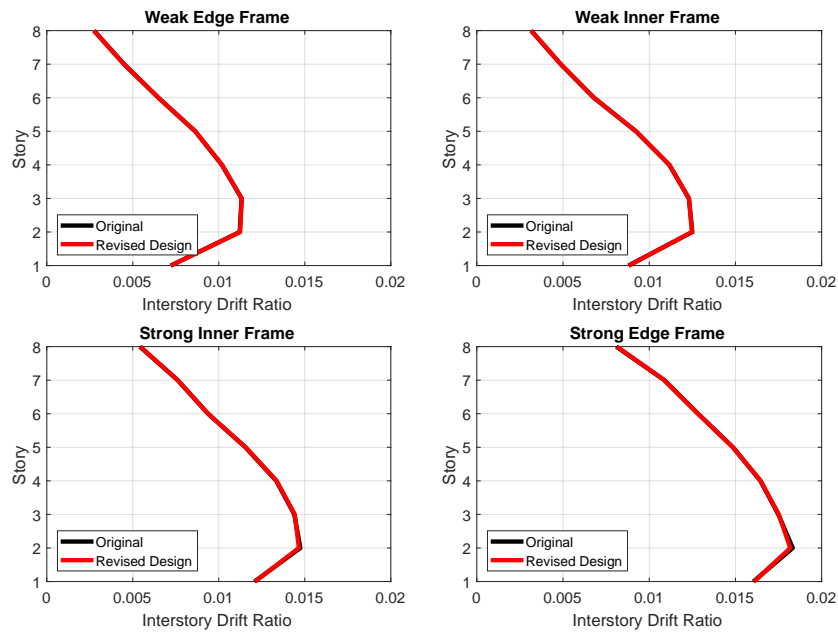


Figure 6.17: Comparison of mean maximum interstory drift ratios calculated for the existing and revised designs.

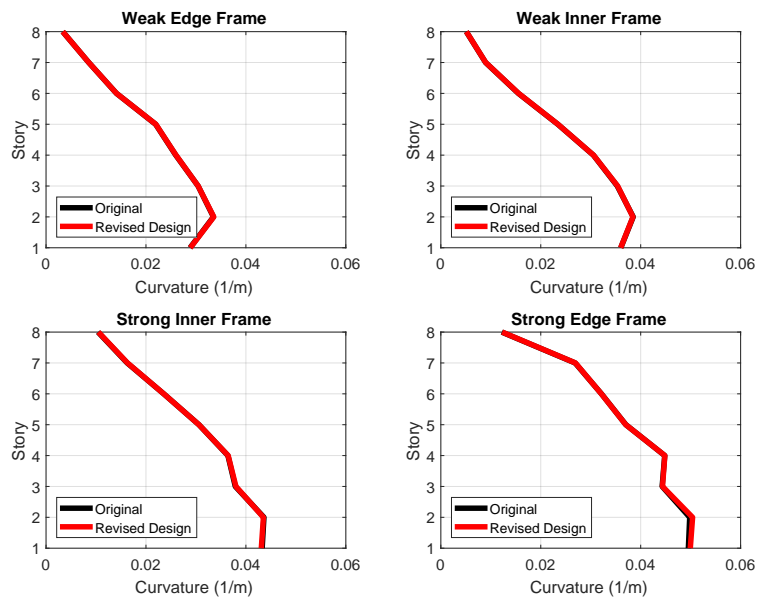


Figure 6.18: Comparison of the mean maximum beam-end curvatures calculated for the existing and revised designs.

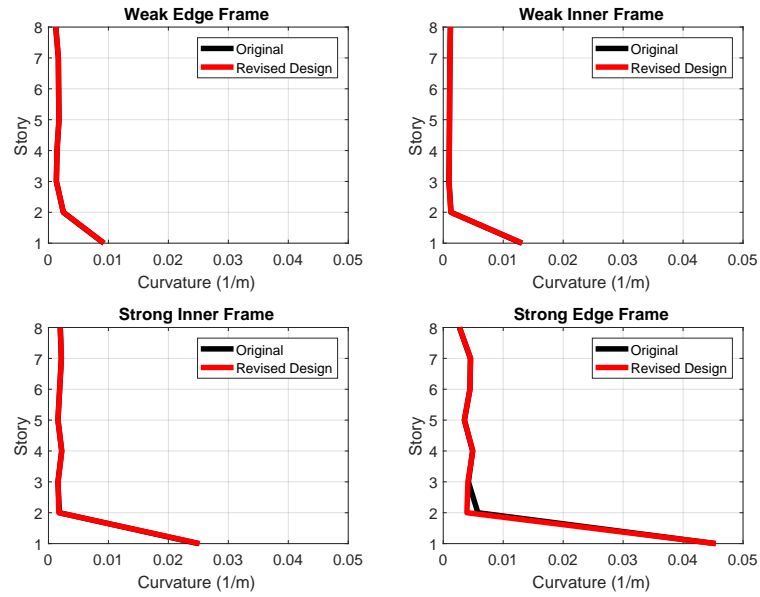


Figure 6.19: Comparison of the mean maximum column bottom-end curvatures calculated for the existing and revised designs.

the weak edge, weak inner, strong inner and strong edge frames, respectively.

It can be observed in Tables 6.10 – 6.13 that there is virtually no difference in curvature ductility demands in all beams in the case of existing and revised systems. It can therefore be concluded that the minor alteration that has been made in revised system does not affect the response of beams in all four frames.

In a similar manner to the beam tables, mean curvature ductilities calculated at both ends of the columns of two systems are compared in Tables 6.14 – 6.17 for the four frames. Column curvature ductility demands are essentially the same for both existing and revised systems in the weak edge, weak inner and strong inner frames as seen in Tables 6.14 – 6.16. However, improvement is observed in the case of strong edge frame in Table 6.17. Modified columns display lower curvature ductilities in the case of revised design. The effect of strengthening the first story columns also manifest itself in the second and third stories where reductions in ductilities are detected. In the upper stories of the strong edge frame, ductility levels of columns showing inelastic deformations stay the same.

Table 6.10: Beam curvature ductility comparison for the Weak Edge Frame

Story	Beam Name	Existing Design		Revised Design	
		I End	J End	I End	J End
1	BEAM1	5.5	5.7	5.5	5.7
	BEAM2	6.1	5.9	6.1	5.9
	BEAM3	5.2	6.2	5.2	6.2
2	BEAM1	6.4	6.7	6.4	6.7
	BEAM2	7.1	6.8	7.2	6.8
	BEAM3	6.1	7.1	6.1	7.1
3	BEAM1	5.9	6.0	5.9	6.0
	BEAM2	6.4	6.2	6.4	6.2
	BEAM3	5.5	6.5	5.5	6.5
4	BEAM1	4.9	5.0	5.0	5.0
	BEAM2	5.4	5.8	5.4	5.8
	BEAM3	4.7	5.4	4.7	5.4
5	BEAM1	4.3	4.6	4.3	4.6
	BEAM2	4.1	4.3	4.1	4.3
	BEAM3	3.8	5.1	3.8	5.1
6	BEAM1	3.1	2.8	3.1	2.8
	BEAM2	2.4	2.6	2.4	2.6
	BEAM3	2.6	3.4	2.6	3.4
7	BEAM1	2.0	1.6	2.0	1.6
	BEAM2	1.5	1.5	1.5	1.5
	BEAM3	1.7	2.0	1.7	2.0
8	BEAM1	0.8	0.7	0.8	0.7
	BEAM2	0.6	0.6	0.6	0.6
	BEAM3	0.7	0.8	0.7	0.8
Beam End Average		4.0	4.3	4.0	4.3
Frame Average		4.2		4.2	

Table 6.11: Beam curvature ductility comparison for the Weak Inner Frame

Story	Beam Name	Existing Design		Revised Design	
		I End	J End	I End	J End
1	BEAM1	6.7	7.7	6.7	7.7
	BEAM2	7.3	7.3	7.3	7.3
	BEAM3	6.3	8.0	6.3	8.0
2	BEAM1	7.0	8.2	7.0	8.2
	BEAM2	7.9	7.8	7.8	7.8
	BEAM3	6.7	8.6	6.7	8.6
3	BEAM1	6.3	7.6	6.3	7.6
	BEAM2	7.2	7.1	7.2	7.1
	BEAM3	6.0	8.1	6.0	8.1
4	BEAM1	5.4	6.6	5.4	6.6
	BEAM2	5.8	6.7	5.8	6.7
	BEAM3	5.0	7.2	5.0	7.2
5	BEAM1	4.3	4.9	4.3	4.9
	BEAM2	4.3	5.0	4.3	5.0
	BEAM3	3.9	5.6	3.9	5.6
6	BEAM1	2.9	3.2	2.9	3.2
	BEAM2	2.9	3.4	2.9	3.4
	BEAM3	2.5	3.8	2.5	3.8
7	BEAM1	1.7	1.8	1.7	1.8
	BEAM2	1.6	2.1	1.6	2.1
	BEAM3	1.2	2.3	1.2	2.3
8	BEAM1	1.0	1.1	1.0	1.1
	BEAM2	0.6	0.9	0.6	0.9
	BEAM3	0.8	1.6	0.8	1.6
Beam End Average		4.4	5.3	4.4	5.3
Frame Average		4.8		4.8	

Table 6.12: Beam curvature ductility comparison for the Strong Inner Frame

Story	Beam Name	Existing Design		Revised Design	
		I End	J End	I End	J End
1	BEAM1	8.3	8.4	8.2	8.4
	BEAM2	8.5	8.5	8.5	8.5
	BEAM3	7.9	8.9	7.8	8.9
2	BEAM1	7.9	8.8	7.9	8.7
	BEAM2	8.8	8.7	8.8	8.7
	BEAM3	7.6	9.2	7.5	9.1
3	BEAM1	6.3	7.4	6.3	7.4
	BEAM2	7.9	7.7	7.9	7.7
	BEAM3	5.8	8.0	5.9	8.0
4	BEAM1	6.4	7.3	6.4	7.3
	BEAM2	7.6	7.6	7.6	7.6
	BEAM3	6.1	7.8	6.1	7.9
5	BEAM1	6.0	6.4	6.0	6.4
	BEAM2	5.9	5.9	5.9	5.9
	BEAM3	5.4	7.1	5.4	7.1
6	BEAM1	4.1	4.9	4.1	4.9
	BEAM2	4.5	5.2	4.5	5.2
	BEAM3	3.7	5.7	3.7	5.7
7	BEAM1	2.7	3.5	2.7	3.6
	BEAM2	3.0	3.8	3.0	3.8
	BEAM3	2.4	4.1	2.4	4.1
8	BEAM1	2.1	2.3	2.1	2.3
	BEAM2	1.2	2.0	1.3	2.0
	BEAM3	1.5	3.4	1.5	3.4
Beam End Average		5.5	6.4	5.5	6.4
Frame Average		5.9		5.9	

Table 6.13: Beam curvature ductility comparison for the Strong Edge Frame

Story	Beam Name	Existing Design		Revised Design	
		I End	J End	I End	J End
1	BEAM1	9.5	8.6	9.5	8.7
	BEAM2	9.5	9.6	9.6	9.7
	BEAM3	8.8	9.5	8.9	9.5
2	BEAM1	9.3	8.9	9.3	9.1
	BEAM2	9.6	9.6	9.8	9.8
	BEAM3	8.6	9.6	8.8	9.7
3	BEAM1	8.3	8.0	8.3	8.0
	BEAM2	8.5	8.5	8.5	8.5
	BEAM3	7.5	8.9	7.5	8.9
4	BEAM1	8.8	8.4	8.8	8.4
	BEAM2	9.1	8.8	9.1	8.8
	BEAM3	8.2	9.0	8.2	9.0
5	BEAM1	7.2	6.8	7.2	6.8
	BEAM2	7.9	7.8	7.9	7.8
	BEAM3	6.7	7.4	6.7	7.4
6	BEAM1	6.4	6.3	6.4	6.3
	BEAM2	6.6	6.4	6.6	6.4
	BEAM3	5.8	7.0	5.8	7.0
7	BEAM1	4.9	5.9	4.9	5.9
	BEAM2	5.0	5.5	5.1	5.5
	BEAM3	4.5	6.5	4.5	6.5
8	BEAM1	3.2	2.0	3.2	2.0
	BEAM2	1.5	2.2	1.5	2.2
	BEAM3	1.6	4.2	1.6	4.2
Beam End Average		7.0	7.3	7.0	7.3
Frame Average		7.1		7.2	

Table 6.14: Column curvature ductility comparison for the Weak Edge Frame

Story	Column Name	Existing Design		Revised Design	
		Bottom End	Top End	Bottom End	Top End
1	COLUMN1	2.0	0.3	2.0	0.3
	COLUMN2	1.8	0.3	1.8	0.3
	COLUMN3	1.7	0.3	1.7	0.3
	COLUMN4	1.8	0.3	1.8	0.3
2	COLUMN1	0.4	0.3	0.4	0.3
	COLUMN2	0.6	0.5	0.6	0.5
	COLUMN3	0.5	0.5	0.5	0.5
	COLUMN4	0.3	0.3	0.4	0.3
3	COLUMN1	0.2	0.4	0.2	0.4
	COLUMN2	0.3	0.6	0.3	0.6
	COLUMN3	0.3	0.6	0.3	0.6
	COLUMN4	0.2	0.4	0.2	0.4
4	COLUMN1	0.2	0.4	0.2	0.4
	COLUMN2	0.3	0.6	0.3	0.6
	COLUMN3	0.3	0.6	0.3	0.6
	COLUMN4	0.2	0.4	0.2	0.4
5	COLUMN1	0.2	0.4	0.2	0.4
	COLUMN2	0.4	0.6	0.4	0.6
	COLUMN3	0.4	0.5	0.4	0.5
	COLUMN4	0.2	0.4	0.2	0.4
6	COLUMN1	0.2	0.4	0.2	0.4
	COLUMN2	0.3	0.6	0.3	0.6
	COLUMN3	0.3	0.6	0.3	0.6
	COLUMN4	0.2	0.4	0.2	0.4
7	COLUMN1	0.2	0.3	0.2	0.3
	COLUMN2	0.3	0.5	0.3	0.5
	COLUMN3	0.3	0.5	0.3	0.5
	COLUMN4	0.2	0.3	0.2	0.3
8	COLUMN1	0.1	0.4	0.1	0.4
	COLUMN2	0.3	0.5	0.3	0.5
	COLUMN3	0.2	0.5	0.2	0.5
	COLUMN4	0.1	0.4	0.1	0.4
Column End Average		0.5	0.4	0.5	0.4
Frame Average		0.5		0.5	

Table 6.15: Column curvature ductility comparison for the Weak Inner Frame

Story	Column Name	Existing Design		Revised Design	
		Bottom End	Top End	Bottom End	Top End
1	COLUMN1	3.3	0.2	3.3	0.2
	COLUMN2	3.0	0.3	3.1	0.3
	COLUMN3	3.0	0.3	3.0	0.3
	COLUMN4	3.2	0.2	3.2	0.2
2	COLUMN1	0.3	0.2	0.2	0.2
	COLUMN2	0.3	0.4	0.3	0.4
	COLUMN3	0.3	0.3	0.3	0.3
	COLUMN4	0.2	0.3	0.2	0.3
3	COLUMN1	0.2	0.3	0.2	0.3
	COLUMN2	0.2	0.4	0.3	0.4
	COLUMN3	0.2	0.4	0.2	0.4
	COLUMN4	0.2	0.3	0.2	0.3
4	COLUMN1	0.2	0.3	0.2	0.3
	COLUMN2	0.2	0.5	0.2	0.5
	COLUMN3	0.2	0.4	0.2	0.4
	COLUMN4	0.2	0.3	0.2	0.3
5	COLUMN1	0.2	0.3	0.2	0.3
	COLUMN2	0.2	0.5	0.2	0.5
	COLUMN3	0.3	0.4	0.3	0.4
	COLUMN4	0.2	0.4	0.2	0.4
6	COLUMN1	0.2	0.3	0.2	0.3
	COLUMN2	0.2	0.6	0.2	0.6
	COLUMN3	0.2	0.5	0.2	0.5
	COLUMN4	0.2	0.4	0.2	0.4
7	COLUMN1	0.1	0.3	0.1	0.3
	COLUMN2	0.2	0.5	0.2	0.5
	COLUMN3	0.2	0.5	0.2	0.5
	COLUMN4	0.2	0.4	0.2	0.4
8	COLUMN1	0.2	0.3	0.2	0.3
	COLUMN2	0.2	0.5	0.2	0.5
	COLUMN3	0.2	0.4	0.2	0.4
	COLUMN4	0.2	0.4	0.2	0.4
Column End Average		0.6	0.4	0.6	0.4
Frame Average		0.5		0.5	

Table 6.16: Column curvature ductility comparison for the Strong Inner Frame

Story	Column Name	Existing Design		Revised Design	
		Bottom End	Top End	Bottom End	Top End
1	COLUMN1	6.0	0.3	6.0	0.3
	COLUMN2	6.1	0.4	6.1	0.4
	COLUMN3	6.0	0.4	6.1	0.4
	COLUMN4	5.9	0.3	5.9	0.3
2	COLUMN1	0.4	0.4	0.3	0.3
	COLUMN2	0.5	0.5	0.5	0.5
	COLUMN3	0.5	0.5	0.4	0.5
	COLUMN4	0.3	0.4	0.3	0.4
3	COLUMN1	0.3	0.5	0.3	0.5
	COLUMN2	0.4	0.7	0.4	0.8
	COLUMN3	0.4	0.7	0.4	0.7
	COLUMN4	0.3	0.5	0.3	0.6
4	COLUMN1	0.4	0.5	0.4	0.5
	COLUMN2	0.5	0.7	0.5	0.7
	COLUMN3	0.5	0.7	0.5	0.7
	COLUMN4	0.4	0.5	0.4	0.5
5	COLUMN1	0.3	0.5	0.3	0.5
	COLUMN2	0.3	0.7	0.3	0.7
	COLUMN3	0.4	0.6	0.4	0.6
	COLUMN4	0.3	0.5	0.3	0.5
6	COLUMN1	0.3	0.5	0.3	0.5
	COLUMN2	0.4	0.7	0.4	0.7
	COLUMN3	0.3	0.6	0.3	0.6
	COLUMN4	0.3	0.5	0.3	0.5
7	COLUMN1	0.3	0.5	0.3	0.5
	COLUMN2	0.4	0.7	0.4	0.7
	COLUMN3	0.4	0.6	0.4	0.6
	COLUMN4	0.3	0.5	0.3	0.5
8	COLUMN1	0.3	0.4	0.3	0.4
	COLUMN2	0.3	1.0	0.3	1.0
	COLUMN3	0.4	0.7	0.4	0.7
	COLUMN4	0.3	0.4	0.3	0.4
Column End Average		1.1	0.5	1.1	0.5
Frame Average		0.8		0.8	

Table 6.17: Column curvature ductility comparison for the Strong Edge Frame

Story	Column Name	Existing Design		Revised Design	
		Bottom End	Top End	Bottom End	Top End
1	COLUMN1	8.6	0.5	6.7	0.4
	COLUMN2	9.6	0.8	7.0	0.6
	COLUMN3	9.5	0.7	6.9	0.5
	COLUMN4	8.4	0.5	6.6	0.4
2	COLUMN1	0.9	0.8	0.6	0.6
	COLUMN2	1.5	1.4	1.0	1.0
	COLUMN3	1.3	1.4	0.9	0.9
	COLUMN4	0.7	0.8	0.5	0.6
3	COLUMN1	0.6	0.9	0.6	0.9
	COLUMN2	1.1	1.6	1.0	1.5
	COLUMN3	1.0	1.6	0.9	1.5
	COLUMN4	0.5	0.9	0.5	0.9
4	COLUMN1	0.6	0.8	0.6	0.8
	COLUMN2	1.2	1.3	1.2	1.3
	COLUMN3	1.1	1.3	1.1	1.4
	COLUMN4	0.6	0.8	0.6	0.8
5	COLUMN1	0.5	0.8	0.5	0.8
	COLUMN2	0.7	1.2	0.7	1.2
	COLUMN3	0.7	1.2	0.7	1.2
	COLUMN4	0.5	0.9	0.5	0.9
6	COLUMN1	0.6	0.7	0.6	0.7
	COLUMN2	0.9	1.2	0.9	1.2
	COLUMN3	0.8	1.1	0.8	1.1
	COLUMN4	0.6	0.7	0.6	0.7
7	COLUMN1	0.6	0.7	0.6	0.7
	COLUMN2	0.8	1.0	0.8	1.0
	COLUMN3	0.9	1.0	0.9	1.0
	COLUMN4	0.6	0.7	0.6	0.7
8	COLUMN1	0.3	0.5	0.3	0.5
	COLUMN2	0.5	2.4	0.5	2.4
	COLUMN3	0.5	1.8	0.5	1.8
	COLUMN4	0.3	0.5	0.3	0.5
Column End Average		1.8	1.0	1.5	1.0
Frame Average		1.4		1.2	

6.12 Summary and Discussions

A mass-asymmetric eight-story reinforced concrete structure is investigated as a case study in this Chapter. Inelastic dynamic response of the code-designed system, which is labeled as the existing design, is investigated first. Next, Optimal Strength Distribution Method is implemented to the existing structure and the revised design has been obtained. Seismic response of the revised design has been discussed accordingly. Finally, response quantities such as frame interstory drifts, beam-column curvatures and curvature ductilities obtained from the existing and revised systems are compared. Performance of the Optimal Strength Distribution Method in improving the response of the mass-asymmetric structure has been evaluated.

Upon applying the proposed procedure, difference between $SFSR_{existing}$ and $SFSR_{opt}$ is determined to be small. As can be seen in Figure 6.9, there is little difference between the strength distributions of the existing and revised designs. By inspecting the given diagram in the Figure, the designer could decide that the existing seismic design is satisfactory and a design revision is not necessary. In fact, this conclusion is supported by dynamic analysis results of the existing system. Although there is ductility unbalance, maximum ductilities measured at the bottom ends of the first story columns are lower than or close to the value of response reduction factor employed in the design. By considering the existing strength distribution and the dynamic analysis results, it is concluded that the code compliant seismic design successfully achieves acceptable seismic performance in the case of particular eight-story mass-asymmetric structure.

Even though a small improvement is expected in the case of revised design due to the minor difference in strength distributions, the method is applied in its full extent so that a throughout performance comparison between existing and revised systems could be carried out. The updated demands obtained in the case of revised design necessitate a modest increase in the capacity of first story columns located at the strong edge. The overall seismic response of the revised system is virtually unchanged when compared with the existing design. The minor design revision only yields a reduction in the curvature ductilities in columns of the strong edge frame. Revised columns as well as columns located in the second and third stories of the strong

edge frame attained lower ductilities in the case of revised structure. Although the curvature ductilities at the bottom of strong side frames has been brought to similar levels, they are still higher from what has been observed at the first story columns of weak side frames. Yet, overall maximum column ductilities measured throughout the structure are still at acceptable levels.

Due to reasons discussed above, the optimal strength distribution method provides a limited improvement to an already acceptable existing design. Overall, the method has reduced the maximum ductilities in the system. However, some ductility unbalance still exists in the seismic response of the revised sign.

In the next chapter, seismic response of a twelve-story structure is investigated as the final case study. This system bears a shear wall, and an “L” shaped structural layout.

CHAPTER 7

CASE STUDY 3: 12-STORY ASYMMETRIC STRUCTURE

7.1 Introduction

In this Chapter, a twelve-story asymmetric frame-wall structure is presented as the third case study of the thesis. Performance of the Optimal Strength Distribution Method is assessed by comparing the inelastic dynamic responses of existing and revised designs of the structure. Organization of the Chapter closely follows the two previous chapters.

7.2 General Information

A twelve-story building is designed according to ASCE 7-10 [4], the Turkish Earthquake Code [73] and Reinforced Concrete Standard of Turkey (TS-500) [87]. Capacity design principles are imposed in structural design. There are twelve identical stories in the building with an “L” shaped floor plan. The reinforced concrete building is composed of moment-frames and a shear wall in the direction of analysis. Story height is 3.5 meters throughout the structure. All beams in the building have a span length of six meters. All beams are 0.30 m wide and their depth is 0.55 m. Slab thickness is 0.14 m at all stories. Inner and outer columns have different dimensions in the building. In the typical story plan, there are four inner columns with dimensions of 0.70 m by 0.70 m. Rest of the columns are 0.50 by 0.50 m. Dimensioning of the columns has been made according to gravity design requirements.

Typical story plan and elevation view are presented in Figure 7.1. Direction of excitation is the Y axis shown in the Figure. There are five frames in the direction of

analysis. Labeling of these frames are made according to their expected deformation patterns. Stiff edge frame is by far the stiffest frame where the shear wall is located. The stiff inner frame is a three-span frame that is composed of two inner and two outer columns. Center frame is also a three span frame that is located in the middle of the structure. It is less stiff compared to stiff inner frame since only one inner column is located in this frame. Flexible inner and flexible edge frames are two bay frames. Flexible edge frame is more flexible than the flexible inner frame due to smaller column sizes.

Characteristic strengths of concrete and reinforcing steel are 35 MPa and 420 MPa, respectively. Cracked section properties, which are defined in the Turkish Earthquake Code [73], are utilized in design and analysis of the system. Section stiffnesses of beams and columns are multiplied by 0.35 and 0.70, respectively.

Due to the geometry of floor plan, building possesses two-way asymmetry. In addition, center of mass is not coincident with the geometric center of the structure. Since story plan and corresponding floor masses show no variation, location of the center of mass does not change along stories.

7.3 Free Vibration Properties

Dynamic properties associated with the first six modes of the structure are presented in Table 7.1. Modes denoted with X and Y are translation dominant modes in respective directions, and modes denoted with θ are the rotation dominant modes. Effective modal masses and their ratios calculated in both directions for each mode are given in the Table along with their associated periods. The frequency ratios (ω_θ) for X and Y directions are 2.1 and 1.92, respectively. Therefore, it can be stated that the system is torsionally stiff in both directions.

7.4 Determination of Static Eccentricity

All stories of the twelve-story structure exhibit rigid diaphragm behaviour and center of rigidity (CR) location at each floor diaphragm varies along the height of the

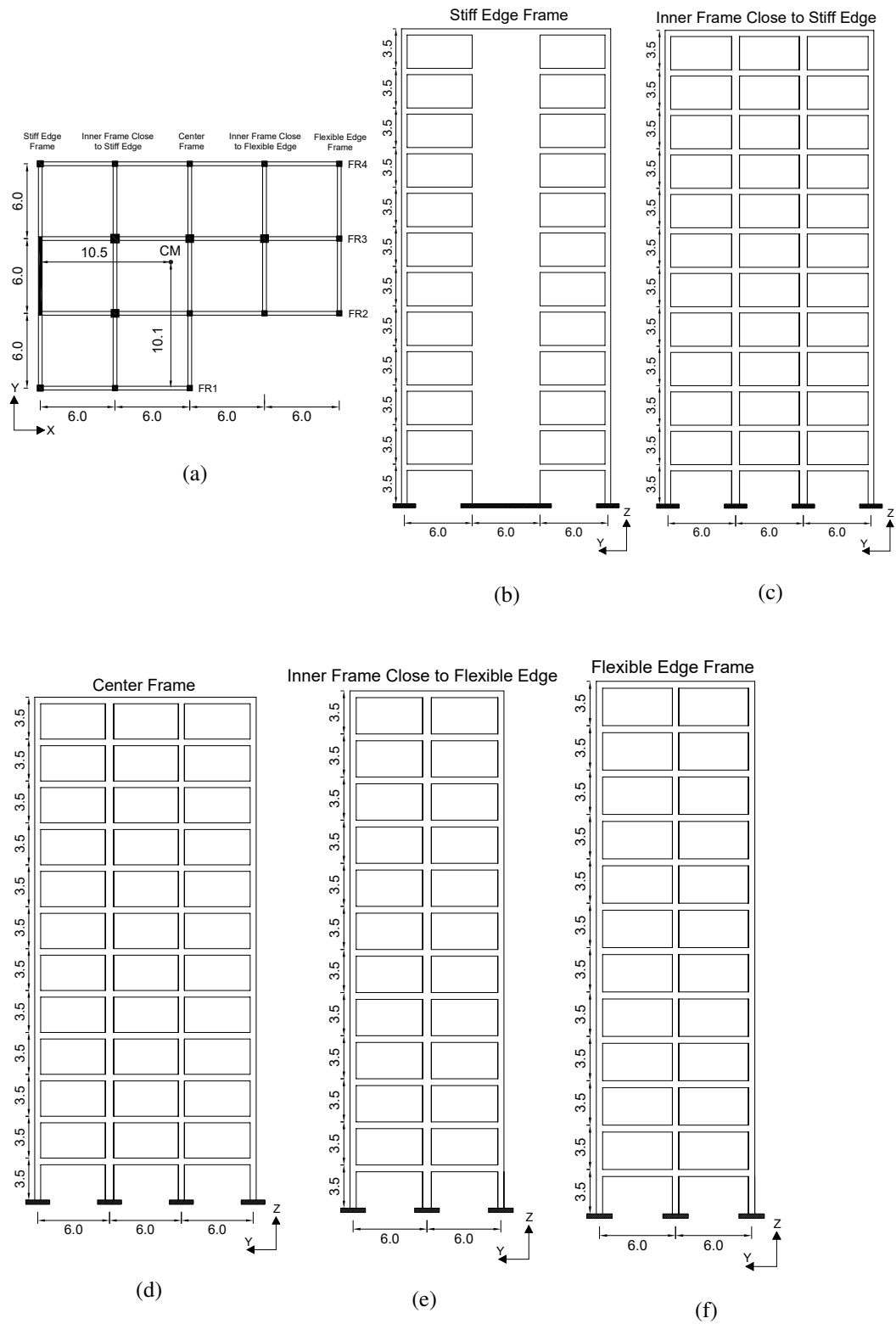


Figure 7.1: Typical floor plan of the twelve story asymmetric structure and elevation view of the frames in the direction of analysis. Center of mass (CM) is marked on the plan. (Units in meters)

Table 7.1: Free vibration properties of the twelve story asymmetric structure

Mode	Period (Seconds)	Effective Modal Mass - Y (tons)	Effective Modal Mass Ratio - Y	Effective Modal Mass - X (tons)	Effective Modal Mass Ratio - X
1X	2.536	10	0.003	2517	0.784
1Y	2.325	1550	0.483	16	0.005
1 θ	1.21	809	0.252	0	0
2X	0.806	0	0	314.6	0.098
2Y	0.741	238	0.074	0	0
2 θ	0.414	61	0.019	0	0

structure. CR of every floor diaphragm can be determined by using the procedure suggested by Basu and Jain [7] as explained in Section 5.4. Through application of the procedure, location of CR, $x_{CR,i}$, is computed at each floor with respect to the center of mass (CM). Thus, stiffness eccentricity (e) of every floor is obtained. Values $x_{CR,i}$ and the corresponding stiffness eccentricities that are calculated in the X direction are given in Table 7.2. It should be noted that only stiffness eccentricity in the X direction is considered in the scope of this case study, since X direction is perpendicular to the direction of analysis.

Table 7.2: Position of CR with respect to CM and the corresponding stiffness eccentricity (e) at each story perpendicular to the direction of analysis. Negative x_{CR} value implies that CR is located at left side of the CM as indicated in Figure 7.1.

Story	x_{CR} (m)	e (%)
1	-9.53	40
2	-9.60	40
3	-9.39	39
4	-9.09	38
5	-8.74	36
6	-8.36	35
7	-7.96	33
8	-7.54	31
9	-7.11	30
10	-6.66	28
11	-6.19	26
12	-5.74	24

After $x_{CR,i}$ values are calculated, equivalent stiffness eccentricity of the structure can be determined. In Section 5.4, equivalent structural eccentricity was defined as the e value which is calculated at the floor which is located at the shear span height (L_s). Shear span of the structure is obtained as 24.6 meters according to Equation 5.2. The shear span height is approximately equal to the height of seventh story. Consequently, the equivalent value of e is determined as $33\% \approx 30\%$.

7.5 Linear Elastic Design Spectrum

Design spectrum is constructed for an imaginary location at the Anatolian side of Istanbul on Site Class C. Short period (S_S) and 1 second (S_1) MCE_R spectral acceleration parameters associated with the site has been determined as $1.01g$ and $0.28g$, respectively. While performing seismic design, design spectrum was reduced by a response reduction factor of $R = 7$. It is determined according to the type of load resisting system of the structure. Linear elastic design spectrum as well as spectrum-matched spectra of ground motion records selected for inelastic dynamic analyses are presented in Figure 7.2. The spectrum matched ground motion set will be explained later in Section 7.7

7.6 Seismic Design

Seismic design is performed per capacity design principles. Beams are designed optimally to resist their force demands; therefore there is little overstrength in the beam members. Column and shear wall design, however, are governed by seismic detailing requirements given in the relevant seismic standards.

Along with reinforcement placement requirements for column sections, minimum longitudinal reinforcement ratio ($\rho_{min} = 1\%$) is satisfied in column design. Consequently, 0.50 m by 0.50 m columns are detailed with twelve 18 mm longitudinal bars, resulting in $\rho_l = 1.22\%$. Twelve 24 mm bars are provided for the 0.70 m by 0.70 m columns, leading to $\rho_l = 1.1\%$.

Critical shear wall height (H_{cr}) is determined as 7 meters. This height corresponds

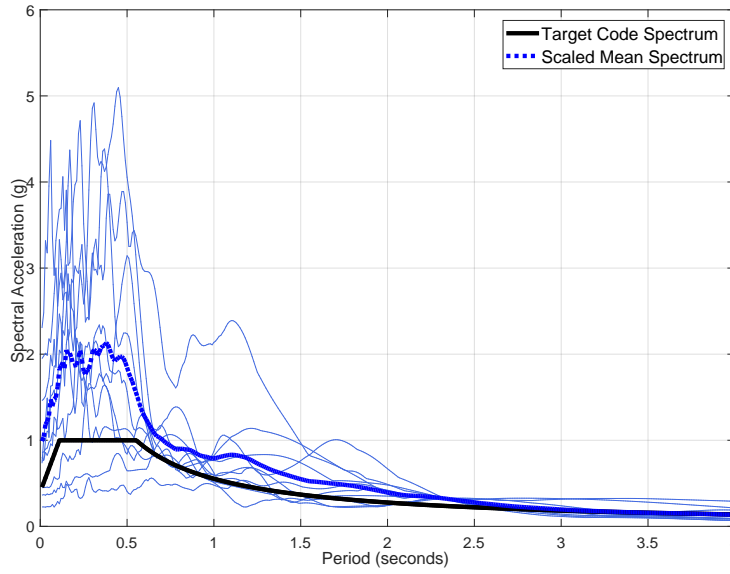


Figure 7.2: Linear elastic design spectrum and acceleration response spectra of the amplitude scaled strong ground motions. Mean response spectrum of the scaled records is plotted in dotted line.

to the first two stories of the shear wall. Confined end regions of the shear wall along the critical height has been determined as 1.2 meters, and 0.6 meters for the rest of the shear wall. As in the case of columns, minimum longitudinal reinforcement requirements governed the detailing of shear wall. Sixteen reinforcement bars having a diameter of 18 mm is provided in the confined end regions of the shear wall along the critical height. Eight 16 mm bars are provided in the confined end regions in the upper regions of shear wall. The ρ_l value of the end regions throughout the shear wall is 1.13%. In the web region of shear wall, 28 bars with a diameter of 12 mm are provided along the critical height. The detailing given for the critical height satisfies the minimum longitudinal web reinforcement ratio of 0.25%, which is required by the Turkish Earthquake Code [73]. In the stories above the critical wall height, shear wall web has 38 longitudinal bars with 12 mm diameter.

Code compliant seismic design (*Existing Design*) which is presented herein is studied in further detail in the following sections. Inelastic dynamic response of the existing design is calculated and it is used as a reference to assess the performance of *Revised*

Design that is obtained through the proposed design methodology.

7.6.1 Frame Design Shears

Design base shear forces are determined under reduced design spectrum at the bases of all five frames. These values are given in Table 7.3. The least amount of base shear force demand is obtained in the *SI* frame. Due to the high stiffness on the side where shear wall is located, both *SE* and *SI* frames experience very low displacement demands. This situation results in a limited design base shear force at the *SI* frame. Yet, the base shear force at the *SE* frame is the highest among all frames due to the presence of a shear wall.

On the flexible side of the structure, *FI* frame attains a base shear demand higher than the *FE* frame. Larger columns located in the mid-axis of the *FI* frame results in higher stiffness, thus increased base shear forces are observed in this frame compared to the *FE* frame.

Table 7.3: Frame design shear force demands ($V_{d,Frame}$) for the *Existing Design*. Units in kN.

<i>SE</i> Frame	<i>SI</i> Frame	CF Frame	FI Frame	FE Frame
885	98	143	170	140

7.6.2 Frame Strengths and Determination of Existing Stiff-to-Flexible Strength Ratio

Frame strengths are determined as discussed in Section 4.6. The column capacity shears are computed at the instant of first story column yielding mechanism, while the shear wall strength is calculated when the wall reaches its plastic moment capacity at the base. The resulting lateral frame strengths are given in Table 7.4. Seemingly, the *SE* frame has considerable amount of strength due to the high capacity of shear wall. In the case of other frames, reduced column sizes as well as lesser number of spans result in lower strengths towards the flexible edge.

Table 7.4: Frame base shear strengths (F_{Frame}) of the *Existing Design*. Units in kN.

SE Frame	SI Frame	CF Frame	FI Frame	FE Frame
2300	1324	1000	844	484

Using the frame base shear strengths given in Table 7.4, $SFSR_{existing}$ value for the system can be determined. Summation of *SE* - *SI* frame strengths yields the strength of the stiff side. Similarly, strength of the *CF*, *FI* and *FE* frames, which are located on the right side of the CM in Figure 7.1, are added together to obtain the flexible side strength. Consequently, $SFSR_{existing}$ value is determined as 1.56 according to Equation 7.1.

$$SFSR = \frac{(F_{SE} + F_{SI})}{(F_{FE} + F_{FI} + F_{CF})} \quad (7.1)$$

7.6.3 System Overstrength and Computation of Ductility Reduction Factor

Frame design shear demands and base shear strengths given in Tables 7.3 and 7.4 respectively, are plotted along the frame axis of the structure in Figure 7.3. As can be seen in the figure, there is significant amount of overstrength throughout the system. Gravity design governs column sizes as well as the seismic detailing of structural members results in very high strengths compared with the seismic demands. This situation is most pronounced in the *SI* frame.

The amount of overstrength in all frames are computed according to Equation 5.4. These Ω_{Frame} values are also displayed in Figure 7.3. In a similar manner, global overstrength (Ω_{Global}) of the twelve story structure is calculated as 4.14, which is the ratio of total base shear capacity to total base shear demand. The ductility reduction factor (R_{mu}), can be calculated as shown in Equation 6.1 by using Ω_{Global} and $R = 7$ that is employed in design. Hence, R_{mu} is determined as 1.70 for the entire structure.

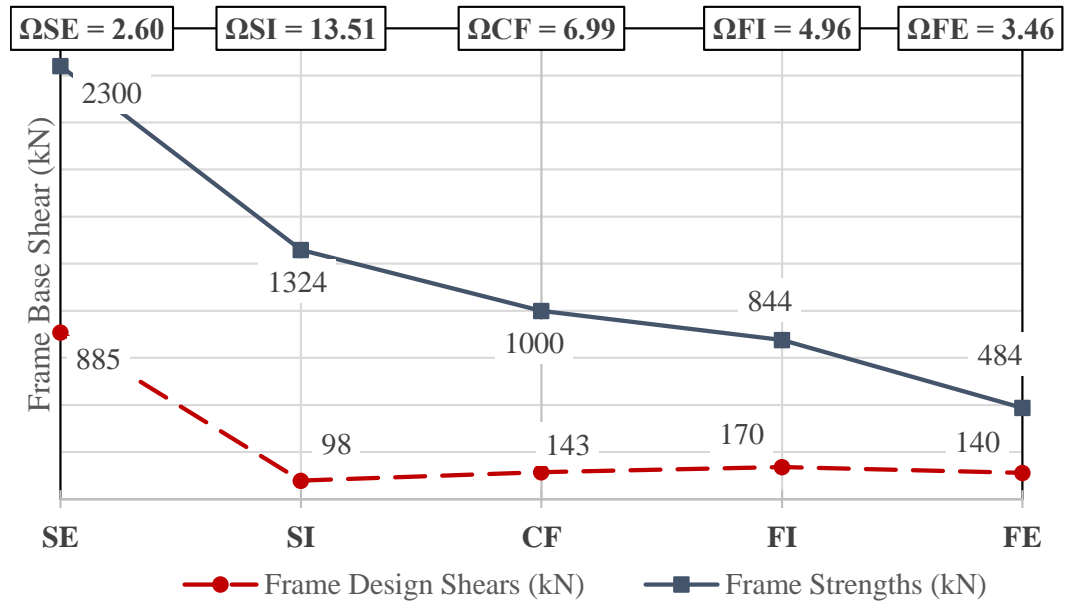


Figure 7.3: Distribution of frame base shear demands and base shear strengths along all frames of the structure (units in kN).

7.7 Analytical Modeling and Strong Ground Motions

Three-dimensional mathematical model of the structure is prepared by using Perform-3D 5.0 [16]. Inelastic section definitions are implemented in the model such that nonlinear dynamic analyses can be performed for seismic performance assessment. Rather than modeling slabs as shell elements, rigid diaphragm constraints are defined at each story level and slab loads are directly transferred to beams. Diaphragm centers of mass are defined at the position shown in Figure 7.1.

Several modeling decisions have been made depending on the type of structural members. Beams and columns are modeled with frame members having moment hinges. These moment hinges are defined for member end regions. The length of the member end region is the half of the section depth for all beams and columns. While member specific inelastic force-deformation relationships are implemented for the hinge regions, rest of the members are defined with linear elastic cracked section properties.

Moment-curvature relationships of each designed beam-end section are obtained, idealized and assigned to the associated beam-end throughout the structure. In the case

of columns, Inelastic P-M2-M3 hinge relationships are utilized at member ends. This type of hinge considers the interaction of axial load and bi-axial bending in calculating the section response during inelastic behaviour. In order to utilize this hinge property properly, moment-curvature relationships of columns as well as their interaction diagrams are calculated and implemented in the mathematical model.

Shear wall at the *SE* frame is modeled by using shell elements. Shear wall shell elements are meshed thoroughly so that a more accurate analytical model could be obtained. A denser mesh is defined in confined end regions of the wall member as compared with the web region. Section of the shear wall is modeled using structural fibers. Inelastic section behaviour is achieved by defining nonlinear concrete and steel reinforcement material models and assigning these to the associated structural fibers. By employing these structural fibers, separate sections have been constructed for confined and body regions of the shear wall according to their reinforcement detailings. The defined sections have later been assigned to the corresponding shell elements. Consequently, nonlinear behaviour in the shell elements that are utilized in modeling of the shear wall has been ensured.

Strong ground motion set that was explained previously in Section 5.7 is used for nonlinear response history analyses. The set is composed of ten strong ground motion records, which have been selected from the PEER NGA Database [66]. Detailed information regarding the selected strong ground motions were given in Table 5.6.

Simple amplitude scaling procedure that was discussed in Section 5.7 is performed for the ground motion set by using the fundamental period of the twelve-story structure in the direction of analysis. The resulting scale factors obtained with this procedure is given in Table 7.5, along with basic information about the strong ground motion records.

7.8 Dynamic Analysis Results for the Existing Design

Convergence has been achieved for all of the ten dynamic analysis performed under the strong ground motion set. Interstory drifts for both orthogonal directions, beam end curvatures and column bottom-end curvatures are determined for each frame

Table 7.5: Strong ground motion records that are employed in dynamic analyses.

Earthquake Name	GMCODE	YEAR	Mw	Scale Factor
Manjil, Iran	ABBAR-L	1990	7.37	1.43
Superstition Hills-02	B-PTS225	1987	6.54	4.59
Parkfield	C05085	1966	6.19	0.49
Victoria, Mexico	CPE045	1980	6.33	3.29
Duzce, Turkey	375-E	1999	7.14	3.63
Kocaeli, Turkey	DZC270	1999	7.51	1.25
Imperial Valley-06	H-E07230	1979	6.53	0.78
Imperial Valley-06	H-E08230	1979	6.53	1.73
Hector Mine	HEC090	1999	7.13	2.20
Kobe, Japan	KAK090	1995	6.9	2.48

throughout inelastic dynamic analyses. Maximum interstory drift ratios of the five frames obtained under each ground motion are given in Figure 7.4. Furthermore, story mean of maximum beam end curvatures computed at five frames for each ground motion are presented in Figure 7.5. In a similar format, story mean column bottom-end curvatures computed at each story of five frames are presented in Figure 7.6. Maximum curvatures computed at each story of the shear wall are shown in Figure 7.7. Finally, interstory drift ratios compiled for the frames in the orthogonal direction are also shown in Figure 7.8. Ground motion set means are plotted in red bold line in Figures 7.4 – 7.8.

Interstory drift ratios of the frames in the direction of analysis given in Figure 7.4 show an increasing trend towards the flexible edge. Effect of shear wall at the stiff edge frame can be seen on the interstory drift distribution observed in that frame. Mean beam end curvature demands presented in Figure 7.5 exhibit a similar deformation pattern as the interstory drift distribution of five frames. Beam-end curvatures of the stiff edge frame is found to be higher compared to the stiff inner frame. Presence of the shear wall at the stiff edge frame results in higher deformation demands in beams located in that frame. In addition, curvature demands in the flexible edge beams are observed to be highest among all members. Significant curvature demands are observed only in the first story columns of the five frames as shown in Figure 7.6. Calculated bottom end curvatures are highest in the first story columns located in

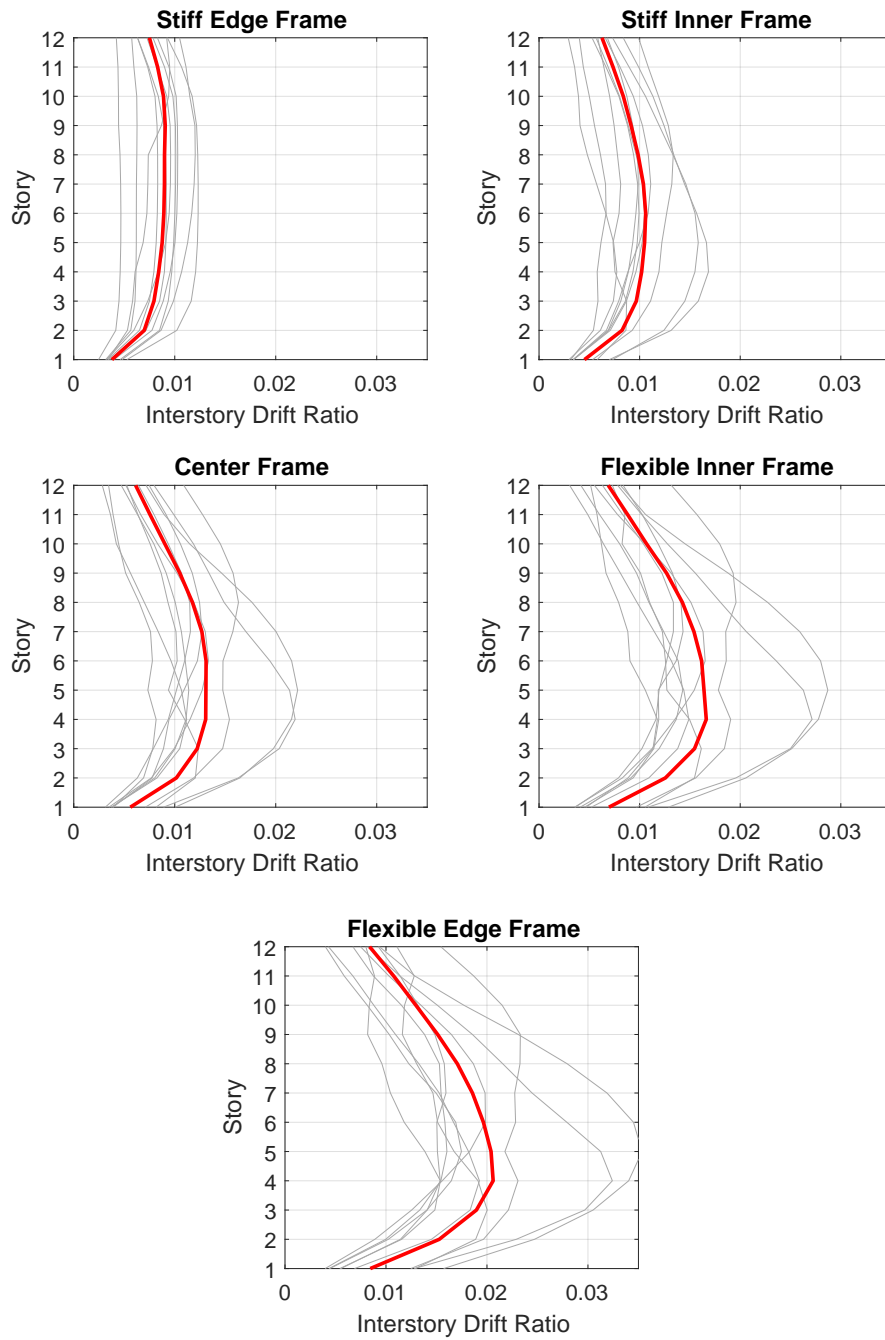


Figure 7.4: Maximum interstory drift ratios obtained from inelastic dynamic analyses of the existing design under ground motion set, and the corresponding mean of maximum values for 10 GM records.

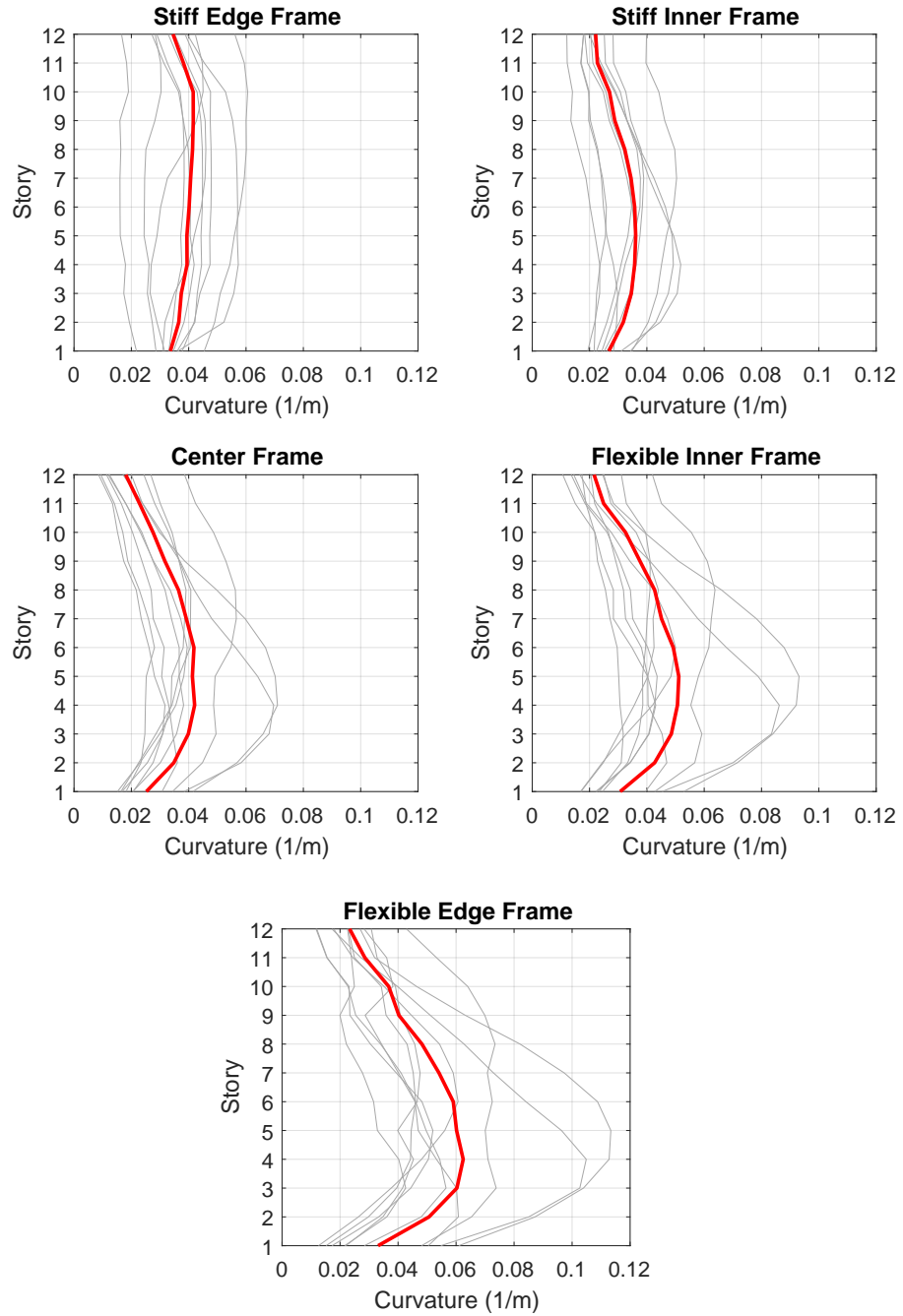


Figure 7.5: Beam-end curvatures obtained from inelastic dynamic analyses of the existing design under ground motion set and the corresponding mean values for 10 GM records.

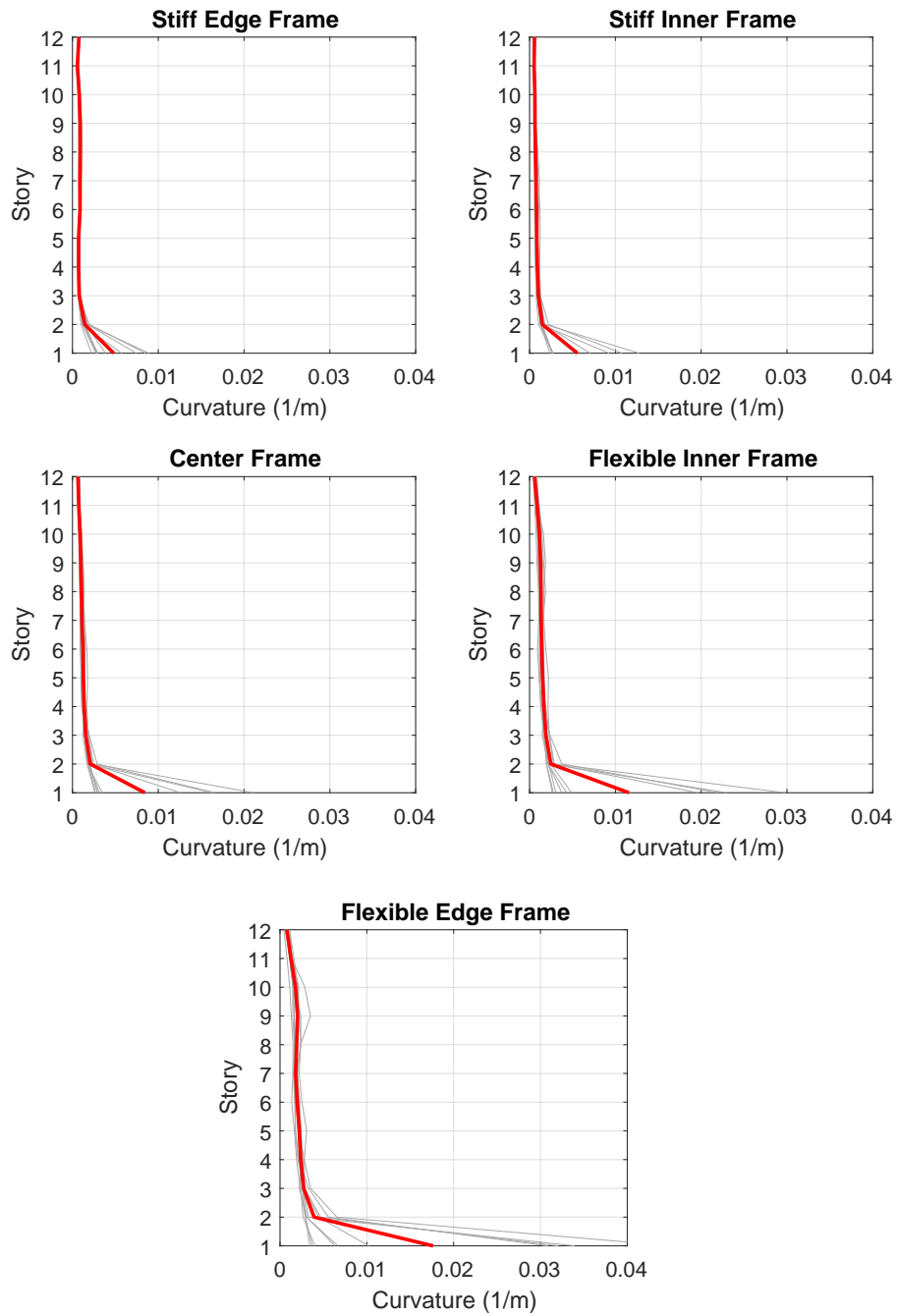


Figure 7.6: Column bottom-end curvatures obtained from inelastic dynamic analyses of the existing design under ground motion set, and the corresponding mean values for 10 GM records.

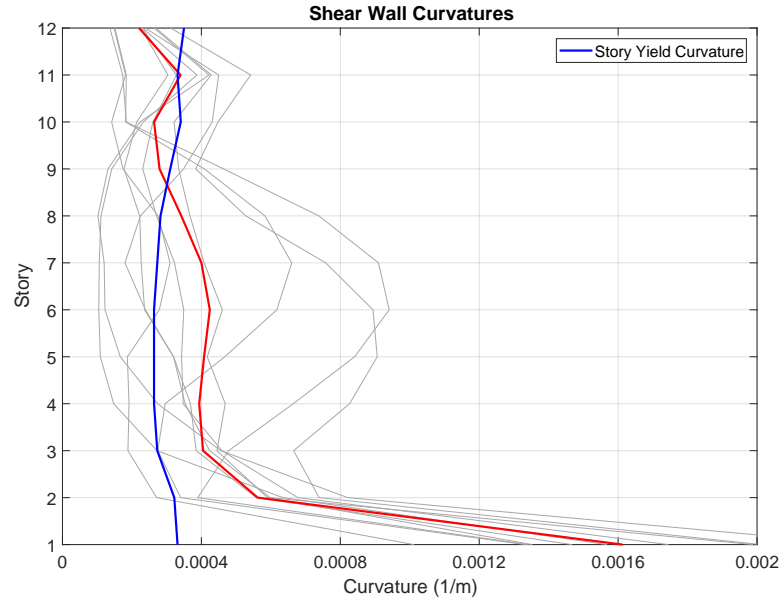


Figure 7.7: *SE* frame shear wall curvatures obtained from inelastic dynamic analyses of the existing design under the ground motion set, and the corresponding mean values for 10 GM records.

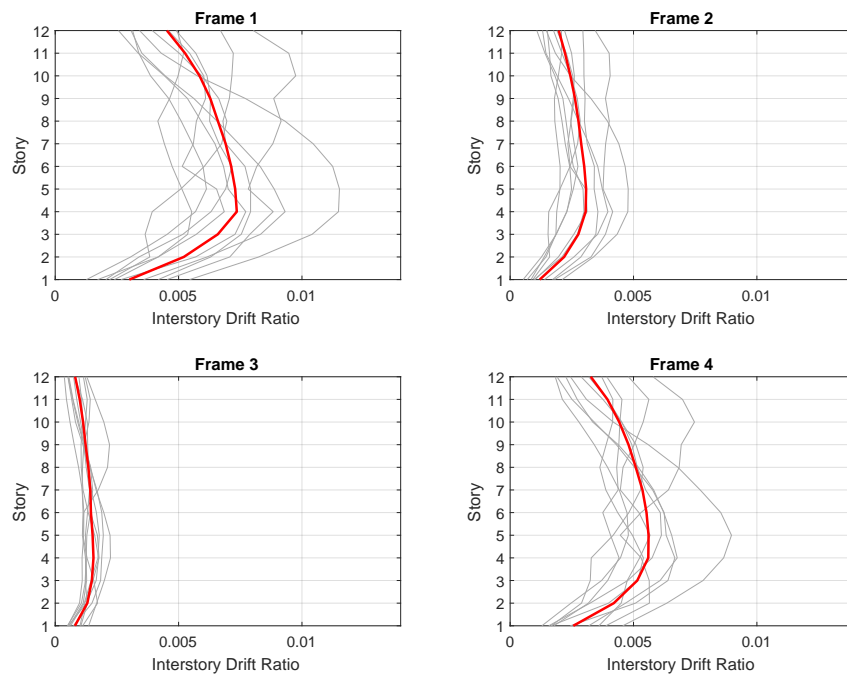


Figure 7.8: Maximum interstory drift ratios of the frames in orthogonal direction determined under ground motion set and the corresponding mean of maximum values for 10 GM records.

the flexible edge frame, while those located at the stiff edge frame exhibit a slightly limited deformation.

As shown in Figure 7.7 curvature demands occur predominantly at the bottom of the shear wall. Estimated yield curvatures are also given in Figure 7.7. Shear wall yield curvatures are calculated from idealized bilinear moment curvature relationships determined at each story through section analysis under gravity loads. It is known that shear walls deform towards inelastic range in a progressive manner and usually a definitive yielding event is not apparent in section response of these members. Therefore, wall yield curvatures can only be estimated approximately through idealized curves. Although computed curvature demands and estimated yield curvatures are small, it can be seen that significant amount of inelastic deformation is concentrated at the bottom end of the shear wall.

Interstory drift ratios determined in the X direction frames (Figure 7.8) are very limited since earthquake excitation is applied only in the Y direction.

The ground motion set mean curvature ductilities of each beam end (denoted as I and J ends) in all five frames are given in Table 7.6. Number of beams on each frame is different; hence, notation of beams located at each story is grouped for $SI-CF$ and $FI-FE$ frames while SE beam ductilities are given separately. For each frame, beams are numbered in order from right to left as shown in frame elevation views given in Figure 7.1.

In general, all beams throughout the structure experience average ductility levels around the value of response reduction factor ($R = 7$). Middle story beams located on the FE frame undergo highest ductility demands due to higher deformation demands. Least frame average ductility is observed in the SI frame, while SE frame beam ductilities are higher due to the shear wall. Results given in Table 7.6 are in close conjunction with what has been observed in Figures 7.4 and 7.5 for interstory drift ratios and mean beam end curvatures of five frames.

Table 7.6: Mean beam curvature ductilities of existing design under the ground motion set.

STORY	SE BEAMS	I End	J End	STORY	SI BEAMS	I End	J End	CF BEAMS	I End	J End	STORY	FI BEAMS	I End	J End	FE BEAMS	I End	J End
1	BSE101	6.6	6.7	1	BSI101	6.7	4.3	BCF101	4.6	4.5	1	BFI201	6.0	5.7	BFE201	5.8	6.7
	BSE301	7.3	6.3		BSI201	4.8	4.6	BCF201	5.3	4.5		BFI301	6.2	5.5	BFE301	5.6	7.1
	BSE102	7.5	6.8		BSI301	5.4	5.6	BCF301	5.0	5.3		BFI202	8.2	7.8	BFE202	8.7	10.5
2	BSE302	7.2	7.4	2	BSI102	6.6	5.8	BCF102	6.8	6.5	2	BFI302	7.2	8.8	BFE302	9.4	9.6
	BSE103	8.1	6.2		BSI202	6.1	6.0	BCF202	7.2	6.6		BFI203	9.3	8.8	BFE203	10.4	12.4
	BSE303	6.7	8.4		BSI302	6.8	5.7	BCF302	7.0	6.1		BFI303	8.3	9.9	BFE303	11.2	11.5
3	BSE104	8.5	6.5	3	BSI103	7.1	6.4	BCF103	7.6	7.4	3	BFI204	10.3	8.5	BFE204	10.8	12.8
	BSE304	7.1	8.9		BSI203	6.5	6.7	BCF203	8.0	7.4		BFI304	10.2	9.3	BFE304	11.6	11.9
	BSE105	7.6	6.8		BSI303	7.2	6.3	BCF303	7.6	8.2		BFI205	10.0	9.4	BFE205	11.1	11.9
4	BSE305	7.6	8.4	4	BSI104	7.2	6.7	BCF104	7.7	8.9	4	BFI305	10.2	9.2	BFE305	11.1	11.4
	BSE106	7.8	7.0		BSI204	6.7	7.0	BCF204	8.3	7.7		BFI206	9.6	9.1	BFE206	10.2	12.4
	BSE306	7.7	8.5		BSI304	7.4	6.6	BCF304	7.9	8.5		BFI306	9.8	8.9	BFE306	11.2	11.4
5	BSE107	8.0	7.2	5	BSI105	7.2	6.9	BCF105	7.6	8.8	5	BFI207	8.7	8.4	BFE207	10.0	11.0
	BSE307	7.8	8.5		BSI205	6.8	7.1	BCF205	8.8	7.5		BFI307	8.9	8.2	BFE307	10.1	10.5
	BSE108	8.2	7.4		BSI305	7.4	6.7	BCF305	8.0	7.1		BFI208	9.1	7.3	BFE208	8.8	9.9
6	BSE308	7.8	8.5	6	BSI106	7.2	6.8	BCF106	7.4	8.7	6	BFI308	7.9	8.4	BFE308	9.7	8.8
	BSE109	8.4	7.7		BSI206	6.7	7.0	BCF206	8.5	7.3		BFI209	7.9	6.1	BFE209	7.3	8.3
	BSE309	7.7	8.4		BSI306	7.3	6.6	BCF306	8.7	8.2		BFI309	7.9	7.1	BFE309	8.1	7.3
7	BSE110	8.9	7.5	7	BSI107	7.0	6.5	BCF107	6.9	8.1	7	BFI210	6.5	6.1	BFE210	6.6	8.0
	BSE310	7.4	8.8		BSI207	6.6	6.7	BCF207	8.0	6.8		BFI310	6.7	5.9	BFE310	7.5	7.0
	BSE111	8.2	6.9		BSI307	7.2	6.3	BCF307	8.2	7.6		BFI211	5.1	4.8	BFE211	4.8	6.5
8	BSE311	6.7	8.1	8	BSI108	6.6	6.0	BCF108	6.3	7.2	8	BFI311	4.7	4.8	BFE311	5.9	5.4
	BSE112	7.2	6.4		BSI208	6.2	6.2	BCF208	8.8	6.0		BFI212	4.7	3.7	BFE212	4.9	4.5
	BSE312	6.2	7.2		BSI308	6.8	5.8	BCF308	7.6	6.8		BFI312	4.0	4.5	BFE312	3.8	5.4
12	END AVERAGE	7.6	7.5		BSI109	4.8	5.6	BCF109	5.4	6.2	12	END AVERAGE	7.8	7.3		8.5	9.3
FRAME AVERAGE			7.6		BSI209	5.7	5.8	BCF209	7.8	5.1	FRAME AVERAGE		7.6			8.9	
9				9	BSI309	6.2	5.4	BCF309	6.8	5.9							
					BSI110	5.5	5.0	BCF110	4.4	5.1							
					BSI210	5.1	5.2	BCF210	6.8	5.3							
10				10	BSI310	5.6	4.9	BCF310	5.8	4.9							
					BSI111	4.2	4.5	BCF111	3.4	4.1							
					BSI211	4.4	4.5	BCF211	5.6	4.3							
11				11	BSI311	4.9	4.1	BCF311	4.2	5.4							
					BSI112	5.1	3.6	BCF112	3.9	2.9							
					BSI212	5.0	3.8	BCF212	3.8	3.4							
12				12	BSI312	4.2	4.4	BCF312	3.5	3.9							
					END AVERAGE	6.2	5.7		6.6	6.3							
					FRAME AVERAGE		6.0										

Shear wall curvature ductilities obtained under the ground motion set is presented in Table 7.7. As seen in Table 7.7, mean ductility demand at the bottom of the shear wall is around 5.0. In addition, limited inelastic action is observed along the shear wall, expressed with curvature ductilities exceeding 1.0 in the majority of upper stories.

Table 7.7: Shear wall curvature ductilities of existing design computed under the ground motion set.

Story	Curvature Ductility
1	4.9
2	1.8
3	1.5
4	1.5
5	1.6
6	1.6
7	1.5
8	1.2
9	0.9
10	0.8
11	1.1
12	0.6

Similar to what has been presented for beams, ground motion set mean curvature ductilities of each column end (denoted as top and bottom ends) in all five frames are given in three separate tables. Frames having same number of columns are grouped and their results are presented in combined tables. Column ductilities of the *SE* frame are given in Table 7.8. *CF* and *FI* frame column ductilities are presented in Table 7.9. Finally, column ductilities of *FI* and *FE* frames are given in Table 7.10. Similar to beam notation, columns are named from right to left as shown in frame elevation views shown in Figure 7.1. The column ends exhibiting inelastic behavior are indicated in colored cells.

It can be seen in Table 7.8 that all columns remain linear elastic in the *SE* frame. This is not the case for *SE* frame shear wall as shown in Table 7.7. Inelastic action is only limited to bottom end of the first story columns of the *SI* frame, which is given in Table 7.9. It can be concluded from these results that the majority of inelastic

Table 7.8: Mean stiff edge frame column curvature ductilities of existing design under the ground motion set.

STORY	SE COLUMNS	I End	J End
1	SE101	0.9	0.2
	SE301	0.9	0.2
2	SE102	0.3	0.1
	SE302	0.3	0.1
3	SE103	0.1	0.2
	SE303	0.1	0.2
4	SE104	0.1	0.2
	SE304	0.1	0.2
5	SE105	0.1	0.2
	SE305	0.1	0.2
6	SE106	0.1	0.2
	SE306	0.1	0.2
7	SE107	0.1	0.2
	SE307	0.1	0.2
8	SE108	0.1	0.2
	SE308	0.1	0.1
9	SE109	0.1	0.1
	SE309	0.1	0.1
10	SE110	0.1	0.1
	SE310	0.1	0.1
11	SE111	0.1	0.1
	SE311	0.1	0.1
12	SE112	0.1	0.2
	SE312	0.1	0.2
END AVERAGE		0.2	0.2
FRAME AVERAGE		0.2	

Table 7.9: Mean stiff inner and center frame column curvature ductilities of the existing design under the ground motion set.

STORY	SI COLUMNS	I End	J End	CF COLUMNS	I End	J End
1	SI101	1.3	0.2	CF101	1.8	0.3
	SI201	1.6	0.3	CF201	1.9	0.3
	SI301	1.5	0.3	CF301	2.3	0.4
	SI401	1.3	0.2	CF401	1.9	0.3
2	SI102	0.3	0.2	CF102	0.4	0.3
	SI202	0.4	0.2	CF202	0.6	0.5
	SI302	0.4	0.2	CF302	0.5	0.4
	SI402	0.4	0.2	CF402	0.4	0.3
3	SI103	0.2	0.3	CF103	0.3	0.3
	SI203	0.3	0.3	CF203	0.4	0.5
	SI303	0.2	0.3	CF303	0.3	0.4
	SI403	0.2	0.2	CF403	0.3	0.3
4	SI104	0.2	0.2	CF104	0.2	0.3
	SI204	0.2	0.3	CF204	0.4	0.4
	SI304	0.2	0.2	CF304	0.3	0.3
	SI404	0.2	0.2	CF404	0.3	0.3
5	SI105	0.2	0.2	CF105	0.2	0.2
	SI205	0.2	0.2	CF205	0.3	0.4
	SI305	0.2	0.2	CF305	0.3	0.3
	SI405	0.2	0.2	CF405	0.2	0.3
6	SI106	0.2	0.2	CF106	0.2	0.2
	SI206	0.2	0.2	CF206	0.3	0.4
	SI306	0.2	0.2	CF306	0.2	0.3
	SI406	0.2	0.2	CF406	0.2	0.3
7	SI107	0.1	0.2	CF107	0.2	0.2
	SI207	0.2	0.2	CF207	0.3	0.3
	SI307	0.1	0.2	CF307	0.2	0.3
	SI407	0.2	0.2	CF407	0.2	0.2
8	SI108	0.1	0.1	CF108	0.2	0.2
	SI208	0.1	0.2	CF208	0.2	0.3
	SI308	0.1	0.1	CF308	0.2	0.2
	SI408	0.1	0.2	CF408	0.2	0.2
9	SI109	0.1	0.2	CF109	0.1	0.2
	SI209	0.1	0.2	CF209	0.2	0.3
	SI309	0.1	0.1	CF309	0.2	0.2
	SI409	0.1	0.2	CF409	0.2	0.2
10	SI110	0.1	0.2	CF110	0.1	0.2
	SI210	0.1	0.2	CF210	0.2	0.2
	SI310	0.1	0.2	CF310	0.1	0.2
	SI410	0.1	0.2	CF410	0.1	0.2
11	SI111	0.1	0.1	CF111	0.1	0.2
	SI211	0.1	0.1	CF211	0.2	0.2
	SI311	0.1	0.1	CF311	0.1	0.2
	SI411	0.1	0.1	CF411	0.1	0.1
12	SI112	0.1	0.2	CF112	0.1	0.1
	SI212	0.1	0.1	CF212	0.1	0.2
	SI312	0.1	0.1	CF312	0.1	0.1
	SI412	0.1	0.2	CF412	0.1	0.1
END AVERAGE		0.3	0.2		0.4	0.3
FRAME AVERAGE		0.2			0.3	

Table 7.10: Mean flexible inner and flexible edge frame column curvature ductilities of existing design under the ground motion set.

STORY	FI COLUMNS	I End	J End	FE COLUMNS	I End	J End
1	FI201	2.5	0.4	FE201	3.3	0.4
	FI301	3.2	0.5	FE301	3.7	0.5
	FI401	2.6	0.3	FE401	3.4	0.4
2	FI202	0.5	0.4	FE202	0.7	0.5
	FI302	0.7	0.5	FE302	0.9	0.7
	FI402	0.6	0.4	FE402	0.7	0.6
3	FI203	0.4	0.4	FE203	0.5	0.6
	FI303	0.5	0.5	FE303	0.6	0.8
	FI403	0.4	0.5	FE403	0.5	0.6
4	FI204	0.3	0.4	FE204	0.4	0.5
	FI304	0.4	0.4	FE304	0.5	0.7
	FI404	0.3	0.4	FE404	0.4	0.5
5	FI205	0.3	0.4	FE205	0.3	0.5
	FI305	0.4	0.4	FE305	0.5	0.7
	FI405	0.3	0.4	FE405	0.3	0.5
6	FI206	0.3	0.3	FE206	0.3	0.4
	FI306	0.3	0.4	FE306	0.4	0.6
	FI406	0.3	0.4	FE406	0.3	0.4
7	FI207	0.3	0.3	FE207	0.3	0.4
	FI307	0.3	0.4	FE307	0.4	0.6
	FI407	0.3	0.3	FE407	0.3	0.4
8	FI208	0.2	0.3	FE208	0.3	0.3
	FI308	0.3	0.3	FE308	0.4	0.5
	FI408	0.2	0.3	FE408	0.3	0.4
9	FI209	0.2	0.3	FE209	0.3	0.3
	FI309	0.3	0.3	FE309	0.3	0.5
	FI409	0.2	0.3	FE409	0.3	0.4
10	FI210	0.2	0.2	FE210	0.2	0.3
	FI310	0.2	0.3	FE310	0.3	0.4
	FI410	0.2	0.3	FE410	0.3	0.3
11	FI211	0.1	0.2	FE211	0.2	0.2
	FI311	0.2	0.2	FE311	0.2	0.3
	FI411	0.1	0.2	FE411	0.2	0.2
12	FI212	0.1	0.1	FE212	0.1	0.2
	FI312	0.1	0.1	FE312	0.1	0.4
	FI412	0.1	0.2	FE412	0.1	0.2
END AVERAGE		0.5	0.3		0.6	0.4
FRAME AVERAGE		0.4			0.5	

deformations on the stiff side of the structure occurs at the shear wall, accumulated at its base.

Only the bottom ends of the first story columns located in *CF*, *FI* and *FE* frames exhibit curvature ductilities over 1.0 as shown in Tables 7.9 and 7.10. The level of computed column ductilities increases towards *FE* frame, indicating an unbalanced damage distribution. First story columns located in the *FE* frame experience curvature ductilities up to 4; while first story *SI* and *CF* columns attain ductilities around 1.5 to 2.0.

7.9 Revised Design: Implementation of the Optimal Strength Distribution Method

Existing design of the twelve-story structure is revised through the implementation of Optimal Strength Distribution Method. The objective is obtaining a more balanced ductility distribution, by increasing the lateral strength of vertical members that are indicated by the procedure.

7.9.1 Determination of $SFSR_{opt}$

The optimal Stiff-to-Flexible side Strength Ratio ($SFSR_{opt}$) is determined by utilizing the system parameters e , T_n , and ductility reduction factor R_{mu} . Previously, it was determined that $T_n = 2.33$ seconds. Equivalent stiffness eccentricity of the structure is 30% and R_{mu} is 1.70, as discussed in Sections 7.4 and 7.6.3, respectively. Using these values, $SFSR_{opt}$ is determined as 1.48 from the associated Uniform Ductility Spectrum given in Figure 3.15. Comparison of existing and optimal values of $SFSR$ indicates that strengthening of the flexible side is necessary in order to achieve the optimal strength distribution. This situation corresponds to Case II variant of the Optimal Strength Distribution that was previously discussed in Section 4.3.2.

7.9.2 Strength Allocation Diagram

Equivalent Strength Allocation Diagram of the twelve-story structure is shown in Figure 7.9. Distances of flexible and stiff side elements to the center of mass in the Figure are computed as described in Section 4.6.1. The target flexible edge strength (F'_F) is computed as shown in Equation 5.6 and determined as 2436 kN. Nominal design strengths F_S and F_F are obtained by summing the design shears of the flexible and stiff side frames given in Table 7.3. Existing stiff side strength $\Omega_S F_S$ is the summation of the shear strengths of *SE* and *SI* frames. Similarly, existing flexible side strength $\Omega_F F_F$ is computed from shear strengths of flexible side frames.

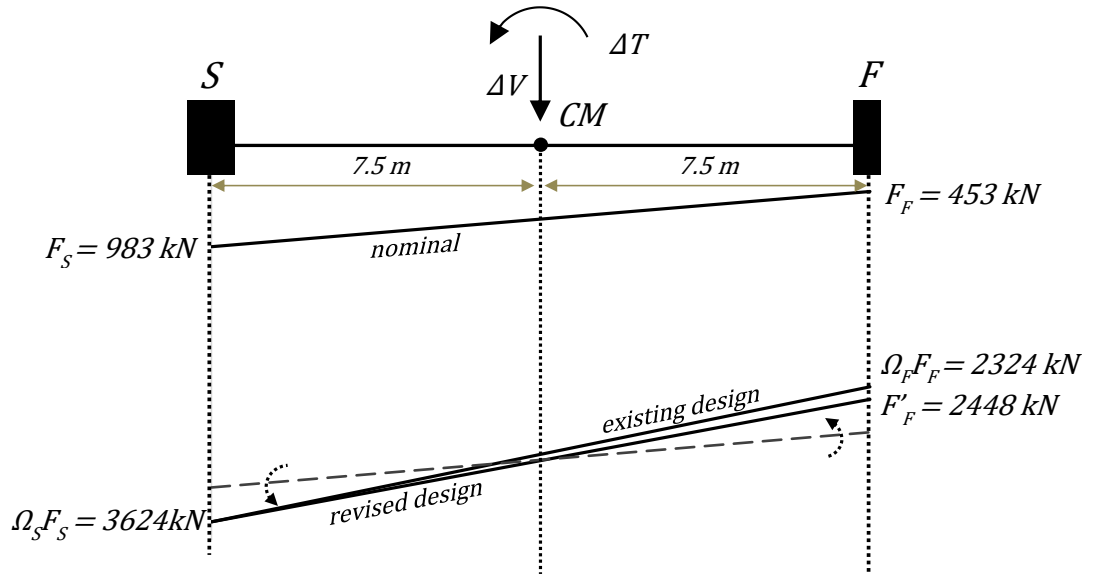


Figure 7.9: Equivalent Strength Allocation Diagram constructed for the twelve story frame-wall structure.

ΔV and ΔT are computed according to Section 4.3.2. Optimal Load Vector that is composed of ΔV and ΔT is given below in Equation 7.2.

$$\Delta F = \begin{bmatrix} 4622 \text{ kN} \\ 4920 \text{ kNm} \end{bmatrix} \quad (7.2)$$

According to the adopted sign convention, resulting torque ΔT is applied towards the flexible side. The dashed line in Figure 7.9 represents the combination of ΔV with the nominal strength distribution, which should be rotated by applying ΔT so that the

revised design strength distribution is obtained.

By comparing the value of F'_F and the existing strength ($\Omega_F F_F$) shown in Figure 7.9, it can be deduced that the correction provided by the proposed method to the existing strength distribution is very limited. Furthermore, the small difference between existing and revised strength distributions clearly indicate that the code-compliant existing design provides a close approximation to the optimal strength allocation on both sides of the system. This observation further validates the conclusions reached at the end of the previous section regarding the seismic performance of existing design.

Considering that similar strength distributions are obtained for the revised and existing systems, further application of the proposed procedure in order to obtain the revised design is a matter of engineering judgment. The performance gain expected from the revised design could be estimated as minimal and the existing design could be considered as satisfactory. However; in order to fully inspect the change in behaviour of the system through application of the method, the Optimal Strength Distribution Method is applied at its full extent in scope of this study and revised design is finalized.

7.9.3 Linear Elastic Analysis and Revised Seismic Design

Upon calculation of the Optimal Load Vector given in Equation 7.2, rest of the Optimal Strength Distribution Method algorithm presented in Section 4.6.5 is followed. Linear elastic analysis of the revised model is performed under combined effect of seismic loads and the Optimal Load Vector. Revised force demands in the columns members and the shear wall are determined. Columns that require increase in their capacities associated with the revised demands are marked in Figure 7.10. In addition to columns, the stories where shear wall should be strengthened are marked in the Figure, as well. The updated frame design base shears, $V_{d,Frame}$, are also written beneath each frame in Figure 7.10

Only the longitudinal reinforcement ratios (ρ_l) of the marked columns and marked shear wall members are increased while revising the design. No additional modification has been performed. Two different revised sections are provided for the 0.50

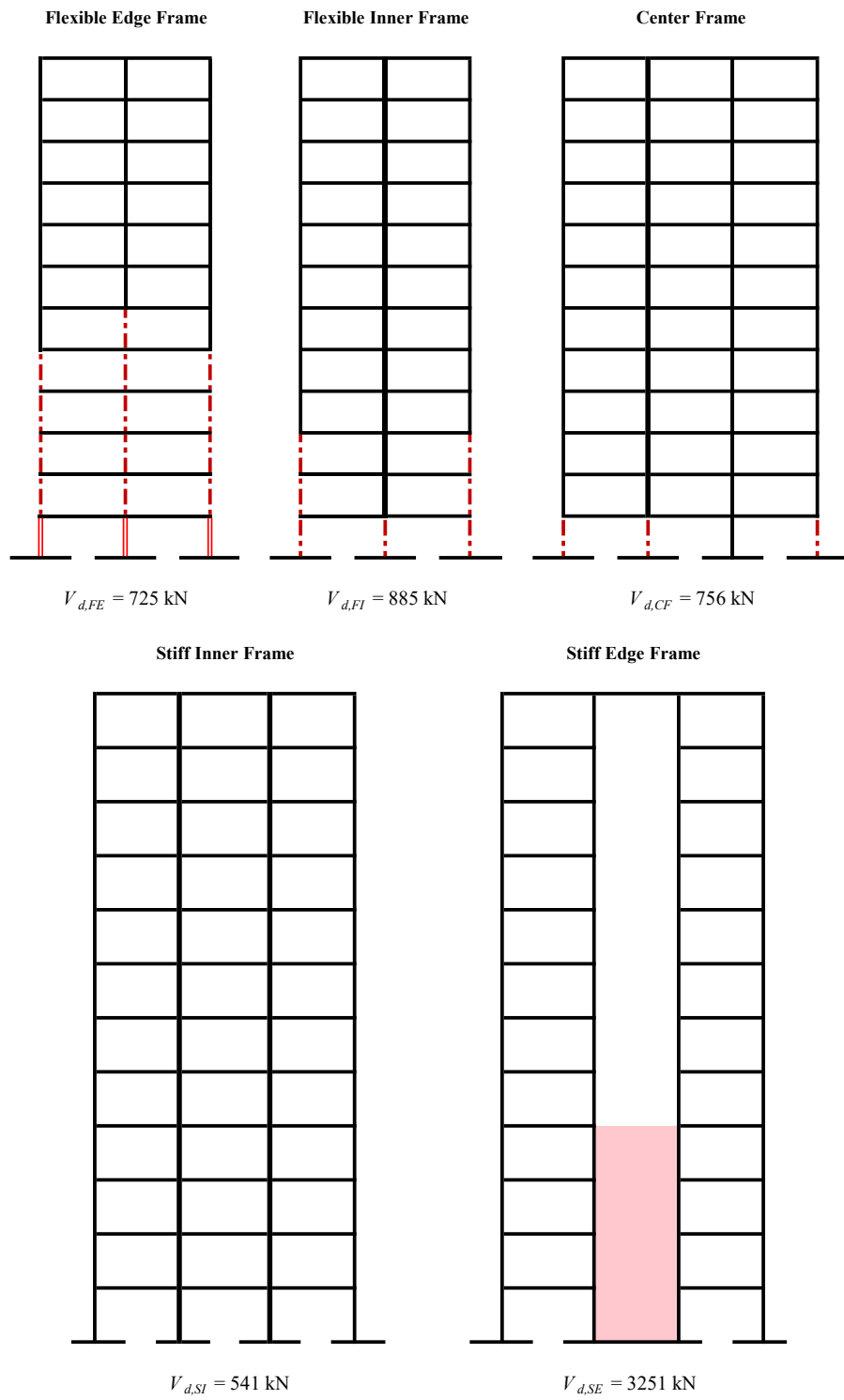


Figure 7.10: Schematic view of the five frames where columns and the shear wall that require strengthening at the related stories are marked.

m by 0.50 m columns. ρ_l value of the first story columns located at the *FE* frame has been increased from 1.22% to 3.86%. This ratio is achieved by providing twelve 32 mm diameter bars in these columns. These four columns are marked with bright red double lines in Figure 7.10. The other strengthened 0.50 m by 0.50 m columns possess a ρ_l value of 2.96%, while the original ratio was 1.1%. Twelve bars having 28 mm diameter are utilized in these members. They are represented with bold dark red dash-dot lines in Figure 7.10.

Similarly, 0.70 m by 0.70 m columns are strengthened by using twelve reinforcement bars having a diameter of 38 mm. This reinforcement arrangement yields a ρ_l value of 2.78%. It should be mentioned here again that the initial ρ_l value of these columns was 1.1%. These revised columns are marked in Figure 7.10 with bold dark red dash-dot lines, as well.

As can be seen in Figure 7.10, shear wall should be strengthened in the first four stories. As discussed previously, critical shear wall height corresponds to the first two stories of the structure. Hence, the section along the critical height is to be revised completely. In addition, another strengthened section is also provided for the third and fourth stories.

Longitudinal reinforcement ratio of the confined end regions along the critical height has been increased from 1.13% to 2.74% by providing sixteen 28 mm bars. Similarly, twenty-eight bars of 14 mm diameter is used in the web region rather than 12 mm diameter bars in the existing design. In the third and fourth stories, same ratio increase is achieved by using eight 28 mm bars in confined end regions. Diameter of the body reinforcement has been increased from 12 mm to 16 mm.

A capacity increase is necessary in the lower part of the shear wall as well as in the specified flexible side columns. As discussed in the previous section, shear wall displayed significant ductility demands throughout the dynamic analyses of the existing structure. The proposed method successfully detects the portion of the shear wall where high inelastic demands are anticipated and indicated a strength increase for the first four stories.

7.10 Dynamic Analysis Results for the Revised Design

Inelastic dynamic analyses have been performed on the mathematical model of the revised structure under the scaled strong ground motion set. Same scaled strong ground motion set is utilized in these analyses. Interstory drifts of all frames in the direction of analysis, beam end curvatures and column bottom-end curvatures determined for five frames, and the maximum curvatures computed at each story of the shear wall throughout the inelastic dynamic analyses are presented in Figures 7.11 – 7.14. In addition, interstory drifts of the frames in the orthogonal direction are shown in Figure 7.15. Ground motion set mean of the result parameters are also plotted in red bold line in Figures 7.11 – 7.15.

Figure 7.11 shows the interstory drift ratios computed at the five frames increases towards the *FE* frame. Effect of the shear wall is prominent in the drift profile of the *SE* frame. A very similar beam end curvature demand distribution to that of interstory drift ratios of the five frames is presented in Figure 7.12. Member end curvature demands of the *SE* frame beams are higher on the upper stories compared with the lower ones due to presence of the shear wall. Moreover, *FE* frame beam end curvature demands are observed to be highest among all *Y* direction beams. Column bottom-end curvature demands computed at the five frames of the revised design exhibit a slightly uniform demand distribution as shown in Figure 7.13. While highest demands are registered at the first story columns, their levels are quite similar with each other. Upper story columns located at the *FE* frame shows slightly greater bottom-end curvature demands compared with the other columns at the remaining frames.

Maximum shear wall curvature demand of the revised design is computed at the first story where significant inelastic deformations are present as shown in Figure 7.14. Story yield curvatures of the strengthened shear wall are also shown in the same Figure. Calculation of these yield curvatures were explained in Section 7.8. A marginally elastic response between second and fourth stories is observed in Figure 7.14. Rest of the shear wall above the fourth story slightly deform into the inelastic range. Interstory drift ratios observed in the orthogonal direction frames given in Figure 7.15 is very limited because seismic excitation is in the perpendicular direction. Frame 3, which is the stiffest frame in orthogonal direction yields the least demands.

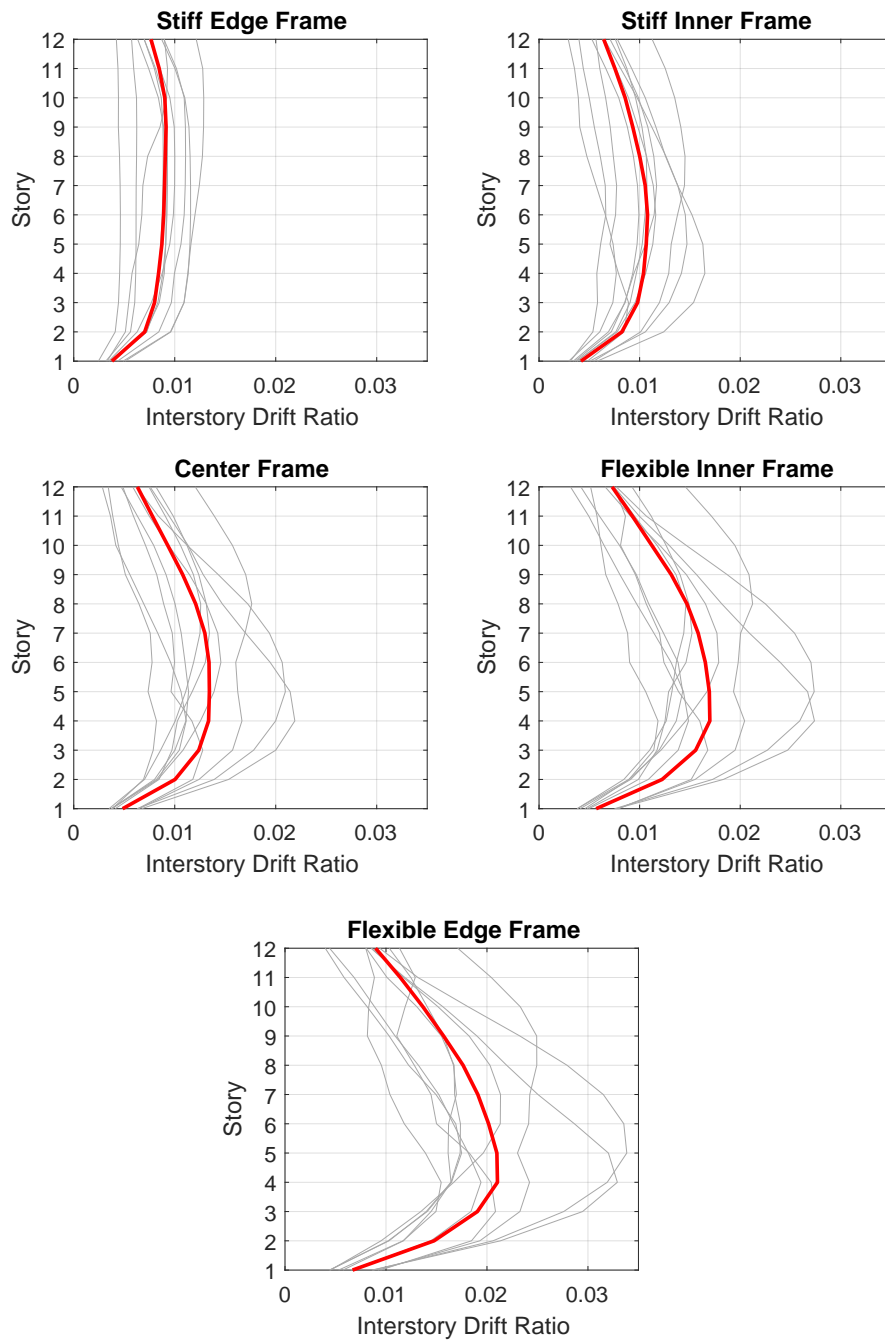


Figure 7.11: Maximum interstory drift ratios obtained from inelastic dynamic analyses of the revised design under ground motion set and the corresponding mean of maximum values for 10 GM records.

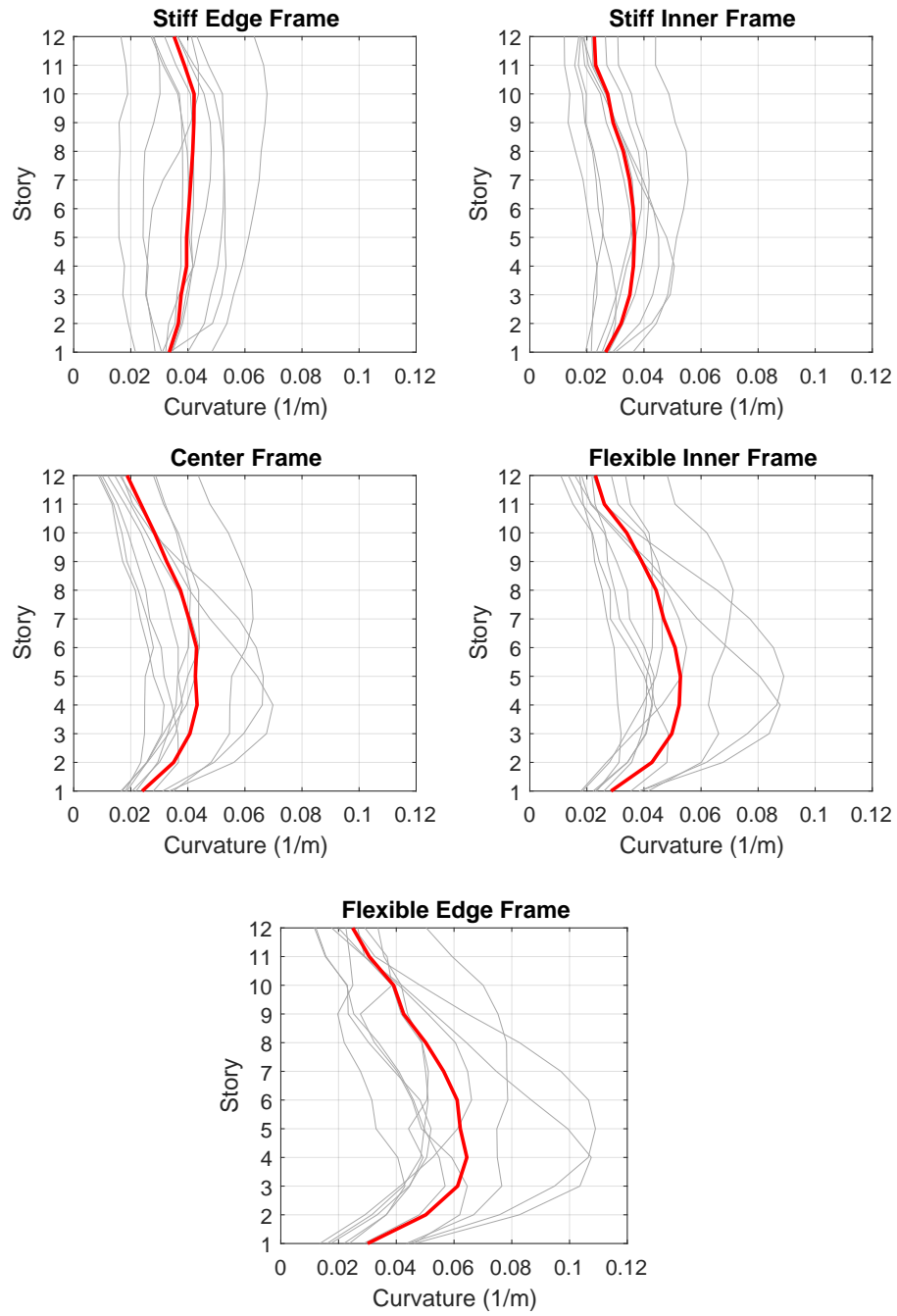


Figure 7.12: Beam end curvatures obtained from inelastic dynamic analyses of the revised design under ground motion set and the corresponding mean values for 10 GM records.

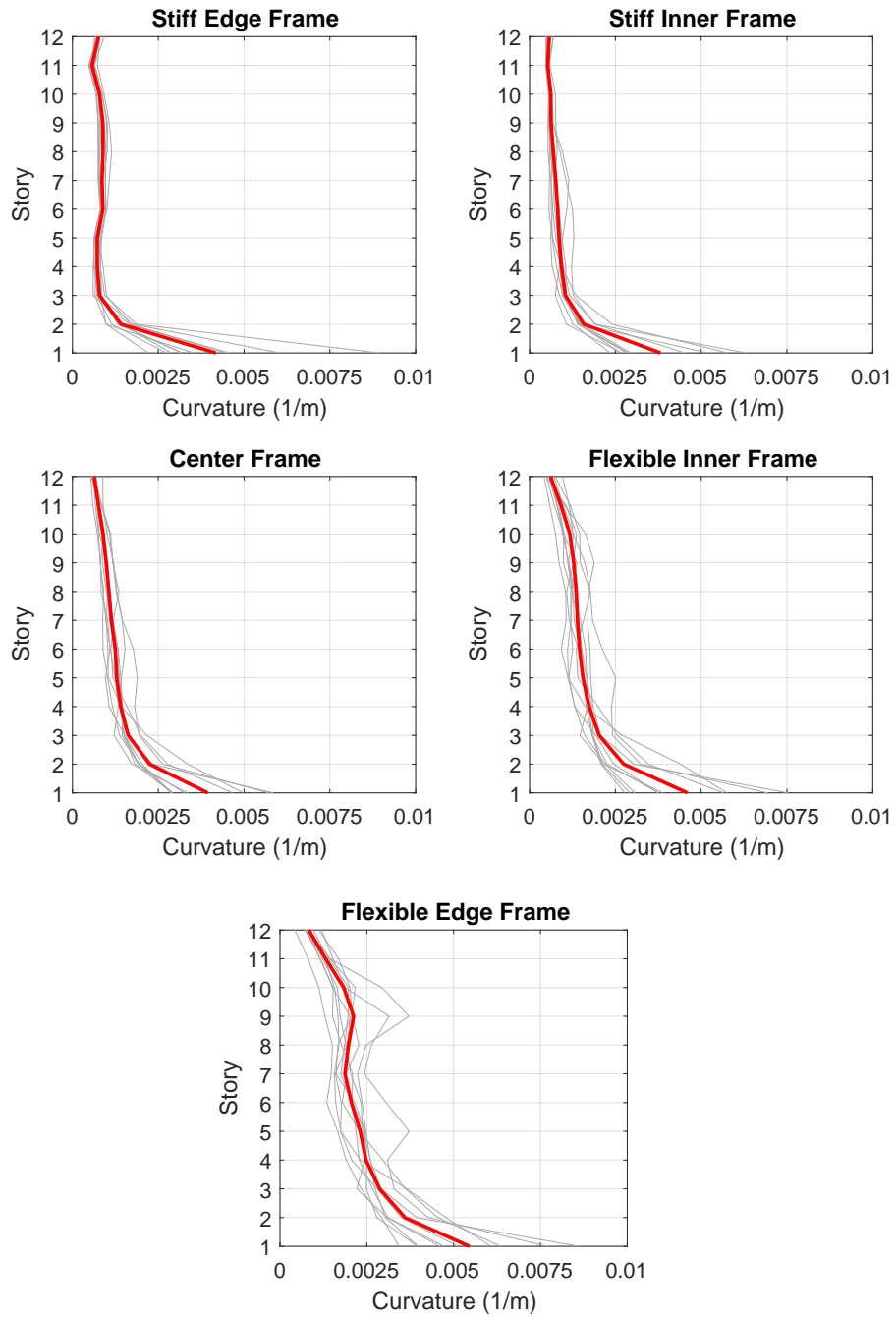


Figure 7.13: Column bottom-end curvatures obtained from inelastic dynamic analyses of the revised design under ground motion set and the corresponding mean values for 10 GM records.

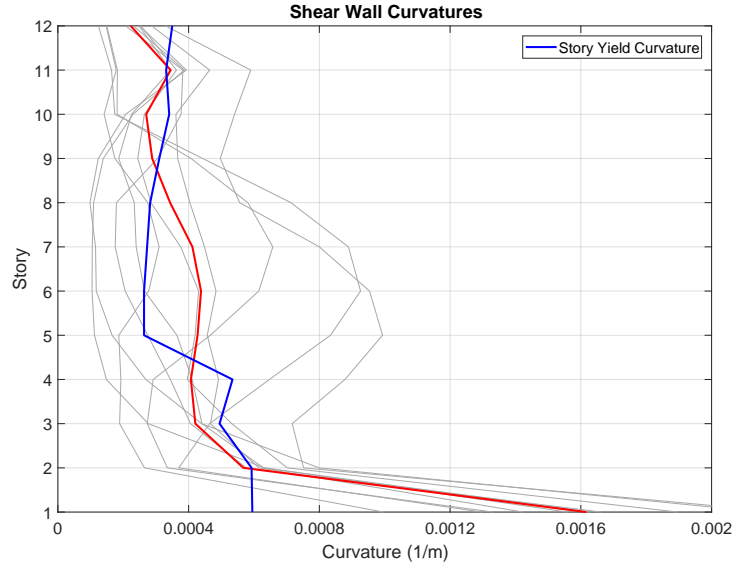


Figure 7.14: *SE* frame shear wall curvatures obtained from inelastic dynamic analyses of the revised design under ground motion set and the corresponding mean values for 10 GM records.

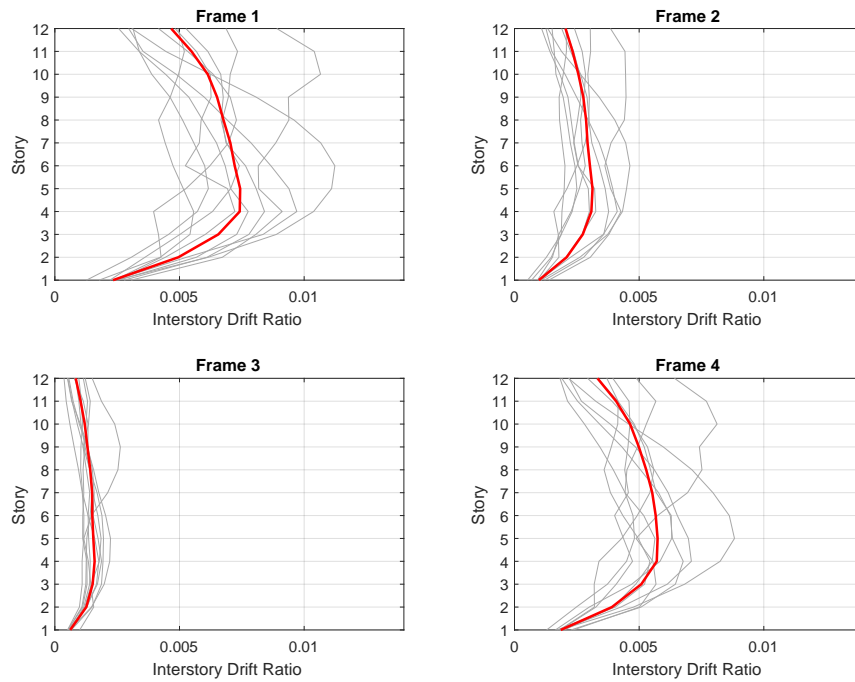


Figure 7.15: Maximum interstory drift ratios of the frames in orthogonal direction of the revised structure determined under ground motion set and the corresponding mean of maximum values for 10 GM records.

Member-end curvature ductilities recorded at every beam located in all five frames are given in Table 7.11. The format of the table is the same that have been given for existing beam designs in Section 7.8. Generally, all beams in the direction of analysis undergo inelastic deformations with global frame ductilities close to response reduction factor of the structure. Beams located in the middle stories FE and FI frames exhibit highest ductilities among all beams, with a maximum value of 12. Due to the presence of shear wall, *SE* frame beams also display somewhat larger ductilities compared to those measured in the *SI* frame. Overall, it could be concluded that the beam end ductility distribution is quite uniform, with FI and FE frames giving slightly higher responses.

Table 7.11: Mean beam curvature ductilities of revised design under the ground motion set.

STORY	SE BEAMS	I End	J End	STORY	SI BEAMS	I End	J End	CF BEAMS	I End	J End	STORY	FI BEAMS	I End	J End	FE BEAMS	I End	J End
1	BSE101	6.5	6.5	1	BSI101	6.6	6.6	BCF101	4.4	4.4	1	BFI201	5.6	5.6	BFE201	5.3	5.3
	BSE301	7.2	7.2		BSI201	4.7	4.7	BCF201	5.1	5.1		BFI301	5.8	5.8	BFE301	5.0	5.0
	BSE102	7.5	7.5		BSI301	5.3	5.3	BCF301	4.8	4.8		BFI202	8.2	8.2	BFE202	8.6	8.6
2	BSE302	7.2	7.2	2	BSI102	6.6	6.6	BCF102	6.8	6.8	2	BFI302	7.3	7.3	BFE302	9.3	9.3
	BSE103	8.3	8.3		BSI202	6.1	6.1	BCF202	7.3	7.3		BFI203	9.5	9.5	BFE203	10.6	10.6
	BSE303	6.6	6.6		BSI302	6.8	6.8	BCF302	7.0	7.0		BFI303	8.6	8.6	BFE303	11.4	11.4
3	BSE104	8.5	8.5	3	BSI103	7.2	7.2	BCF103	7.8	7.8	3	BFI204	10.7	10.7	BFE204	11.1	11.1
	BSE304	7.0	7.0		BSI203	6.6	6.6	BCF203	8.2	8.2		BFI304	10.6	10.6	BFE304	12.0	12.0
	BSE105	7.8	7.8		BSI303	7.3	7.3	BCF303	7.8	7.8		BFI205	10.4	10.4	BFE205	11.5	11.5
4	BSE305	7.5	7.5	4	BSI104	7.3	7.3	BCF104	7.9	7.9	4	BFI305	10.5	10.5	BFE305	11.5	11.5
	BSE106	7.9	7.9		BSI204	6.8	6.8	BCF204	8.6	8.6		BFI206	9.9	9.9	BFE206	10.6	10.6
	BSE306	7.6	7.6		BSI304	7.5	7.5	BCF304	8.1	8.1		BFI306	10.1	10.1	BFE306	11.6	11.6
5	BSE107	8.2	8.2	5	BSI105	7.3	7.3	BCF105	7.9	7.9	5	BFI207	9.1	9.1	BFE207	10.5	10.5
	BSE307	7.7	7.7		BSI205	6.8	6.8	BCF205	9.1	9.1		BFI307	9.2	9.2	BFE307	10.5	10.5
	BSE108	8.4	8.4		BSI305	7.5	7.5	BCF305	8.3	8.3		BFI208	9.4	9.4	BFE208	9.2	9.2
6	BSE308	7.7	7.7	6	BSI106	7.2	7.2	BCF106	7.6	7.6	6	BFI308	8.2	8.2	BFE308	10.1	10.1
	BSE109	8.6	8.6		BSI206	6.8	6.8	BCF206	8.8	8.8		BFI209	8.2	8.2	BFE209	7.8	7.8
	BSE309	7.7	7.7		BSI306	7.4	7.4	BCF306	8.9	8.9		BFI309	8.2	8.2	BFE309	8.6	8.6
7	BSE110	9.1	9.1	7	BSI107	7.0	7.0	BCF107	7.1	7.1	7	BFI210	6.6	6.6	BFE210	7.0	7.0
	BSE310	7.4	7.4		BSI207	6.6	6.6	BCF207	8.2	8.2		BFI310	6.8	6.8	BFE310	8.0	8.0
	BSE111	8.4	8.4		BSI307	7.2	7.2	BCF307	8.4	8.4		BFI211	5.2	5.2	BFE211	5.2	5.2
8	BSE311	6.7	6.7	8	BSI108	6.6	6.6	BCF108	6.5	6.5	8	BFI311	4.8	4.8	BFE311	6.3	6.3
	BSE112	7.5	7.5		BSI208	6.2	6.2	BCF208	8.9	8.9		BFI212	5.0	5.0	BFE212	5.1	5.1
	BSE312	6.2	6.2		BSI308	6.8	6.8	BCF308	7.7	7.7		BFI312	4.1	4.1	BFE312	4.0	4.0
END AVERAGE		7.6	7.6		BSI109	4.8	4.8	BCF109	5.5	5.5	END AVERAGE	8.0	8.0		8.8	8.8	
FRAME AVERAGE			7.6		BSI209	5.7	5.8	BCF209	7.9	7.9	FRAME AVERAGE						
9				9	BSI309	6.2	6.2	BCF309	6.9	6.9	9						
					BSI110	5.5	5.5	BCF110	4.5	4.5							
					BSI210	5.1	5.1	BCF210	6.9	6.9							
10				10	BSI310	5.6	5.6	BCF310	5.8	5.8	10						
					BSI111	4.2	4.2	BCF111	3.5	3.5							
					BSI211	4.4	4.4	BCF211	5.7	5.7							
11				11	BSI311	4.9	4.9	BCF311	4.3	4.3	11						
					BSI112	5.1	5.1	BCF112	4.0	4.0							
					BSI212	5.0	5.0	BCF212	3.9	3.9							
12				12	BSI312	4.2	4.2	BCF312	3.6	3.6	12						
					END AVERAGE	6.2	6.2		6.8	6.8							
					FRAME AVERAGE												

Shear wall curvature ductilities computed at each story of the revised structure are given in Table 7.12. The results in the Table are consistent with what has been discussed for Figure 7.15. Maximum curvature demand in the wall occurs at the bottom with a value of 2.7. Strengthened sections of the wall located between second and fourth stories remain elastic while small amounts of ductility are observed in mid-height of the wall.

Table 7.12: Shear wall curvature ductilities of revised design computed under the ground motion set.

Story	Curvature Ductility
1	2.7
2	0.9
3	0.9
4	0.8
5	1.6
6	1.7
7	1.5
8	1.2
9	0.9
10	0.8
11	1.0
12	0.6

Ground motion set mean curvature ductilities of every column end in all five frames are presented in Tables 7.13 – 7.15. Format of these tables have been previously discussed in Section 7.8. Column end ductilities of the *SE* frame are given in Table 7.13, those of *SI* and *CF* frames are given in 7.14. Ductilities computed at the ends of columns located in *FE* and *FI* frames are presented in 7.15.

In Tables 7.13 – 7.15 it could be seen that all columns remain essentially elastic throughout the dynamic analyses. Only bottom ends of the inner columns located in *SI* and *CF* frames display slight inelastic behavior with computed ductilities just over 1.0. Therefore, it could be concluded that the strengthening of the marked members given in Figure 7.10 results in elastic response in columns of the revised structure under the scaled strong ground motion set which is compatible with the Design Basis Earthquake (DBE) level of seismic excitation.

Table 7.13: Mean stiff edge frame column curvature ductilities of revised design under the ground motion set.

STORY	SE COLUMNS	Bottom End	Top End
1	SE101	0.8	0.2
	SE301	0.8	0.2
2	SE102	0.3	0.2
	SE302	0.3	0.1
3	SE103	0.1	0.2
	SE303	0.1	0.2
4	SE104	0.1	0.2
	SE304	0.1	0.2
5	SE105	0.1	0.2
	SE305	0.1	0.2
6	SE106	0.1	0.2
	SE306	0.1	0.2
7	SE107	0.1	0.2
	SE307	0.1	0.2
8	SE108	0.1	0.2
	SE308	0.1	0.1
9	SE109	0.1	0.1
	SE309	0.1	0.2
10	SE110	0.1	0.1
	SE310	0.1	0.1
11	SE111	0.1	0.1
	SE311	0.1	0.1
12	SE112	0.1	0.2
	SE312	0.1	0.2
END AVERAGE		0.2	0.2
FRAME AVERAGE		0.2	

Table 7.14: Mean stiff inner and center frame column curvature ductilities of revised design under the ground motion set.

STORY	SI COLUMNS	Bottom End	Top End	CF COLUMNS	Bottom End	Top End
1	SI101	0.8	0.2	CF101	0.5	0.2
	SI201	1.2	0.3	CF201	1.0	0.4
	SI301	1.2	0.3	CF301	0.8	0.3
	SI401	0.8	0.2	CF401	0.6	0.2
2	SI102	0.3	0.2	CF102	0.4	0.3
	SI202	0.4	0.3	CF202	0.6	0.5
	SI302	0.4	0.3	CF302	0.6	0.4
	SI402	0.4	0.2	CF402	0.5	0.3
3	SI103	0.2	0.3	CF103	0.3	0.3
	SI203	0.3	0.3	CF203	0.4	0.5
	SI303	0.3	0.3	CF303	0.4	0.4
	SI403	0.3	0.3	CF403	0.3	0.4
4	SI104	0.2	0.3	CF104	0.2	0.3
	SI204	0.2	0.3	CF204	0.4	0.5
	SI304	0.2	0.3	CF304	0.3	0.4
	SI404	0.2	0.3	CF404	0.3	0.3
5	SI105	0.2	0.2	CF105	0.2	0.3
	SI205	0.2	0.2	CF205	0.3	0.4
	SI305	0.2	0.2	CF305	0.3	0.3
	SI405	0.2	0.2	CF405	0.2	0.3
6	SI106	0.2	0.2	CF106	0.2	0.2
	SI206	0.2	0.2	CF206	0.3	0.4
	SI306	0.2	0.2	CF306	0.3	0.3
	SI406	0.2	0.2	CF406	0.2	0.3
7	SI107	0.2	0.2	CF107	0.2	0.2
	SI207	0.2	0.2	CF207	0.3	0.3
	SI307	0.2	0.2	CF307	0.2	0.3
	SI407	0.2	0.2	CF407	0.2	0.3
8	SI108	0.1	0.2	CF108	0.2	0.2
	SI208	0.1	0.2	CF208	0.2	0.3
	SI308	0.1	0.1	CF308	0.2	0.2
	SI408	0.1	0.2	CF408	0.2	0.2
9	SI109	0.1	0.2	CF109	0.1	0.2
	SI209	0.1	0.2	CF209	0.2	0.3
	SI309	0.1	0.1	CF309	0.2	0.2
	SI409	0.1	0.2	CF409	0.2	0.2
10	SI110	0.1	0.2	CF110	0.1	0.2
	SI210	0.1	0.2	CF210	0.2	0.2
	SI310	0.1	0.2	CF310	0.1	0.2
	SI410	0.1	0.2	CF410	0.1	0.2
11	SI111	0.1	0.1	CF111	0.1	0.2
	SI211	0.1	0.2	CF211	0.2	0.2
	SI311	0.1	0.1	CF311	0.1	0.2
	SI411	0.1	0.1	CF411	0.1	0.2
12	SI112	0.1	0.2	CF112	0.1	0.1
	SI212	0.1	0.1	CF212	0.1	0.3
	SI312	0.1	0.1	CF312	0.1	0.1
	SI412	0.1	0.2	CF412	0.1	0.2
END AVERAGE		0.2	0.2		0.3	0.3
FRAME AVERAGE		0.2			0.3	

Table 7.15: Mean flexible inner and flexible edge frame column curvature ductilities of revised design under the ground motion set.

STORY	FI COLUMNS	Bottom End	Top End	FE COLUMNS	Bottom End	Top End
1	FI201	0.6	0.3	FE201	0.7	0.3
	FI301	0.9	0.4	FE301	0.7	0.4
	FI401	0.7	0.3	FE401	0.7	0.3
2	FI202	0.4	0.3	FE202	0.6	0.5
	FI302	0.8	0.6	FE302	0.9	0.7
	FI402	0.4	0.3	FE402	0.6	0.5
3	FI203	0.3	0.3	FE203	0.5	0.5
	FI303	0.5	0.6	FE303	0.7	0.7
	FI403	0.3	0.3	FE403	0.5	0.5
4	FI204	0.2	0.3	FE204	0.4	0.5
	FI304	0.5	0.6	FE304	0.5	0.6
	FI404	0.3	0.3	FE404	0.4	0.4
5	FI205	0.3	0.4	FE205	0.4	0.6
	FI305	0.4	0.4	FE305	0.5	0.6
	FI405	0.3	0.4	FE405	0.4	0.6
6	FI206	0.3	0.4	FE206	0.3	0.5
	FI306	0.3	0.4	FE306	0.4	0.6
	FI406	0.3	0.4	FE406	0.3	0.5
7	FI207	0.3	0.3	FE207	0.3	0.5
	FI307	0.3	0.4	FE307	0.4	0.6
	FI407	0.3	0.3	FE407	0.3	0.5
8	FI208	0.2	0.3	FE208	0.3	0.4
	FI308	0.3	0.3	FE308	0.4	0.5
	FI408	0.3	0.3	FE408	0.3	0.5
9	FI209	0.2	0.3	FE209	0.3	0.4
	FI309	0.3	0.3	FE309	0.3	0.5
	FI409	0.2	0.3	FE409	0.3	0.4
10	FI210	0.2	0.2	FE210	0.2	0.3
	FI310	0.2	0.3	FE310	0.3	0.4
	FI410	0.2	0.3	FE410	0.3	0.3
11	FI211	0.1	0.2	FE211	0.2	0.2
	FI311	0.2	0.3	FE311	0.2	0.3
	FI411	0.1	0.2	FE411	0.2	0.3
12	FI212	0.1	0.1	FE212	0.1	0.2
	FI312	0.1	0.1	FE312	0.1	0.4
	FI412	0.1	0.2	FE412	0.1	0.2
END AVERAGE		0.3	0.3		0.4	0.4
FRAME AVERAGE		0.3			0.4	

Overall, the revised design which has been obtained under the updated seismic demands estimated by the Optimal Strength Distribution Method reduces the seismic response of the structure to the elastic range. The increase in capacity of the marked elements given in Figure 7.10 yields significantly reduced deformation levels. Consequently, unbalance in damage distribution could no longer be observed in the revised system.

7.11 Performance Comparison between Existing and Revised Designs

Seismic response quantities which have been compiled for the two designs through inelastic dynamic analyses and discussed individually in the previous sections are compared herein. The performance of the Optimal Strength Distribution Method in improving the seismic response of the twelve-story structure is evaluated.

7.11.1 Comparison of Frame Responses

Ground motion set mean interstory drift ratios in the direction of analysis obtained from inelastic dynamic analyses of existing and revised structures are presented in Figure 7.16. Similarly, ground motion set mean beam end curvatures computed for both designs through dynamic analyses are given in Figure 7.17. Mean column bottom-end curvatures which were compiled for both designs are shown in Figure 7.18. Ground motion set mean shear wall curvatures computed for both existing and revised designs are displayed in Figure 7.19. Finally, mean interstory drift ratios in the orthogonal direction are given in Figure 7.20

Black line in Figures 7.16 - 7.20 indicate the mean response of existing design; whereas red line illustrates the mean deformations associated with the revised design. Story yield curvatures of the shear wall computed for both existing and revised designs are also displayed in Figure 7.19

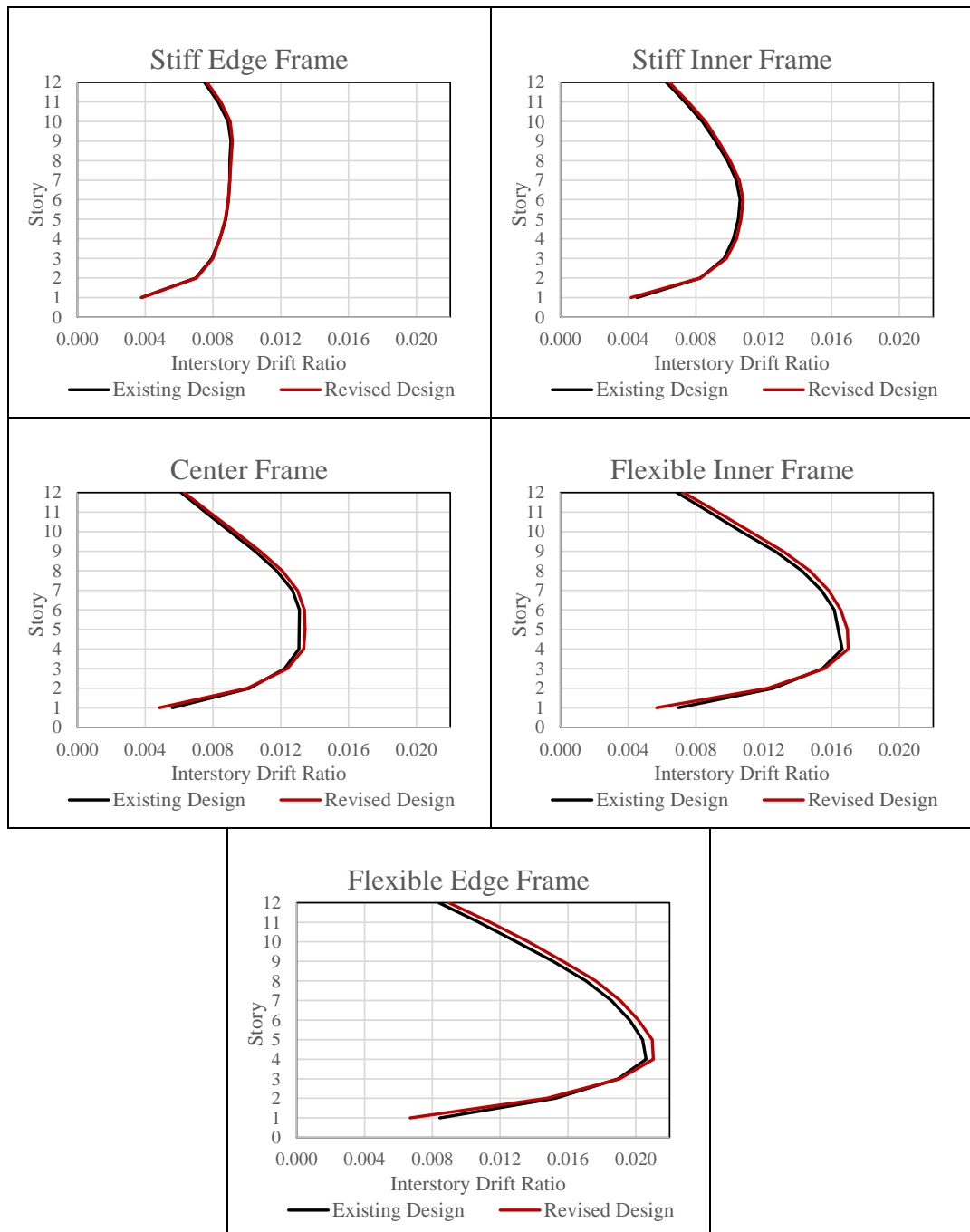


Figure 7.16: Comparison of the mean interstory drift ratios in direction of analysis calculated for the existing and revised designs.

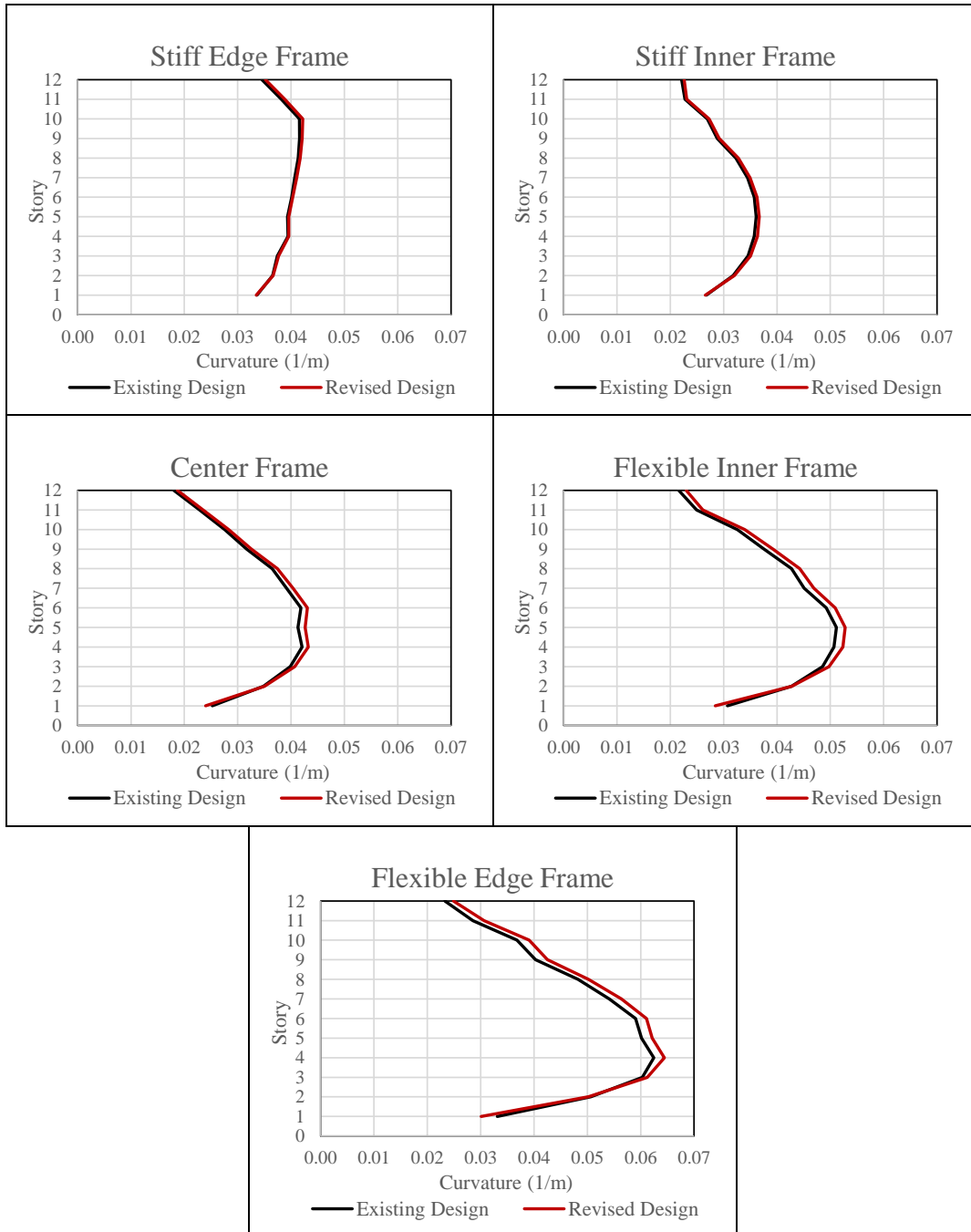


Figure 7.17: Comparison of the mean beam-end curvatures calculated for the existing and revised designs.

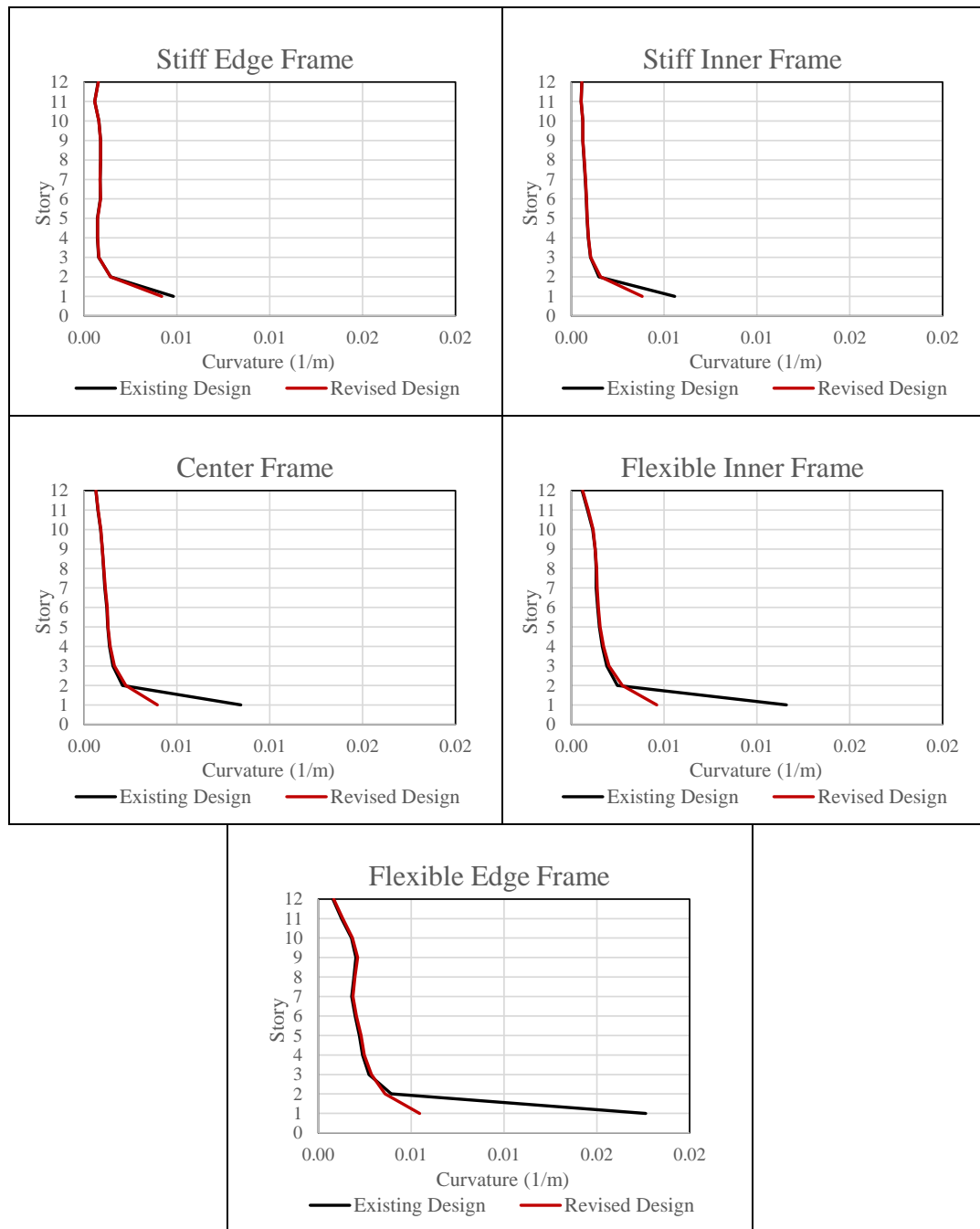


Figure 7.18: Comparison of the mean column bottom end curvatures calculated for the existing and revised designs.

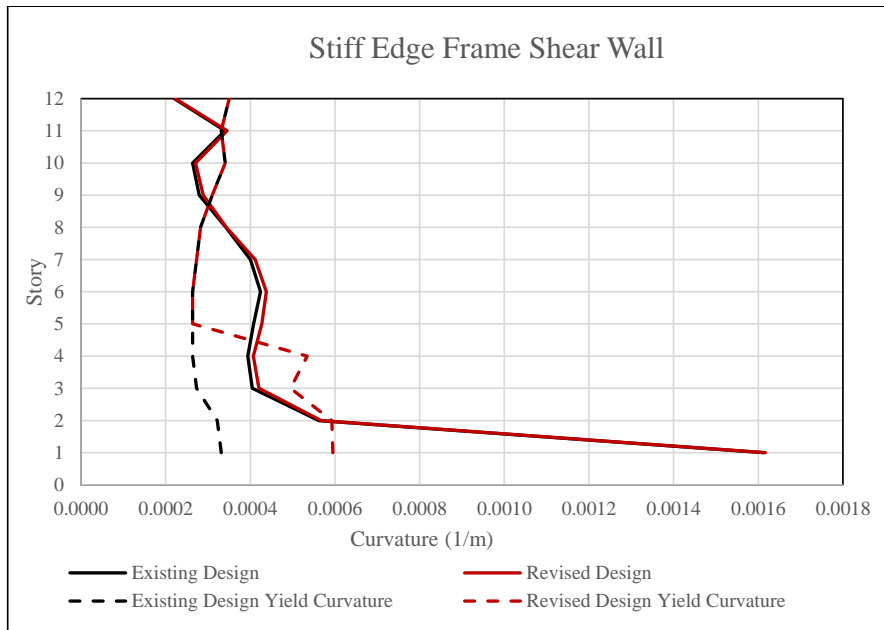


Figure 7.19: Comparison of the shear wall curvatures calculated for the existing and revised designs.

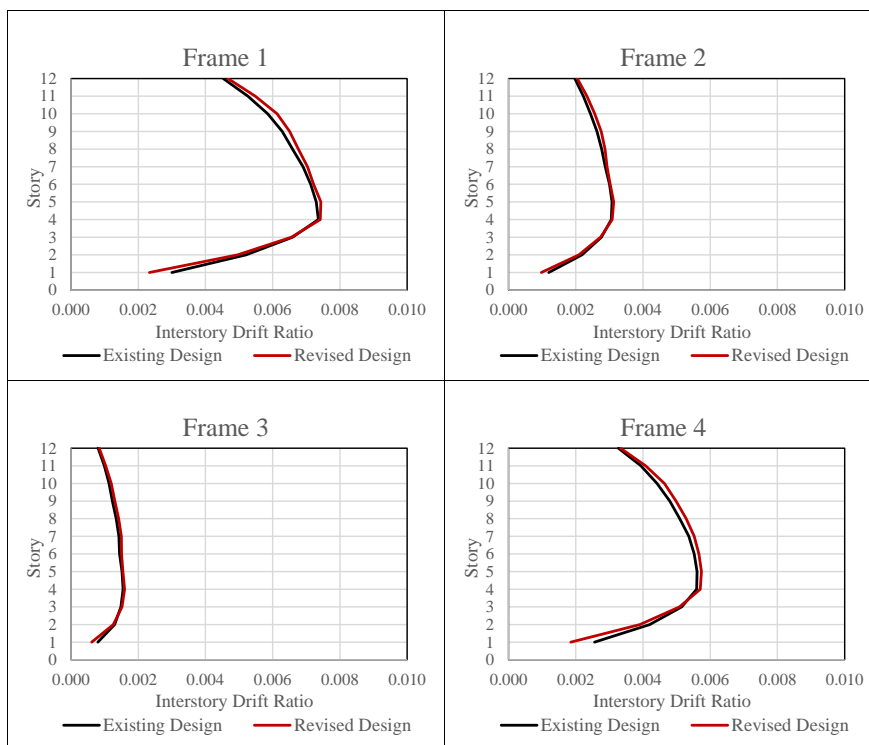


Figure 7.20: Comparison of the mean interstory drift ratios calculated in the orthogonal direction frames for the existing and revised designs.

As can be seen in Figures 7.16, 7.17 and 7.20, interstory drift ratios and beam curvature demands registered in upper stories are slightly bigger in the of revised structure. However, seismic demands at the first two stories are marginally lower. This behavior is more pronounced in flexible side frames. Overall, frame interstory drifts and beam end curvatures exhibit limited variation between existing and revised structures.

A considerable change in curvature demands of first story column ends is seen in Figure 7.18. Highly unbalanced demand distribution observed in the case of existing design is not seen in revised structure results. Ground motion set mean first story column curvature demands are around 0.01/m at all five frames in the direction of analysis. Major improvement in balancing the deformation demands of columns is obtained through application of the Optimal Strength Distribution Method. Apart from first story column bottom-ends, curvature demands computed at the rest of the columns do not vary at all between both systems.

Comparison of the mean curvature demands measured at the shear wall given in 7.19 indicate a reduction in inelastic deformations. Even though the curvature demand distribution along height of the shear wall do not change considerably, yield deformation of the strengthened portion of the shear wall increases significantly. As mentioned in previous sections, yield deformation of the shear wall is computed approximately through bilinearization of the moment-curvature relationship obtained at each story. Since shear wall sections exhibit progressive yielding behavior, capacity increase associated with the strengthened sections significantly affects the idealized yield deformations. Consequently, reduced ductilities are observed at the first story of the shear wall. Between second and fourth stories, revised shear wall remain elastic. These outcomes regarding the behavior of the wall are further discussed while member ductilities are given in the next subsection.

7.11.2 Comparison of Member Ductility Demands

Mean curvature ductility demands of all beam, column ends as well as shear wall ductilities obtained for two systems are compared with each other in this subsection. Beam end ductilities are compared in Tables 7.16 – 7.20 for *SE*, *SI*, *CF*, *FI* and *FE* frames, respectively.

Table 7.16: Beam curvature ductility comparison for the Stiff Edge Frame

Story	Beam	Existing Design		Revised Design	
		I End	J End	I End	J End
1	BSE101	6.6	6.7	6.5	6.5
	BSE301	7.3	6.3	7.2	7.2
2	BSE102	7.5	6.8	7.5	7.5
	BSE302	7.2	7.4	7.2	7.2
3	BSE103	8.1	6.2	8.3	8.3
	BSE303	6.7	8.4	6.6	6.6
4	BSE104	8.5	6.5	8.5	8.5
	BSE304	7.1	8.9	7.0	7.0
5	BSE105	7.6	6.8	7.8	7.8
	BSE305	7.6	8.4	7.5	7.5
6	BSE106	7.8	7.0	7.9	7.9
	BSE306	7.7	8.5	7.6	7.6
7	BSE107	8.0	7.2	8.2	8.2
	BSE307	7.8	8.5	7.7	7.7
8	BSE108	8.2	7.4	8.4	8.4
	BSE308	7.8	8.5	7.7	7.7
9	BSE109	8.4	7.7	8.6	8.6
	BSE309	7.7	8.4	7.7	7.7
10	BSE110	8.9	7.5	9.1	9.1
	BSE310	7.4	8.8	7.4	7.4
11	BSE111	8.2	6.9	8.4	8.4
	BSE311	6.7	8.1	6.7	6.7
12	BSE112	7.2	6.4	7.5	7.5
	BSE312	6.2	7.2	6.2	6.2
Beam End Average		7.6	7.5	7.6	7.6
Frame Average		7.6		7.6	

Table 7.17: Beam curvature ductility comparison for the Stiff Inner Frame

Story	Beam	Existing Design		Revised Design	
		I End	J End	I End	J End
1	BSI101	6.7	4.3	6.6	6.6
	BSI201	4.8	4.6	4.7	4.7
	BSI301	5.4	5.6	5.3	5.3
2	BSI102	6.6	5.8	6.6	6.6
	BSI202	6.1	6.0	6.1	6.1
	BSI302	6.8	5.7	6.8	6.8
3	BSI103	7.1	6.4	7.2	7.2
	BSI203	6.5	6.7	6.6	6.6
	BSI303	7.2	6.3	7.3	7.3
4	BSI104	7.2	6.7	7.3	7.3
	BSI204	6.7	7.0	6.8	6.8
	BSI304	7.4	6.6	7.5	7.5
5	BSI105	7.2	6.9	7.3	7.3
	BSI205	6.8	7.1	6.8	6.8
	BSI305	7.4	6.7	7.5	7.5
6	BSI106	7.2	6.8	7.2	7.2
	BSI206	6.7	7.0	6.8	6.8
	BSI306	7.3	6.6	7.4	7.4
7	BSI107	7.0	6.5	7.0	7.0
	BSI207	6.6	6.7	6.6	6.6
	BSI307	7.2	6.3	7.2	7.2
8	BSI108	6.6	6.0	6.6	6.6
	BSI208	6.2	6.2	6.2	6.2
	BSI308	6.8	5.8	6.8	6.8
9	BSI109	4.8	5.6	4.8	4.8
	BSI209	5.7	5.8	5.7	5.7
	BSI309	6.2	5.4	6.2	6.2
10	BSI110	5.5	5.0	5.5	5.5
	BSI210	5.1	5.2	5.1	5.1
	BSI310	5.6	4.9	5.6	5.6
11	BSI111	4.2	4.5	4.2	4.2
	BSI211	4.4	4.5	4.4	4.4
	BSI311	4.9	4.1	4.9	4.9
12	BSI112	5.1	3.6	5.1	5.1
	BSI212	5.0	3.8	5.0	5.0
	BSI312	4.2	4.4	4.2	4.2
Beam End Average		6.2	5.7	6.2	6.2
Frame Average		6.0		6.2	

Table 7.18: Beam curvature ductility comparison for the Center Frame

Story	Beam	Existing Design		Revised Design	
		I End	J End	I End	J End
1	BCF101	4.6	4.5	4.4	4.4
	BCF201	5.3	4.5	5.1	5.1
	BCF301	5.0	5.3	4.8	4.8
2	BCF102	6.8	6.5	6.8	6.8
	BCF202	7.2	6.6	7.3	7.3
	BCF302	7.0	6.1	7.0	7.0
3	BCF103	7.6	7.4	7.8	7.8
	BCF203	8.0	7.4	8.2	8.2
	BCF303	7.6	8.2	7.8	7.8
4	BCF104	7.7	8.9	7.9	7.9
	BCF204	8.3	7.7	8.6	8.6
	BCF304	7.9	8.5	8.1	8.1
5	BCF105	7.6	8.8	7.9	7.9
	BCF205	8.8	7.5	9.1	9.1
	BCF305	8.0	7.1	8.3	8.3
6	BCF106	7.4	8.7	7.6	7.6
	BCF206	8.5	7.3	8.8	8.8
	BCF306	8.7	8.2	8.9	8.9
7	BCF107	6.9	8.1	7.1	7.1
	BCF207	8.0	6.8	8.2	8.2
	BCF307	8.2	7.6	8.4	8.4
8	BCF108	6.3	7.2	6.5	6.5
	BCF208	8.8	6.0	8.9	8.9
	BCF308	7.6	6.8	7.7	7.7
9	BCF109	5.4	6.2	5.5	5.5
	BCF209	7.8	5.1	7.9	7.9
	BCF309	6.8	5.9	6.9	6.9
10	BCF110	4.4	5.1	4.5	4.5
	BCF210	6.8	5.3	6.9	6.9
	BCF310	5.8	4.9	5.8	5.8
11	BCF111	3.4	4.1	3.5	3.5
	BCF211	5.6	4.3	5.7	5.7
	BCF311	4.2	5.4	4.3	4.3
12	BCF112	3.9	2.9	4.0	4.0
	BCF212	3.8	3.4	3.9	3.9
	BCF312	3.5	3.9	3.6	3.6
Beam End Average		6.6	6.3	6.8	6.8
Frame Average		6.5		6.8	

Table 7.19: Beam curvature ductility comparison for the Flexible Inner Frame

Story	Beam	Existing Design		Revised Design	
		I End	J End	I End	J End
1	BFI201	6.0	5.7	5.6	5.6
	BFI301	6.2	5.5	5.8	5.8
2	BFI202	8.2	7.8	8.2	8.2
	BFI302	7.2	8.8	7.3	7.3
3	BFI203	9.3	8.8	9.5	9.5
	BFI303	8.3	9.9	8.6	8.6
4	BFI204	10.3	8.5	10.7	10.7
	BFI304	10.2	9.3	10.6	10.6
5	BFI205	10	9.4	10.4	10.4
	BFI305	10.2	9.2	10.5	10.5
6	BFI206	9.6	9.1	9.9	9.9
	BFI306	9.8	8.9	10.1	10.1
7	BFI207	8.7	8.4	9.1	9.1
	BFI307	8.9	8.2	9.2	9.2
8	BFI208	9.1	7.3	9.4	9.4
	BFI308	7.9	8.4	8.2	8.2
9	BFI209	7.9	6.1	8.2	8.2
	BFI309	7.9	7.1	8.2	8.2
10	BFI210	6.5	6.1	6.6	6.6
	BFI310	6.7	5.9	6.8	6.8
11	BFI211	5.1	4.8	5.2	5.2
	BFI311	4.7	4.8	4.8	4.8
12	BFI212	4.7	3.7	5.0	5.0
	BFI312	4.0	4.5	4.1	4.1
Beam End Average		7.8	7.3	8.0	8.0
Frame Average		7.6		8.0	

Table 7.20: Beam curvature ductility comparison for the Flexible Edge Frame

Story	Beam	Existing Design		Revised Design	
		I End	J End	I End	J End
1	BFE201	5.8	6.7	5.3	5.3
	BFE301	5.6	7.1	5.0	5.0
2	BFE202	8.7	10.5	8.6	8.6
	BFE302	9.4	9.6	9.3	9.3
3	BFE203	10.4	12.4	10.6	10.6
	BFE303	11.2	11.5	11.4	11.4
4	BFE204	10.8	12.8	11.1	11.1
	BFE304	11.6	11.9	12.0	12.0
5	BFE205	11.1	11.9	11.5	11.5
	BFE305	11.1	11.4	11.5	11.5
6	BFE206	10.2	12.4	10.6	10.6
	BFE306	11.2	11.4	11.6	11.6
7	BFE207	10.0	11.0	10.5	10.5
	BFE307	10.1	10.5	10.5	10.5
8	BFE208	8.8	9.9	9.2	9.2
	BFE308	9.7	8.8	10.1	10.1
9	BFE209	7.3	8.3	7.8	7.8
	BFE309	8.1	7.3	8.6	8.6
10	BFE210	6.6	8.0	7.0	7.0
	BFE310	7.5	7.0	8.0	8.0
11	BFE211	4.8	6.5	5.2	5.2
	BFE311	5.9	5.4	6.3	6.3
12	BFE212	4.9	4.5	5.1	5.1
	BFE312	3.8	5.4	4.0	4.0
Beam End Average		8.5	9.3	8.8	8.8
Frame Average		8.9		8.8	

In general, there is little variation in beam end curvature ductilities computed for both designs as seen in Tables 7.16 – 7.20. A very minor ductility demand increase is spotted in frame averages. However, a noticeable decrease in curvature ductilities of the first and second story beams located at the *FE* frame is observed in Table 7.20. First story *FE* columns are the most strengthened members in the structure and this reduction in the beam inelastic response could be associated with this design revision.

Moreover, overall frame average ductility is slightly lower in the *FE* frame of the revised system when compared with that of existing structure.

Shear wall ductilities computed for the existing and revised designs are given in Table 7.21. As can be seen in Table 7.21, the capacity increase at the first four stories of the shear wall results in nearly 50% drop in first story curvature ductility demand. Second, third and fourth stories remain elastic in the revised structure. At the rest of the wall, amount of inelastic deformations is at similar levels for both systems. These observations further support the findings while comparing the shear wall curvature demands given in Figure 7.20.

Table 7.21: Shear wall ductility comparison for both designs.

Story	Existing Design	Revised Design
1	4.9	2.7
2	1.7	1.0
3	1.5	0.9
4	1.5	0.8
5	1.5	1.6
6	1.6	1.7
7	1.5	1.5
8	1.2	1.2
9	0.9	0.9
10	0.8	0.8
11	1.0	1.0
12	0.6	0.6

Finally, column end curvature ductilities computed for the *SE*, *SI*, *FI*, *CF* and *FE* frames are compared in Tables 7.22 - 7.26, respectively. As can be seen in Table 7.22, there is virtually no difference in computed mean column end ductilities throughout the *SE* frame. The inelastic deformations which are limited to first story column bottom-ends in *SI*, *FI*, *CF* and *FE* frames in the case of existing design are reduced significantly for revised design. This situation can be observed in Figures 7.22 – 7.25. While *FI* and *FE* frames exhibit elastic column behavior in the case of revised design, only ductilities that are over 1.0 are measured in inner columns of *SI* and *CF* frames.

Table 7.22: Column curvature ductility comparison for the Stiff Edge Frame

Story	Column	Existing Design		Revised Design	
		Bottom End	Top End	Bottom End	Top End
1	SE101	0.9	0.2	0.8	0.2
	SE401	0.9	0.2	0.8	0.2
2	SE102	0.3	0.1	0.3	0.2
	SE402	0.3	0.1	0.3	0.1
3	SE103	0.1	0.2	0.1	0.2
	SE403	0.1	0.2	0.1	0.2
4	SE104	0.1	0.2	0.1	0.2
	SE404	0.1	0.2	0.1	0.2
5	SE105	0.1	0.2	0.1	0.2
	SE405	0.1	0.2	0.1	0.2
6	SE106	0.1	0.2	0.1	0.2
	SE406	0.1	0.2	0.1	0.2
7	SE107	0.1	0.2	0.1	0.2
	SE407	0.1	0.2	0.1	0.2
8	SE108	0.1	0.2	0.1	0.2
	SE408	0.1	0.1	0.1	0.1
9	SE109	0.1	0.1	0.1	0.1
	SE409	0.1	0.1	0.1	0.2
10	SE110	0.1	0.1	0.1	0.1
	SE410	0.1	0.1	0.1	0.1
11	SE111	0.1	0.1	0.1	0.1
	SE411	0.1	0.1	0.1	0.1
12	SE112	0.1	0.2	0.1	0.2
	SE412	0.1	0.2	0.1	0.2
Column End Average		0.2	0.2	0.2	0.2
Frame Average		0.2		0.2	

Table 7.23: Column curvature ductility comparison for the Stiff Inner Frame

Story	Column	Existing Design		Revised Design	
		Bottom End	Top End	Bottom End	Top End
1	SI101	1.3	0.2	0.8	0.2
	SI201	1.6	0.3	1.2	0.3
	SI301	1.5	0.3	1.2	0.3
	SI401	1.3	0.2	0.8	0.2
2	SI102	0.3	0.2	0.3	0.2
	SI202	0.4	0.2	0.4	0.3
	SI302	0.4	0.2	0.4	0.3
	SI402	0.4	0.2	0.4	0.2
3	SI103	0.2	0.3	0.2	0.3
	SI203	0.3	0.3	0.3	0.3
	SI303	0.2	0.3	0.3	0.3
	SI403	0.2	0.2	0.3	0.3
4	SI104	0.2	0.2	0.2	0.3
	SI204	0.2	0.3	0.2	0.3
	SI304	0.2	0.2	0.2	0.3
	SI404	0.2	0.2	0.2	0.3
5	SI105	0.2	0.2	0.2	0.2
	SI205	0.2	0.2	0.2	0.2
	SI305	0.2	0.2	0.2	0.2
	SI405	0.2	0.2	0.2	0.2
6	SI106	0.2	0.2	0.2	0.2
	SI206	0.2	0.2	0.2	0.2
	SI306	0.2	0.2	0.2	0.2
	SI406	0.2	0.2	0.2	0.2
7	SI107	0.1	0.2	0.2	0.2
	SI207	0.2	0.2	0.2	0.2
	SI307	0.1	0.2	0.2	0.2
	SI407	0.2	0.2	0.2	0.2
8	SI108	0.1	0.1	0.1	0.2
	SI208	0.1	0.2	0.1	0.2
	SI308	0.1	0.1	0.1	0.1
	SI408	0.1	0.2	0.1	0.2
9	SI109	0.1	0.2	0.1	0.2
	SI209	0.1	0.2	0.1	0.2
	SI309	0.1	0.1	0.1	0.1
	SI409	0.1	0.2	0.1	0.2
10	SI110	0.1	0.2	0.1	0.2
	SI210	0.1	0.2	0.1	0.2
	SI310	0.1	0.2	0.1	0.2
	SI410	0.1	0.2	0.1	0.2
11	SI111	0.1	0.1	0.1	0.1
	SI211	0.1	0.1	0.1	0.2
	SI311	0.1	0.1	0.1	0.1
	SI411	0.1	0.1	0.1	0.1
12	SI112	0.1	0.2	0.1	0.2
	SI212	0.1	0.1	0.1	0.1
	SI312	0.1	0.1	0.1	0.1
	SI412	0.1	0.2	0.1	0.2
Column End Average		0.3	0.2	0.2	0.2
Frame Average		0.2		0.2	

Table 7.24: Column curvature ductility comparison for the Center Frame

Story	Column	Existing Design		Revised Design	
		Bottom End	Top End	Bottom End	Top End
1	CF101	1.8	0.3	0.5	0.2
	CF201	1.9	0.3	1.0	0.4
	CF301	2.3	0.4	0.8	0.3
	CF401	1.9	0.3	0.6	0.2
2	CF102	0.4	0.3	0.4	0.3
	CF202	0.6	0.5	0.6	0.5
	CF302	0.5	0.4	0.6	0.4
	CF402	0.4	0.3	0.5	0.3
3	CF103	0.3	0.3	0.3	0.3
	CF203	0.4	0.5	0.4	0.5
	CF303	0.3	0.4	0.4	0.4
	CF403	0.3	0.3	0.3	0.4
4	CF104	0.2	0.3	0.2	0.3
	CF204	0.4	0.4	0.4	0.5
	CF304	0.3	0.3	0.3	0.4
	CF404	0.3	0.3	0.3	0.3
5	CF105	0.2	0.2	0.2	0.3
	CF205	0.3	0.4	0.3	0.4
	CF305	0.3	0.3	0.3	0.3
	CF405	0.2	0.3	0.2	0.3
6	CF106	0.2	0.2	0.2	0.2
	CF206	0.3	0.4	0.3	0.4
	CF306	0.2	0.3	0.3	0.3
	CF406	0.2	0.3	0.2	0.3
7	CF107	0.2	0.2	0.2	0.2
	CF207	0.3	0.3	0.3	0.3
	CF307	0.2	0.3	0.2	0.3
	CF407	0.2	0.2	0.2	0.3
8	CF108	0.2	0.2	0.2	0.2
	CF208	0.2	0.3	0.2	0.3
	CF308	0.2	0.2	0.2	0.2
	CF408	0.2	0.2	0.2	0.2
9	CF109	0.1	0.2	0.1	0.2
	CF209	0.2	0.3	0.2	0.3
	CF309	0.2	0.2	0.2	0.2
	CF409	0.2	0.2	0.2	0.2
10	CF110	0.1	0.2	0.1	0.2
	CF210	0.2	0.2	0.2	0.2
	CF310	0.1	0.2	0.1	0.2
	CF410	0.1	0.2	0.1	0.2
11	CF111	0.1	0.2	0.1	0.2
	CF211	0.2	0.2	0.2	0.2
	CF311	0.1	0.2	0.1	0.2
	CF411	0.1	0.1	0.1	0.2
12	CF112	0.1	0.1	0.1	0.1
	CF212	0.1	0.2	0.1	0.3
	CF312	0.1	0.1	0.1	0.1
	CF412	0.1	0.1	0.1	0.2
Column End Average		0.4	0.3	0.3	0.3
Frame Average		0.3		0.3	

Table 7.25: Column curvature ductility comparison for the Flexible Inner Frame

Story	Column	Existing Design		Revised Design	
		Bottom End	Top End	Bottom End	Top End
1	FI201	2.5	0.4	0.6	0.3
	FI301	3.2	0.5	1.0	0.4
	FI401	2.6	0.3	0.7	0.3
2	FI202	0.5	0.4	0.4	0.3
	FI302	0.7	0.5	0.8	0.6
	FI402	0.6	0.4	0.4	0.3
3	FI203	0.4	0.4	0.3	0.3
	FI303	0.5	0.5	0.5	0.6
	FI403	0.4	0.5	0.3	0.3
4	FI204	0.3	0.4	0.2	0.3
	FI304	0.4	0.4	0.5	0.6
	FI404	0.3	0.4	0.3	0.3
5	FI205	0.3	0.4	0.3	0.4
	FI305	0.4	0.4	0.4	0.4
	FI405	0.3	0.4	0.3	0.4
6	FI206	0.3	0.3	0.3	0.4
	FI306	0.3	0.4	0.3	0.4
	FI406	0.3	0.4	0.3	0.4
7	FI207	0.3	0.3	0.3	0.3
	FI307	0.3	0.4	0.3	0.4
	FI407	0.3	0.3	0.3	0.3
8	FI208	0.2	0.3	0.2	0.3
	FI308	0.3	0.3	0.3	0.3
	FI408	0.2	0.3	0.3	0.3
9	FI209	0.2	0.3	0.2	0.3
	FI309	0.3	0.3	0.3	0.3
	FI409	0.2	0.3	0.2	0.3
10	FI210	0.2	0.2	0.2	0.2
	FI310	0.2	0.3	0.2	0.3
	FI410	0.2	0.3	0.2	0.3
11	FI211	0.1	0.2	0.1	0.2
	FI311	0.2	0.2	0.2	0.3
	FI411	0.1	0.2	0.1	0.2
12	FI212	0.1	0.1	0.1	0.1
	FI312	0.1	0.1	0.1	0.1
	FI412	0.1	0.2	0.1	0.2
Column End Average		0.5	0.3	0.3	0.3
Frame Average		0.4		0.3	

Table 7.26: Column curvature ductility comparison for the Flexible Edge Frame

Story	Column	Existing Design		Revised Design	
		Bottom End	Top End	Bottom End	Top End
1	FE201	3.3	0.4	0.7	0.3
	FE301	3.7	0.5	0.7	0.4
	FE401	3.4	0.4	0.7	0.3
2	FE202	0.7	0.5	0.6	0.5
	FE302	0.9	0.7	0.9	0.7
	FE402	0.7	0.6	0.6	0.5
3	FE203	0.5	0.6	0.5	0.5
	FE303	0.6	0.8	0.7	0.7
	FE403	0.5	0.6	0.5	0.5
4	FE204	0.4	0.5	0.4	0.5
	FE304	0.5	0.7	0.5	0.6
	FE404	0.4	0.5	0.4	0.4
5	FE205	0.3	0.5	0.4	0.6
	FE305	0.5	0.7	0.5	0.6
	FE405	0.3	0.5	0.4	0.6
6	FE206	0.3	0.4	0.3	0.5
	FE306	0.4	0.6	0.4	0.6
	FE406	0.3	0.4	0.3	0.5
7	FE207	0.3	0.4	0.3	0.5
	FE307	0.4	0.6	0.4	0.6
	FE407	0.3	0.4	0.3	0.5
8	FE208	0.3	0.3	0.3	0.4
	FE308	0.4	0.5	0.4	0.5
	FE408	0.3	0.4	0.3	0.5
9	FE209	0.3	0.3	0.3	0.4
	FE309	0.3	0.5	0.3	0.5
	FE409	0.3	0.4	0.3	0.4
10	FE210	0.2	0.3	0.2	0.3
	FE310	0.3	0.4	0.3	0.4
	FE410	0.3	0.3	0.3	0.3
11	FE211	0.2	0.2	0.2	0.2
	FE311	0.2	0.3	0.2	0.3
	FE411	0.2	0.2	0.2	0.3
12	FE212	0.1	0.2	0.1	0.2
	FE312	0.1	0.4	0.1	0.4
	FE412	0.1	0.2	0.1	0.2
Column End Average		0.6	0.4	0.4	0.4
Frame Average		0.5		0.4	

7.11.3 Discussion of Results

One major difference between seismic responses of existing and revised systems is that the revised structure behaves elastic except for the bottom end of the shear wall. This observation may further indicate that a design revision was not necessary for this particular twelve-story structure, as discussed in Section 7.9.2.

Since the seismic behavior of the structure changes completely, a proper comparison of seismic response between the existing and revised designs could not be made from the dynamic analysis results. These results have been obtained under the ground motion set that has been previously scaled according to linear elastic design spectrum which represents the Design Basis Earthquake Level. In the next section, seismic response of the existing and revised systems are investigated under Maximum Considered Earthquake (MCE) level of dynamic excitation.

7.12 Performance Comparison between Existing and Revised Designs under Scaled Ground Motion Set

Due to reasons explained in the previous section, both versions of the structure are analyzed using scaled ground motions that represents Maximum Considered Earthquake (MCE) level described in the Turkish Earthquake Code [73]. This has been achieved by introducing a scale factor of 1.5 to each strong ground motion record that has been utilized. Ground motion scale factors previously given in Table 7.5 for each record have been further multiplied with 1.5 and inelastic dynamic analyses performed again.

Convergence has been achieved for seven of the ten dynamic analyses performed under the scaled ground motion set. Dynamic analyses under scaled CPE045, H-E07230 and H-E08230 records have led to excessive frame deformations, indicating collapse. Therefore, analysis results obtained under these records have been left out of the response set.

7.12.1 Comparison of Frame Responses

Mean response parameters obtained under the MCE scaled ground motion set are compared and performance of the proposed method is further evaluated in this section. In a similar format to previous section, scaled ground motion set mean of frame interstory drifts for the direction of analysis, beam end curvatures and column bottom-end curvatures are presented in Figures 7.21 – 7.23. In addition, maximum curvatures computed at each story of the shear wall are shown in Figure 7.24. Moreover, mean interstory drift ratios of the frames in the orthogonal direction are given in 7.25. Mean response of the existing structure is denoted with black lines in Figures 7.21 – 7.25. Red lines indicate the mean response of the revised structure. Shear wall yield curvatures computed at all stories for both designs are also in given their respective colors in Figure 7.24.

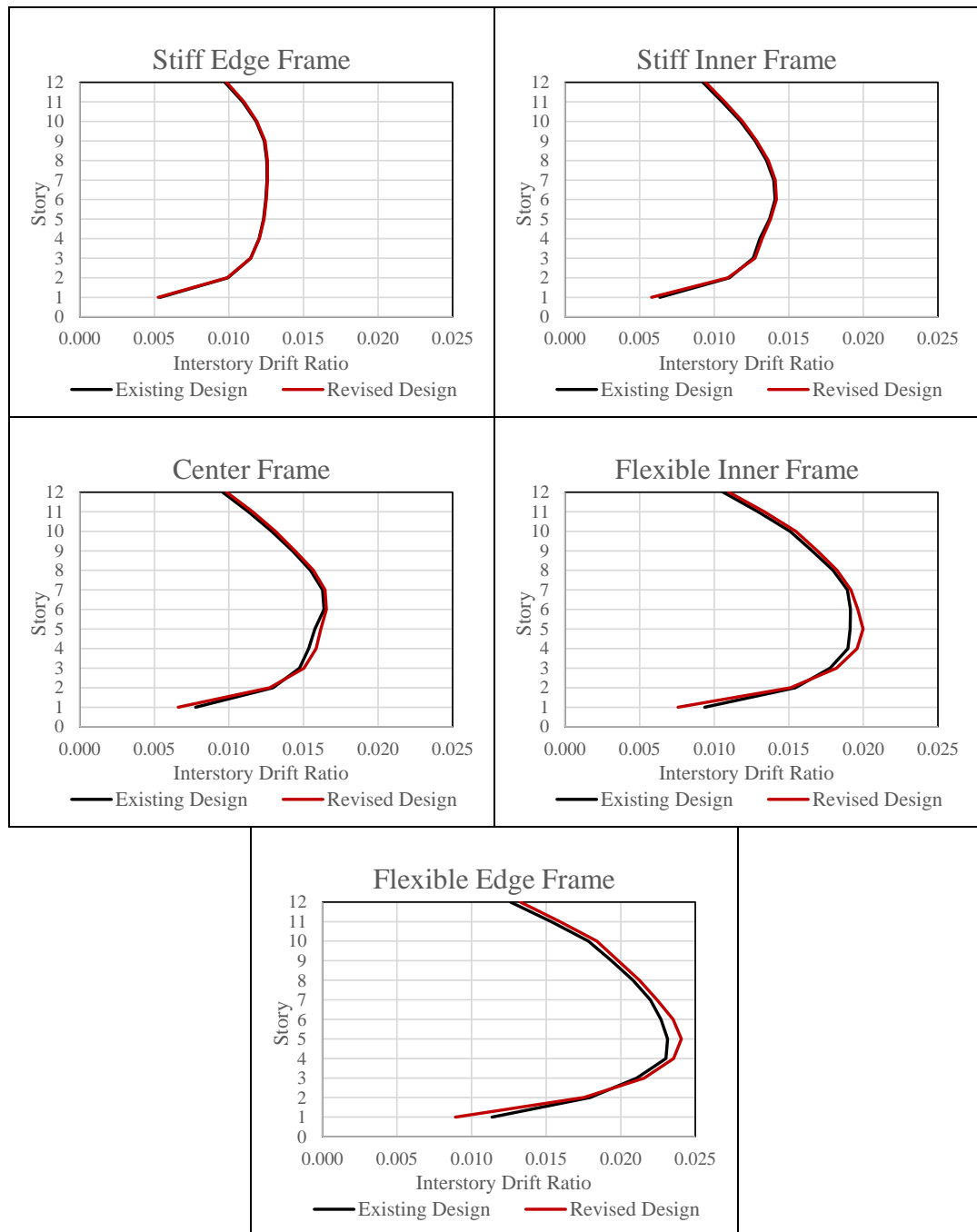


Figure 7.21: Comparison of the mean interstory drift ratios in direction of analysis calculated for the existing and revised designs under the MCE scaled ground motion set.

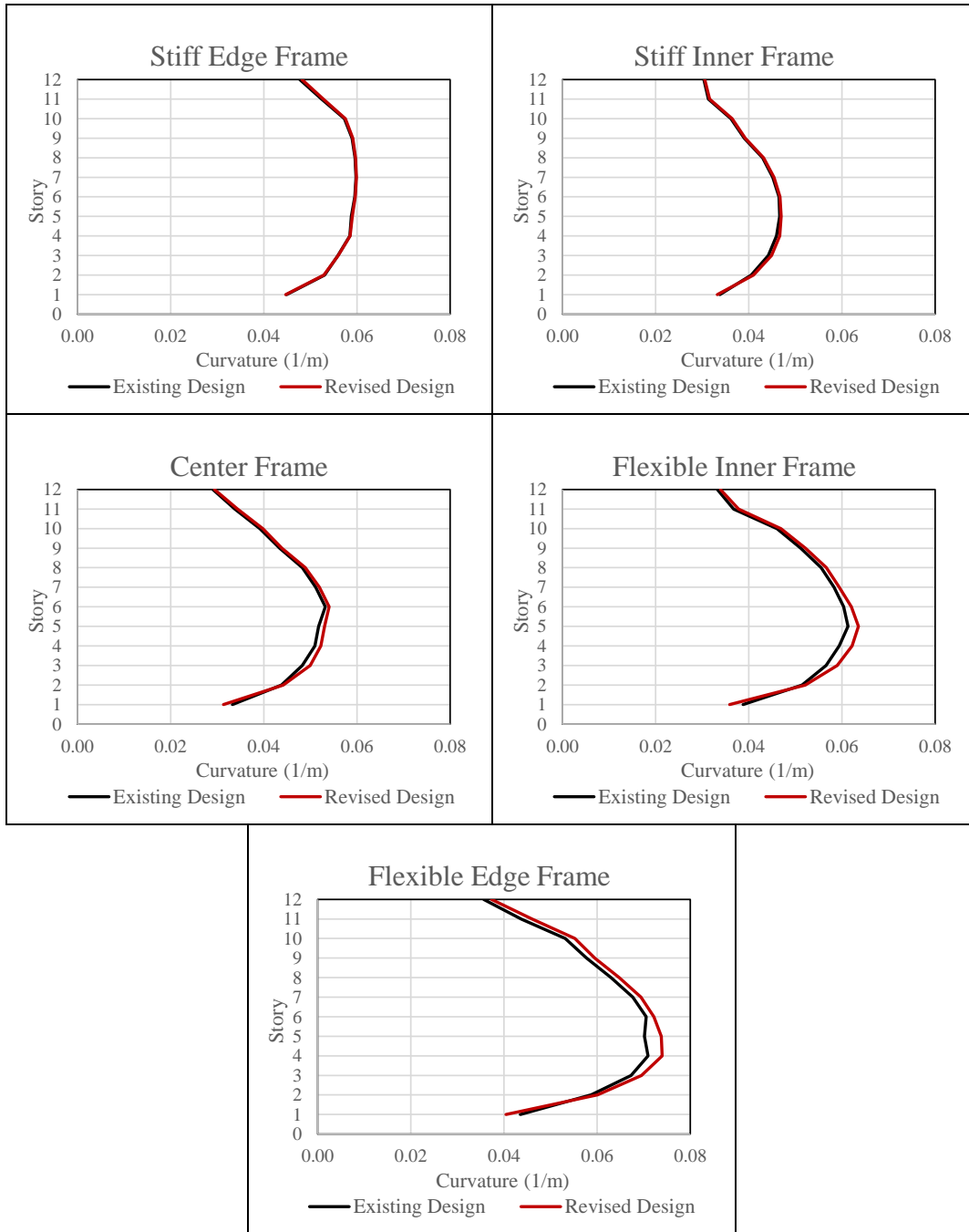


Figure 7.22: Comparison of the mean beam-end curvatures calculated for the existing and revised designs under the MCE scaled ground motion set.

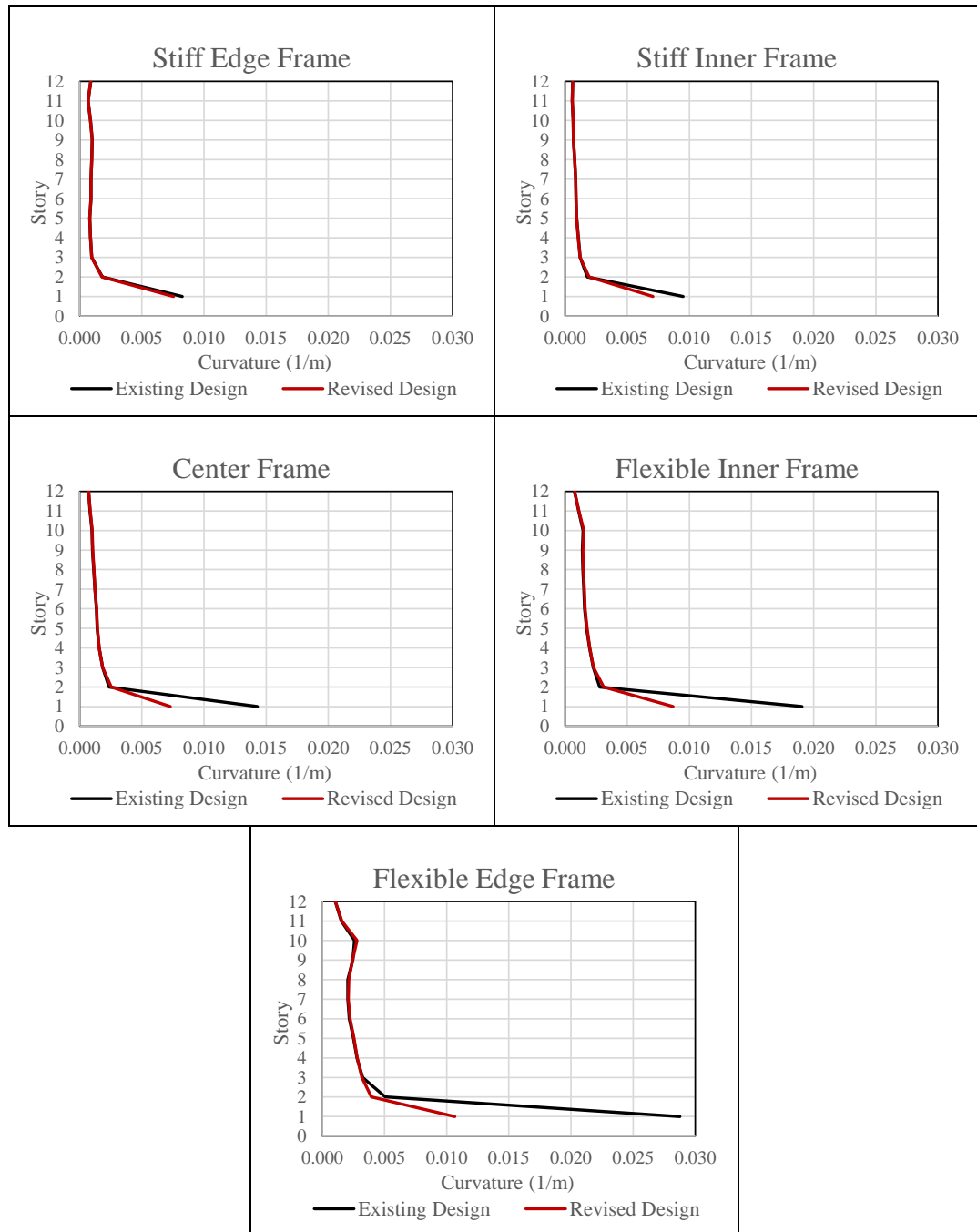


Figure 7.23: Comparison of the mean column bottom end curvatures calculated for the existing and revised designs under the MCE scaled ground motion set.

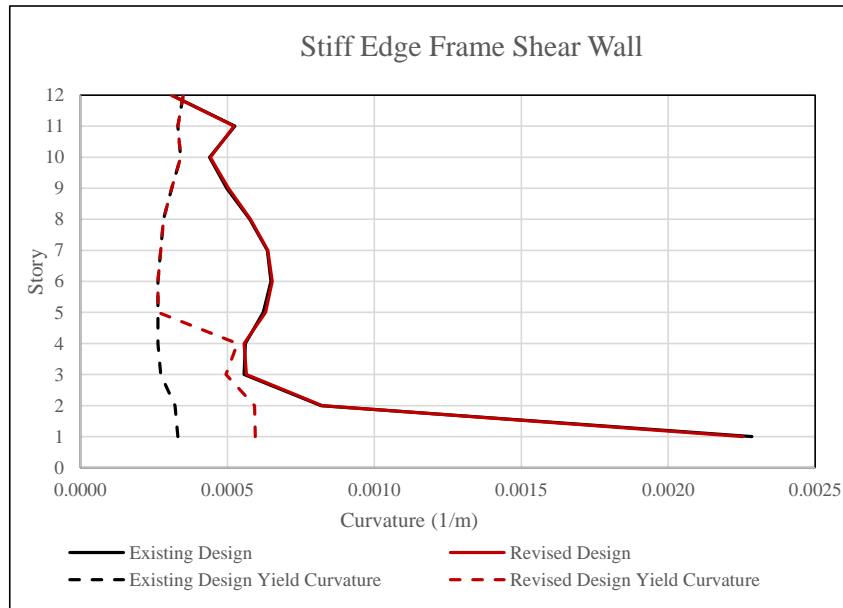


Figure 7.24: Comparison of the shear wall curvatures calculated for the existing and revised designs under the MCE scaled ground motion set.

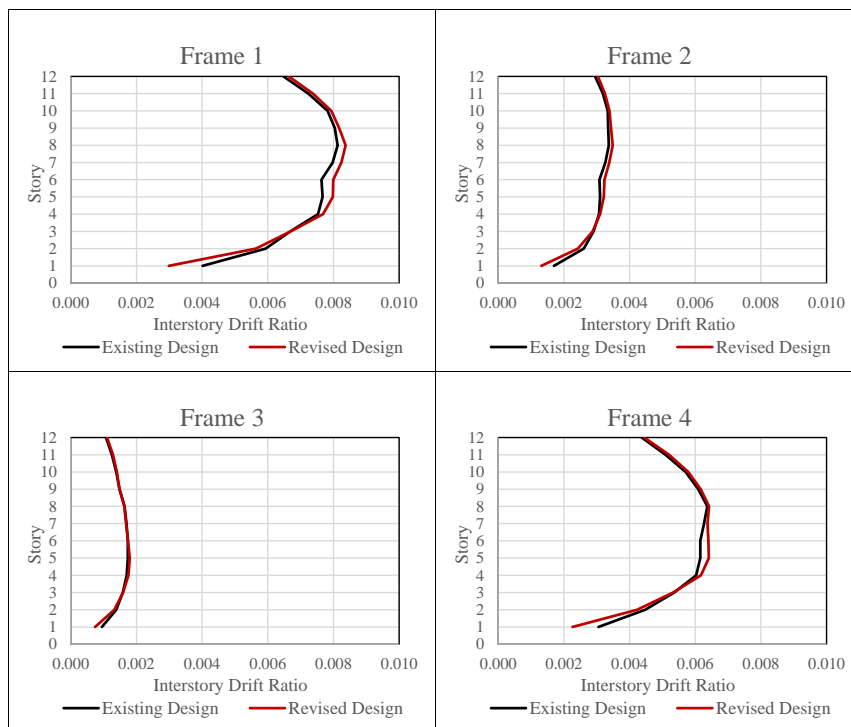


Figure 7.25: Comparison of the mean interstory drift ratios calculated in the orthogonal direction frames for the existing and revised designs under the MCE scaled ground motion set.

Upon inspecting Figures 7.21 and 7.25, it could be seen that interstory drift ratio distribution of all frames is quite similar for both designs. In the direction of analysis, a maximum drift ratio demand of about 2.5% is recorded at the flexible edge frame. It should also be noted that the effect of the shear wall can be seen at the interstory drift distribution of stiff edge frame. Interstory drifts recorded at first two stories of the flexible side frames are slightly lower in the case of revised structure. A minor increase in drift demands in the middle stories is also evident for these frames.

Ground motion set mean beam end curvature demands recorded for both systems exhibit very minor variation as shown in Figure 7.22. A small increase in curvature demands is notable at the middle stories of flexible side frames. Accompanying to this, a very slight demand decrease at the first story of these frames is also observed.

The major behavior difference is observed in column bottom end curvature demands given in Figure 7.23. In the case of existing system, first story column bottom end curvature demands reach up to 0.03/m at flexible edge frame. A significant unbalanced demand distribution is noted. On the other hand, first story curvatures of the revised systems are quite similar. All frames exhibit curvature demands about 0.01/m. In addition, there is decrease in demands at first story column bottom ends. This is very noticeable in flexible side frames; while a slight reduction in demands is also noted for stiff side frames. Apart from first story, curvature demands at the rest of the columns remain unchanged. Upon inspecting the results, it could be concluded that the revised system exhibits balanced damage distribution in first story columns under the MCE level seismic extrication.

Mean shear wall curvature demands computed at all stories for both designs are virtually the same, as given in Figure 7.24. However, ductility levels measured in the case of revised system is lower. The yield curvatures of the revised sections are higher due to reasons discussed in previous sections. Changes in measured ductilities are further discussed in the next Subsection.

7.12.2 Comparison of Member Ductility Demands

Scaled ground motion set mean beam end ductilities of both systems are compared in Tables 7.27 – 7.31 for *SE*, *SI*, *CF*, *FI* and *FE* frames, respectively.

Table 7.27: Beam curvature ductility comparison for the Stiff Edge Frame

Story	Beam	Existing Design		Revised Design	
		I End	J End	I End	J End
1	BSE101	8.3	10.0	8.2	10.0
	BSE301	9.0	8.7	8.9	8.7
2	BSE102	10.8	10.3	10.8	10.3
	BSE302	10.1	10.8	10.0	10.7
3	BSE103	12.0	9.9	12.0	9.9
	BSE303	9.9	12.1	9.9	12.1
4	BSE104	12.5	10.4	12.5	10.4
	BSE304	10.3	12.6	10.3	12.6
5	BSE105	11.8	10.9	11.9	10.9
	BSE305	10.8	11.9	10.9	11.9
6	BSE106	12.0	11.0	12.0	11.0
	BSE306	11.0	12.0	11.0	12.1
7	BSE107	12.0	11.1	12.0	11.1
	BSE307	11.0	12.0	11.1	12.1
8	BSE108	12.0	11.1	12.0	11.1
	BSE308	11.0	12.0	11.0	12.0
9	BSE109	12.0	11.3	12.0	11.3
	BSE309	10.7	11.6	10.7	11.7
10	BSE110	12.4	11.2	12.5	11.2
	BSE310	9.6	11.7	9.6	11.7
11	BSE111	11.6	10.5	11.7	10.5
	BSE311	8.4	10.5	8.5	10.6
12	BSE112	10.4	10.0	10.5	10.0
	BSE312	7.6	9.3	7.8	9.5
Beam End Average		10.7	10.9	10.7	11.0
Frame Average		10.8		10.9	

Table 7.28: Beam curvature ductility comparison for the Stiff Inner Frame

Story	Beam	Existing Design		Revised Design	
		I End	J End	I End	J End
1	BSI101	8.0	5.8	7.9	5.8
	BSI201	5.9	5.9	5.7	5.9
	BSI301	6.6	7.2	6.4	7.2
2	BSI102	8.2	7.6	8.3	7.7
	BSI202	7.9	7.7	7.9	7.8
	BSI302	8.4	7.3	8.5	7.5
3	BSI103	8.8	8.4	8.9	8.6
	BSI203	8.4	8.5	8.5	8.7
	BSI303	9.0	8.2	9.1	8.4
4	BSI104	9.0	9.0	9.1	9.1
	BSI204	8.6	9.1	8.7	9.2
	BSI304	9.1	8.8	9.3	8.9
5	BSI105	9.0	9.2	9.1	9.2
	BSI205	8.6	9.3	8.7	9.4
	BSI305	9.2	9.0	9.2	9.0
6	BSI106	8.9	9.2	9.0	9.2
	BSI206	8.5	9.3	8.6	9.4
	BSI306	9.1	9.0	9.2	9.0
7	BSI107	8.6	9.0	8.7	9.0
	BSI207	8.2	9.1	8.3	9.1
	BSI307	8.8	8.8	8.8	8.8
8	BSI108	8.2	8.6	8.2	8.6
	BSI208	7.8	8.7	7.9	8.7
	BSI308	8.3	8.4	8.4	8.4
9	BSI109	6.5	8.0	6.6	8.0
	BSI209	7.2	8.0	7.2	8.0
	BSI309	7.8	7.8	7.8	7.8
10	BSI110	6.9	7.3	7.0	7.3
	BSI210	6.5	7.3	6.6	7.3
	BSI310	7.0	7.1	7.1	7.1
11	BSI111	5.5	6.6	5.6	6.6
	BSI211	5.6	6.5	5.7	6.5
	BSI311	6.1	6.2	6.2	6.3
12	BSI112	6.3	5.7	6.3	5.8
	BSI212	5.8	5.8	5.9	5.8
	BSI312	5.1	6.9	5.2	6.9
Beam End Average		7.7	7.9	7.8	7.9
Frame Average		7.8		7.9	

Table 7.29: Beam curvature ductility comparison for the Center Frame

Story	Beam	Existing Design		Revised Design	
		I End	J End	I End	J End
1	BCF101	6.4	6.2	6.1	5.7
	BCF201	7.0	5.8	6.5	5.5
	BCF301	6.5	6.6	6.2	6.4
2	BCF102	8.7	8.3	8.7	8.3
	BCF202	9.1	8.1	9.2	8.2
	BCF302	8.9	7.6	9.0	7.6
3	BCF103	9.3	9.0	9.6	9.4
	BCF203	9.7	8.9	10.1	9.3
	BCF303	9.3	9.6	9.6	10.0
4	BCF104	9.3	10.7	9.5	11.0
	BCF204	9.9	9.5	10.2	9.7
	BCF304	9.5	10.3	9.8	10.6
5	BCF105	9.5	11.1	9.8	11.3
	BCF205	10.6	9.6	10.9	9.8
	BCF305	9.8	9.3	10.1	9.5
6	BCF106	9.7	11.1	9.8	11.3
	BCF206	10.6	9.6	10.8	9.7
	BCF306	10.6	10.5	10.8	10.6
7	BCF107	9.2	10.7	9.4	10.9
	BCF207	10.2	9.3	10.3	9.4
	BCF307	10.1	10.1	10.2	10.3
8	BCF108	8.4	10.1	8.6	10.2
	BCF208	10.5	8.6	10.6	8.7
	BCF308	9.4	9.5	9.4	9.6
9	BCF109	7.4	9.1	7.6	9.3
	BCF209	9.5	7.7	9.6	7.7
	BCF309	8.4	8.6	8.5	8.7
10	BCF110	6.4	8.1	6.5	8.3
	BCF210	8.2	8.2	8.4	8.3
	BCF310	7.3	7.7	7.4	7.8
11	BCF111	5.1	6.9	5.2	7.2
	BCF211	7.0	7.2	7.2	7.2
	BCF311	5.4	8.4	5.5	8.5
12	BCF112	5.2	5.9	5.2	6.0
	BCF212	5.2	6.2	5.3	6.2
	BCF312	4.8	7.0	4.9	7.1
Beam End Average		8.4	8.6	8.5	8.8
Frame Average		8.5		8.6	

Table 7.30: Beam curvature ductility comparison for the Flexible Inner Frame

Story	Beam	Existing Design		Revised Design	
		I End	J End	I End	J End
1	BFI201	7.8	6.9	7.3	6.4
	BFI301	7.9	6.8	7.4	6.2
2	BFI202	10.1	9.1	10.2	9.3
	BFI302	9.1	10.1	9.2	10.3
3	BFI203	10.8	10.3	11.3	10.7
	BFI303	9.9	11.4	10.2	11.8
4	BFI204	11.9	10.3	12.4	10.8
	BFI304	11.7	11.1	12.2	11.7
5	BFI205	11.7	11.6	12.2	12.0
	BFI305	11.9	11.4	12.3	11.8
6	BFI206	11.6	11.4	11.9	11.7
	BFI306	11.7	11.1	12.0	11.5
7	BFI207	11.1	11.1	11.3	11.3
	BFI307	11.2	10.8	11.4	11.0
8	BFI208	11.0	10.2	11.2	10.4
	BFI308	9.9	11.4	10.1	11.6
9	BFI209	9.8	9.3	10.0	9.5
	BFI309	9.8	10.4	10.0	10.6
10	BFI210	8.2	9.6	8.5	9.6
	BFI310	8.4	9.3	8.6	9.4
11	BFI211	6.4	8.0	6.7	8.1
	BFI311	6.2	7.9	6.4	8.1
12	BFI212	6.1	6.8	6.3	6.8
	BFI312	5.1	7.9	5.2	8.1
Beam End Average		9.6	9.8	9.8	10.0
Frame Average		9.7		9.9	

Table 7.31: Beam curvature ductility comparison for the Flexible Edge Frame

Story	Beam	Existing Design		Revised Design	
		I End	J End	I End	J End
1	BFE201	7.9	8.7	7.3	8.0
	BFE301	7.6	8.9	7.0	8.4
2	BFE202	10.1	12.1	10.4	12.3
	BFE302	10.9	11.2	11.1	11.5
3	BFE203	11.8	13.7	12.2	14.1
	BFE303	12.5	12.7	13.0	13.1
4	BFE204	12.4	14.4	13.0	15.0
	BFE304	13.2	13.5	13.8	14.0
5	BFE205	12.9	13.9	13.5	14.7
	BFE305	13.0	13.3	13.7	13.9
6	BFE206	12.1	15.0	12.4	15.2
	BFE306	13.1	13.9	13.4	14.3
7	BFE207	12.6	13.7	12.9	14.1
	BFE307	12.5	13.2	12.8	13.6
8	BFE208	11.6	12.8	11.9	13.2
	BFE308	12.6	11.7	12.9	12.0
9	BFE209	10.5	11.8	10.9	12.2
	BFE309	11.4	10.8	11.8	11.1
10	BFE210	9.2	11.8	9.6	12.2
	BFE310	10.3	10.7	10.7	11.1
11	BFE211	7.4	9.9	7.8	10.4
	BFE311	8.5	8.7	9.0	9.2
12	BFE212	5.9	8.1	6.4	8.3
	BFE312	5.2	9.3	5.6	9.6
Beam End Average		10.6	11.8	11.0	12.1
Frame Average		11.2		11.6	

As can be seen in Tables 7.27 – 7.31, ductility levels in all beams are quite high when compared with the value of response reduction factor ($R = 7$). This is an expected outcome due to both structures being analyzed under scaled ground motion set. As can be seen in Table 7.26 beams connecting to the shear wall exhibit high ductility demands. In addition, flexible side frames also register ductility values up to 15.0.

Beam end ductility demands show very little variation between two designs. Most

notable change is observed at the first stories of the flexible side frames, where ductility reductions up to 10% are attained. However, a minor ductility demand increase is observed at the upper stories of these frames, as well.

Scaled ground motion set mean shear wall ductilities computed for existing and revised designs are given in Table 7.32. Overall, ductility demands recorded at the first four stories of the shear wall where the member has been strengthened are reduced by half. The increase in the idealized yield curvature of these sections result in a significant reduction in inelastic response of the shear wall. However, it should be added that the shear wall undergoes inelastic action throughout its height for both systems.

Table 7.32: Shear wall ductility comparison for both designs under the MCE scaled ground motion set.

Story	Existing Design	Revised Design
1	6.9	3.8
2	2.5	1.4
3	2.0	1.1
4	2.1	1.0
5	2.4	2.4
6	2.5	2.5
7	2.3	2.3
8	2.0	2.0
9	1.6	1.6
10	1.3	1.3
11	1.6	1.6
12	0.9	0.9

Existing and revised structure mean column end curvature ductilities obtained through scaled ground motions for the *SE*, *SI*, *FI*, *CF* and *FE* frames are compared in Tables 7.33 - 7.37, respectively. As can be seen from the Tables, the only inelastic action observed in columns is at the first story of all frames of both existing and revised structures. Rest of the columns remain elastic, except for second story columns of the flexible edge frame. However, it should be noted reduction in ductility is observed at the revised system in all columns which behave inelastic. This is most pronounced in flexible side frames. Observations made here is in conjunction with

what has been discussed for column curvature demand distributions given previously in Figure 7.24. The revised system, which has been obtained through application the Optimal Strength Distribution Method, exhibits a more balanced demand a ductility distribution at its frame bases under MCE level scaled ground motion set. Moreover, it registers lower ductilities at the shear wall, compared with the existing design.

Table 7.33: Column curvature ductility comparison for the Stiff Edge Frame

Story	Column	Existing Design		Revised Design	
		Bottom End	Top End	Bottom End	Top End
1	SE101	1.6	0.3	1.4	0.3
	SE401	1.5	0.3	1.4	0.3
2	SE102	0.3	0.2	0.3	0.2
	SE402	0.3	0.2	0.3	0.2
3	SE103	0.2	0.2	0.2	0.2
	SE403	0.2	0.2	0.2	0.2
4	SE104	0.1	0.2	0.1	0.2
	SE404	0.1	0.2	0.1	0.2
5	SE105	0.1	0.2	0.1	0.2
	SE405	0.1	0.2	0.1	0.2
6	SE106	0.1	0.2	0.1	0.2
	SE406	0.1	0.2	0.1	0.2
7	SE107	0.1	0.2	0.1	0.2
	SE407	0.1	0.2	0.1	0.2
8	SE108	0.2	0.2	0.2	0.2
	SE408	0.1	0.2	0.1	0.2
9	SE109	0.1	0.2	0.1	0.2
	SE409	0.1	0.2	0.1	0.2
10	SE110	0.1	0.2	0.1	0.2
	SE410	0.1	0.2	0.1	0.2
11	SE111	0.1	0.1	0.1	0.1
	SE411	0.1	0.1	0.1	0.1
12	SE112	0.1	0.3	0.1	0.3
	SE412	0.1	0.2	0.1	0.2
Column End Average		0.3	0.2	0.3	0.2
Frame Average		0.2		0.2	

Table 7.34: Column curvature ductility comparison for the Stiff Inner Frame

Story	Column	Existing Design		Revised Design	
		Bottom End	Top End	Bottom End	Top End
1	SI101	2.2	0.3	1.5	0.3
	SI201	2.8	0.4	2.2	0.5
	SI301	2.6	0.4	2.2	0.5
	SI401	2.1	0.3	1.4	0.3
2	SI102	0.4	0.3	0.4	0.3
	SI202	0.5	0.3	0.6	0.4
	SI302	0.5	0.3	0.6	0.4
	SI402	0.4	0.3	0.4	0.3
3	SI103	0.3	0.3	0.3	0.3
	SI203	0.3	0.3	0.3	0.4
	SI303	0.3	0.3	0.3	0.4
	SI403	0.3	0.3	0.3	0.3
4	SI104	0.2	0.3	0.2	0.3
	SI204	0.3	0.3	0.3	0.3
	SI304	0.3	0.3	0.3	0.3
	SI404	0.2	0.3	0.2	0.3
5	SI105	0.2	0.3	0.2	0.3
	SI205	0.2	0.3	0.2	0.3
	SI305	0.2	0.3	0.2	0.3
	SI405	0.2	0.3	0.2	0.3
6	SI106	0.2	0.2	0.2	0.2
	SI206	0.2	0.3	0.2	0.3
	SI306	0.2	0.3	0.2	0.3
	SI406	0.2	0.2	0.2	0.3
7	SI107	0.2	0.2	0.2	0.2
	SI207	0.2	0.2	0.2	0.2
	SI307	0.2	0.2	0.2	0.2
	SI407	0.2	0.2	0.2	0.2
8	SI108	0.1	0.2	0.1	0.2
	SI208	0.2	0.2	0.2	0.2
	SI308	0.2	0.2	0.2	0.2
	SI408	0.2	0.2	0.2	0.2
9	SI109	0.1	0.2	0.1	0.2
	SI209	0.1	0.2	0.1	0.2
	SI309	0.1	0.2	0.1	0.2
	SI409	0.1	0.2	0.1	0.2
10	SI110	0.1	0.2	0.1	0.2
	SI210	0.1	0.2	0.1	0.2
	SI310	0.1	0.2	0.1	0.2
	SI410	0.1	0.2	0.1	0.2
11	SI111	0.1	0.2	0.1	0.2
	SI211	0.1	0.2	0.1	0.2
	SI311	0.1	0.2	0.1	0.2
	SI411	0.1	0.2	0.1	0.2
12	SI112	0.1	0.2	0.1	0.2
	SI212	0.1	0.1	0.1	0.1
	SI312	0.1	0.1	0.1	0.1
	SI412	0.1	0.2	0.1	0.2
Column End Average		0.4	0.3	0.3	0.3
Frame Average		0.3		0.3	

Table 7.35: Column curvature ductility comparison for the Center Frame

Story	Column	Existing Design		Revised Design	
		Bottom End	Top End	Bottom End	Top End
1	CF101	3.2	0.4	0.9	0.2
	CF201	3.3	0.5	2.0	0.5
	CF301	3.9	0.5	1.3	0.4
	CF401	3.1	0.4	1.0	0.3
2	CF102	0.4	0.4	0.5	0.4
	CF202	0.6	0.6	0.7	0.6
	CF302	0.6	0.5	0.7	0.5
	CF402	0.5	0.4	0.5	0.4
3	CF103	0.3	0.4	0.3	0.4
	CF203	0.5	0.6	0.5	0.6
	CF303	0.4	0.5	0.4	0.5
	CF403	0.4	0.4	0.4	0.4
4	CF104	0.3	0.3	0.3	0.4
	CF204	0.4	0.5	0.4	0.6
	CF304	0.4	0.4	0.4	0.5
	CF404	0.3	0.4	0.3	0.4
5	CF105	0.2	0.3	0.2	0.3
	CF205	0.3	0.5	0.3	0.5
	CF305	0.3	0.4	0.3	0.4
	CF405	0.3	0.4	0.3	0.4
6	CF106	0.2	0.3	0.2	0.3
	CF206	0.3	0.4	0.3	0.4
	CF306	0.3	0.3	0.3	0.4
	CF406	0.3	0.3	0.3	0.3
7	CF107	0.2	0.2	0.2	0.2
	CF207	0.3	0.4	0.3	0.4
	CF307	0.2	0.3	0.3	0.3
	CF407	0.2	0.3	0.2	0.3
8	CF108	0.2	0.2	0.2	0.2
	CF208	0.3	0.3	0.3	0.4
	CF308	0.2	0.3	0.2	0.3
	CF408	0.2	0.3	0.2	0.3
9	CF109	0.1	0.2	0.2	0.2
	CF209	0.2	0.3	0.2	0.3
	CF309	0.2	0.3	0.2	0.3
	CF409	0.2	0.2	0.2	0.2
10	CF110	0.1	0.2	0.1	0.2
	CF210	0.2	0.3	0.2	0.3
	CF310	0.2	0.3	0.2	0.3
	CF410	0.1	0.2	0.2	0.2
11	CF111	0.1	0.2	0.1	0.2
	CF211	0.2	0.2	0.2	0.2
	CF311	0.1	0.2	0.1	0.2
	CF411	0.1	0.2	0.1	0.2
12	CF112	0.1	0.2	0.1	0.2
	CF212	0.1	0.3	0.1	0.3
	CF312	0.1	0.1	0.1	0.1
	CF412	0.1	0.2	0.1	0.2
Column End Average		0.5	0.3	0.4	0.3
Frame Average		0.4		0.3	

Table 7.36: Column curvature ductility comparison for the Flexible Inner Frame

Story	Column	Existing Design		Revised Design	
		Bottom End	Top End	Bottom End	Top End
1	FI201	4.2	0.5	1.2	0.4
	FI301	5.2	0.7	1.8	0.5
	FI401	4.5	0.4	1.3	0.3
2	FI202	0.6	0.6	0.4	0.4
	FI302	0.8	0.7	0.9	0.7
	FI402	0.7	0.6	0.4	0.4
3	FI203	0.5	0.6	0.3	0.4
	FI303	0.6	0.7	0.6	0.7
	FI403	0.5	0.6	0.3	0.4
4	FI204	0.4	0.5	0.3	0.4
	FI304	0.5	0.6	0.5	0.7
	FI404	0.4	0.6	0.3	0.4
5	FI205	0.3	0.5	0.3	0.6
	FI305	0.4	0.6	0.4	0.7
	FI405	0.4	0.5	0.4	0.6
6	FI206	0.3	0.4	0.3	0.5
	FI306	0.4	0.5	0.4	0.5
	FI406	0.3	0.4	0.3	0.5
7	FI207	0.3	0.4	0.3	0.4
	FI307	0.3	0.4	0.3	0.5
	FI407	0.3	0.4	0.3	0.5
8	FI208	0.2	0.3	0.2	0.3
	FI308	0.3	0.4	0.3	0.4
	FI408	0.3	0.3	0.3	0.4
9	FI209	0.2	0.3	0.2	0.3
	FI309	0.3	0.4	0.3	0.4
	FI409	0.2	0.3	0.2	0.3
10	FI210	0.2	0.3	0.2	0.3
	FI310	0.3	0.3	0.3	0.3
	FI410	0.2	0.3	0.2	0.3
11	FI211	0.2	0.2	0.2	0.2
	FI311	0.2	0.3	0.2	0.3
	FI411	0.2	0.2	0.2	0.3
12	FI212	0.1	0.1	0.1	0.1
	FI312	0.1	0.1	0.2	0.1
	FI412	0.1	0.2	0.1	0.2
Column End Average		0.7	0.4	0.4	0.4
Frame Average		0.6		0.4	

Table 7.37: Column curvature ductility comparison for the Flexible Edge Frame

Story	Column	Existing Design		Revised Design	
		Bottom End	Top End	Bottom End	Top End
1	FE201	5.4	0.5	1.3	0.4
	FE301	6.0	0.6	1.4	0.4
	FE401	5.5	0.5	1.3	0.4
2	FE202	0.8	0.8	0.7	0.6
	FE302	1.1	1.0	0.9	0.9
	FE402	1.0	0.7	0.7	0.6
3	FE203	0.5	0.9	0.5	0.6
	FE303	0.7	1.2	0.7	0.8
	FE403	0.6	0.8	0.6	0.6
4	FE204	0.4	0.9	0.4	0.6
	FE304	0.6	1.1	0.6	0.8
	FE404	0.5	0.8	0.5	0.5
5	FE205	0.4	0.8	0.4	0.8
	FE305	0.5	1.0	0.5	0.7
	FE405	0.4	0.7	0.4	0.8
6	FE206	0.3	0.6	0.3	0.7
	FE306	0.5	0.8	0.5	0.7
	FE406	0.3	0.6	0.4	0.7
7	FE207	0.3	0.5	0.3	0.6
	FE307	0.4	0.8	0.4	0.8
	FE407	0.3	0.6	0.3	0.7
8	FE208	0.3	0.4	0.3	0.5
	FE308	0.4	0.6	0.4	0.8
	FE408	0.3	0.5	0.3	0.6
9	FE209	0.3	0.3	0.3	0.4
	FE309	0.4	0.5	0.4	0.5
	FE409	0.4	0.4	0.4	0.4
10	FE210	0.3	0.3	0.4	0.3
	FE310	0.4	0.4	0.4	0.4
	FE410	0.4	0.3	0.4	0.3
11	FE211	0.2	0.3	0.2	0.3
	FE311	0.3	0.3	0.3	0.3
	FE411	0.2	0.3	0.2	0.3
12	FE212	0.1	0.2	0.1	0.2
	FE312	0.2	0.4	0.2	0.5
	FE412	0.1	0.2	0.1	0.2
Column End Average		0.9	0.6	0.5	0.5
Frame Average		0.7		0.5	

7.12.3 Discussion of the Results

One major observation that could be made from the results is that existing system behaves within expected damage levels under MCE level seismic action. Computed beam-end ductilities, first story column bottom-end and shear wall ductilities are consistent with the earthquake level that the system has been analyzed. A ductility unbalance manifests itself at the bottom end of first story columns. Considering these results, it can be concluded that the performance of the code-compliant design in terms of ductility demands is satisfactory.

The revised system exhibits significantly low ductility levels in vertical members even for the MCE level seismic excitation. In terms of performance-based engineering approach, this observation is questionable because it clearly indicates an overdesign. This conclusion is in parallel with what has been discussed previously for response comparison that has been made for DBE level dynamic analyses. On the other hand, there is one clear positive effect observed in the seismic response of revised system. The unbalanced ductility distribution at first story columns that has been seen in the case of existing design diminishes remarkably in the revised system. However, this positive outcome could be regarded as a minor gain considering the level of overdesign in the revised structure.

7.13 Summary and Discussions

In this chapter, a twelve-story reinforced concrete structure with a shear wall is designed according to seismic standards. Inelastic dynamic response of the system has been investigated under a set of design spectrum compatible ground motions. Next, Optimal Strength Distribution Method is applied to the structure and the existing design is revised by strengthening some of the columns as well as first four stories of the shear wall. Then, seismic performance of the revised structure has been investigated. Performance comparison between the existing and revised systems has been carried out. Finally, both existing and revised structures have been analyzed under the strong ground motion set that has been scaled up to maximum considered earthquake (MCE) level and their seismic responses have been compared for a second time.

When the analysis results of the code compliant existing system is investigated, some amount of ductility is observed in the first story flexible side columns and lower stories of the shear wall. Rest of the columns behave elastic. All beams located in the frames in the direction of analysis exhibit similar ductility values with flexible side beam ductilities being slightly higher. Although these results indicate a ductility unbalance in the existing design, amounts of measured ductilities are at expected levels throughout the structure. This observation is also valid for the MCE level seismic excitation. Therefore one major outcome that can be stated is that the seismic design codes are successful in terms of achieving acceptable amounts of ductilities at the twelve-story structure.

The equivalent strength allocation diagram given in Figure 7.9 shows that the existing design attains almost optimal strength distribution along its frames. Considering the seismic response of the existing system along with this observation, it may be deduced that the code compliant existing design is satisfactory. Since the estimated correction in the strength distribution is small, rest of the procedure may not be followed. This is considered as a decision left to the design engineer.

When the revised design is obtained according to updated demands, it results in a significant capacity increase for the vertical members that are marked in Figure 7.10. Hence, seismic response of the columns of the revised system reduces to an essentially elastic response in the case of DBE level excitation. Analyses performed under MCE level scaled ground motion set provides a better opportunity to assess inelastic performance changes. A considerable reduction in ductilities of these members as well as decrease in ductility imbalance is observed in the case of revised structure. Although the Optimal Strength Distribution Method successfully reduces the amount of measured ductility, it results in an overdesign of the system while intending to correct the near-optimal strength distribution of the existing design. Nevertheless, a balanced ductility distribution is observed at the bottom end of first story under MCE level dynamic analyses.

Finally, it should also be added that even if the Optimal Strength Distribution Method aims to increase the strength of the flexible side in its general application for this particular system, it correctly estimates a capacity increase for the stiff side shear

wall as well. This design revision has resulted in a decrease in ductility demand at the shear wall for both levels of seismic action. Consequently, it is deduced that the proposed method has been successful in detecting the critical stiff side members in terms of the expected inelastic deformations as well as the flexible side ones.

CHAPTER 8

SUMMARY AND CONCLUSIONS

8.1 Summary

Inelastic seismic response of torsionally coupled systems has been investigated in this thesis study. The problem of uneven damage distribution that is closely associated with the unsymmetrical placement of lateral load resisting members and/or uneven mass distribution along a story plan is a well-known phenomenon in the literature. However, there are no definitive outcomes achieved in the past studies regarding the improvement of the seismic response of torsionally coupled systems. Moreover, contemporary code provisions which utilize a single global ductility demand among all structural members yield poor seismic performance in terms of ductility imbalance in asymmetric systems.

These identified problems have been inspected in detail throughout the thesis study. First, basic characteristics of the seismic response of torsionally coupled systems have been studied on basic, conceptual single-story structures. Both reinforced concrete and steel designs are provided for the basic system and the effect of inherent over-strength on the unbalanced ductility distribution is investigated. Next, a comprehensive single-story parametric case study is conceived in order to further inspect the effect of fundamental structural parameters such as eccentricity, fundamental period, strength distribution (Stiff to Flexible Strength Ratio - SFSR) and response reduction factor on the torsionally coupled response. Results of the parametric study are compiled in the form of Unsymmetrical Response Spectra and Uniform Ductility Spectra. Implementation of these proposed spectra to the seismic design for improving the ductility distribution has been tested on a set of single-story systems with notable

success.

Following this part of the study, Optimal Strength Distribution Method, which utilizes the Uniform Ductility Spectra, is proposed as a procedure to improve the ductility distribution of asymmetric, torsionally coupled structures. In the proposed method, optimal value of Stiff to Flexible Strength Ratio associated with an asymmetric structure is determined from the related Uniform Ductility Spectrum and it is compared with the existing strength ratio of the system. Upon this comparison, strength allocation diagram for the structure is prepared and identified the side of the structure that require strengthened in order to achieve the optimal strength distribution. After the procedure is explained in detail and sensitivity of the parameters associated with the method is evaluated, its performance is tested on single-story asymmetric systems. Results of this verification study indicates that the method is successful in improving the ductility distribution.

Next, the method is expanded to multi degree of freedom, actual structures. Strategies for determining flexible and stiff side strengths of the actual structures are discussed. While determining the shear strengths of moment-frames or shear walls in an actual multi degree of freedom structure is not a trivial task, some simple concepts are utilized with satisfactory accuracy. Strengths of stiff and flexible sides of building structures are determined by using the existing section capacities. Finally, an algorithm for the implementation of Optimal Strength Method for torsionally coupled structures is developed.

After the proposed method is discussed in detail, its performance on improving the ductility distribution of actual multi degree of freedom structures is evaluated by using three separate case study buildings. First, a reinforced concrete eight-story stiffness-asymmetric structure is investigated. After its seismic design is discussed, inelastic dynamic analysis results of the existing, original structure have been presented. Then the Optimal Strength Distribution Method has been utilized and the revised structure has been obtained. Inelastic dynamic analysis results compiled for the revised system has also been discussed and seismic responses of existing and revised structures have been compared. The application of the method and strengthening of the members indicated by the procedure affected the ductility distribution of the system positively.

Similarly, a reinforced concrete mass-asymmetric structure is inspected as the second case study. The flow of the discussion is the same as the one explained for the stiffness asymmetric structure. Finally, a twelve-story reinforced concrete, highly irregular structure is investigated as the last case study. This building possesses an “L” shaped story plan and a shear wall in one of its frames. The resulting system has a high stiffness asymmetry. Inelastic Seismic response of the existing and revised designs are compared under both DBE and MCE level earthquake excitations.

8.2 Conclusion

According to the results obtained in this study, the following conclusions are reached.

- Through the inspection of two basic single-story systems designed by using reinforced concrete and steel elements, the interdependency between strength and stiffness of structural members has been clearly demonstrated in the initial phase of the thesis study. As can be seen in the results given in Chapter 2, the inherent overstrength that is present in the code designed structural members results in an unbalanced damage distribution in torsionally coupled systems.
- The detailed parametric study performed in Chapter 3 has yielded some interesting results. As can be seen from Unsymmetrical Response Spectra, ductility demands on the flexible and stiff sides depend on quite different system parameters. Further, nominal design (i.e. no overstrength) of the parametric systems results in an unbalanced ductility distribution in seismic response. There is an optimal strength distribution however, that yields balanced ductilities along the plan of each parametric structure. Compilation of these optimal strength distributions for different system parameters yielded the Uniform Ductility Spectra. These two sets of spectra have been presented as practical design tools from which the expected level of ductility imbalance of a structure could be estimated at the preliminary design phase. The Uniform Ductility Spectra, in particular, is considered as an important product of this thesis study. Using the spectrum associated with the fundamental structural properties, the design engineer can determine the optimal strength distribution of system members accordingly.

- The proposed Optimal Strength Distribution Method employs the basic principles of static force superposition procedure in the design phase of a torsionally coupled system. The superimposed Optimal Load Vector applied along with the seismic forces yields the revised demands on structural members. Hence, a more optimal strength distribution is achieved. In addition to the classical design procedure, a single additional linear elastic static analysis step is performed in order to compute the additional demands under the Optimal Load Vector. Because of its simplicity, Optimal Strength Distribution Method is considered as a handy tool that can easily be integrated into the linear elastic seismic design procedures. Hence, it can proactively provide the correct strength distribution for the designed structure; ultimately yielding a better inelastic seismic response distribution.
- As revealed in Chapter 5, revised version of the eight-story stiffness asymmetric structure clearly exhibits a better damage distribution compared with the existing one. The design revision, which significantly corrects the existing strength distribution improves the seismic response considerably. Ductility imbalance and high amounts of curvature demands that are observed at the first story columns of the existing design decreased in the case of revised design. On the other hand, interstory drift ratios and beam-end curvature demands have slightly increased in the revised structure. However, the change in these demands is considered negligible when compared with the global improvement of seismic response.
- Compared with the stiffness asymmetric systems, the eight-story mass asymmetric structure presented in Chapter 6 poses more challenge in terms of balancing the inelastic seismic response. Since section dimensions are uniform throughout the structure, there is no definitive stiffness asymmetry in the system. However, mass asymmetry due to the shift in the location of CM , requires one side of the structure to be designed stronger than the other side. Due to the relationship between strength and stiffness, the stronger side frames are stiffer than the weaker frames of the structure. Throughout this analogy, the proposed method is also implemented on a mass-asymmetric system.
- The code compliant, existing designs of eight-story mass asymmetric and twelve-

story stiffness asymmetric structures that are investigated in Chapters 6 and 7 respectively, exhibit near optimal strength distribution. Moreover, measured ductilities throughout these two systems at the end of inelastic dynamic analyses are at acceptable levels. Therefore, it can be concluded that the seismic design that was performed according to the design codes yields satisfactory performance in terms of strength distribution and inelastic deformations for these two particular systems.

- As observed from the Equivalent Strength Allocation Diagrams that are constructed for eight-story mass asymmetric and twelve-story stiffness asymmetric structures (Figures 6.8 and 7.9), the correction to the strength distribution estimated by the Optimal Strength Distribution Method is minimal. This conclusion further verifies that the existing designs of these systems can be considered satisfactory. At this stage, implementation of the further steps of the proposed method is an engineering decision in terms of performance-based earthquake engineering. The Optimal Strength Distribution Method algorithm given in Chapter 4 could further be followed and revised design with updated capacities could be obtained in order to remedy the slight uneven ductility distribution that is observed in the case study buildings given in Chapters 6 and 7. Alternatively, the existing designs could be left without any modifications by considering the seismic performances of these systems as acceptable.
- Due to the reasons discussed above, minor design modification is obtained through the application of the proposed method on the mass asymmetric structure in Chapter 6. However it yields a limited improvement in the seismic response of the revised system. Overall seismic behavior remains essentially unchanged. Nevertheless, maximum member ductilities measured in first story columns of the strong side members of the existing system are reduced.
- When design revision is performed on the twelve-story structure in Chapter 7, the proposed method indicates a considerable number of columns to be strengthened on the flexible side. In addition, it accurately points out to a capacity increase in the shear wall located on the stiff side, as well. However, these increases in member capacities result in a significant overdesign of the revised system. Maximum ductilities recorded at the bottom of the shear wall

and columns located in the flexible side frames reduce significantly. In fact, columns of the revised structure remain essentially elastic under DBE level seismic excitation.

- A similar observation can be made for the dynamic analyses results obtained under MCE scaled ground motion set in Chapter 7. The existing design presented in Chapter 7 performs well under the MCE level seismic excitation in terms of member ductilities. However, a slight uneven ductility distribution at the bottom end of first story columns is observed. In the revised system, the ductility unbalance present in the columns reduces significantly. In addition, a significant reduction in column deformations is also detected. Although ductility unbalance is reduced, these results indicate an overdesign of the revised system similar to the case of DBE level seismic performance comparison. As mentioned previously, this situation arises when the proposed method is applied to the twelve-story structure which already possess a near-optimal strength distribution. The revised design overcorrects the seismic behaviour of the existing system as can be seen from performance comparisons made for two levels of seismic excitations.
- Optimal Strength Distribution Method indicated a capacity increase for the first story Stiff Edge frame columns of the eight-story stiffness asymmetric structure discussed in Chapter 5. This could be related with the redistribution of response when the Optimal Load Vector is applied. Due to combined reaction of the four frames of the structure, additional force demands could be observed on the stiffer side elements, as well. The proposed procedure could further be refined to remedy this situation as part of a possible future study.
- Optimal Strength Distribution Method could be further developed in order to perform better in the case of mass-asymmetric structures. The method is based on Uniform Ductility Spectra, which are compiled through inelastic seismic response of stiffness asymmetric single story parametric structures. By developing the same set of spectra through mass-asymmetric parametric systems, seismic response of actual multi-degree of freedom structures having same type of asymmetry could be better estimated. By doing so, seismic response of a very comprehensive class of torsionally coupled structures could be improved

through application of the proposed method. This is also considered as a future expansion of the procedure.

- As clearly demonstrated in Chapters 6 and 7, the structural design that has been performed according to seismic design codes actually yields acceptable performance in the case of some asymmetric structures. Many requirements such as minimum member dimensions or reinforcement detailing remedy the expected uneven seismic response in these systems. However, this correction may not be sufficient for a more irregular and/or asymmetric structure. In addition, the positive effect of seismic detailing is absent from buildings that has not been designed according to seismic regulations. The main advantage of the proposed Optimal Strength Distribution Method could become clearer while inspecting the behaviour of these type of structures. Further progressing the work laid out here on these types of structures is also one of the possible future extensions of this thesis study.

8.3 Recommendations for Future Research

In addition to planned future expansions of this thesis study discussed in the Conclusions Section, several additional topics for future research are also recommended.

- The formulation of the Optimal Strength Distribution Method is independent of the direction of seismic excitation and it can be applied to a structure at any desired direction. However, dynamic analysis results of a structure on which the procedure is implemented will definitely show variation with respect to the direction of seismic excitation. The seismic responses of the structural members obtained under bidirectional excitation may differ considerably from those determined from the unidirectional case. In this thesis study, performance assessment of the proposed method is conducted by inspecting the inelastic dynamic responses of building structures under strong motions acting in the direction of analysis. As a further expansion to what has been done in scope of the study, inelastic dynamic responses of existing and revised systems can be obtained under bidirectional earthquake excitation. Due to reasons explained, incorpo-

rating the more realistic application of the seismic excitation is considered as the next stage in verification studies.

- The case study systems that are investigated herein are all reinforced concrete structures which exhibit vertical regularity. In the case of structures that possess very prominent soft stories or member irregularities in their elevations, determination of the stiffness eccentricity is a significant challenge that needs to be addressed. The proposed Optimal Strength Distribution Method can be implemented and its effectiveness can be tested on these type of systems in the subsequent studies.
- The necessary capacity increase that has been determined upon application of the Optimal Strength Distribution Method to the case study building structures is achieved by increasing the longitudinal reinforcement ratios of vertical members. This procedure resulted in higher shear strengths in reinforced concrete load resisting systems with minor changes in yield deformations and member stiffnesses. While a simple design modification has been sufficient in the case of reinforced concrete systems, this may not be the case for buildings having steel load resisting members. Due to relationship between strength and stiffness, increasing the capacities of steel structural elements would ultimately yield an increase in the stiffness of these members. The resulting change in the stiffness eccentricity of the system may alter the seismic response of the revised system dramatically. This effect may be positive or negative depending on the structural layout. This issue definitely needs more investigation and it is considered as a major future study subject. The Optimal Strength Distribution Method could be developed further and design procedures specific to building structures having steel structural members could be implemented to the proposed method as part of the future research.

REFERENCES

- [1] J. L. Almazan and J. C. De la Llera. Torsional balance as new design criterion for asymmetric structures with energy dissipation devices. *Earthquake Engineering and Structural Dynamics*, 38(12):1421–1440, 2009.
- [2] American Institute of Steel Construction. *Specification for Structural Steel Buildings*. June 2010.
- [3] American Institute of Steel Construction. Steel construction manual shapes database v14.1: <http://www.aisc.org/content.aspx?id=2868>, December 2014.
- [4] American Society of Civil Engineers. *Minimum Design Loads for Buildings and Other Structures (ASCE/SEI 7-10)*. 2010.
- [5] American Society of Civil Engineers. *Seismic Evaluation and Retrofit of Existing Buildings (ASCE/SEI 41-13)*. 2013.
- [6] S. A. Anagnostopoulos, M. T. Krykos, and K. G. Stathopoulos. Earthquake induced torsion in buildings: critical review and state of the art. *Earthquakes and Structures*, 8(2):463–484, 2015.
- [7] D. Basu and S. K. Jain. Alternative method to locate centre of rigidity in asymmetric buildings. *Earthquake Engineering and Structural Dynamics*, 36(8):965–973, 2007.
- [8] R. Bertero. Inelastic torsion for preliminary seismic design. *Journal of Structural Engineering*, 121(8):1183–1189, 1995.
- [9] M. Bosco, A. Ghersi, E. M. Marino, and P. P. Rossi. Comparison of nonlinear static methods for the assessment of asymmetric buildings. *Bulletin of Earthquake Engineering*, 11(6):2287–2308, 2013.
- [10] J. I. Bustamante and E. Rosenblueth. Building code provisions on torsional oscillations. In *Proceedings of 2nd World Conference on Earthquake Engineering*, volume 2, pages 879–894, Tokyo, 1960.

- [11] A. M. Chandler and X. N. Duan. A modified static procedure for the design of torsionally unbalanced multistorey frame buildings. *Earthquake Engineering and Structural Dynamics*, 22(5):447–462, 1993.
- [12] A. M. Chandler and X. N. Duan. Performance of asymmetric code-designed buildings for serviceability and ultimate limit states. *Earthquake Engineering and Structural Dynamics*, 26(7):717–735, 1997.
- [13] A. M. Chandler, X. N. Duan, and A. Rutenberg. Evaluation and further development of the ec8 static torsional provisions. In *European Seismic Design Practice*, pages 531–540. Balkema, 1995.
- [14] A. K. Chopra and R. K. Goel. A modal pushover analysis procedure for estimating seismic demands for buildings. *Earthquake Engineering and Structural Dynamics*, 31(3):561–582, 2002.
- [15] A. K. Chopra and R. K. Goel. A modal pushover analysis procedure to estimate the seismic demands for unsymmetrical-plan buildings. *Earthquake Engineering and Structural Dynamics*, 33(8):903–927, 2004.
- [16] Computers & Structures Inc. Perform-3d version 5.0.0: Nonlinear analysis and performance assessment of 3d structures, 2011.
- [17] J. C. Correnza, G. L. Hutchinson, and A. M. Chandler. Seismic response of flexible-edge elements in code-designed torsionally unbalanced structures. *Engineering Structures*, 17(3):158–166, 1995.
- [18] E. F. Cruz and S. Cominetti. Three-dimensional buildings subjected to bi-directional earthquakes: Validity of analysis considering unidirectional earthquakes. In *Proceedings of the 12th World Conference on Earthquake Engineering*, New Zealand, 2000.
- [19] J. De-la Collina. Assessment of design recommendations for torsionally unbalanced multistory buildings. *Earthquake Spectra*, 19(1):47–66, 2003.
- [20] J. C. De la Llera, J. L. Almazan, and I. J. Vial. Torsional balance of plan-asymmetric structures with frictional dampers: Analytical results. *Earthquake Engineering and Structural Dynamics*, 34(9):1089–1108, 2005.

- [21] J. C. De la Llera and A. K. Chopra. Understanding the inelastic seismic behaviour of asymmetric-plan buildings. *Earthquake Engineering and Structural Dynamics*, 24(4):549–572, 1995.
- [22] M. De Stefano, G. Faella, and R. R. Seismic response of 3d r/c frame: Effect of plan irregularity. In A. S. Elnashai, editor, *European Seismic Design Practice - Research and Application: Proceedings of the 5th SECED Conference*, Chester, UK, 1995.
- [23] M. De Stefano, G. Faella, and R. Ramasco. Inelastic seismic response of one-way plan-asymmetric systems under bi-directional ground motions. *Earthquake Engineering and Structural Dynamics*, 27(4):363–376, 1998.
- [24] M. De Stefano, E. M. Marino, and P. P. Rossi. Effect of overstrength on the seismic behaviour of multi-storey regularly asymmetric buildings. *Bulletin of Earthquake Engineering*, 4(1):23–42, 2006.
- [25] M. De Stefano and B. Pintucchi. A model for analyzing the inelastic seismic response of plan-irregular building structures. In *Proceedings of the 15th ASCE Engineering Mechanics Conference*, New York, 2002.
- [26] M. De Stefano and B. Pintucchi. A review of the research on seismic behaviour of irregular structures since 2002. *Bulletin of Earthquake Engineering*, 6:285–308, 2008.
- [27] X. N. Duan and A. M. Chandler. Inelastic seismic response of code-designed multistorey frame buildings with regular asymmetry. *Earthquake Engineering and Structural Dynamics*, 22(5):431–445, 1993.
- [28] X. N. Duan and A. M. Chandler. An optimized procedure for seismic design of torsionally unbalanced structure. *Earthquake Engineering and Structural Dynamics*, 26(7):737–757, 1997.
- [29] E. Erduran and K. L. Ryan. Effects of torsion on the behaviour of peripheral steel-braced frame systems. *Earthquake Engineering and Structural Dynamics*, 40(5):491–507, 2011.
- [30] European Committee for Standardization. *EN 1998-3 Eurocode 8: Design of structures for earthquake resistance*. 2004.

- [31] P. Fajfar, V. Kilar, D. Marusic, I. Perus, and G. Magluilo. The extension of the n2 method to asymmetric buildings. In *Proceedings of the 4th European workshop on the seismic behaviour of irregular and complex structures*, Thessaloniki, 2005.
- [32] P. Fajfar, G. Magluilo, D. Marusic, and I. Perus. Simplified non-linear analysis of asymmetric buildings. In *Proceedings of the 3rd European workshop on the seismic behaviour of irregular and complex structures*, Florence, 2002.
- [33] G. K. Georgoussis. Optimum design of multistory uniform structures with simple eccentricity. *The Structural Design of Tall and Special Buildings*, 17(3):719–738, 2008.
- [34] A. Gherzi, E. M. Marino, and P. P. Rossi. Static versus modal analysis: Influence on inelastic response of multi-storey asymmetric buildings. *Bulletin of Earthquake Engineering*, 5(4):511–532, 2007.
- [35] A. Gherzi and P. P. Rossi. Formulation of design eccentricity to reduce ductility demand in asymmetric buildings. *Engineering Structures*, 22(7):857–871, 2000.
- [36] R. K. Goel. Seismic response of asymmetric systems: Energy-based approach. *Journal of Structural Engineering*, 123(11):1444–1453, 1997.
- [37] R. K. Goel. Effects of supplemental viscous damping on seismic response of asymmetric-plan systems. *Earthquake Engineering and Structural Dynamics*, 27(2):125–141, 1998.
- [38] R. K. Goel. Effects of supplemental viscous damping on inelastic seismic response of asymmetric-plan systems. *Earthquake Engineering and Structural Dynamics*, 30(3):411–430, 2001.
- [39] R. K. Goel and A. K. Chopra. Effects of plan asymmetry in inelastic seismic response of one-story systems. *Journal of Structural Engineering*, 117(5):1492–1513, 1991.
- [40] R. K. Goel and A. K. Chopra. Dual-level approach for seismic design of asymmetric-plan buildings. *Journal of Structural Engineering*, 120(1):161–179, 1994.

- [41] R. K. Goel and A. K. Chopra. Extension of modal pushover analysis to compute member forces. *Earthquake Spectra*, 21(1):125–139, 2005.
- [42] J. Hancock, J. Watson-Lamprey, N. A. Abrahamson, J. J. Bommer, A. Markatis, E. McCoy, and R. Mendis. Improved method of matching response spectra of recorded earthquake ground motion using wavelets. *Journal of Earthquake Engineering*, 10(Special Issue 1):67–89, 2006.
- [43] H. Hao and X. N. Duan. Seismic response of asymmetric structures to multiple ground motions. *Journal of Structural Engineering*, 121(11):1557–1564, 1995.
- [44] R. Hejal and A. K. Chopra. Earthquake response of torsionally coupled frame buildings. *Journal of Structural Engineering*, 115(4):834–851, 1989.
- [45] R. Hejal and A. K. Chopra. Lateral-torsional coupling in earthquake response of frame buildings. *Journal of Structural Engineering*, 115(4):852–867, 1989.
- [46] J. L. Humar and P. Kumar. Effect of orthogonal inplane structural elements on inelastic torsional response. *Earthquake Engineering and Structural Dynamics*, 28(10):1071–1097, 1999.
- [47] K. Kaatsiz and H. Sucuoglu. Generalized force vectors for multi-mode pushover analysis of torsionally coupled systems. *Earthquake Engineering and Structural Dynamics*, 43(13):2015–2033, 2014.
- [48] C. L. Kan and A. K. Chopra. Elastic earthquake analysis of torsionally coupled multistorey buildings. *Earthquake Engineering and Structural Dynamics*, 5(4):395–412, 1977.
- [49] C. L. Kan and A. K. Chopra. Effects of torsional coupling on earthquake forces in buildings. *Journal of the Structural Division*, 103(4):805–819, 1977.
- [50] C. L. Kan and A. K. Chopra. Torsional coupling and earthquake response of simple elastic and inelastic systems. *Journal of the Structural Division*, 107(8):1569–1588, 1981.
- [51] D. C. Kent and R. Park. Flexural members with confined concrete. *Journal of the Structural Division*, 97(7):1969–1990, 1971.

- [52] V. Kilar and P. Fajfar. On the applicability of pushover analysis to the seismic performance evaluation of asymmetric buildings. *European Earthquake Engineering*, 15:20–31, 2001.
- [53] A. J. Kosmopoulos and M. N. Fardis. Estimation of inelastic seismic deformations in asymmetric multistorey rc buildings. *Earthquake Engineering and Structural Dynamics*, 36(9):1209–1234, 2007.
- [54] M. Kreslin and P. Fajfar. The extended n2 method considering higher mode effects in both plan and elevation. *Bulletin of Earthquake Engineering*, 10(2):695–715, 2012.
- [55] M. T. Kyrkos and S. A. Anagnostopoulos. Improved earthquake resistant design of eccentric steel buildings. *Soil Dynamics and Earthquake Engineering*, 47:144–156, 2013.
- [56] J. L. Lin, M. T. Bui, and K. C. Tsai. An energy-based approach to the generalized optimal locations of viscous dampers in two-way asymmetrical buildings. *Earthquake Spectra*, 30(2):867–889, 2014.
- [57] D. Marusic and P. Fajfar. Torsional effects on seismic response of asymmetric buildings. In Grundman and Schueller, editors, *Structural Dynamics - EURO-DYN2002*. 2002.
- [58] D. Marusic and P. Fajfar. On the inelastic seismic response of asymmetric buildings under bi-axial excitation. *Earthquake Engineering and Structural Dynamics*, 34(8):943–963, 2005.
- [59] M. S. Medhekar and D. J. L. Kennedy. Displacement-based seismic design of buildings - application. *Engineering Structures*, 22(3):210–221, 2000.
- [60] M. S. Medhekar and D. J. L. Kennedy. Displacement-based seismic design of buildings - theory. *Engineering Structures*, 22(3):201–209, 2000.
- [61] A. S. Moghadam and W. K. Tso. Damage assessment of eccentric multistory buildings using 3-d pushover analysis. In *Proceedings of the 11th World Conference on Earthquake Engineering*, Acapulco, 1996.

- [62] A. S. Moghadam and W. K. Tso. 3-d pushover analysis for damage assessment of buildings. *Journal of Seismology and Earthquake Engineering*, 2(3):23–31, 2000.
- [63] B. Myslimaj and W. K. Tso. A design-oriented approach to strength distribution in single-story asymmetric systems with elements having strength-dependent stiffness. *Earthquake Spectra*, 21(1):197–212, 2005.
- [64] T. K. L. Nelson, J. L. Wilson, and G. L. Hutchinson. Review of the torsional coupling of asymmetrical wall-frame buildings. *Engineering Structures*, 19(3):233–246, 1997.
- [65] Pacific Earthquake Engineering Research Center. Opensees: Open system for earthquake engineering simulation, <http://opensees.berkeley.edu>, June 2015.
- [66] Pacific Earthquake Engineering Research Center. Peer ground motion database available from: <http://ngawest2.berkeley.edu>, October 2018.
- [67] T. Paulay. A behaviour-based design approach to earthquake-induced torsion in ductile buildings. In P. Fajfar and H. Krawinkler, editors, *Seismic Design Methodologies for the Next Generation of Codes*. Balkema, Rotterdam, 1997.
- [68] T. Paulay. Some design principles relevant to torsional phenomena in ductile buildings. *Journal of Earthquake Engineering*, 5(3):273–308, 2001.
- [69] T. Paulay. An estimation of displacement limits for ductile systems. *Earthquake Engineering and Structural Dynamics*, 31(3):583–599, 2002.
- [70] I. Perus and P. Fajfar. On the seismic response of idealized asymmetric single-story structures. eace task group 8: Asymmetric and irregular structures. In *Proceedings of the 2nd Workshop*, volume 1, Istanbul, 1999.
- [71] I. Perus and P. Fajfar. On inelastic torsional response of single-story structures under bi-axial excitation. *Earthquake Engineering and Structural Dynamics*, 34(8):931–941, 2005.
- [72] J. D. Pettinga, M. J. N. Priestley, and S. Pampanin. The role of inelastic torsion in determination of residual deformations. *Journal of Earthquake Engineering*, 11(1):133–157, 2007.

- [73] Presidency of Disaster and Emergency Management. *Turkish Earthquake Code for Building Structures: Specifications for Design of Buildings under Earthquake Forces*. 2018.
- [74] M. J. N. Priestley. Myths and fallacies in earthquake engineering - conflicts between design and reality. *Bulletin of the New Zealand National Society for Earthquake Engineering*, 26:329–341, 1993.
- [75] R. Riddell and H. Santa-Maria. Inelastic response of one-story asymmetric-plan systems to bi-directional earthquake motions. *Earthquake Engineering and Structural Dynamics*, 28(3):273–285, 1999.
- [76] R. Roy and S. Chakrobotry. Seismic demand of plan-asymmetric structures: a revisit. *Earthquake Engineering and Engineering Vibration*, 12(1):99–117, 2013.
- [77] A. Rutenberg. Nonlinear response of asymmetric building structures and seismic codes: A state of the art review. In P. Fajfar and H. Krawinkler, editors, *Nonlinear Seismic Analysis and Design of Reinforced Concrete Buildings*, pages 281–305. Amsterdam, 1992.
- [78] A. Rutenberg. Eae task group 8: Behavior of irregular and complex structures - state of the art report: Seismic nonlinear response of code-designed asymmetric structures. In *Proceedings of the 11th European Conference on Earthquake Engineering*, Paris, 1998.
- [79] A. Rutenberg. Eae task group 8: Behavior of irregular and complex structures asymmetric structures - progress since 1998. In *Proceedings of the 12th European Conference on Earthquake Engineering, CD-ROM*, London, 2002.
- [80] A. Rutenberg and M. De Stefano. On the seismic performance of yielding asymmetric multistorey buildings: A review and a case study. In P. Fajfar and H. Krawinkler, editors, *Seismic Design Methodologies for the Next Generation of Codes*. Balkema, Rotterdam, 1997.
- [81] A. Sahin. A new algorithm for geometrical design of asymmetric tall buildings against seismic torsional behaviour. *The Structural Design of Tall and Special Buildings*, 21(9):642–668, 2012.

- [82] H. Sedarat and V. V. Bertero. *Effects of Torsion on the Linear and Nonlinear Seismic Response of Structures*. UCB/EERC-90/12, Earthquake Engineering Research Center, University of California, Berkeley, 1990.
- [83] K. G. Stathopoulos and S. A. Anagnostopoulos. Elastic and inelastic torsion in buildings. In *Proceedings of the 11th European Conference on Earthquake Engineering*, Paris, 1998.
- [84] K. G. Stathopoulos and S. A. Anagnostopoulos. Inelastic torsion of multistory buildings under earthquake excitations. *Earthquake Engineering and Structural Dynamics*, 34(12):1449–1465, 2005.
- [85] W. K. Tso and B. Myslimaj. A yield displacement distribution-based approach for strength assignment to lateral force-resisting elements having strength dependent stiffness. *Earthquake Engineering and Structural Dynamics*, 32(15):2319–2351, 2003.
- [86] W. K. Tso and C. M. Wong. Seismic displacements of torsionally unbalanced buildings. *Earthquake Engineering and Structural Dynamics*, 24(10):1371–1387, 1995.
- [87] Turkish Standard Institute. *Requirements for Design and Construction of Reinforced Concrete Structures (TS 500)*. February 2000.
- [88] B. Wu, J. P. Ou, and T. T. Soong. Optimal placement of energy dissipation devices for three-dimensional structures. *Engineering Structures*, 19(2):113–125, 1997.

CURRICULUM VITAE

PERSONAL INFORMATION

Surname, Name: Kaatsız, Kaan

Nationality: Turkish (TC)

Date and Place of Birth: 02.10.1986, Ankara

Marital Status: Single

Phone: 0 312 2105401

Fax: 0 312 2102411

EDUCATION

Degree	Institution	Year of Graduation
M.S.	METU Civil Engineering	2012
B.S.	METU Civil Engineering	2009
High School	Ankara Atatürk High School	2004

PROFESSIONAL EXPERIENCE

Year	Place	Enrollment
2018 - Present	METU Civil Engineering Department	Part Time Instructor
2010 - 2018	METU Civil Engineering Department	Research Assistant
2009 - 2010	METU Structural Mechanics Laboratory	Project Assistant

PUBLICATIONS

Refereed Papers and Journal Articles

1. K. Kaatsız, H. Sucuoğlu. The Role of Overstrength on the Seismic Performance of Asymmetric-Plan Structures. *Earthquake Engineering and Structural Dynamics*, 2018:1–20. <https://doi.org/10.1002/eqe.3142>
2. K. Kaatsız, H. Sucuoğlu. Generalized Force Vectors for Multi-Mode Pushover Analysis of Torsionally Coupled Systems. *Earthquake Engineering and Structural Dynamics*, 43(13):2015-2033, October 2014

Conference Proceedings

1. K. Kaatsız, H. Sucuoğlu. Investigation of Overstrength in Asymmetric-Plan Structures. 16th European Conference on Earthquake Engineering, Thessaloniki, Greece, 2018.
2. K. Kaatsız, H. Sucuoğlu. Investigation of Overstrength in Asymmetric-Plan Structures as an Optimum Design Strategy. Fourth International Earthquake Engineering and Seismology Conference, Eskişehir, Turkey, 2017
3. K. Kaatsız, F.S. Alıcı, and H. Sucuoğlu. Generalized Pushover Analysis for Torsionally Coupled Systems. 16th World Conference on Earthquake Engineering, Santiago, Chile, 2017.
4. K. Kaatsız, F.S. Alıcı, and H. Sucuoğlu. Burulmalı Sistemler İçin Genel Yük Vektörleri İle Çok Modlu İtme Analizi. Third Turkish Earthquake Engineering and Seismology Conference, İzmir, Turkey,
5. F.S. Alıcı, K. Kaatsız, and H. Sucuoğlu. Bina Yapılarının Çok Modlu İtme Analizi için Genel Yük Vektörlerinin Pratik Uygulaması, Third National Earthquake Engineering and Seismology Conference, İzmir, Turkey, 2015.
6. K. Kaatsız, F.S. Alıcı, and H. Sucuoğlu. Generalized Force vectors for Analysis of Torsionally Coupled Systems, 2015 World Congress on Advances in Structural Engineering and Mechanics (ASEM15), Incheon, South Korea, 2015.

7. F.S. Alıcı, K. Kaatsız, and H. Sucuoğlu. Practical Implementation of Generalized Pushover Analysis for Multimodal Pushover Analysis. 2015 World Congress on Advances in Structural Engineering and Mechanics (ASEM15), Incheon, South Korea, 2015
8. F.S. Alıcı, K. Kaatsız, and H. Sucuoğlu. Genel İtme Analizinin Pratik Uygulaması. Second Turkish Earthquake Engineering and Seismology Conference, Hatay, Turkey, 2013.
9. F.S. Alıcı, K. Kaatsız, and H. Sucuoğlu. Practical Implementation of Generalized Pushover Analysis. 15th World Conference on Earthquake Engineering, Lisbon, Portugal, 2012.
10. F.S. Alıcı, K. Kaatsız, and H. Sucuoğlu. Multi Modal Pushover Analysis with Generalized Force Vectors (Generalized Pushover Analysis). The Turkish Earthquake Engineering and Seismology Conference, Ankara, Turkey, 2011.

HOBBIES

Computers and Programming, Scale Model Making, Music (Guitar), Reading, Motor Sports